SYNCHROPHASORS BASED POWER SYSTEM MONITORING AND VOLTAGE CONTROL

Ph. D. THESIS

by

K S SAJAN

DEPARTMENT OF ELECTRICAL ENGINEERING
INDIAN INSTITUTE OF TECHNOLOGY ROORKEE
ROORKEE - 247667, INDIA
DECEMBER, 2015

SYNCHROPHASORS BASED POWER SYSTEM MONITORING AND VOLTAGE CONTROL

A THESIS

Submitted in partial fulfilment of the requirements for the award of the degree

of

DOCTOR OF PHILOSOPHY

in

ELECTRICAL ENGINEERING

by

K S SAJAN

DEPARTMENT OF ELECTRICAL ENGINEERING
INDIAN INSTITUTE OF TECHNOLOGY ROORKEE
ROORKEE – 247 667 (INDIA)
DECEMBER, 2015

INDIAN INSTITUTE OF TECHNOLOGY ROORKEE
ROORKEE

CANDIDATE'S DECLARATION

I hereby certify that the work which is being presented in the thesis entitled **"SYNCHROPHASORS BASED POWER SYSTEM MONITORING AND VOLTAGE CONTROL"** in partial fulfilment of the requirements for the award of the Degree of Doctor of Philosophy and submitted in the Department of Electrical Engineering of the Indian Institute of Technology Roorkee, Roorkee is an authentic record of my own work carried out during a period from December, 2010 to December, 2015 under the supervision of Dr. Barjeev Tyagi, Associate Professor and Dr. Vishal Kumar, Assistant Professor, Department of Electrical Engineering, Indian Institute of Technology, Roorkee.

The matter presented in this thesis has not been submitted by me for the award of any other degree of this or any other Institute.

(K S SAJAN)

This is to certify that the above statement made by the candidate is correct to the best of our knowledge.

(Vishal Kumar)
Supervisor

(Barjeev Tyagi)
Supervisor

Date:_____

ABSTRACT

Real time monitoring and control is the prime requirement for reliable and secure operation of large interconnected power system. The invention of the Phasor Measurement Unit (PMU) in mid 1980's enabled the synchronized measurements of voltages and currents in real time that has become the foundation of today's Wide Area Measurement, Protection And Control (WAMPAC) systems. A wide area monitoring system consists of PMUs, which are geographically dispersed in the system, and are time-synchronized through Global Positioning System (GPS) clock. The PMU measures instantaneous voltage, current, frequency and rate of change in frequency from dispersed locations of a wide network. These measured phasors with precise time stamp are collected at a centralized location, called as the Phasor Data Concentrator (PDC) that provides a real-time picture of the large interconnected power system. This synchronized data aids in all kinds of monitoring, control, and protection applications. This thesis primarily focuses on application of PMU measurements in wide area monitoring and control of real power system.

In the implementation of WAMPAC, the first and the foremost step is the installation of optimally placed PMUs in the power system. The principal objective of PMUs installation is to make the system observable, either completely or incompletely. In practical scenario, PMU installation requires large expenditure. In addition to this, the proper site preparation, establishment of adequate communication and GPS are other essential requirements, which further increase these financial constraints. Many Optimal Placement of PMUs (OPP) techniques have been reported in the literature, such as integer programming, depth-first search, spanning tree method etc. Intelligent techniques like nondominated genetic algorithm, Tabu search, simulated annealing, particle swarm optimization techniques etc. have also been used for the solution of the problem. Different OPP methods, discussed so far, provide the optimal number and locations; the optimization of the number of branch current phasors of PMU has not been taken into account. A branch current phasor of PMU installed bus is used for calculating the voltage phasor of the other end bus by applying KVL. The current phasors measurement requires the number of current transformers and other auxiliary equipment equal to the number of lines connected to the bus, which increases the overall cost. In addition, measuring the current phasors of all the connected lines to a PMU installed bus becomes unnecessary if the bus connected to these lines are already under observation of neighboring PMU through its current phasor in the same power system. Hence, number of current phasors

need to be measured by a PMU can be optimized, which will reduce the overall installation cost.

In present work, a new approach for the optimal placement of PMUs with optimal number of current phasor measurements considering the different cases of observability has been proposed. In first case, the problem for OPP has been solved for the complete observability and then the optimal current phasors are determined. In second case, the OPP problems have been formulated with the optimal current phasors for incomplete observability with Depth-of-One unobservability and Depth-of-Two unobservability. In another case, the similar OPP problems have been formulated that ensures complete power system observability with N-1 contingency. The ultimate goal is to find the minimum number of PMUs and their corresponding locations with optimal current phasor measurements so that the state estimation could be performed with measured phasor data at the lowest possible cost. The problems are formulated as a generalized binary linear programming problem and genetic algorithm is used to search the solution for deriving the optimal configuration.

In a large power system, a large quantum of PMUs is required for full observability that entails high capital cost, in the installation. These requirements pose physical and financial constraints on the PMUs installation process. It is imperative to formulate a staging program for PMUs installation in a phased manner and effectively utilize the PMUs even during the installation process in a power system network. Some of the authors have considered phased placement with additional benefits in terms of generator bus and tie line observability. This thesis addresses the problem of phased PMUs placement based on voltage stability monitoring and control.

In this thesis, a new multi-phase PMUs placement approach based on voltage stability monitoring has been proposed. The approach uses Revised Analytical Hierarchy Process (RAHP). In this process, the first step is to determine the optimal number and the optimal locations of PMUs along with the channel limit that ensure complete power system observability even under a branch outage or a PMU failure. The second step is to identify the critical buses, which are more prone to voltage collapse using the Fast Voltage Stability Index (FVSI). The objective of the present work is to monitor the most critical buses in first phase either directly (PMU bus) or indirectly (neighboring bus). RAHP is used for decision-making in phasing of PMUs allocation. To get the maximum priority to the critical buses in multiphase installation of PMUs, Critical Load bus Observability

Criteria (CLOC) has been introduced in the decision making process in addition to five other observability criteria (OC) namely, Noncritical Load bus Observability Criteria (NLOC), Generator Observability Criteria (GOC), PMUs Distribution Criteria (PDC), Tie Line Observability Criteria (TOC), and Bus Connectivity Criteria (BCC).

As the synchrophasor measurements become available from the PMUs placed in phases, it is useful to integrate the conventional SCADA measurements and the phasor measurements to improve the accuracy of the State Estimation (SE). Therefore, developing a hybrid state estimator that includes both conventional and phasor measurements is required to get better results. Several hybrid SE approaches have been suggested in the literature, such as multi-area SE, distributed hybrid SE and quadratic hybrid SE. Most of the proposed hybrid SE methods result in an increased accuracy of the SE.

This thesis provides a state estimation model, which can integrate both the SCADA measurements and the available phasor measurements obtained from multi-phasing installation of PMUs. The bad data detection and elimination in both the conventional measurement and the phasor measurements have been carried out using the normalized residual test method.

In the recent years, voltage collapse is a major cause for many power system blackouts around the globe. The traditional method for voltage stability analysis relied on static analysis using the conventional power flow methods such as Gauss-Seidel or Newton-Raphson. In literature a number of voltage stability indexes, based upon conventional power flow have been proposed. The main drawback of these techniques is the singularity of the Jacobian matrix at the maximum loading point. To overcome this problem, Continuation Power Flow (CPF) method is used to compute voltage stability margin. The aforementioned techniques require comparatively large computations and are not time efficient for on-line applications. The ability of synchrophasor measurements to capture the fast power system dynamics makes the voltage stability monitoring of the power system more accurate and fast.

A Genetic Algorithm based Support Vector Machine (GA-SVM) approach for online monitoring of long-term voltage instability has been proposed in this work. To improve the accuracy and minimize the training time of SVM, the optimal values of SVM parameters are obtained using genetic algorithm. The proposed approach uses the voltage magnitude and phase angle obtained from PMUs as the input vectors to SVM and the output vector is the Voltage Stability Margin Index (VSMI). Total Vector Error (TVE) in

PMU measurement may be maximum of 1% which may include some uncertainty in phasor measurement. Thus, the impact of these uncertainties in synchrophasor measurements is also analyzed to detect the deviation of VSMI at the operating point. The results of the proposed GA-SVM approach for voltage stability monitoring are compared with Grid Search SVM (GS-SVM) and Artificial Neural Networks (ANN) based approach with same data set to prove its superiority.

Flexible Alternating Current Transmission Systems (FACTS) devices are usually used for the dynamic control of voltage, impedance, and phase angle of high-voltage ac lines. FACTS devices provide strategic benefits for improved transmission system power flow management through better utilization of existing transmission assets, increased transmission system security and reliability. The STATCOM plays an important role in reactive power compensation and voltage control because of its operating characteristics, which have been well studied in the past years. In the literature, various control methods have been proposed for STATCOM control. In most of the work, the control logic is implemented with the Proportional Integral (PI) controllers. The PI controller gives only a control point not the range of control. This is due to the integer nature of PI controller. Therefore, PI controller required to be tuned time to time.

For the dynamic operation of the STATCOM, Fractional order PI (FOPI) controller has been proposed in this work. FOPI controllers have been designed using the fractional calculus. These controllers have more degrees of freedom and provide a complete range of control. FOPI controllers have better capability of handling uncertainties and provide better stability. The voltage phasors and current phasors, which are assumed to be obtained from PMU have been transformed into their d-q components. Voltage and current components in d-q frame have been used as input to the FOPI controller. The simulation studies have been carried out in MATLAB version 2013a. The performance of FOPI controller has been compared with the Integer Order PI (IOPI) controller. Simulation results of FOPI controller obtained in MATLAB have also been validated in Real Time Digital Simulator (RTDS).

ACKNOWLEDGEMENT

I express my deepest sense of gratitude towards my supervisors Dr. Barjeev Tyagi, Associate Professor, Department of Electrical Engineering and Dr. Vishal Kumar, Assistant Professor, Department of Electrical Engineering of Indian Institute of Technology Roorkee, Roorkee, for their patience, inspiring guidance, constant encouragement, moral support, and keen interest in minute details of the work.

My deepest gratitude and sincere thanks to Dr. Vinay Pant, Assistant Professor, Department of Electrical Engineering, Indian Institute of Technology Roorkee, Roorkee without whose encouragement and support my Ph.D would not have been possible. I am thankful to Dr. G. N. Pillai, Chairmen DRC, Department of Electrical Engineering, Indian Institute of Technology Roorkee, Roorkee and Prof. S. P. Srivastava, Professor and Head, Department of Electrical Engineering, Indian Institute of Technology Roorkee, Roorkee for their invaluable direction, encouragement and support, and above all the noblest treatment extended by them during the course of my studies at IIT Roorkee. I am also grateful to the Ministry of Human Resources and Development, Government of India, AICTE, New Delhi for sponsoring me for doctoral research work.

I extend my sincere thanks to all research scholars especially to Dr. Devender Saini, Dr. Himanshu Chaudhary, Dr. Deep Gupta, Dr. Neeraj Gupta, Mr Pushkar Tripathi, Mr. Ashok Manori, Mr. Anubhav Agrawal, Mr. Shailendra Bhaskar, Mr. Nagendra Gautam, for sharing and supporting me during my research work. I am also thankful to Mr. Akhilesh Mishra for their help and involvement in my research work. I am extremely thankful to Dr. Satish, Mrs Sonal Jain, and Mrs Pallavi Verma for supporting me during my research work.

I am also very grateful to my B.Tech & M.Tech group for their help and co-operation during my study. I owe a debt of gratitude to my parents, my sister, and family members for their consistent encouragement, moral support, patience and care. Last but not the least; I am thankful to the almighty who gave me the strength and health for completing the work.

(K S Sajan)

CONTENTS

LIST OF FIGURES

LIST OF TABLES

ABBREVIATIONS AND SYMBOLS

The abbreviations used in the text have been defined at appropriate places, however, for easy reference, the list of abbreviations are given below.

Abbreviations	**Stands for**
ANN	Artificial Neural Network
BCC	Bus Connectivity Criteria
CLOC	Critical Load bus Observability criteria
CPF	Continuation Power Flow
et al.	and others
etc	et cetera
FACTS	Flexible AC Transmission System
FOPI	Fractional Order Proportional Integral
GA	Genetic Algorithm
GOC	Generator Observability Criteria
GPS	Global Positioning System
i.e	that is to say
ICT	Information Communication Technology
IEEE	Institute of Electrical and Electronics Engineers
ILP	Integer Linear Programming
IOPI	Integer Order Proportional Integral
KCL	Kirchhoff's Current Law
KVL	Kirchhoff's Voltage Law
NLOC	Noncritical Load bus Observability criteria
OPP	Optimal Placement of PMU
p.u.	Per Unit
PDC	PMUs Distribution Criteria
PMU	Phasor Measurement Unit

RAHP	Revised Analytical Hierarchy Process
RMS	Root Mean Square
RTDS	Real Time Digital Simulator
RTU	Remote Terminal Units
SCADA	Supervisory Control and Data Acquisition
SE	State Estimation
SVM	Support Vector Machine
TOC	Tie Line Observability Criteria
VSMI	Voltage Stability Monitoring Index
WAMS	Wide Area Monitoring System
WLS	Weighted Least Square

Chapter 1: Introduction

1.1 Overview

Initially generation, transmission, and distribution of electric power were restricted to comparatively small geographical areas but today these power systems are widely spread and form large interconnected systems. This leads to complexity, and disturbance or fault in one part of the system may adversely influence the performance of the whole system. These complexities are also due to the introduction of new generation technologies in the form of distributed generators and renewable energy resources. Transmission networks in many countries around the globe are being crushed between two conflicts. On the one side, there is continuous increase in the demand for electricity, the privatization and the deregulation of the electricity markets and the economic pressures are forcing transmission and grid operators to maximize the use of transmission assets. On the other side, there is rising concerns about the reliability of supply. The above mentioned conflicts can be overcome either by strengthening the existing networks by building more transmission lines and expansion of the infrastructure or by maximizing the use of the existing networks by using more efficient controllers. However, taking into account the cost, time and environmental related issues, it seems that the first course of action is not the suitable solution to these challenges. Therefore, utilities are more focused on the dynamic monitoring and control of power system to face these chalenges. The Supervisory Control and Data Acquisition (SCADA) system has been employed to provide steady state monitoring of the electrical power systems, however SCADA system are not capable to sense dynamic changes in the network and are unable to avoid severe blackouts. This has encouraged the development of the synchrophasor technology, and paved its way to the emerging form of Wide Area Monitoring System (WAMS). The WAMS is a combination of power system, synchronized measurement, protection and control using Information, Communication Technology (ICT).

SCADA system consists of Remote Terminal Units (RTUs) which are only capable of procuring Root Mean Square (RMS) values of voltages and currents, and not capable of providing the corresponding phase angles. The phase angle provides important information about the current state of the power system. The WAMS with synchrophasor technology can provide phasor values of voltages and currents measurements. The Phasor Measurement Unit (PMU) is the main technology enabler of WAMS [1]. PMUs are geographically dispersed in

the power system networks and can provide the phasor measurements. The measurements include both the magnitude and the phase angles of the bus voltage and branch current signals, and synchronization in PMU is achieved through timing signals from the common referenced clock of Global Positioning System (GPS) with an accuracy of 1 microsecond. The PMU based applications, analysis, monitoring, and control with exact time synchronization is making the centralized monitoring and control a reality.

In WAMS, optimal placement of PMUs is a prerequisite for the complete observability of the power system as deployment of PMUs required high capital investment. Further, the measurements obtained from these devises are benefited in various stability and control applications. Recently, it is recognized that PMU measurements can be used to enhance the voltage stability analysis. These measurements can assist in real time identification of various causes, which lead to voltage instability as well as these can also help in scheming various protective and control scheme for voltage instabilities. This thesis explores various issues related to PMU Placement and their application in the field of voltage stability monitoring and control.

1.2 PMU based WAMS Implementation

1.2.1 WAMS Architecture

The WAMS includes mainly four components: (1) Phasor measurement Unit (PMU) (2) Phasor Data Concentrator (PDC) (3) Application and Data processing (4) Communication Network to integrate all these components. The general layout of the WAMS architecture is shown in Figure 1-1. The components perform unique and distinguished function in the form of four layers of WAMS architecture, the first layer consist of data acquisition layer which collects the sampled data of analog phasors from the PMUs located at substation interfacing with the electrical system. The second layer consist the communication network, which integrate the components placed in substations to the control room to transfer real time data. The third layer consists of PDC with data management layer where the synchronized data from PMUs are collected and sorted in the form of single time-aligned data set and the fourth layer consists of data services and application layer where all the time-aligned data are utilized to execute protection and restoration controls. In next subsection, the detailed description of synchrophasor measurement is given to explain the importance of these measurements in WAMS implementation.

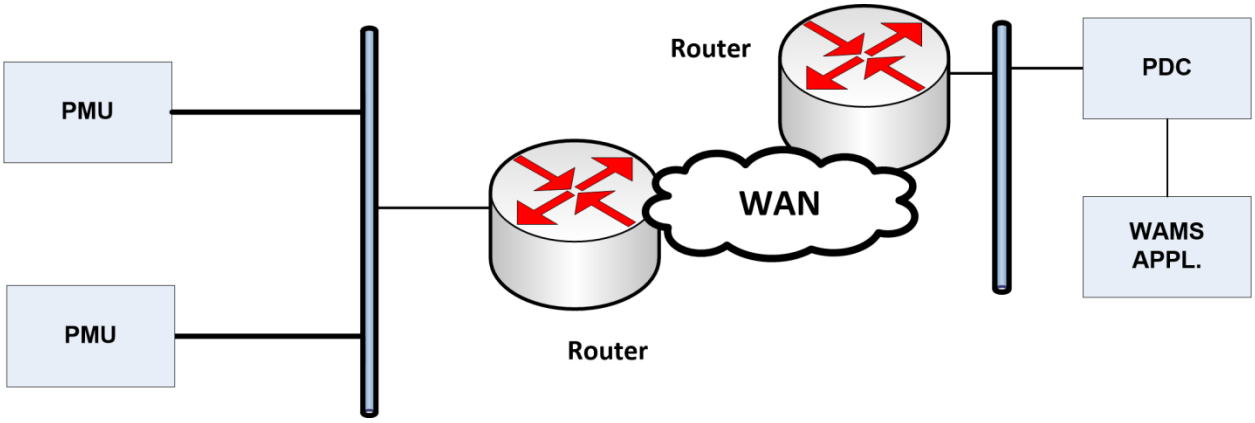

Figure 1-1: Architecture of Wide Area Monitoring System

1.2.2 Synchrophasor measurements

Synchrophasor is defined as the complex representation of voltage or current phasor. These phasors contains a time-tag defining the time instant at which the sample is being recorded. The sampling instant in the data window must be able to be correlated with the absolute time provided by GPS clock. A sinusoidal signal, $x(t)$ of a known frequency f, with magnitude X_m and angular position ϕ with respect to time reference 't' is given by;

$$x(t) = X_m \cos\{2\pi ft + \phi\} \tag{1.1}$$

The phasor representation of a signal $x(t)$ is given by

$$\bar{X} = (X_m / \sqrt{2})e^{j\phi} \tag{1.2}$$

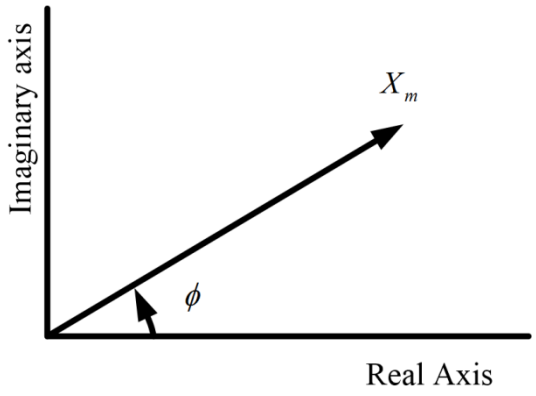

Figure 1-2: Phasor Representation of signal $x(t)$

The phasor representation of signal $x(t)$ is illustrated in Figure 1-2. Typically, the PMUs installed at various buses of the power system measure the data and send these data in real time

to PDC. Many PDCs belonging to different utilities are connected to a common central or super PDC, which provide an interconnection-wide snapshot of the power system [2]. The high data rate and low latency associated with phasor measurement provide the desired ability to respond to abnormal conditions.

The IEEE C37.118 [3] specifies the standards for synchronization of data sampling, data to phasor conversions, formats for timing input and phasor data output. This standard also adds the dynamic phasor measurement and frequency measurement requirements and specifies the suitable communication protocol for real-time communication between PMU, PDC and other application.

1.2.3 Phasor Measurement Units (PMUs)

According to North American Synchro Phasor Initiative (NASPI), PMU is "a device that provides, as a minimum, synchro phasor measurement for one or more phases of an AC voltage and /or current waveform. The synchro-phasor can be single phase or symmetrical component values." PMUs measure the positive sequence voltage phasor and positive sequence current phasor at a measurement rate of 60 measurements per second. Therefore, this feature makes PMU a suitable device to obtain power system dynamics. Figure 1-3 shows the generic PMU structure describing its principal components.

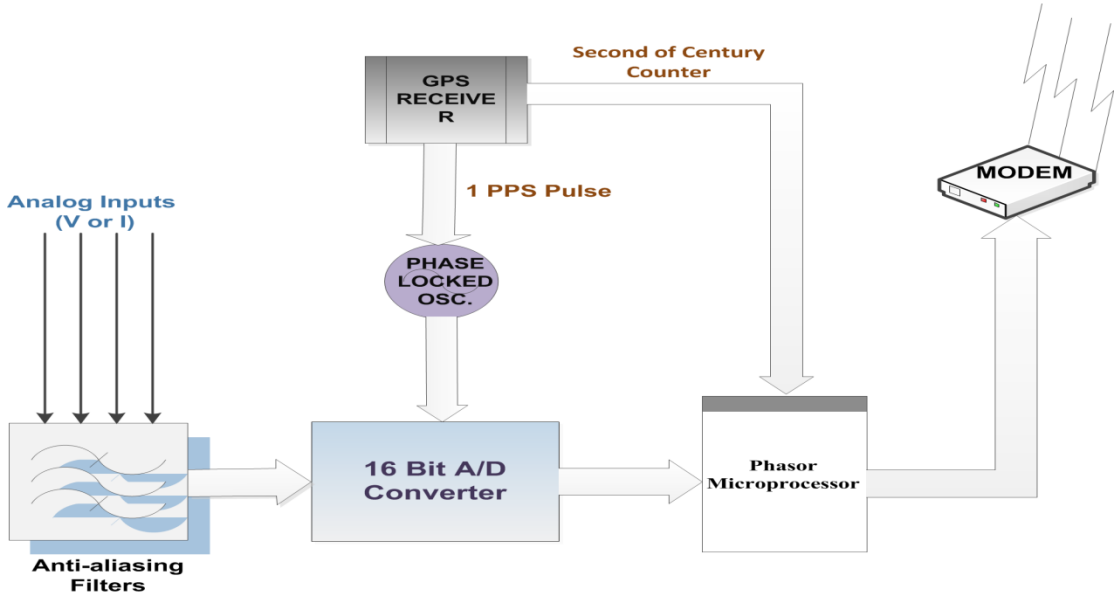

Figure 1-3: Generic Phasor Measurement Unit (PMU)

In Figure 1-3, phase-locked oscillator, anti-aliasing filters, analog to digital converter and phasor microprocessor are the different components in PMU used for phasor computation. The

analog signals i.e. voltage and current measurements obtained from secondary side of potential transformers and current transformers are fed to PMUs as analog inputs. These analog inputs are pre-processed by anti-aliasing filter to remove alias of the reconstructed signals. The analog to digital converter samples the pre-processed analog data according to Nyquist criterion. The phase-locked oscillator along with a GPS signal as reference source provides high-speed synchronized sampling with accuracy up to 1 microsecond. This GPS signal is also used to give a time stamp using coordinated universal time as the reference for each measurement. The internal GPS receiver-clock synchronizes the sampling process to guarantee that the data is sampled at the same instant by all the PMUs installed at different buses in the power system. Microprocessor based phasor estimator further processes these time-synchronized samples. Estimated phasors are time tagged with the synchronizing signal. Finally, this time tagged phasors are transferred over the communication links through suitable modems to a higher level in the measurement system hierarchy using IEEEC37.118 data format.

According to IEEE standards, Total Vector Error (TVE) is used to define the accuracy of phasor measurements. The IEEE C37.118 standard [3] states that TVE in PMU should be less than 1%, which corresponds to the phase error of 0.01 radian or 0.57degrees. Other few desired specifications of PMU are:

- Time Tagging of PMUs should have accuracy of 50 micro second
- Phase angle calculation should have accuracy of 1 degree
- Synchronizing source should have accuracy of 1 micro second
- Analog to digital converter should have resolution of 16 bit or more.

The various applications of the phasor data obtained from various PMUs in WAMS are state estimation, power system stability monitoring, Flexible AC Transmission System (FACTS) set-point optimization using feedback control, real-time congestion management, real-time power system control etc. At present, power systems, are still not having large deployment of PMUs in the network. However, in near future looking at the growing popularity of the WAMS, it is likely to have at least a minimum set of optimally placed PMUs in the networks, which will be able to completely observe the power systems with only the phasor measurements.

1.3 Literature Review

In last two decades, synchronized phasor technology has gained a lot of research interest in power system applications. The utilization of the synchronized phasor based application mainly focuses on the following three main areas.

1) Wide area monitoring applications
2) Wide area control applications
3) Wide area protection applications

This thesis is primarily focused on the comprehensive study on first two applications *viz.* the wide-area monitoring and control application. It is specifically focused on the optimal PMUs deployment techniques, followed by using the synchronized phasor measurement obtained from these PMUs for the improvement of wide-area state estimation, wide-area voltage monitoring and wide-area voltage control. A literature review is presented below discussing some of the major techniques used for optimal placement of PMUs and monitoring and voltage control of power system using synchrophasor measurements.

1.3.1 Review on Optimal PMU Placement techniques

Deployment of PMUs is the backbone of WAMS. PMU placement helps in monitoring the dynamics of large interconnected power system. PMUs are capable of measuring the voltage phasor of the bus on which it is installed and the current phasor of all the lines connected to that bus. It is not practical and economical to install PMU at each bus location due to the high cost factor, which includes associated communication equipment and the cost of the installation. Reduction of number of PMU installed also helps in reducing the size of data received from installed PMUs for further analysis. In literature, work has been carried out for PMU placement on the basis of some specific applications such as state estimation [4]–[6], voltage stability [7], and fault location in the network [8].

Apart from the PMU placement based on specific application, significant research has been done for Optimal Placement of PMU (OPP) in the literature to ensure the complete observability of the large interconnected power system. The initial works have been carried out by Phadke et. al [1], [9] on the PMU placement ensuring system observability. This work has later been extended for optimally locating the PMUs with the assumption that each PMU provides voltage at its associated bus and the current phasors of all the incident branches. It has

been, therefore, possible to fully monitor the system by using relatively much small number of PMUs as compared to the number of buses in the system. This problem has been formulated and solved by using a graph theoretic based observability analysis and an optimization method based on simulated annealing [10]. L. Mili et al. in [11] presented a new approach for OPP problem has been presented and then using the PMUs data for calculating states of the system for voltage stability monitoring. B. Milosevic et al. in [12] presented a new approach for PMU placement using Genetic Algorithm. The OPP problem has been formulated with simultaneous optimization of two contradictory objectives viz. minimization of the number of PMUs and maximization of the measurement redundancy. The two objectives are contradictory in nature because the progress of one of the objective function leads to the depreciation of the other objective function. Thus, instead of a unique optimal solution, there exists a trade-off between the competing objectives. In this work, the authors have not considered the possible loss or failure of PMUs in the problem formulation.

S. Chakrabarti et al. [13], explains the OPP problem for the complete observability of a power system under both normal operating conditions and single branch outages. A binary search algorithm is used to find the optimal number of PMUs needed to make the system completely observable. In case, if the problem has more than one solutions, then the authors have also proposed a strategy to select the solution that results in maximum measurement redundancy. S. Chakrabarti et al. in another reference [14], developed an integer quadratic approach for OPP problem. In the category of multi-objectives, a Binary Particle Swarm Optimization (BPSO) based methodology has also been proposed for solving the OPP in [15]. In [16], authors has proposed a approach for OPP problem using multi-objective biogeography based optimization technique. This approach has achieved dual objectives i.e., minimization of the number of PMUs required for making the system fully observable, and maximization of the measurement redundancy. However, presence of conventional measurements and depth of observability has not been considered.

Abur et al. in [17] presented a novel approach for optimal PMU placement problem. In this formulation, the authors have considered conventional power flow and power injection measurements in addition to PMUs. Solution for this optimization problem is obtained through integer programming approach. It also established that by considering conventional measurements, the number of PMUs can further be reduced. However, the formulated optimization problem for OPP becomes non-linear.

In [18], B. Gou proposed an Integer Linear Programming (ILP) problem formulation for the OPP considering both with and without conventional measurements. In [19], the problem formulation has been expanded for the incomplete observability i.e. depth-one unobservability and depth–two unobservability cases, with and without conventional measurements.

In view of observability along with voltage phasor measurement, the PMUs should have sufficient number of channels to measure all the current phasors of the line connected to that bus, to make the neighboring buses observable. Therefore, the number of channels is a critical factor in the OPP formulation. In [20], the authors have revised the OPP formulation to illustrate the impact of having limited number of channels on the location and number of PMUs required to make the system observable. Literature reveals that mostly the OPP formulations are carried out for the complete topological observability[10], [18], [19]. R. Sodhi et al. [21] considered both for the complete topological observability and the numerical observability in the reported PMU placement algorithm. R.F. Nuqui et al. [22] addressed the physical and financial constraints in the PMU installation process. This compels utilities to place the limited number of PMUs in the system. As a solution, phase-wise/stage-wise solution was proposed which utilizes the concept of depth of observability to place PMUs in stages/phases.

In 2008, D. Dua et.al. proposed an enumeration of trees for finding OPP and simulated annealing (SA) formulation for solving pragmatic based phased installation. However this requires more number of PMUs than single-phased installation [23]. R. Sodhi et al. [24] proposed a multi-phased PMU placement technique using multi criteria decision making approach considering various criteria like bus, tie line, and voltage observability. The authors utilized ILP problem for OPP and Analytical Hierarchy Process (AHP) is used for phasing of PMUs. In reference [25], authors proposed a scheme for PMUs placement that ensures the monitoring and protection of critical buses of the system while moving towards the complete observability of the network. C. Sharma et. al. [26] proposed a multistage PMU placement problem by incorporating critical buses based on small signal stability.

The PMU deployment in the power system is the first step towards developing synchrophasor-assisted state estimators. These estimators utilize the conventional SCADA measurements along with the PMU measurements. This type of state estimator has also been termed as hybrid state estimators. In literature, many alternatives have been proposed to combine the SCADA and the PMU measurements, as discussed in the following subsection.

1.3.2 Review on Phasor Assisted State Estimation

In 1970, Schweppe et al. was the first to introduce the concept of State Estimation (SE) [27]–[29]. This algorithm plays a key role in the monitoring and control of power system. The inclusion of the phasor measurements obtained from the PMUs in the power system SE is a research area, which received a lot of attention in the recent past. A number of algorithms have been developed for the refinement of parameter estimation and the bad data detection in SE with the inclusion of phasor measurements. Literature survey reveals that the SE using PMU data can be classified into two complementary approaches. In first approach, the SE is carried out with only PMU measurements. This approach requires large number of PMU deployment, but provides much faster and accurate SE solution [9], [30]. In second approach, the SE has been performed by including phasor measurements obtained from PMUs along with the conventional SCADA measurement set [31]–[38].

In [9], Phadke et al. proposed a linear state estimator where static SE is done using phasor measurements. In the linear SE, synchronized positive sequence voltage and current phasors received from PMUs have been linearly expressed in terms of the system states thus eliminating the iterative calculation needed in traditional SE. In this approach, SE problem is reduced to state calculation. However, the linear SE can only be applied if there are sufficient number of PMUs installed in power system grid, which make the system completely observable [10]. At present, the PMUs are expensive and the utilities like to install these devices in stages. Therefore, research has been carried out to develop a SE technique, which can utilize both the PMU measurements and the conventional SCADA measurements.

A multi-area state estimator has been suggested for the large scale power system SE [33]. In the proposed method, each area has its own state estimator that processes measurements for its own area and estimates the states. This estimated data from each area is send to a central coordinator along with the phasor measurements from their boundaries, and finally central coordinator finds the system-wide solution. This method has assumption that the neighboring subsystems affect only the boundary buses.

Zhou et al [31] has proposed an alternative method to use phasor measurements in post processing step of the traditional weighted least square (WLS) method by keeping the existing SE method unchanged. A hybrid non-linear state estimator has been proposed in [39], where the voltage phasor measurements have been transformed into indirect equivalent branch current measurements and use these measurements along with the SCADA measurements in WLS

method. In [40], a new mixed measurement state estimator has been developed. In this approach, the PMU measurements i.e. bus voltage and branch current phasor measurements, and equivalent current phasor measurements obtained by transforming the power flow measurements of the branches obtained from SCADA system are used for SE. Similarly, Bi et al [34] proposed a hybrid SE method where the voltage phasor measurements and current phasor measurements obtained from PMUs are included with the traditional measurements. In reference [41], authors have carried out a comparative study of some of these methods, which includes the branch current phasor measurements in a hybrid SE. All these methods have resulted in more accurate/reliable SE, but at the cost of considerable modifications in the existing SE model and the measurement set. Ranjana et al [37] proposed two different techniques to add the available PMU measurements to the existing SCADA measurements to increase the accuracy of the SE without altering the existing SE model.

One of the major issues in most of the state estimators is to identify the presence of bad data in the measurement set. The most frequently used technique for bad data detection is normalized measurement residual test where predefined measurement weights are used for calculation as discussed in [42]–[45]. Jun and Abur [46] presented a rectangular coordinate formulation which enables bad data processing for both the phasor and the conventional measurements. In [47], authors have proposed a projected Kalman filter approach for dynamic state estimator considering zero injection constraint. Guo et al [48] proposed a novel method for SE with accuracy evaluation of estimated value using a scalar index of correntropy. Thukaram et al. [49] proposed a linear programing approach for SE using upper bound optimization technique.

The phasor-assisted SE is one of the applications of the synchrophasor measurements obtained from PMUs. Once the states are obtained for all the buses in the system with maximum accuracy, the next step is to use these states for different power system applications. Another promising application, addressed in this thesis, is the synchrophasors based voltage stability monitoring and control. The following subsection provides an insight into some of the existing solutions for voltage stability monitoring and control, based on the synchrophasor measurements.

1.3.3 Review on voltage stability monitoring and control

In recent years, voltage collapse is a major cause for many power system blackouts around the globe [50]. This is because of the steadily growing loads that force the grid to operate closer to its limits. At the same time, the transmission networks are also not strengthen because of social

and economic constraints. The deregulation of electricity market increases the operating uncertainty. Facing these factors, operators are currently experiencing many unpredictable challenges in the electric power system operation.

Typically, voltage instability is the proof of system low voltage profile, high reactive power losses, and insufficient reactive power support to heavily loaded power systems. Generally, voltage collapse occurs suddenly after a symptomatic period which may last for few seconds to several minutes [51]. The beginning of the voltage collapse is often caused by single or multiple contingencies. The traditional method for voltage stability analysis relied on static analysis using the conventional power flow methods such as Gauss-Seidel or Newton-Raphson. In reference [52]–[56], numerous voltage stability indexes based upon conventional power flow methods have been proposed. The main drawback of these techniques is the singularity of the Jacobian matrix at the maximum loading point. To overcome this problem, Continuation Power Flow (CPF) method is used to compute voltage stability margin [57]. In reference [58], P-Q-V curve technique is proposed for voltage stability margin assessment which demonstrates the maximum limits of power demand and its corresponding voltage magnitude. The aforementioned techniques require comparatively large computations and are not efficient for wide area on-line applications. Since voltage instability is a system-wide phenomenon, and knowledge of local conditions alone is not enough to describe this instability, therefore it requires complementary use of dynamic and static analysis techniques. WAMS opens up new opportunities for the application of system-wide phasor measurements in monitoring the voltage stability. This is mainly because of the time synchronization of the phasor measurements and their high refreshing rate, which provides a wide area dynamic picture of the system state.

The voltage stability monitoring approaches and the following preventive/corrective solutions against the voltage instability are suggested at local busbar level or at centralized level. The literature review reveals that the increase in the utilization of synchrophasor measurements has widened the scope of improvement in the assessment techniques at both the levels i.e. at the local as well as at the control center levels [59][60] .

In [61], the authors proposed an algorithm for real-time prediction and mitigation of the voltage collapse problem using combinations of both the slow SCADA measurements and the fast synchrophasor measurements, so that the critical parts of the power system in the context of voltage security in real time operating environment can be pinpointed. In this work, the authors

have also suggested an optimal load-shedding scheme to make the system stable. In [62], authors have proposed an ant colony optimization algorithm for solving the optimal load shedding problem to enhance the voltage stability of the power system.

In [63]–[65], authors have proposed an real-time monitoring of voltage stability using synchronized phasor measurement obtained from PMUs. Y Gong et.al. [66], developed a synchronized phasor measurement based voltage stability index to determine the voltage stability margins for all system load buses in an informative format and identified the load bus that is the most vulnerable to voltage collapse. In order to apply this approach to a large power system, a method is developed to simplify the large network behind a load bus into an equivalent circuit. This circuit consists of a single source and a single transmission line obtained by using time-synchronized phasor measurements and network parameters. Reference [67] presents a novel approach for analyzing power system static voltage stability considering all possible active and reactive power controls based on the multi-input multi- output (MIMO) transfer function. In [68], the authors has proposed an approach for voltage stability analysis by visualizing the changes in topological structure of the system potential with respect to the change in power system loading. In [69], the author has proposed a voltage stability index to indicate the most venerable bus in the system. The key role of this index is to determine the voltage stability status (stable or unstable) of the system. In [70], the authors has proposed a new approach for detection of voltage instability and identification of critical buses in the system using PMU data. However, this method uses only the voltage magnitude not the voltage vector and requires the information of the network topology as well as the status of the generators.

In recent years, the machine learning techniques such as artificial neural network (ANN), fuzzy logic, pattern recognition, Support Vector Machine (SVM) etc. have been used for power system analysis. Zhou et.al. [71], proposed a new online monitoring technique for voltage stability margin using synchrophasor measurements. Reference [72] introduces a method based on ANN model for on-line voltage security assessment. The proposed approach uses radial basis function (RBF) networks to estimate the voltage stability level of the system under contingency state. Hashemi et al. uses wavelet transformation for feature extraction of voltage profile along with RBF network to estimate the voltage stability margin [73].

In the last decade, the advancement in power-semiconductor devices have led to the development of the static compensator. STATCOM operation is based on Gate TurnOff (GTO)

thyristors, and has been used for reactive power control for improvement of power system stability [74]. The main objective of a STATCOM is to regulate the voltage at the Point of Common Coupling (PCC) by dynamically absorbing or delivering reactive power from or to the transmission network respectively. In literature, most of the proposed schemes involve traditional linear control techniques in which the nonlinear models of STATCOMs are linearized around a specific operating point [75]–[82]. In [75], authors have proposed two different types of inverters and their control schemes for the dynamic operation of STATCOM. In this work, the results are illustrated with the measured waveforms obtained from a scaled analogue model of an 80 MVAR STATCOM. Lehn et. al. in [76], have proposed a new approach for the dynamic control of FACTS devices such as STATCOM and UPFC, which utilize voltage source inverters (VSI) as the main building block. P. Rao et. al. in [77], proposed a STATCOM with linear optimal control, based on LQR controller, for power system voltage control application. In [80], the authors have presented a space vector modulation based switching strategy for STATCOM. The main feature of the proposed switching strategy is that it enables balancing voltages of the dc capacitors, without the requirement of additional controls or auxiliary devices. El-Moursi et. al. in [82] investigates the dynamic operation of novel control scheme for both STATCOM and Static Synchronous Series Compensator (SSSC). The scheme is based on a new model comprising of a 48-pulse GTO thyristor voltage source converter for combined reactive power compensation and voltage stabilization of the electric grid network. However, most of the techniques discussed in the literature uses integer order PI controller that experiences certain drawback, especially in case of uncertainty in system parameters. The PI controller gives only a control point not the range of control. Therefore, there is still a lot of scope for improvement in the design of controller.

1.4 Motivation and Objectives

The primary requirement of large interconnected power system is to provide a highly reliable and uninterrupted power supply. This requires the real-time information of the system. PMUs are the key elements in synchrophasor technology based WAMS. In different parts of the world, PMUs are progressively being installed. The objective of these PMU deployments is to develop new dynamic, robust, and advance metering system to have more "situational awareness". This will help utilities to take necessary real-time protection and control action to avoid emergent and severe shutdowns. PMU deployment requires high capital investment, which confirms the need of developing an OPP scheme that will help in determining optimal number and the corresponding locations in order to attain system observability.

Many techniques for OPP have been reported in the literature, such as integer programming, depth-first search, spanning tree-based method etc. Intelligent techniques like nondominated genetic algorithm, Tabu search, simulated annealing, particle swarm optimization etc. have also been reported. Different OPP methods discussed so far provide only the optimal bus locations in power system where PMUs have to be placed. The branch current phasor measured by a PMU is used for calculating the voltage phasor of the bus at other end of the line with the help of KVL. In order to measure the line current phasors, the scheme requires as many numbers of auxiliary equipment to connect current transformer and PMU as the number of lines connected to the bus. This increases the overall installation cost. However, measuring the current phasor of all the connected lines is not essential because, the bus connected to the line may be observed by other PMUs in the same power system. Therefore, number of current phasors can be reduced which in turn reduces the number of auxiliary equipment. It reduces the overall installation cost.

In a large power system, there will be a large quantum of PMUs to be deployed for the complete observability and will entail high capital cost in their installation. Therefore, it is essential to formulate a staging program for PMU installation in a phased manner and effectively utilize the PMU measurements even during the installation process in power system network. Some of the authors have considered phased placement with additional benefits in terms of generator bus and tie line observability. However, these approaches do not considered the problem of phased PMU placement based on power system voltage stability monitoring and control.

As the synchrophasor measurements from PMUs become available, by placing them in multiple phases, it is useful to integrate the conventional SCADA measurements and the phasor measurements to improve the accuracy of the SE. Therefore, developing a hybrid state estimator that includes both conventional and phasor measurements is an alternative to get better results. Several hybrid SE approaches have been suggested in the literature, such as multi-area SE, distributed hybrid SE and quadratic hybrid SE. Most of the proposed hybrid SE methods result in an increased accuracy of the state estimation. In practice, a SE model is of concern, which can integrate the phased PMUs measurements in the SE model, keeping the existing SE model unchanged.

In recent years, voltage collapse is a major cause for many power system blackouts around the globe. In literature, numerous voltage stability indexes based on conventional SCADA

measurements have been proposed. Since the data scan rate of these measurements are of the order of several seconds, therefore require comparatively large computation time and are not efficient for on-line applications. In the other hand, PMUs provides time-synchronized phasor measurements from dispersed locations. These measurements are capable of providing a snapshot of the system dynamics, which opens up new promising ways for voltage stability monitoring in an accurate and fast manner. Therefore, the ability of synchrophasor measurements for the voltage stability monitoring of the power system is still of research interest.

Many voltage stability control scheme have suggested in literature, which utilizes STATCOM for enhancing voltage stability limits. In the literature, various control methods have been proposed for STATCOM control. In most of the work, the control logic is implemented with the Proportional Integral (PI) controllers. The PI controller gives only a control point, not the range of control. This is due to the integer nature of PI controller. Therefore, PI controller required to be tuned time to time.

Considering previously mentioned technical challenges for PMU placement for monitoring and control of voltage stability, the main objectives behind the research work carried out in this thesis are summarized below:

- To develop a new approach for the optimal placement of PMUs with optimal number of current phasor measurements for the complete and the incomplete observability of the power system with N-1 contingency.
- To develop an algorithm for multi-phase PMU placement, using RAHP based on voltage stability monitoring, that ensures the complete power system observability even under a branch outage or a PMU failure.
- To develop hybrid state estimators, utilizing the available phasor measurements along with the conventional SCADA measurements to increase the estimation accuracy.
- To develop an approach for online monitoring of long-term voltage instability condition in the power system with the use of Genetic Algorithm based Support Vector Machine (GA-SVM).
- To develop a control scheme for the dynamic operation of STATCOM based on Fractional Order Proportional Integral (FOPI) controller, which receives system state measurements from optimally placed PMUs.

1.5 Thesis Organization

The work carried out in this thesis has been organized in seven chapters. The current chapter demonstrates the fundamentals of the synchrophasor technology based WAMS and its applications. Further, it presents the literature review on the problem areas and gives the motivation behind the presented work. Finally, it outlines the organization of the thesis.

In Chapter 2 a new approach has been proposed for the optimal placement of PMUs with optimal number of current phasors measurements considering different cases. In first case, the OPP formulation has been carried out for the complete observability. In second case, the OPP problem has been formulated for the incomplete observability with Depth-of-One unobservability and Depth-of-Two unobservability. In another case, the OPP problem has been formulated that ensures the complete power system observability even under a branch outage or a PMU failure considering channel limit. The proposed method has been illustrated on four test systems viz. IEEE 14-bus system, IEEE 30-bus system, IEEE 57-bus system and Northern Region Power Grid (NRPG) 246-bus Indian system.

In Chapter 3 an algorithm has been developed for multi-phase PMU placement, using RAHP based on voltage stability monitoring that ensures the complete power system observability even under a branch outage or a PMU failure. In this approach, the optimal number and locations of PMUs that ensures complete power system observability with N-1 contingency considering channel limit (as in chapter 2) have been identified. These PMUs are placed in phased manner due to their high installation cost. The RAHP is used for decision-making to prioritize these PMU locations in terms of phases. The indices which have been used to achieve this objective are Critical Load bus Observability criteria (CLOC), Noncritical Load bus Observability Criteria (NLOC), Generator Observability Criteria (GOC), PMUs Distribution Criteria (PDC), Tie Line Observability Criteria (TOC), and Bus Connectivity Criteria (BCC). The proposed methodology has been applied on IEEE 30-bus system and the Northern Regional Power Grid (NRPG) 246-bus system.

In Chapter 4 hybrid state estimator has been developed, utilizing the available phasor measurements along with the conventional SCADA measurements to improve the estimation accuracy. The inclusion of synchrophasors have been carried out in the same phased manner as in chapter 3 to enhance the accuracy of conventional WLS-based SE. The bad data detection in both the conventional measurements and the phasor measurements have been carried out using

the normalized residual test method. The effectiveness of the approach has been tested on IEEE-30 bus test system and the Indian Northern Region Power Grid (NRPG) 246-bus Indian system.

In Chapter 5 an approach for online monitoring of long-term voltage instability condition in the power system has been developed with the use of GA-SVM. GA is used to optimize the SVM parameter such as RBF kernel, regularization parameter and insensitive loss function to improve the performance of SVM. The input features of GA-SVM are voltage magnitude and voltage phase angle, which are assumed to be obtained from PMU. Although the PMUs have high precision level, still there are possibilities that the signal processing may introduce some errors in phasor calculation. Thus, the impacts of these uncertainties in synchrophasor measurements have also been analyzed to detect the deviation of Voltage Stability Monitoring Index (VSMI) at the operating point. The effectiveness of the proposed approach has been tested on New England 39-bus test system and Northern Region Power Grid (NRPG) 246-bus real Indian system. The results obtained are compared with other models i.e. Grid Search based Support Vector Machine (GS-SVM) model and Multilayer Perceptron-back propagation neural network (MLP-BPNN)

In Chapter 6 a control scheme for the dynamic operation of STATCOM based on Fractional Order Proportional Integral (FOPI) controller has been developed. The controller receives system state measurements from optimally placed PMUs. GA has been used to obtain the optimal parameters of FOPI controller. The performance of FOPI controller has been evaluated by connecting a STATCOM of rating 15KV, 100 MVar to the 230-kV grid. The voltage phasors and current phasors, which are assumed to be obtained from PMU have been transformed into their d-q components which have been used as input to the FOPI controller. The designed control scheme for STATCOM has been tested on Real–Time Digital Simulator (RTDS). The simulation results of FOPI controller have been compared with integer order PI controllers.

Chapter 7 concludes the main findings of the work presented in this thesis and presents the suggestion for the future work.

Chapter 2: Optimal Placement of PMUs

2.1 Introduction

The power system observability is a necessary condition for state estimation and prerequisite for effective implementation of Wide Area Monitoring Protection and Control Systems (WAMPC). The Phasor Measurement Unit (PMU) is the main technology enabler of WAMPC [1]. It is not practical and economical to install PMUs at each bus location due to the following reasons: (1) high cost factor, which includes associated communication equipment and the cost of the installation. (2) Reduction of number of PMU installation also helps in reducing the size of data received from installed PMUs for further analysis. The real-time measurements received from PMUs are used for different power system applications such as state estimation, transient and dynamic stability analysis, voltage stability monitoring [9], [35], [83], [84].

Since the voltage and current phasors are measured, the state estimation equations become linear and it is easier to find the solution than the nonlinear system state estimation [4]. In view of observability, the PMUs should have a sufficient number of channels to measure the voltage phasor and all the line current phasors connected to that bus, making the neighboring buses observable. Therefore, the number of channels is a critical factor in optimal placement of PMUs (OPP) problem [20]. In [45] the author has proposed a strategic PMU placement algorithm to improve the bad data processing capability of state estimation. The problem of PMU placement becomes an important issue in the power system state estimation as this device is increasingly being used for state estimation. Several OPP algorithms using different techniques have been proposed by different researchers across the world. An algorithm, which finds the minimal set of PMUs placement needed for power system state estimation, has been developed in [22] and [10]. In this paper, the graph theory and the simulated annealing method has been used to achieve the goal. In[82] the author has proposed a new integer linear programming based algorithm with and without conventional measurements, which is computationally effective. In [19], the author proposed a generalized approach for integer programming based method for OPP problem for the complete and the incomplete observability with and without considering conventional measurements. Similarly there are number of PMU placement algorithms proposed by different researchers across the world using non-dominated Genetic Algorithm (GA) [12], particle swarm optimization [85] etc.

Different OPP methods discussed so far provides only the optimal bus locations in power system where PMUs has to be placed. A branch current phasor measured by a PMU is used for calculating the voltage phasor of the other end bus using Kirchhoff's Voltage Law (KVL). In this approach the number of auxiliary equipments (i.e. current transformers, relays, circuit breakers etc.) required to measure the line currents are equal to the number of lines connected to the buses. This increase the overall installation cost. However, measuring the current phasor of all the connected lines is not essentially required because; the bus connected to the line may be observed by another PMU in the same power system. Hence, number of current phasors need to be measured by a PMUs can be reduced. This reduces the number of auxiliary equipment required for branch current phasor measurement and hence, reduces the overall installation cost.

In this chapter, a new approach for the OPP problem with optimal number of current phasors measurements for different cases has been proposed. In first case, the OPP formulation is done for complete observability without considering channel limit and N-1 contingency. In second case, the OPP formulation is done for incomplete observability with Depth-of-One unobservability and Depth-of-Two unobservability. In another case, the OPP problem is formulated that ensures complete power system observability even under a branch outage or a PMU failure considering channel limit. The ultimate goal is to find the minimum number of PMUs and their corresponding locations with optimal current phasor measurements so that the state estimation could be performed with measured phasor data at the lowest possible cost. For assessment of network observability, topological approach has been considered. The problem is formulated as a Binary Integer Linear Programming (BILP) problem. GA is used to solve BILP problem for deriving the optimal configuration.

The above problem is solved in two steps. The first step finds the optimal locations of PMUs using GA for each case. Second step utilizes the results of the first step to obtain the optimal set of branch current phasor measurement for each case.

2.2 PMU placement for complete observability analysis

Unlike traditional meters, the ability of PMU is to measure the voltage phasor of a bus at which it is placed and the current phasors of all lines connected to that bus. That means PMU can make the installed bus and its neighboring buses observable. The objective of placing PMUs is to determine a minimal set of PMUs such that the whole system becomes observable.

2.2.1 Optimal PMU Placement Problem

The optimal PMU placement problem for N bus system can be formulated as given below.

$$\begin{aligned} &Minimize \sum_{i=1}^{N} x_i \\ &such\,that \\ &\quad A_{PMU} X \geq b_{PMU} \\ &where,\ X = \left[x_1, x_2, \ldots\ldots, x_N\right]^T ; x_i \in \{0,1\}; i = 1,2,\ldots\ldots, N \\ &\quad b_{PMU} = [1,1,\ldots\ldots\ldots,1]_{N\times 1} \end{aligned} \tag{2.1}$$

where xi is a binary PMU placement variable whose entries are defined as:

$$x_i = \begin{cases} 1 & When\ PMU\ is\ installed\ at\ i^{th}\ bus \\ 0 & otherwise \end{cases} \tag{2.2}$$

The matrix A_{PMU} is bus connectivity matrix and the elements of this matrix are defined as follows:

$$a_{i,j} = \begin{cases} 1 & if\ i = j \\ 1 & if\ \ buses\ i\ and\ j\ are\ connected \\ 0 & otherwise \end{cases} \tag{2.3}$$

This is a BILP problem. The solution of this problem gives the optimal number and the location of PMU buses in the system considered. This problem is solved by using the GA in this chapter.

2.2.2 Determination of the Optimal Branch Current Phasor

PMUs can measure the current of all the lines connected to that bus. Let PMU is placed at bus *m* and this bus is connected to buses *p, q* and *r*. Current phasor of line *m- p* can observe (i.e. can determine voltage phasor) the p^{th} bus. Similarly *m-q* and *m-r* current phasors can observer the q^{th} and r^{th} buses.

Let us define a matrix B_{CO} whose rows correspond to the non-PMU buses in the system and the columns correspond to branches connected to the PMU buses. The entries of B_{CO} can be defined as.

$$B_{CO(i,j)} = \begin{cases} 1, if\ bus\ i\ is\ observed\ by\ branch\ current\ phasor\ of\ j^{th}\ line \\ 0, \qquad\qquad otherwise \end{cases} \tag{2.4}$$

Therefore, the optimal branch current phasor measurements problem is to find out the minimum set of branch current phasors such that a bus must be observed at least and at most by one branch current phasor and can be formulated as a BILP as given below.

$$\begin{aligned} & Minimize \sum_{j=1}^{NB} y_j \\ & such\ that \\ & \qquad B_{CO} Y = b \\ & where, \quad Y = \left[y_1, y_2, \ldots\ldots, y_{NB} \right]^T ; y_j \in \{0,1\}; j = 1,2,\ldots., NB \\ & \qquad b = \left[1,1, \ldots\ldots ,1 \right]^T_{(N-NP)} \end{aligned} \tag{2.5}$$

N is the number of buses, NP is the number of optimal PMUs, NB is the number of initial set of branch current phasor; and y_i is the branch current phasor variable.

Since there is no need of branch current phasors to observe the PMU buses as they are being already observed by PMU installed on them, the rows correspond to PMU buses can be removed from the matrix $\mathrm{B_{CO}}$. Hence, the size of matrix $\mathrm{B_{CO}}$ is $\left((\mathrm{N} - \mathrm{NP}) \times \mathrm{NB}\right)$ and the length of vector b is $(\mathrm{N} - \mathrm{NP})$.

The above formulation of BILP for complete observability has been explained using a seven bus system as shown in Figure 2-1. It is assumed that there are no conventional measurements in the system.

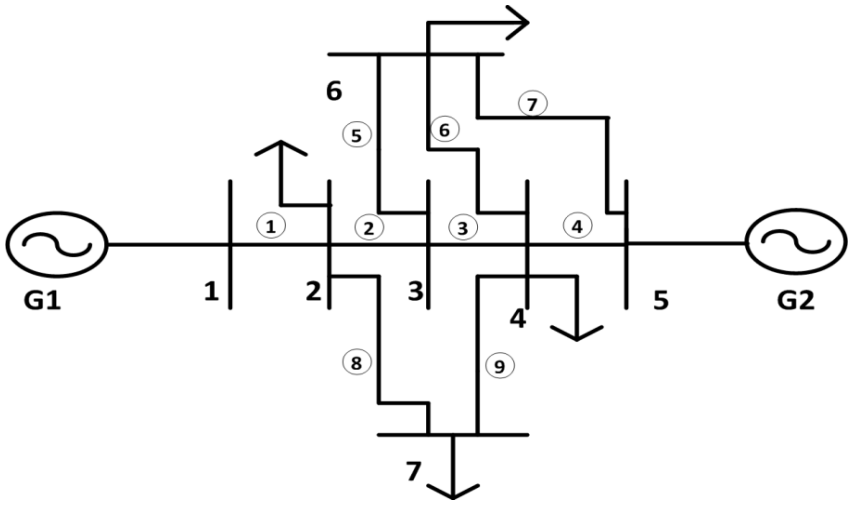

Figure 2-1: Single-line diagram of a 7-bus sample system

For the above system, A_{PMU} can be written as explained in (2.3)

$$A_{PMU} = \begin{bmatrix} 1 & 1 & 0 & 0 & 0 & 0 & 0 \\ 1 & 1 & 1 & 0 & 0 & 0 & 1 \\ 0 & 1 & 1 & 1 & 0 & 1 & 0 \\ 0 & 0 & 1 & 1 & 1 & 1 & 1 \\ 0 & 0 & 0 & 1 & 1 & 1 & 0 \\ 0 & 0 & 1 & 1 & 1 & 1 & 0 \\ 0 & 1 & 0 & 1 & 0 & 0 & 1 \end{bmatrix} \tag{2.6}$$

The optimal PMU placement problem given by (2.1) can be written as:

$$Minimize \sum_{i=1}^{7} x_i$$

$$such\,that$$

$$\begin{bmatrix} 1 & 1 & 0 & 0 & 0 & 0 & 0 \\ 1 & 1 & 1 & 0 & 0 & 0 & 1 \\ 0 & 1 & 1 & 1 & 0 & 1 & 0 \\ 0 & 0 & 1 & 1 & 1 & 1 & 1 \\ 0 & 0 & 0 & 1 & 1 & 1 & 0 \\ 0 & 0 & 1 & 1 & 1 & 1 & 0 \\ 0 & 1 & 0 & 1 & 0 & 0 & 1 \end{bmatrix} \begin{bmatrix} x_1 \\ x_2 \\ x_3 \\ x_4 \\ x_5 \\ x_6 \\ x_7 \end{bmatrix} \geq \begin{bmatrix} 1 \\ 1 \\ 1 \\ 1 \\ 1 \\ 1 \\ 1 \end{bmatrix} \tag{2.7}$$

This BILP problem is solved using GA. The optimal solution is $X = [0\ \ 1\ \ 0\ \ 1\ \ 0\ \ 0\ \ 0]^T$, which means PMUs are placed at buses 2 and 4. So the initial set of branch current phasors are 2-1, 2-3, 2-7, 4-3, 4-5, 4-6, and 4-7(total 7-phasors) representing the lines 1, 2, 8, 3, 4, 6 and 9 respectively as shown in Figure 2-1. In this system, 7 branch current phasors are obtained. Therefore, the matrix B_{CO} defined in Eq. (2.4) can be written as:

$$B_{CO} = \left[\begin{array}{c|ccccccc} lines \rightarrow & 1 & 2 & 8 & 3 & 4 & 6 & 9 \\ non-PMU\ bus \downarrow & & & & & & & \\ \hline 1 & 1 & 0 & 0 & 0 & 0 & 0 & 0 \\ 3 & 0 & 1 & 0 & 1 & 0 & 0 & 0 \\ 5 & 0 & 0 & 0 & 0 & 1 & 0 & 0 \\ 6 & 0 & 0 & 0 & 0 & 0 & 1 & 0 \\ 7 & 0 & 0 & 1 & 0 & 0 & 0 & 1 \end{array}\right] \tag{2.8}$$

The optimal branch current phasors problem for the seven bus system can be formulated as:

$$\begin{bmatrix} 1 & 0 & 0 & 0 & 0 & 0 & 0 \\ 0 & 1 & 0 & 1 & 0 & 0 & 0 \\ 0 & 0 & 0 & 0 & 1 & 0 & 0 \\ 0 & 0 & 0 & 0 & 0 & 1 & 0 \\ 0 & 0 & 1 & 0 & 0 & 0 & 1 \end{bmatrix} \begin{bmatrix} y_1 \\ y_2 \\ y_3 \\ y_4 \\ y_5 \\ y_6 \\ y_7 \end{bmatrix} = \begin{bmatrix} 1 \\ 1 \\ 1 \\ 1 \\ 1 \end{bmatrix} \tag{2.9}$$

This BILP problem can also be solved using GA. The optimal solution is $Y = [1\ \ 1\ \ 1\ \ 0\ \ 1\ \ 1\ \ 0]^T$. This means that the branch current phasors needed to be monitored are 2-1, 2-3, 2-7, 4-5 and 4-6 (total 5 branches).

2.3 PMU placement for incomplete observability analysis

Incomplete observability refers to the network condition in which number and location of the PMUs are insufficient to determine the complete set of bus voltage phasors. A detailed discussion on incomplete observability is given in reference [22]. Incomplete observability may be of two types:

1) Depth-of-One unobservability: It is defined as "A situation in which all of the neighboring buses of any unobservable bus must be observable". Figure 2-2 shows a system with Depth-of-One unobservability. The bus D is unobservable bus and all other neighboring buses are observed either directly or indirectly by PMU.

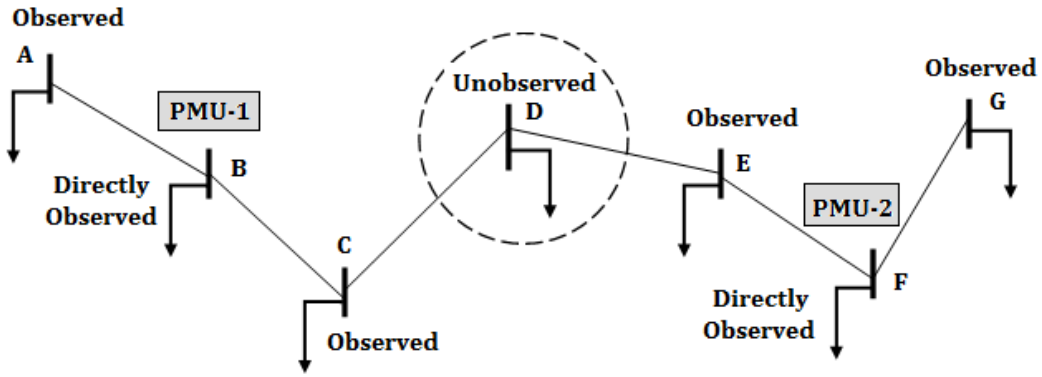

Figure 2-2: Depth-of-One unobservability

2) Depth-of-Two unobservability: It is defined as "A situation in which all of the neighboring buses of any two consecutive unobservable buses must be observable". Figure 2-3 shows a system with Depth-of-Two unobservability. The bus D and the bus E are unobservable buses and all other neighboring buses are observed either directly or indirectly by PMU.

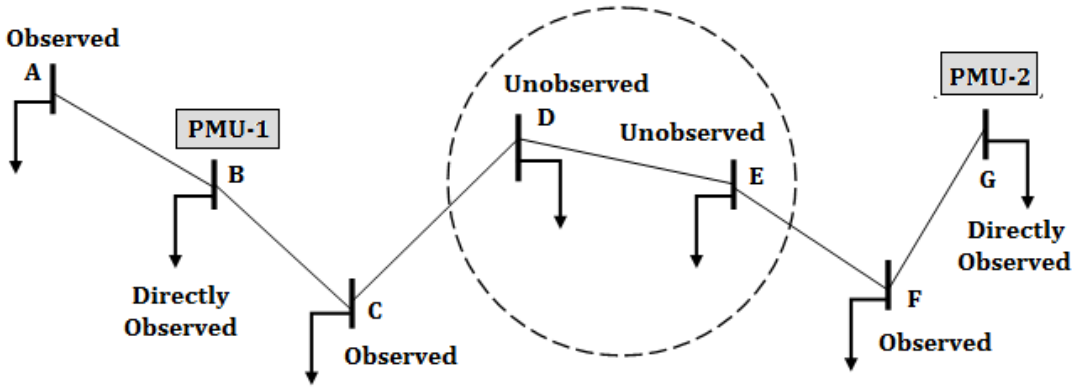

Figure 2-3: Depth-of-Two Unobservability

2.3.1 Optimal PMU Placement Problem for Depth-of-one unobservability

The depth-of-one unobservability can be modeled as a set of linear inequalities and can be formulated as:

$$\begin{aligned} &Minimize \sum_{i=1}^{N} x_i \\ &such\,that \\ &A_I A_{PMU} X \geq b_1 \\ &where, X = [x_1, x_2, ..., x_N]^t ; x_i \in \{0,1\}; i = 1,2,....N \\ &b_1 = [1,1,.....,1]^t_{M_1 \times 1} \end{aligned} \tag{2.10}$$

where, A_I is the branch-to-node incident matrix and M_1 is the total numbers of branches. x_i is the PMU placement variable and N is the total number of buses in the system.

2.3.2 Optimal PMU Placement Problem for Depth-of-two unobservability

The depth-of-two unobservability can be modeled as a set of linear inequalities and can be formulated as:

$$\begin{aligned} &Minimize \sum_{i=1}^{N} x_i \\ &such\,that \\ &BA_{PMU} X \geq b_2 \\ &where, X = \left[x_1, x_2, ..., x_N\right]^t ; x_i \in \{0,1\}; i = 1,2,....N \\ &b_2 = \left[1,1,.....,1\right]^t_{M_2 \times 1} \end{aligned} \tag{2.11}$$

Where, B is the matrix in which each row corresponds to three connecting buses and contains all of the possible combinations of three connecting buses and M_2 is the total numbers of possible combinations of three connecting buses. x_i is the PMU placement variable and N is the total number of buses in the system.

2.3.3 Determination of the Optimal Branch Current Phasor

Optimal branch current phasor measurements problem for incomplete observability is same for depth-of-one unobservability and depth-of-two unobservability. Let us define a matrix B_{CUO} whose rows correspond to the buses in the system excluding the PMU buses and the unobservable buses and the columns correspond to the branches connected to PMU buses. The entries of B_{CUO} is defined as:

$$B_{CUO(i,j)} = \begin{cases} 1, & if\ bus\ i\ is\ observed\ by\ branch\ current\ phasor\ of\ j^{th}\ line \\ 0, & otherwise \end{cases} \tag{2.12}$$

Therefore, the optimal branch current phasor measurements problem is to find out the minimum set of branch current phasors. This problem can be formulated as BILP as given below.

$$\begin{aligned} &Minimize \sum_{j=1}^{NB} y_j \\ &such\,that \\ &B_{CUO} Y = b_3 \\ &where, \quad Y = \left[y_1, y_2, ... , y_{NB}\right]^t ; y_j \in \{0,1\}; j = 1,2,...., NB \\ &b_3 = \left[1,1, ... ,1\right]^t_{(N-(NP+NUB))} \end{aligned} \tag{2.13}$$

Where, N is the number of buses; NP is the number of optimal PMUs; NB is the number of initial set of branch current phasor; NUB is the number of unobserved buses and y_i is the branch current phasor variable.

The branch current phasors need not to observe the PMU buses as they are already observed by the PMU installed on them and the unobserved buses, the rows correspond to PMU buses and unobserved buses can be removed from the matrix $\mathrm{B_{CUO}}$. Hence, the size of matrix $\mathrm{B_{CUO}}$ is $\big((\mathrm{N}-(\mathrm{NP}+\mathrm{NUB}))\times \mathrm{NB}\big)$ and the length of vector b is $\big(\mathrm{N}-(\mathrm{NP}+\mathrm{NUB})\big)$.

The formulation given in section 2.3.1 for depth-of-one unobservability is explained using the seven-bus system shown in Figure 2-1. First, the OPP problem have been formulated for incomplete observability is explained then optimal current phasor problem is considered. $\mathrm{A_{PMU}}$ is same as (2.6) and the branch-to-node incident matrix $\mathrm{A_I}$ for the sample system is:

$$A_I = \begin{bmatrix} 1 & 1 & 0 & 0 & 0 & 0 & 0 \\ 0 & 1 & 1 & 0 & 0 & 0 & 0 \\ 0 & 1 & 0 & 0 & 0 & 0 & 1 \\ 0 & 0 & 1 & 1 & 0 & 0 & 0 \\ 0 & 0 & 1 & 0 & 0 & 1 & 0 \\ 0 & 0 & 0 & 1 & 1 & 0 & 0 \\ 0 & 0 & 0 & 1 & 0 & 0 & 1 \\ 0 & 0 & 0 & 1 & 0 & 1 & 0 \\ 0 & 0 & 0 & 0 & 1 & 1 & 0 \end{bmatrix} \tag{2.14}$$

Equation (2.10) can be written as:

$$Minimize \sum_{i=1}^{N} x_i$$

$$such\ that$$

$$\begin{bmatrix} 2 & 2 & 1 & 0 & 0 & 0 & 1 \\ 1 & 2 & 2 & 1 & 0 & 1 & 1 \\ 1 & 2 & 1 & 1 & 0 & 0 & 2 \\ 0 & 1 & 2 & 2 & 1 & 2 & 1 \\ 0 & 1 & 2 & 2 & 1 & 2 & 0 \\ 0 & 0 & 1 & 2 & 2 & 2 & 1 \\ 0 & 1 & 1 & 2 & 1 & 1 & 2 \\ 0 & 0 & 2 & 2 & 2 & 2 & 1 \\ 0 & 0 & 1 & 2 & 2 & 2 & 0 \end{bmatrix} \begin{bmatrix} x_1 \\ x_2 \\ x_3 \\ x_4 \\ x_5 \\ x_6 \\ x_7 \end{bmatrix} \geq \begin{bmatrix} 1 \\ 1 \\ 1 \\ 1 \\ 1 \\ 1 \\ 1 \\ 1 \\ 1 \end{bmatrix} \tag{2.15}$$

GA is used to solve this problem. The optimal solution obtained is $X = [0\ \ 0\ \ 1\ \ 0\ \ 0\ \ 0\ \ 0]^T$, which means PMU is placed at buses 3 and the unobservable buses are 1, 5 and 7. The initial set of branch current phasors is 3-2, 3-4 and 3-6 corresponds to the lines 2, 3 and 5 respectively

as shown in Figure 2-1. In this system, 3 branch-current phasors are obtained. Therefore, the matrix B_{CUO} defined in (2.12) can be written as:

$$B_{CUO} = \left[\begin{array}{c|ccc} \begin{array}{c} Lines \rightarrow \\ buses(excluding\ PMU\ buses \\ \&\ Unobservable\ buses) \\ \downarrow \end{array} & 2 & 3 & 5 \\ \hline 2 & 1 & 0 & 0 \\ 4 & 0 & 1 & 0 \\ 6 & 0 & 0 & 1 \end{array}\right] \tag{2.16}$$

Now, the optimal branch current phasors problem for the example system can be formulated as:

$$\begin{aligned} & Minimize \sum_{j=1}^{3} y_j \\ & such\ that \\ & \begin{bmatrix} 1 & 0 & 0 \\ 0 & 1 & 0 \\ 0 & 0 & 1 \end{bmatrix} \begin{bmatrix} y_1 \\ y_2 \\ y_3 \end{bmatrix} = \begin{bmatrix} 1 \\ 1 \\ 1 \end{bmatrix} \end{aligned} \tag{2.17}$$

The optimal solution is$Y = [1 \ \ 1 \ \ 1]^{T}$. This means that the branch current phasors needed to be monitored are 3-2, 3-4 and 3-6.

For the seven-bus system, depth-of-two unobservability also gives the same results due to its very small size.

2.4 PMU placement for complete observability with N-1 contingency analysis

For an N-bus system, the PMU placement problem can be formulated as:

$$\begin{aligned} & Minimize \sum_{i=1}^{N} x_i \\ & such\ that \\ & [A_{PMU}]_{N\times N}[X]_{N\times 1} \geq [b_{PMU}]_{N\times 1} \\ & X_{np} = 0 \\ & where,\ X = [x_1, x_2, \ldots\ldots, x_N]^T ; x_i \in \{0,1\}; i = 1, 2, \ldots\ldots, N \\ & b_{PMU} = [2, 2, \ldots\ldots\ldots, 2]_{N\times 1} \end{aligned} \tag{2.18}$$

Where, A_{PMU} is bus connectivity matrix and the elements of this matrix is same as explained in (2.3). The elements of b_{PMU} is "two", so that i[th] bus (of connectivity matrix in LHS) is observed by atleast "two" PMUs either directly or indirectly. This ensure that a PMU outage or failure of a communication link does not lead to loss of observability. N is the total number of buses in the system. In the system, there may be few buses on which PMU placement is not possible due to various reasons such as physical constraints etc. Therefore, 'np' is the set of those buses, which are not suitable for PMU placement.

To include the effect of the channel limits on the number of PMUs required to make the system completely observable, a "B" matrix [20] is formed using the matrix "A_{PMU}". Number of rows of matrix B for each bus can be found as follows:

$$r_k = \begin{cases} \binom{N_k}{L} = \dfrac{N_k!}{(N_k - L)!L!} & if\ L < N_k \\ 1 & if\ N_k \le L \end{cases} \tag{2.19}$$

Where N_k is the number of branches connected to bus k, L is the specified channel limits for the PMUs. Matrix B is the formed based on the number of L-combination of N_k. By incorporating this effect in optimal PMU placement, the constraint $[A_{PMU}]_{N\times N}[X]_{N\times 1} \ge [b_{PMU}]_{N\times 1}$ in (2.18) is replaced by:

$$B^T X \ge b_{PMU} \tag{2.20}$$

Each row associated with bus k in the matrix B can be defined as:

If $r_k = 1$, the row associated with bus k in matrix A_{PMU} is kept with no change and if $r_k > 1$, then each row of the matrix B is formed based on the number of L combination of N_k.

In the present work, the PMU channel limit (L) is considered as 24 channels that can measure eight phasor values [86]. Presence of conventional measurements like real or reactive power injections, real or reactive power flow and current injection measurements further reduces the number of PMUs required for complete observability[13, 14]. If n buses are associated with zero injection bus and the voltage phasors of (n-1) bus are known, then the n[th] bus voltage phasor can be calculated by applying KCL at zero injection bus. To explain the effect of zero injection bus, let us assume that four-bus system with injection measurement at bus k as shown in Figure 2-4.

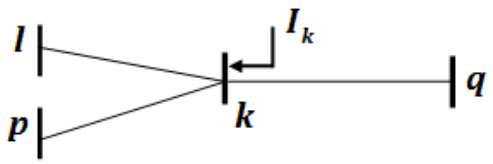

Figure 2-4: Injection measurement at bus k

The constraints for the above figure can be formulated as:

$$\begin{aligned} f_l &= x_l + x_k && \geq 1 \\ f_p &= x_p + x_k && \geq 1 \\ f_k &= x_l + x_p + x_k + x_q && \geq 1 \\ f_q &= x_q + x_k && \geq 1 \end{aligned} \tag{2.21}$$

By incorporating the effect of zero injection bus at kth bus, (2.21) can be written as:

$$f_{lpkq} = f_l + f_p + f_k + f_q \geq n-1, \ \ where\, n = 4 \tag{2.22}$$

And for (N-1) contingency the constraints will be:

$$f_{lpkq} = f_l + f_p + f_k + f_q \geq 2n-1, \ \ where\, n = 4 \tag{2.23}$$

In this work, the zero injection measurements are included into the OPP formulation. The aforementioned BILP problem is solved using the GA to obtain optimal allocations for PMUs.

2.4.1 Determination of the Optimal Branch Current Phasor

Let us define a matrix $B_{CO(N-1)}$whose rows correspond to the buses in the system and the columns correspond to the branches connected to PMU buses. The entries of $B_{CO(N-1)}$ can be defined as:

$$B_{CO(N-1)_{(i,j)}} = \begin{cases} 1, if\ bus\ i\ is\ observed\ by\ branch\ current\ phasor\ of\ \ j^{th}\ line \\ 0, \qquad\qquad\qquad\qquad\qquad\qquad otherwise \end{cases} \tag{2.24}$$

Therefore, the optimal branch current phasor measurements problem is to find out the minimum set of branch current phasors and can be formulated as a BILP as given below.

$$\begin{aligned} & Minimize \sum_{j=1}^{NB} y_j \\ & such\,that \\ & \quad B_{CO(N-1)} Y = b \\ & where, \quad Y = \left[y_1, y_2, \ldots\ldots, y_{NB} \right]^T ; y_j \in \{0,1\}; j = 1,2,\ldots\ldots, NB \\ & \quad b = \left[[1,1,\ldots,1]_{(NP+NZ)\times 1}; [2,2,\ldots,2]_{(N-NP)\times 1} \right] \end{aligned} \tag{2.25}$$

N is the number of buses, NP is the number of optimal PMUs, NB is the number of initial set of branch current phasor; NZ is the number of zero injection bus and y_j is the branch current phasor variable.

The above formulation of BILP problem for complete observability with N-1 contingency has been explained using a seven-bus system as shown in Figure 2-1. In this system, bus 3 is taken as zero injection bus. Buses 2, 3, 4 and 6 are associated with this conventional measurement. Since the number of channel limit to the PMU taken in this work is eight phasors and maximum branch connected to a bus are four, therefore, it will not affect the formulation of seven-bus system. It is assumed that, there is no such buses which are not suitable for PMU placement therefore, np is an empty set, i.e. np = {}.The formulated BILP problem has been solved to find the optimal number of PMUs. The problem considering both conventional measurement and N-1 contingency has formulated as:

$$\begin{aligned} & Minimise \sum_{k=1}^{7} x_k \\ & f(x) = \begin{cases} f_1 = x_1 + x_2 & \geq 2 \\ f_5 = x_4 + x_5 + x_6 & \geq 2 \\ f_7 = x_2 + x_4 + x_7 & \geq 2 \\ f_{2346} = x_1 + 2x_2 + 4x_3 + 3x_4 + 2x_5 + 3x_6 + 2x_7 & \geq 7 \end{cases} \end{aligned} \tag{2.26}$$

The solution of optimal PMU placement problem for the seven-bus system with conventional measurements and N-1 contingency obtained as $X = \begin{bmatrix} 1 & 1 & 0 & 1 & 1 & 0 & 0 \end{bmatrix}^T$ indicating the placement of PMUs at buses 1, 2, 4 and 5. It must be noted that if a bus is observed by at least two PMUs, then a line outage or a PMU failure will not affect the complete observability of the network.

The initial set of branch current phasors are 1-2, 2-1, 2-3, 2-7, 4-3, 4-5, 4-6, 4-7, 5-4 and 5-6 representing the lines 1, 1, 2, 8, 3, 4, 6, 9, 4 and 7 respectively as shown in Figure 2-1. In this

system, 10 branch current phasors are monitored. Therefore, the matrix $B_{CO(N-1)}$ can be written as:

$$B_{CO(N-1)} = \left[\begin{array}{c|cccccccccc} Lines \rightarrow & 1 & 1 & 2 & 8 & 3 & 4 & 6 & 9 & 4 & 7 \\ Buses \downarrow & & & & & & & & & & \\ \hline 1 & 0 & 1 & 0 & 0 & 0 & 0 & 0 & 0 & 0 & 0 \\ 2 & 1 & 0 & 0 & 0 & 0 & 0 & 0 & 0 & 0 & 0 \\ 4 & 0 & 0 & 0 & 0 & 0 & 0 & 0 & 0 & 1 & 0 \\ 5 & 0 & 0 & 0 & 0 & 0 & 1 & 0 & 0 & 0 & 0 \\ 3 & 0 & 0 & 1 & 0 & 1 & 0 & 0 & 0 & 0 & 0 \\ 6 & 0 & 0 & 0 & 0 & 0 & 0 & 1 & 0 & 0 & 1 \\ 7 & 0 & 0 & 0 & 1 & 0 & 0 & 0 & 1 & 0 & 0 \end{array}\right] \quad (2.27)$$

The optimal branch current phasors problem for the seven-bus system can be formulated as:

$$\begin{bmatrix} 0 & 1 & 0 & 0 & 0 & 0 & 0 & 0 & 0 & 0 \\ 1 & 0 & 0 & 0 & 0 & 0 & 0 & 0 & 0 & 0 \\ 0 & 0 & 0 & 0 & 0 & 0 & 0 & 0 & 1 & 0 \\ 0 & 0 & 0 & 0 & 0 & 1 & 0 & 0 & 0 & 0 \\ 0 & 0 & 1 & 0 & 1 & 0 & 0 & 0 & 0 & 0 \\ 0 & 0 & 0 & 0 & 0 & 0 & 1 & 0 & 0 & 1 \\ 0 & 0 & 0 & 1 & 0 & 0 & 0 & 1 & 0 & 0 \end{bmatrix} \begin{bmatrix} y_1 \\ y_2 \\ y_3 \\ y_4 \\ y_5 \\ y_6 \\ y_7 \\ y_8 \\ y_9 \\ y_{10} \end{bmatrix} = \begin{bmatrix} 1 \\ 1 \\ 1 \\ 1 \\ 1 \\ 2 \\ 2 \end{bmatrix} \quad (2.28)$$

This BILP is solved using GA. The optimal solution is $Y = [1\ \ 1\ \ 1\ \ 1\ 0\ \ 1\ \ 1\ \ 1\ \ 1\ \ 1]^T$. This means that the branch current phasors needed to be monitored are 1-2, 2-1, 2-3, 2-7, 4-5, 4-6, 4-7, 5-4 and 5-6 (total 9 phasors).

2.5 Optimal placement of PMUs using Genetic Algorithm

In OPP, each bus in a system is a variable and the objective is to find the minimum set of PMU buses that make the system observable. Figure 2-5 illustrates the procedure of OPP using GA. The detailed description of the GA for PMU placement is as follows:

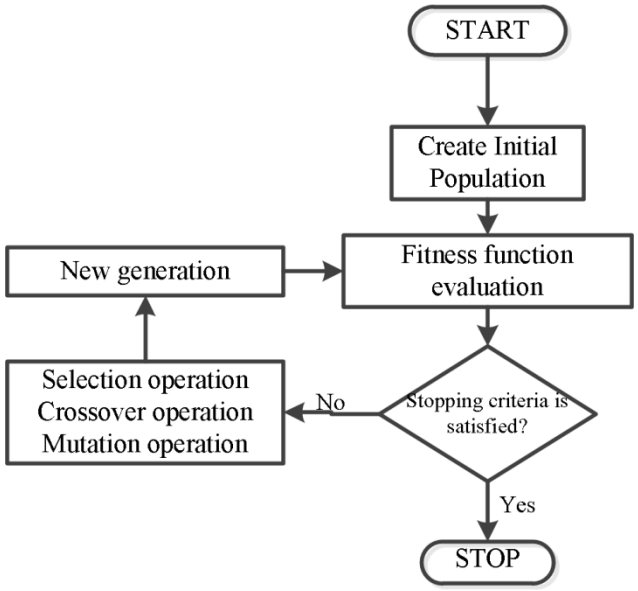

Figure 2-5: GA flowchart

Step I Representation: The chromosomes X is represented as $X = \{x_1, x_2, ..., x_N\}$, where, N is the total number of buses.

Step II Fitness definition: In this chapter, 8 fitness functions are defined given by equation (2.1), (2.5), (2.10), (2.11), (2.13), (2.18) and (2.25). Depending upon the cases, the fitness function is selected and optimized using GA.

Step III Population initialization: In the proposed study, the initial population composed of hundred randomly created chromosomes. The population size is selected as a trade-off between the convergence time and population diversity.

Step IV Fitness evaluation: The fitness value for each randomly generated chromosomes in step III is calculated using fitness function defined in step II.

Step V Creating new population: Selection, crossover, and mutation are carried out to replace the current population by the newer population. The chromosomes with better fitness values are selected into the recombination pool using the roulette wheel. Genes between two parent chromosomes are exchanged to obtain new offspring to attempt to get better solutions, the probability of creating new chromosomes in each pair is set to 0.8. Mutation is performed to alter the binary code with a probability of 0.05.

Step VI Stopping criteria: The process is repeated from step IV to step V until the generation count reaches its limit.

2.6 Simulation Result

The OPP problem has been solved for IEEE-14, IEEE-30, IEEE-57 bus systems and the Northern Regional Power Grid (NRPG) 246-bus system. The details of these systems have been given in Appendix A. For all the system, following cases have been considered.

Case 1: The OPP problem has been formulated for the complete observability.

Case 2: The OPP problem has been formulated for the incomplete observability with Depth-of-One unobservability.

Case 3: The OPP problem has been formulated for the incomplete observability with Depth-of-Two unobservability.

Case 4: The OPP problem has been formulated for the complete observability with cannel limits and N-1 contingency.

2.6.1 IEEE 14 Bus System

For all the cases considered, the optimal number of PMUs and their locations for IEEE-14 bus system are given in Table 2-1. Initial set of branch current phasors and optimal branch current phasors are given in Table 2-2 for all the cases for IEEE 14 bus system. This table shows that if current phasors are optimized, their number may reduce sufficiently.

Table 2-1: Number and Locations of PMUs for IEEE-14 bus system

Cases	No. of PMUs	Location of PMUs
Case 1	4	2, 6,7,9
Case 2	2	4, 6
Case 3	2	4, 6
Case 4	7	2,3,5,6,9,10,13

Table 2-2: Initial and Optimal Branch Current Phasors for IEEE-14 bus system

Cases	Initial Set of Branch Current Phasors		Optimal Branch Current Phasors	
	No. of Branch Current Phasors	Locations	No. of Branch Current Phasors	Locations
Case-1	15	2-1, 2-3, 2-4,2-5, 6-5, 6-11,6-12, 6-13, 7-4,7-8, 7-9, 9-4,9-7, 9-10, 9-14	10	2-1, 2-3, 2-4,2-5, 6-11, 6-12,6-13, 7-8, 9-10,9-14
Case-2	9	4-2,4-3,4-5,4-7,4-9,6-5,6-11,6-12,6-13	8	4-2,4-3,4-5,4-7,4-9,6-1,6-12,6-13

Cases	Initial Set of Branch Current Phasors		Optimal Branch Current Phasors	
Case-3	9	4-2,4-3,4-5,4-7,4-9,6-5,6-11,6-12,6-13	8	4-2,4-3,4-5,4-7,4-9, 6-11,6-12,6-13
Case-4	23	2-1,2-3,2-4,2-5,3-2,3-4,5-1,5-2,5-4,5-6,6-5,6-11,6-12,6-13,9-4,9-7,9-10,9-14,10-9,10-11,13-6,13-12,13-14	20	2-1,2-3,2-4,2-5,3-2,3-4,5-1,5-6,6-5,6-11,6-12,6-13,9-7,9-10,9-14,10-9,10-11,13-6,13-12,13-14

2.6.2 IEEE-30 Bus System

The optimal number of PMUs and their locations for IEEE-30 bus system for all the cases are given in Table 2-3. For all the cases, initial set of branch current phasors and optimal branch current phasors are given in Table 2-4. If current phasors are optimized their number reduces from 40 to 20 phasors for case 1. Similarly, branch current phasors reduces from 18 to 17 for case 2, 15 to 14 for case 3 and 47 to 39 for case 4.

Table 2-3: Number and Locations of PMUs for IEEE-30 bus system

Cases	No. of PMUs	Location of PMUs
Case 1	10	1,2,6,9,10, 12,15,19, 25,27
Case 2	4	2, 10, 15, 27
Case 3	3	6, 15, 27
Case 4	15	1, 2, 4, 5, 10, 12, 13, 15, 17, 18, 20, 23, 25, 27, 28

Table 2-4: Initial and Optimal Branch Current Phasors for IEEE-30 bus system

Cases	Initial Set of Branch Current Phasors		Optimal Branch Current Phasors	
	No. of Branch Current Phasors	Locations	No. of Branch Current Phasors	Locations
Case-1	40	1-2,1-3,2-1,2-4,2-5,2-6,6-2,6-4,6-7,6-8,6-9,6-10,6-28,9-6,9-10,9-11,10-6,10-9,10-17,10-20,10-21,10-22,12-4,12-13,12-14,12-15,12-16,15-12,15-14,15-18,15-23,19-18,19-20,25-24,25-26,25-27,27-25,27-28,27-29,27-30	20	1-3,2-4,2-5,6-7,6-8,6-28,9-11,10-17,10-20,10-21,10-22,12-13,12-14,12-16,15-18,15-23,25-24,25-26,27-29,27-30
Case-2	18	2-1,2-4,2-5,2-6,10-6,10-9,10-17,10-20,10-21,10-22,15-12,15-14,15-18,15-23,27-25,27-28,27-29,27-30	17	2-1,2-4,2-5,2-6,10-9,10-17,10-20,10-21, 10-22,15-12,15-14,15-18,15-23,27-25, 27-28,27-29, 27-30
Case-3	15	6-2,6-4,6-7,6-8,6-9,6-10,6-28,15-12,15-14,15-18,15-23,27-25,27-28,27-29,27-30	14	6-2,6-4,6-7,6-8,6-9,6-10,6-28,15-12,15-14,15-18,15-23,27-25, 27-29,27-30
Case-4	47	1-2,1-3,2-1,2-4,2-5,2-6,4-2,4-3,4-6,4-12,5-2,5-7,10-6,10-9,10-17,10-20,10-21,10-22,12-4,12-13,12-14,12-15,12-16,13-12,15-12,15-14,15-18,15-23,17-10,17-16,18-15,18-19,20-10,20-19,23-15,23-	39	1-2,1-3,2-1,2-4,2-5,2-6,4-12, 5-7, 10-9,10-17,10-20,10-21,10-22,12-13,12-14,12-15,12-16,15-14,15-18,15-23,17-10,17-16,18-15,18-19, 20-19,23-15,23-21,23-24,25-

Cases	Initial Set of Branch Current Phasors		Optimal Branch Current Phasors	
		21,23-24,25-24,25-26,25-27,27-25,27-28,27-29,27-30,28-6,28-8,28-27		24,25-26,25-27,27-25,27-28,27-29,27-30,28-6,28-8,28-27

2.6.3 IEEE-57 Bus System

The optimal number of PMUs and their locations for IEEE-57 bus system for all the cases are given in Table 2-5. Initial set of branch current phasors and optimal current phasors for all the cases given in Table 2-6. The results shows that for case 1, the initial set of branch current phasors are reduced from 54 to 40 measurements, 35 to 31 for case 2, 30 to 29 for case 3 and 83 to 61 for case 4.

Table 2-5: Number and Locations of PMUs for IEEE-57 bus system

Cases	*No. of PMUs*	*Location of PMUs*
Case 1	17	1,4,9,15,20,24,25,26,29,32,36,38,39,41,46,51,54
Case 2	11	4,9,15,21,26,31,36,48,51,52,56
Case 3	8	9,15,18,24,29,34,38,56
Case 4	28	1,3,4,7,9,12,15,19,20,23,24,25,28,29,31,32,33,36,38,39,41,46,48,50,51,53,54,56

Table 2-6: Initial and Optimal Branch Current Phasors for IEEE-57 bus system

Cases	Initial Set of Branch Current Phasors		Optimal Branch Current Phasors	
	No. of Branch Current Phasors	Locations	No. of Branch Current Phasors	Locations
Case-1	54	1-2,1-15.1-16,1-17,4-3,4-5,4-6,4-18,9-8,9-10,9-11,9-12,9-13,9-55,15-1,15-3,15-13,15-14,15-45,20-19,20-21,24-23,24-25,24-26,25-24,25-30,26-24,26-27,29-7,29-28,29-52,32-31,32-33,32-34,36-35,36-37,36-40,38-22,38-37,38-44,38-48,38-49,39-37,39-57,41-11,41-42,41-43,41-56,46-14,46-47,51-10,51-50,54-53,54-55	40	1-2,1-16,1-17,4-3,4-5,4-6,4-18,9-8,9-10,9-11,9-12,9-13,9-55,15-14,15-45,20-19,20-21,24-23,25-30,26-27,29-7,29-28,29-52,32-31,32-33,32-34,36-35,36-37,36-40,38-22,38-44,38-48,38-49,39-57,41-42,41-43,41-56,46-47,51-50,54-53
Case-2	35	4-3,4-5,4-6,4-18,9-8,9-10,9-11,9-12,9-13,9-55,15-1,15-3,15-13,15-14,15-45,21-20,21-22,26-24,26-27,31-30,31-32,36-35,36-37,36-40,48-38,48-47,48-49,51-10,51-50,52-29,52-53,56-40,56-41,56-42,56-57	31	4-3,4-5,4-6,4-18,9-8,9-10,9-11,9-12,9-13,9-55,15-1,15-14,15-45,21-20,21-22,26-24,26-27,31-30,31-32,36-35,36-37,36-40,48-38,48-47,48-49,51-50,52-29,52-53,56-41,56-42,56-57
Case-3	30	9-8,9-10,9-11,9-12,9-13,9-55,15-1,15-3,15-13,15-14,15-45,18-4,18-19,24-23,24-25,24-26,29-7,29-28,29-52,34-32,34-35,38-22,38-37,38-44,38-48,38-49,56-40,56-41,56-42,56-57	29	9-8,9-10,9-11,9-12,9-13,9-55,15-1,15-3,15-14,15-45,18-4,18-19,24-23,24-25,24-26,29-7,29-28,29-52,34-32,34-35,38-22,38-37,38-44,38-48,38-49,56-40,56-41,56-42,56-57
Case-4	83	1-2,1-15,1-16,1-17,3-2,3-4,3-15,4-3,4-5,4-6,4-18,7-6,7-8,7-29,9-8,9-10,9-11,9-12,9-13,9-55,12-9,12-10,12-13,12-16,12-17,15-1,15-3,15-13,15-	61	1-2,1-15,1-16,1-17,3-2,3-4,4-3,4-6,4-18,7-6,7-8,7-29,9-8,9-10,9-11,9-12,9-13,9-55,12-9,12-10,12-13,12-16,12-17,15-1,15-14,19-18,19-20,20-19,23-

		14,15-45,19-18,19-20,20-19,20-21,23-22,23-24,24-23,24-25,24-26,25-24,25-30,28-27,28-29,29-7,29-28,29-52,31-30,31-32,32-31,32-33,32-34,33-32,36-35,36-37,36-40,38-22,38-37,38-44,38-48,38-49,39-37,39-57,41-11,41-42,41-43,41-56,46-14,46-47,48-38,48-47,48-49,50-49,50-51,51-10,51-50,53-52,53-54,54-53,54-55,56-40,56-41,56-42,56-57		22,23-24,24-23,24-25,25-30,29-7,29-28,29-52,31-30,31-32,32-31,32-33,36-37,36-40,38-22,38-37,38-48,38-49,39-57,41-11,41-42,41-56,46-14,46-47,48-38,48-47,48-49,50-51,51-50,53-52,53-54,54-53,54-55,56-40,56-41,56-42,56-57

2.6.4 Northern Regional Power Grid (NRPG – 246 bus system)

The optimal number of PMUs and their locations for NRPG-246 bus system for all the cases considered in this chapter are given in Table 2-7. In the second step of the proposed method, the optimal current phasor measurements for all the cases are determined and are given in Table 2-8. The initial branch current phasors are reduced from 268 phasors to 176 phasor measurements for case 1. Similarly for case 2 measurements reduces from 194 to 161, 85 to 57 for case 3 and 425 to 341 for case 4.

Table 2-7: Number and Locations of PMUs for Northern Regional Power Grid (NRPG) - 246 bus system

Cases	***No. of PMUs***	***Location of PMUs***
Case 1	70	6,21,23,24,29,34,40,45,48,54,55,57,60,61,62,63,65,69,73,74,75,78,80,88,93,95,98,100, 101,102,103,106,109,116,117,121,122,125,126,129,132,134,140,141,142,147,157,158, 160,163,168,173,181,183,185,187,190,191,194,199,201,202,203,215, 216,219,234,235,243,245
Case 2	52	29,40,45,48,55,57,60,61,62,63,65,69,74,75,78,80,93,95,98,101,102,103,106,116, 117,122,125,129,132,140,141,142,147,157,160,163,168,173,181,183, 190,191,194,199,201,203,215,216,219,234,235,245
Case 3	43	29,40,55,60,62,69,74,78,80,88,93,98,100,101,103,106,117,121,125,129,140, 141,142,147,157,160,163,168,173,181,183,190,191, 194,199,201,203,215,216,219,234,235,245
Case 4	136	2, 3, 4, 5, 6, 7, 9, 10, 11, 12, 15, 19, 21, 23, 24, 27, 28, 29, 30, 31, 32, 34, 35, 38, 40, 41, 44, 45, 47, 48, 49, 50, 51, 52, 53, 54, 56, 57, 61, 62, 65, 68, 69, 71, 74, 77, 78, 80, 82, 83, 84, 87, 88, 89, 93, 95, 97, 100, 101, 106, 109, 111, 112, 113, 118, 119, 120, 123, 124, 125, 126, 128, 129, 130, 132, 133, 134, 135, 139, 140, 141, 144, 145, 147, 148, 149, 151, 152, 153, 156, 157, 158, 159, 160, 163, 164, 165, 168, 172, 173, 174, 176, 177, 178, 181, 182, 185, 187, 188, 189, 190, 191, 193, 194, 195, 197, 199, 201, 202, 203, 205, 206, 208, 213, 216, 218, 219, 223, 224, 229, 230, 235, 238, 242, 243, 246

Table 2-8: Initial and Optimal Branch Current Phasors for Northern Regional Power Grid (NRPG) 246-bus system

Cases	Initial Set of Branch Current Phasors		Optimal Branch Current Phasors	
	No. of Branch Current Phasors	Locations	No. of Branch Current Phasors	Locations
Case-1	268	6-5,6-65,21-19,21-20,21-37,21-160,21-165,21-166,23-22,23-180,24-1,24-191,24-192,24-198,29-205,29-206,29-207,34-17,34-135,34-136,34-150,34-158,34-183,40-32,40-41,40-211,40-239,40-241,45-43,45-56,48-47,48-59,48-204,54-49,54-51,54-52,54-55,54-62,55-50,55-54,55-56,57-25,57-44,57-46,60-9,60-11,61-53,61-154,62-4,62-54,62-71,63-58,63-70,65-6,65-7,65-8,65-67,65-68,65-90,65-100,65-110,69-10,69-70,69-115,69-154,73-3,73-72,73-74,74-73,74-86,74-88,74-104,74-246,75-76,75-91,78-84,78-91,80-12,80-44,80-46,80-56,80-82,80-86,88-13,88-64,88-74,88-79,88-94,93-14,93-89,95-83,95-92,98-15,98-66,98-97,100-13,100-65,100-87,101-81,101-96,101-99,102-64,102-83,103-83,103-85,106-107,106-123,106-130,109-16,109-108,109-110,109-121,109-131,109-132,116-128,116-229,117-35,117-119,121-17,121-109,121-111,121-115,121-122,121-162,121-229,122-112,122-121,125-16,125-114,125-124,125-130,126-113,126-120,126-129,129-113,129-118,129-126,129-127,129-232,132-109,132-139,132-140,132-149,134-18,134-146,134-147,140-132,140-137,140-143,140-144,140-154,141-136,141-137,141-138,141-148,141-151,141-155,142-145,142-152,147-134,147-150,147-153,157-22,157-162,157-175,157-176,157-177,157-180,158-34,158-156,158-160,158-181,160-21,160-158,160-161,160-162,160-164,160-179,160-230,163-164,163-167,168-20,168-169,168-170,168-171,168-178,173-166,173-174,181-37,181-158,181-172,181-230,183-34,183-133,183-182,183-194,185-30,185-197,185-209,185-219,187-2,187-186,187-189,187-191,187-210,190-188,190-211,190-222,190-223,190-227,191-24,191-184,191-187,191-208,191-212,194-182,194-183,194-193,194-195,194-198,194-213,194-220,194-228,199-1,199-	176	6-5,21-19,21-20,21-37,21-165,21-166,23-22,23-180,24-1,24-192,24-198,29-205,29-206,29-207,34-17,34-135,34-136,34-150,40-32,40-41,40-211,40-239,40-241,45-43,45-56,48-47,48-59,48-204,54-49,54-51,54-52,55-50,57-25,57-44,57-46,60-9,60-11,61-53,61-154,62-4,62-71,63-58,63-70,65-7,65-8,65-67,65-68,65-90,65-110,69-10,69-115,73-3,73-72,74-86,74-104,74-246,75-76,75-91,78-84,80-12,80-82,88-13,88-64,88-79,88-94,93-14,93-89,95-83,95-92,98-15,98-66,98-97,100-87,101-81,101-96,101-99,103-85,106-107,106-123,106-130,109-16,109-108,109-131,116-128,116-229,117-35,117-119,121-111,121-162,122-112,125-114,125-124,126-113,126-120,129-118,129-127,129-232,132-139,132-149,134-18,134-146,140-137,140-143,140-144,141-138,141-148,141-151,141-155,142-145,142-152,147-153,157-175,157-176,157-177,158-156,160-161,160-164,160-179,160-230,163-167,168-169,168-170,168-171,168-178,173-174,181-172,183-133,183-182,185-30,185-197,185-209,187-2,187-186,187-189,187-210,190-188,190-222,190-223,190-227,191-184,191-208,191-212,194-193,194-195,194-213,194-220,194-228,199-36,199-159,199-200,199-214,201-26,201-226,201-231,202-28,202-225,203-27,203-39,203-224,215-33,215-221,216-217,216-218,219-31,219-77,219-196,234-233,234-237,234-238,235-38,235-236,235-240,243-42,243-242,245-105,245-244

		36,199-159,199-200,199-214,201-26,201-200,201-226,201-231,202-28,202-203,202-225,203-27,203-39,203-202,203-224,215-27,215-33,215-213,215-221,215-239,216-59,216-204,216-217,216-218,219-31,219-77,219-185,219-196,234-233,234-237,234-238,234-239,235-38,235-213,235-233,235-236,235-240,243-42,243-242,243-245,245-42,245-105,245-243,245-244		
Case-2	194	29-205,29-206,29-207,40-32,40-41,40-211,40-239,40-241,45-43,45-56,48-47,48-59,48-204,55-50,55-54,55-56,57-25,57-44,57-46,60-9,60-11,61-53,61-154,62-4,62-54,62-71,63-58,63-70,65-6,65-7,65-8,65-67,65-68,65-90,65-100,65-110,69-10,69-70,69-115,69-154,74-73,74-86,74-88,74-104,74-246,75-76,75-91,78-84,78-91,80-12,80-44,80-46,80-56,80-82,80-86,93-14,93-89,95-83,95-92,98-15,98-66,98-97,101-81,101-96,101-99,102-64,102-83,103-83,103-85,106-107,106-123,106-130,116-128,116-229,117-35,117-119,122-112,122-121,125-16,125-114,125-124,125-130,129-113,129-118,129-126,129-127,129-232,132-109,132-139,132-140,132-149,140-132,140-137,140-143,140-144,140-154,141-136,141-137,141-138,141-148,141-151,141-155,142-145,142-152,147-134,147-150,147-153,157-22,157-162,157-175,157-176,157-177,157-180,160-21,160-158,160-161,160-162,160-164,160-179,160-230,163-164,163-167,168-20,168-169,168-170,168-171,168-178,173-166,173-174,181-37,181-158,181-172,181-230,183-34,183-133,183-182,183-194,190-188,190-211,190-222,190-223,190-227,191-24,191-184,191-187,191-208,191-212,194-182,194-183,194-193,194-195,194-198,194-213,194-220,194-228,199-1,199-36,199-159,199-200,199-214,201-26,201-200,201-226,201-231,203-27,203-39,203-202,203-224,215-27,215-33,215-213,215-221,215-239,216-59,216-204,216-217,216-218,219-31,219-77,219-185,219-196,234-233,234-237,234-238,234-239,235-38,235-213,235-233,235-236,235-240,245-42,245-105,245-243,245-244	161	29-205,29-206,29-207,40-32,40-41,40-211,40-239,40-241,45-43,45-56,48-47,48-59,48-204,55-50,55-54,57-25,57-44,57-46,60-9,60-11,61-53,61-154,62-4,62-71,63-58,63-70,65-6,65-7,65-8,65-67,65-68,65-90,65-100,65-110,69-10,69-115,74-73,74-86,74-88,74-104,74-246,75-76,75-91,78-84,80-12,80-82,93-14,93-89,95-83,95-92,98-15,98-66,98-97,101-81,101-96,101-99,102-64,103-85,106-107,106-123,106-130,116-128,116-229,117-35,117-119,122-112,122-121,125-16,125-114,125-124,129-113,129-118,129-126,129-127,129-232,132-109,132-139,132-149,140-137,140-143,140-144,141-136,141-138,141-148,141-151,141-155,142-145,142-152,147-134,147-150,147-153,157-22,157-162,157-175,157-176,157-177,157-180,160-21,160-158,160-161,160-164,160-179,160-230,163-167,168-20,168-169,168-170,168-171,168-178,173-166,173-174,181-37,181-172,183-34,183-133,183-182,190-188,190-222,190-223,190-227,191-24,191-184,191-187,191-208,191-212,194-193,194-195,194-198,194-213,194-220,194-228,199-1,199-36,199-159,199-200,199-214,201-26,201-226,201-231,203-27,203-39,203-202,203-224,215-33,215-221,216-217,216-218,219-31,219-77,219-185,219-196,234-233,234-237,234-238,235-38,235-236,235-240,245-42,245-105,245-243,245-244

Case-3	85	29-204,29-216,40-44,40-57,55-56,60-58,60-63,62-59,62-216,69-6,69-65,74-8,74-65,78-64,78-102,80-9,80-60,88-66,88-118,93-10,93-131,98-70,98-238,100-72,100-73,101-74,101-86,103-74,103-104,106-75,106-91,117-82,117-83,121-83,121-103,125-85,125-94,129-13,129-88,140-14,140-93,141-96,141-101,142-97,142-98,147-105,147-107,157-16,157-113,160-111,160-128,163-113,163-126,168-115,168-118,173-17,173-229,181-120,181-126,183-121,183-162,190-132,190-139,191-132,191-140,194-133,194-139,199-134,199-147,201-136,201-138,203-136,203-229,215-142,215-145,216-142,216-152,219-147,219-150,234-20,234-37,235-157,235-162,245-160,245-164	57	29-204,40-44,40-57,55-56,60-58,60-63,62-59,69-6,69-65,74-8,78-64,78-102,80-9,88-66,88-118,93-10,93-131,98-70,98-238,100-72,100-73,101-86,103-104,106-75,106-91,117-82,117-83,125-85,125-94,129-13,140-14,141-96,142-97,147-105,147-107,157-16,157-113,160-111,160-128,163-126,168-115,173-17,173-229,181-120,183-162,190-132,190-139,194-133,199-134,201-136,201-138,215-145,216-152,219-150,234-20,234-37,245-164
Case-4	425	2-187,3-71,3-73,4-62,5-6,6-5,6-65,7-65,7-67,7-79,7-105,9-11,9-60,10-8,10-69,10-131,11-9,11-60,11-64,11-86,12-80,15-14,15-89,15-98,15-99,19-21,19-169,21-19,21-20,21-37,21-160,21-165,21-166,23-22,23-180,24-1,24-191,24-192,24-198,27-26,27-203,27-215,27-222,27-231,28-33,28-202,29-205,29-206,29-207,30-185,31-219,32-33,32-40,32-59,32-218,32-221,34-17,34-135,34-136,34-150,34-158,34-183,35-117,35-229,38-235,40-32,40-41,40-211,40-239,40-241,41-40,44-43,44-56,44-57,44-80,45-43,45-56,47-48,48-47,48-59,48-204,49-50,49-54,50-49,50-55,51-54,52-54,53-61,54-49,54-51,54-52,54-55,54-62,56-25,56-44,56-45,56-46,56-55,56-71,56-80,57-25,57-44,57-46,61-53,61-154,62-4,62-54,62-71,65-6,65-7,65-8,65-67,65-68,65-90,65-100,65-110,68-65,68-108,69-10,69-70,69-115,69-154,71-3,71-56,71-62,71-72,74-73,74-86,74-88,74-104,74-246,77-219,78-84,78-91,80-12,80-44,80-46,80-56,80-82,80-86,82-80,82-83,82-92,83-82,83-95,83-102,83-103,83-104,84-72,84-78,84-89,84-94,87-96,87-100,88-13,88-64,88-74,88-79,88-94,89-15,89-84,89-93,93-14,93-89,95-83,95-92,97-81,97-90,97-91,97-98,97-236,100-13,100-65,100-87,101-81,101-96,101-99,106-107,106-123,106-130,109-16,109-108,109-110,109-121,109-131,109-132,111-121,111-128,112-122,113-16,113-114,113-126,113-127,113-129,118-66,118-115,118-129,118-	341	2-187,3-71,3-73,4-62,5-6,6-5,6-65,7-67,7-79,9-11,9-60,10-8,10-69,10-131,11-9,11-60,11-64,11-86,12-80,15-14,15-89,15-98,15-99,19-21,19-169,21-19,21-20,21-37,21-160,21-165,21-166,23-22,23-180,24-1,24-191,24-192,24-198,27-26,27-203,27-215,27-222,27-231,28-33,28-202,29-205,29-206,29-207,30-185,31-219,32-33,32-40,32-59,32-218,34-17,34-135,34-136,34-150,34-158,34-183,35-117,35-229,38-235,40-32,40-41,40-211,44-43,44-56,44-57,45-43,47-48,48-47,48-59,48-204,49-50,49-54,50-49,50-55,53-61,54-51,54-52,54-55,56-25,56-44,56-45,56-46,57-25,57-46,61-53,61-154,62-4,65-7,65-8,65-67,65-68,65-90,65-100,65-110,68-108,69-10,69-70,69-115,69-154,71-3,71-72,74-73,74-86,74-88,74-104,74-246,78-84,78-91,80-12,80-82,82-83,82-92,83-95,83-104,84-72,84-78,84-94,87-96,88-13,88-64,88-74,88-79,88-94,89-15,89-93,93-14,95-92,97-81,97-90,97-91,97-98,97-236,100-13,100-87,101-81,101-96,101-99,106-123,106-130,109-16,109-108,109-110,109-121,109-131,109-132,111-121,111-128,113-16,113-114,113-126,113-127,113-129,118-66,118-115,118-162,118-232,119-117,123-106,124-125,125-114,125-124,126-113,126-120,128-111,128-116,129-118,129-127,129-232,130-66,132-109,132-139,132-140,132-149,133-18,133-182,133-183,134-18,134-146,134-147,135-34,139-133,139-

		162,118-232,119-117,119-229,120-126,123-106,124-125,125-16,125-114,125-124,125-130,126-113,126-120,126-129,128-111,128-116,129-113,129-118,129-126,129-127,129-232,130-66,130-106,130-114,130-125,132-109,132-139,132-140,132-149,133-18,133-139,133-182,133-183,134-18,134-146,134-147,135-34,139-132,139-133,139-145,139-152,139-240,140-132,140-137,140-143,140-144,140-154,141-136,141-137,141-138,141-148,141-151,141-155,144-140,144-143,145-139,145-142,147-134,147-150,147-153,148-141,148-146,149-132,151-138,151-141,152-139,152-142,153-147,156-158,157-22,157-162,157-175,157-176,157-177,157-180,158-34,158-156,158-160,158-181,159-199,160-21,160-158,160-161,160-162,160-164,160-179,160-230,163-164,163-167,164-160,164-163,165-21,165-37,165-167,165-170,165-171,165-174,168-20,168-169,168-170,168-171,168-178,172-181,173-166,173-174,174-165,174-173,176-157,176-161,177-157,177-175,178-168,181-37,181-158,181-172,181-230,182-133,182-183,182-194,182-228,185-30,185-197,185-209,185-219,187-2,187-186,187-189,187-191,187-210,188-186,188-190,189-187,190-188,190-211,190-222,190-223,190-227,191-24,191-184,191-187,191-208,191-212,193-192,193-194,193-197,194-182,194-183,194-193,194-195,194-198,194-213,194-220,194-228,195-194,195-196,195-197,195-220,197-184,197-185,197-193,197-195,199-1,199-36,199-159,199-200,199-214,201-26,201-200,201-226,201-231,202-28,202-203,202-225,203-27,203-39,203-202,203-224,205-29,205-217,205-225,206-29,206-207,208-191,213-194,213-209,213-212,213-214,213-215,213-235,216-59,216-204,216-217,216-218,218-32,218-216,219-31,219-77,219-185,219-196,223-39,223-190,223-227,224-203,229-17,229-35,229-116,229-119,229-121,229-136,229-233,230-160,230-181,230-238,235-38,235-213,235-233,235-236,235-240,238-70,238-179,238-230,238-233,238-234,242-243,243-42,243-242,243-245,246-74		145,139-152,139-240,140-137,140-143,140-144,141-136,141-137,141-138,141-148,141-151,144-143,145-142,147-134,147-150,147-153,148-141,148-146,151-138,152-142,157-22,157-162,157-175,157-176,157-177,157-180,158-156,158-181,159-199,160-161,160-164,160-179,160-230,163-167,164-163,165-37,165-167,165-170,165-171,165-174,168-20,168-169,168-170,168-171,168-178,173-166,174-173,176-157,176-161,177-175,178-168,181-172,182-194,182-228,185-30,185-197,185-209,187-2,187-186,187-189,188-186,188-190,190-188,190-211,190-222,190-223,190-227,191-24,191-184,191-208,191-212,193-192,194-193,194-195,194-198,194-213,194-220,194-228,195-196,195-220,197-184,199-1,199-159,199-200,199-214,201-26,201-200,201-231,202-28,202-225,203-27,203-39,203-224,205-29,205-217,205-225,206-207,213-209,213-212,213-214,213-215,216-204,216-217,218-216,219-31,219-77,219-196,223-39,223-227,229-17,229-35,229-116,229-119,229-233,230-238,235-38,235-233,235-236,235-240,238-70,238-179,242-243,243-242

2.7 Conclusion

In this chapter, a new approach for the optimal placement of PMU with optimal number of current phasor measurements has been proposed. The formulated problem is of Binary Integer Linear Programming (BILP) problem. The Genetic Algorithm (GA) approach has been used to solve this BILP problem. Developed algorithm has been tested on IEEE-14, IEEE-30, IEEE-57 bus systems and the Northern Regional Power Grid (NRPG) 246-bus system. It is clear from the result that using the optimal approach, number of current phasor measurements can be reduced to a considerable amount, hence the overall cost can be reduced.

The result also shows that in a large power system, large number of PMUs needed to be deployed for complete observability and will entail high capital cost in their installation. These requirements pose physical and financial constraints on the PMU installation process. It is commanding to formulate a staging program for PMU installation in a phased manner and effectively utilize the PMU even during the installation process in any power system network. Therefore, the subsequent chapter proposed a technique for the placing the PMUs in phases for the PMUs obtained for case 4. This is because case 4 that ensures complete power system observability even under a branch outage or a PMU failure considering channel limit which is more practical condition.

Chapter 3: Revised Analytical Hierarchy Process based Phased Optimal Placement of PMUs

3.1 Introduction

In a large power system, there will be a large quantum of PMUs to be deployed for full observability and will entail high capital cost in their installation. These requirements pose physical and financial constraints on the PMU installation process. It is imperative to formulate a staging program for PMU installation in a phased manner and effectively utilize the PMU even during the installation process in any power system network. In 2008, enumeration of trees for finding optimal PMU placement and simulated annealing (SA) formulation for solving pragmatic based phased installation has been proposed [23]. This requires more number of PMUs needed in phasing technique than in single-phase installation. In [24], a multiphase optimal PMU placement procedure, based upon certain criteria which are important as per power system observability view point, have been worked out. In reference [25], authors proposed a new PMU placement scheme that ensures the monitoring and protection of critical buses of the system while moving toward complete observability of the network. In [26], multistage PMU placement is carried out by incorporating critical buses based on small signal stability. However, the authors in [24], [26] have not considered the effect of channel limit and the supply capacity of load buses in multistage PMU placement. In [25] authors have considered the monitoring and protection of critical buses in PMU placement but without considering multiphase PMU installation.

In the previous chapter, three different cases for the optimal placement of PMUs with optimal number of current phasors measurements have been proposed. In this chapter, a new multiphase PMU placement procedure based on voltage stability and using Revised Analytical Hierarchy Process (RAHP) has been proposed. In this approach, the first step is to determine the optimal number and locations of PMUs that ensures complete power system observability even under a branch outage or a PMU failure considering channel limit. Second step is to identify the critical buses, which are more prone to voltage collapse. These critical buses are identified using the line stability index determined by fast voltage stability index (FVSI) [88]. The objective of the present work is to monitor the most critical buses in first phase either directly (PMU bus) or indirectly (neighboring bus). To achieve this objective RAHP is used for decision-making for phasing of PMU locations. To get the maximum priority to critical buses

in the multiphase installation of PMUs, Critical Load bus Observability Criteria (CLOC) has been introduced in the decision making process along with five more observability criteria (OB) i.e. Noncritical Load bus Observability Criteria (NLOC), Generator Observability Criteria (GOC), PMUs Distribution Criteria (PDC), Tie Line Observability Criteria (TOC), and Bus Connectivity Criteria (BCC). The proposed methodology is tested on a standard IEEE 30-bus system and the Northern Regional Power Grid (NRPG) 246-bus system.

3.2 Identification of critical buses

Identification of weak or critical buses is an important task in the load dispatch center for a given operating condition. These critical buses play a vital role in view of the threat of voltage instability leading to voltage collapse. In this chapter, voltage stability analysis is conducted using line stability index indicated by fast voltage stability index (FVSI)[88] in order to determine the maximum loadability in a transmission system. The reactive power of each load is increased in small steps until it reaches the instability point at bifurcation. At the instability point, the reactive power loading of a particular bus indicates the maximum loadability for voltage stability of that particular load bus. The maximum loadability for each load bus is sorted in ascending order with the smallest value being ranked highest. The highest rank implies the weakest bus in the system that has the lowest sustainable load.

3.2.1 Line Stability Index FVSI

The line stability index FVSI is based on the concept of power flow through a single line. The FVSI [88] is derived from the voltage quadratic equation of two-bus system as shown in Figure 3-1. In this figure Pi, Qi, Si and $V_i\angle 0$ are the real power, reactive power apparent power and voltage phasor respectively of bus i. Pj, Qj, Sj and $V_j\angle\delta$ are the real power, reactive power apparent power and voltage phasor respectively of bus j.

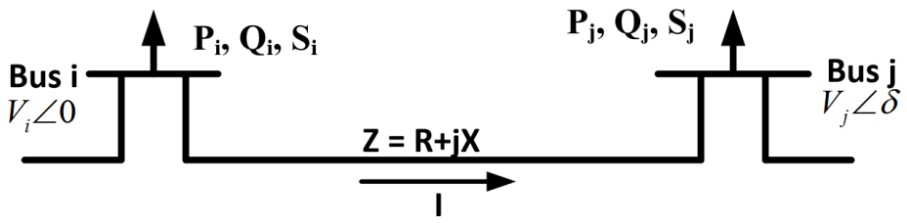

Figure 3-1: Two-bus power system model

For two bus system voltage quadratic equation can be written as:

$$V_j^2 - \left[\left(\frac{R}{X}\right)\sin\delta + \cos\delta\right]V_i V_j + \left(X + \frac{R^2}{X}\right)Q_j = 0 \tag{3.1}$$

Setting the discriminant of the equation to be greater than or equal to zero yields

$$\left[\left(\frac{R}{X}\sin\delta + \cos\delta\right)V_i\right]^2 - 4\left(X + \frac{R^2}{X}\right)Q_j \geq 0 \tag{3.2}$$

Rearranging eq. (3.2), we obtain

$$\frac{4Z^2 Q_j X}{V_i^2\left(R\sin\delta + X\cos\delta\right)^2} \leq 1 \tag{3.3}$$

Since, δ is normally very small, then $R\sin\delta = 0$ is neglected and $X\cos\delta = X$.

If a line is connected between bus *i* and *j*, the FVSI for this line is given as:

$$FVSI_{ij} = \frac{4Z^2 Q_j}{V_i^2 X} \tag{3.4}$$

The line that gives index value closest to 1 is the most critical line of that bus and may lead to a system wide instability scenario. This index can also be used to determine the weakest bus of the system.

The following are the steps have been followed to determine the weakest bus of the system.

Step 1: Run the load flow program for the base case, using Newton-Raphson method.

Step 2: Calculate the value of FVSI for every line in the system for the base case.

Step 3: Gradually increase the reactive power loading at a chosen load bus keeping the loads on the other nodes constant until load flow solution fails to converge. The load prior to divergence is the critical load for that bus.

Step 4: calculate the value of FVSI at that critical load for each line.

Step 5: Repeat steps 3 and 4 for all load buses.

Step 6: Extract the maximum reactive power loading for the maximum computable FVSI for every load bus. The maximum reactive power loading is referred as the maximum loadability of a particular bus.

Step 7: Sort the maximum loadability obtained from step 6 in ascending order. The weakest load bus of the system is that bus which changes the FVSI of a line to its maximum value with minimum increase in the reactive power of that bus.

From voltage stability monitoring point of view all critical buses must be observable in the very first phase.

3.3 Phased PMU Installation

After identifying the optimal PMU locations for complete observability, the Revised Analytical Hierarchical Process (RAHP) approach is the second step in the phases PMU installation. In the intermediate phases of PMU placement, the power system is only partially observable. This suggests that in the intermediate phases, the PMUs installation should be sequenced to maximize the number of observable buses and critical parameters in the system. In order to reach the most preferred sequence of phase wise, optimal PMU installations, certain critical criteria for control and monitoring of wide area power system should be considered. These performance indexes of WAMPCS should be in agreement with the criteria is chosen in the decision making process. As these have a very important bearing in reaching the final goal of the desired phasing process. These important criteria are Load bus Observability criteria (LOC), Generator Observability Criteria (GOC), PMUs Distribution Criteria (PDC), Tie Line Observability Criteria (TOC) and Bus Connectivity Criteria (BCC).

3.3.1 Load bus Observability Criterion (LOC)

Power system stability is one of the major issues in this emerging world of the technologies and development. Due to the excessive load demand and non-linearity in loads leads to voltage instability and ultimately leading to voltage collapse. Voltage collapse has to be given the utmost priority because it led to cascading blackouts in the whole network. Therefore, in order to avoid this voltage collapse it is important to monitor the load buses directly or indirectly using the PMUs. It is to be noted here that there may be few buses that are strategically important and are not present in optimal locations. In such a case, nearest or second nearest optimal location to that critical bus is given priority.

In this chapter, the load buses in a given system are divided into two groups, that is, critical load buses and noncritical load buses. For critical load bus, the critical load observability criteria are represented as CLOC. For the K[th] PMU bus CLOC and is given by,

$$CLOC_K = (w_{c1} \times \sum_{\forall CL} CL_{KL}) + (w_{c2} \times \sum_{\forall NCL} CL_{KNL}) + (w_{c3} \times \sum_{\forall NNCL} CL_{KNN}) \quad (3.5)$$

where $CLOC_K$ is the CLOC for k[th] PMU bus, which are more significant for voltage stability monitoring. CL_{KL} represents number of critical load buses connected to k[th] PMU bus. Similarly, CL_{KNL} and CL_{KNN} represent the number of neighboring critical buses and neighbor to neighboring critical buses, respectively connected to k[th] PMU bus. CL, NCL, and NNCL are set of critical buses, neighbor to critical load bus and neighbor-to-neighbor to critical load buses respectively w_{c1}, w_{c2} and w_{c3} are the weights given to critical load buses, neighbor to critical load bus and neighbor-to-neighbor to critical load buses. The numeric values or magnitude of weight has been chosen based on importance given to the associated parameter in (3.5). Presently, considered weights are 1, 0.8 and 0.6 respectively, which represent that maximum importance is given to critical bus than its neighboring buses.

In case of noncritical load bus, the load bus observability criteria are indicated as NLOC. For the K[th] PMU bus, it is given by the following expression:

$$NLOC_K = (w_{n1} \times \sum_{\forall NL} NL_{KL}) + (w_{n2} \times \sum_{\forall NNL} NL_{KNL}) + (w_{n3} \times \sum_{\forall NNNL} NL_{KNN}) \quad (3.6)$$

NL_{KL} represents number of noncritical load buses connected to k[th] PMU bus. Similarly, NL_{KNL} and NL_{KNN} represent the number of neighboring noncritical buses and neighbor to neighboring noncritical buses, respectively connected to k[th] PMU bus. NL, NNL, and NNNL are set of noncritical load buses, neighbor to noncritical load bus and neighbor-to-neighbor to noncritical load buses respectively. w_{n1}, w_{n2} and w_{n3} are the weights given to noncritical load buses, neighbor to noncritical load bus and neighbor-to-neighbor to noncritical load buses. The weights for w_{n1}, w_{n2} and w_{n3} are taken as 1, 0.8 and 0.6 respectively.

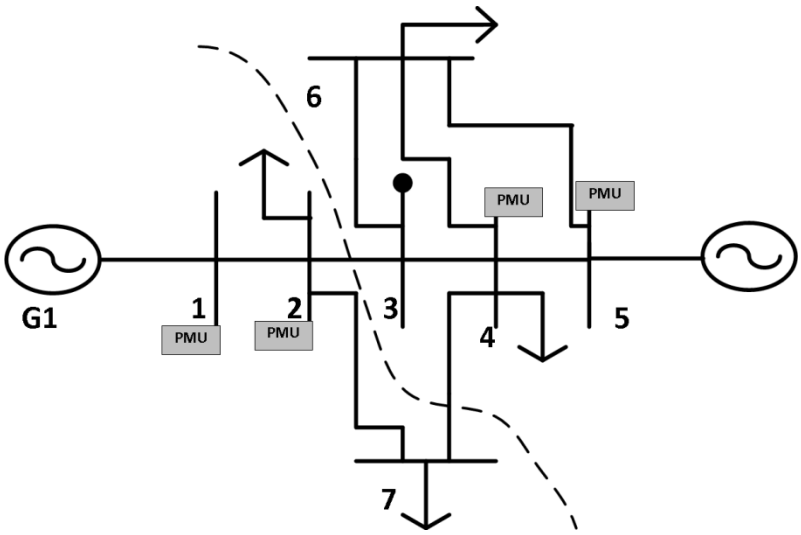

Figure 3-2: Seven-bus system

Let us take the example of seven-bus sample system as shown in Figure 3-2 for clear understating of both CLOC and NLOC. In the given example, Critical load bus buses CL identified using the procedure explained in section 3.2 are {3,7}, neighbor to critical load buses NCL are {2, 4, 6}, neighbor-to-neighbor to critical load buses NNCL is {1,5} and the PMU buses are {1, 2, 4, 5}. The buses connected to PMU bus 1 is {2}, buses connected to PMU bus 2 are {1, 3, 7}, buses connected to PMU bus 4 are {3, 5, 6, 7} and buses connected to PMU bus 5 are {4, 6}. In addition, weights w_{c1}, w_{c2} and w_{c3} are taken as 1, 0.8 and 0.6 respectively. Then the CLOC for PMU buses are:

$$\begin{aligned} CLOC_1 &= 1*0+0.8*1+0.6*1=1.4;\ CLOC_2 = 1*2+0.8*1+0.6*1=3.4 \\ CLOC_4 &= 1*2+0.8*2+0.6*1=4.2;\ CLOC_5 = 1*0+0.8*2+0.6*1=2.2 \end{aligned} \tag{3.7}$$

Similarly Noncritical load bus buses NL is {2, 4, 6}, neighbor to critical load buses NNL is {1, 3, 5, 7}, neighbor-to-neighbor to critical load buses NNCL is { }, i.e. empty. In addition, weights w_{n1}, w_{n2} and w_{n3} are taken as 1, 0.8 and 0.6 respectively. Then the NLOC for PMU buses are:

$$\begin{aligned} NLOC_1 &= 1*1+0.8*1+0.6*0=1.8;\ NLOC_2 = 1*1+0.8*3+0.6*0=3.4 \\ NLOC_4 &= 1*2+0.8*3+0.6*0=4.4;\ NLOC_5 = 1*2+0.8*1+0.6*0=2.8 \end{aligned} \tag{3.8}$$

3.3.2 Generator Observability Criterion (GOC)

Power systems are highly inductive in nature due to the abundance of motors and industrial loads in the system. Generators and synchronous condensers assist in supplying the required

reactive power to such loads in the system. The reactive power generation should be commensurate with the reactive power consumed by the loads. The generators and reactors affect the voltage stability of the power system. The efficiency of these reactors and generators depend upon their location and output. In order to have more close and real time control and to contain damage to the power system in case of eventuality the Generator buses should be observable. In this case, Generator bus will have a higher weight than those connected to neighbor or neighbor-to-neighbor Generator buses. A weighting process related to GOC for PMU buses is given by,

$$GOC_K = (w_1 \times \sum_{\forall G} G_{KG}) + (w_2 \times \sum_{\forall NG} G_{KNG}) + (w_3 \times \sum_{\forall NN} G_{KNN}) \quad (3.9)$$

GOC_K is the GOC for kth PMU bus. G_{KG} is the number of Generator-buses connected to k^{th} PMU bus. G_{KNG} is the number of neighboring Generator buses connected to k^{th} PMU bus. G_{KNN} is the number of neighbor-to-neighbor Generator buses connected to k^{th} PMU bus. G, NG, and NN are set of generator buses, neighbor to generator bus and neighbor-to-neighbor to Generator buses respectively. w_1, w_2 and w_3 are weights given to generator buses, neighbor to generator bus and neighbor-to-neighbor to Generator buses. The numeric values or magnitude of weight has been chosen based on importance given to the associated parameter in (3.9). In this work, the weights considered are 1, 0.8 and 0.6 respectively, which represent that maximum importance is given to the generator bus than its neighboring buses.

For the example of 7-bus sample system, Generator buses G is {1, 5}, neighbor to generator bus NG is {2, 4, 6}, neighbor-to-neighbor to Generator buses NN is {3, 7} and the PMU buses are {1,2, 4,5}. In addition, weights w_1, w_2 and w_3 are taken as 1, 0.8 and 0.6 respectively. Then the Generator Observability Criterion (GOC) for PMU buses are:

$$\begin{aligned} GOC_1 &= 1*1+0.8*1+0.6*0 = 1.8;\ GOC_2 = 1*1+0.8*1+0.6*2 = 3 \\ GOC_4 &= 1*1+0.8*2+0.6*2 = 3.8;\ GOC_5 = 1*1+0.8*2+0.6*0 = 2.6 \end{aligned} \quad (3.10)$$

3.3.3 PMU Distribution Criteria (PDC)

Electrical distance is used as a measure to derive a physical relationship between any two buses in the power system. PMUs should be sparsely located in the power system network during the process of their installation. Using electrical distance as physical relationship, the voltage

control areas are defined. The electrical distance between two buses *i* and *j* in the power network is given as follows [89]:

$$Electrical\ Distance\ \ ed_{ij} = ed_{ji} = -\log_{10}\left(\alpha_{ij} \times \alpha_{ji}\right) \tag{3.11}$$

where α_{ij} is defined as $\left[J_{ij}^{-1} / J_{ii}^{-1}\right]$ and J_{ij}^{-1} is sensitivity matrix $\left[\partial V_i / \partial Q_j\right]$ and this value is inverse of Jacobian matrix, which indicates the effect on a voltage variation at neighboring buses to reactive power injection at a bus. Now the PDC can be calculated for each PMU bus as given by (3.12).

$$PDC_k = \sum_{\forall m} ed_{km} \tag{3.12}$$

where, m ∈ PMU buses

The electrical distance for the 7-bus sample system is shown in Table **3-1** using (3.11).

Table 3-1: Electrical Distance for the 7-bus sample system

Buses	**1**	**2**	**3**	**4**	**5**	**6**	**7**
1	**0**	**0.01043**	0.03767	**0.04281**	**0.06035**	0.04986	0.03665
2	**0.01043**	**0**	0.02723	**0.03237**	**0.04991**	0.03942	0.02621
3	**0.03767**	**0.02723**	0	**0.01693**	**0.03239**	0.01887	0.03216
4	**0.04281**	**0.03237**	0.01693	**0**	**0.02147**	0.01671	0.02650
5	**0.06035**	**0.04991**	0.03239	**0.02147**	**0**	0.02465	0.04595
6	**0.04986**	**0.03942**	0.01887	**0.01671**	**0.02465**	0	0.03826
7	**0.03665**	**0.0262166**	0.032164	**0.026501**	**0.04595**	0.03826	0

The PMU Distribution Criteria (PDC) for the PMU buses is calculated using (3.12) are:

$$\begin{aligned} PDC_1 &= 0.1136;\ PDC_2 = 0.0927 \\ PDC_4 &= 0.0967;\ PDC_5 = 0.1317 \end{aligned} \tag{3.13}$$

3.3.4 Tie Line Observability Criteria (TOC)

The transmission and sub-transmission networks topologically form mesh and ring networks and presence of tie-lines allows power flow on multiple paths between any two points in the power system network. Such redundancy allows power flow to load even when a part of the transmission line or generator goes offline. The power system tie line is a vital health-monitoring index of any power system and PMUs should be placed on priority at such

locations. Especially dynamic changes in tie-line power flows and phase angle difference at its two ends are important precursors to power oscillations in a system[24]. In a power system, TOC measurement can be calculated as discussed below.

Prepare three lists *viz*. list of tie-line buses having elements as $TI_{i,}$ list of tie-line neighboring buses with each element of the list as NT_i bus locations and Optimal PMU locations with elements as $M_{k.}$

If $M_k \in TI_i$ then for bus k, $TOC_k=N_{bk}$, where N_{bk} is the number of buses connected to bus k.

If $M_k \in NT_i$ then for bus k, $TOC_k=NI_{i,}$ where NI_i is the number of tie line buses connected to bus k.

If $M_k \notin TI_i$, $M_k \notin NT_j$, then for bus k, TOC_k=Zero.

The 7-bus sample system has been partitioned using eigenvector based partitioning approach[90]. The two partitioned blocks of the system with bus numbers in block I [1 2 7] and block II [3 4 5 6] are shown in Figure 3-2. There are two tie-lines in the partitioned network viz. 2-3 and 4-7.

List of tie-line buses TI are {2 3 4 7}, and list of tie-line neighboring buses NT are {1 5 6}, then TOC for PMU buses are:

$$\begin{aligned} TOC_1 &= 1; \; TOC_2 = 3 \\ TOC_4 &= 4; \; TOC_5 = 1 \end{aligned} \tag{3.14}$$

3.3.5 Bus Connectivity Criteria (BCC)

Bus Connectivity Criteria (BCC) for any optimal PMU bus location is equal to the total number of buses connected to it [24]. This is a quantitative criterion and is included in the phasing problem to maximize the observability of the power system by giving more preference to the buses have maximum connectivity with other buses. BCC for PMU bus k, is given by (3.15).

$$BCC_k = \sum_{j=1}^{N} B_{kj} \tag{3.15}$$

where, N is the total number of buses.

$$B_{kj} = \begin{cases} 1 \ \ if \ PMU \ bus \ k \ is \ directly \ connected \ to \ bus \ j \\ 0 \qquad\qquad\qquad\qquad\qquad otherwise \end{cases} \tag{3.16}$$

BCCs for the PMU buses connected in 7-bus sample system are

$$\begin{aligned} BCC_1 = 2;\ BCC_2 = 4 \\ BCC_4 = 5;\ BCC_5 = 3 \end{aligned} \tag{3.17}$$

3.4 Revised Analytical Hierarchical Process

Revised Analytical Hierarchical Process (RAHP) is a decision making technique introduced by Belton and Gear in 1983 [91]. The decision making process involves many intangibles that need to be traded off in a decision process. These criteria have to be measured alongside these tangibles and need to be evaluated how well they serve the objectives of decision maker. RAHP is a theory of measurements through pairwise comparisons and relies on judgments of experts to derive priority scales. In this process, the decision maker has to convert the opinion in terms of value of pairwise comparison, one at a time [92]. Decision-making is a formal mathematical science, which involves many criteria and sub criteria that are used to rank the alternatives of a decision process. The approach takes both qualitative and quantitative aspects of a decision into account and involves building the hierarchy of decision elements. The decision-making can be organized in the following steps as shown in Figure 3-3.

The RAHP of decision making starts with defining the main goal and then identifying some main criteria organized in a decision hierarchy which contributes in final decision making [93]. Set these criteria in a hierarchy; make the comparisons based on the importance or dominance of one criterion over other. These comparisons are made on 9-point linguistic scale as given in Table 3-2.

Table 3-2: Scale of relative importance

Scale rating	Linguistic Comparison
1	Equally preferred
3	Moderately preferred
5	Strongly (essentially) preferred
7	Very strongly preferred
9	Extremely strongly preferred
2,4,6,8	Intermediate values

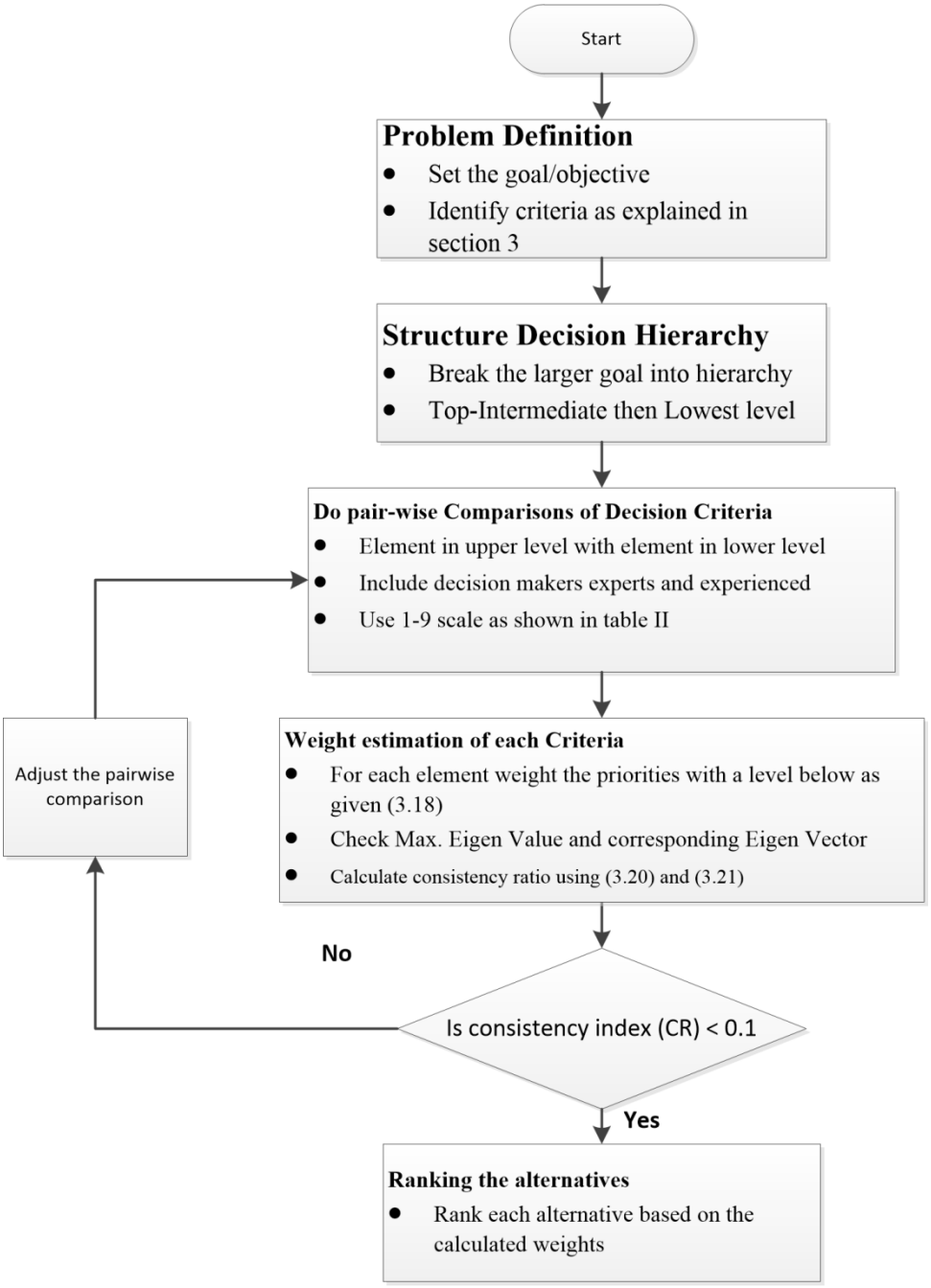

Figure 3-3: Steps in Revised Analytic Hierarchy Process

After doing pairwise comparisons, the first step is to form an Overall Preference Matrix (A). The six criteria: 1. CLOC (weight C_1); 2. GOC (weight C_2); 3. TOC (weight C_3); 4. NLOC (weight C_4); 5. PDC (weight C_5) and 6. BCC (weight C_6) discussed in section 3.3 are used to form the Overall Preference Matrix (A) which is given as:

$$A=\begin{bmatrix} C_1/C_1 & C_1/C_2 & C_1/C_3 & C_1/C_4 & C_1/C_5 & C_1/C_6 \\ C_2/C_1 & C_2/C_2 & C_2/C_3 & C_2/C_4 & C_2/C_5 & C_2/C_6 \\ C_3/C_1 & C_3/C_2 & C_3/C_3 & C_3/C_4 & C_3/C_5 & C_3/C_6 \\ C_4/C_1 & C_4/C_2 & C_4/C_3 & C_4/C_4 & C_4/C_5 & C_4/C_6 \\ C_5/C_1 & C_5/C_2 & C_5/C_3 & C_5/C_4 & C_5/C_5 & C_5/C_6 \\ C_6/C_1 & C_6/C_2 & C_6/C_3 & C_6/C_4 & C_6/C_5 & C_6/C_6 \end{bmatrix} \quad (3.18)$$

The fractional value of criteria C_i / C_j is a relative comparison of criteria *i* against criteria *j*.

Table 3-3: Linguistic statement forming pairwise matrix

SL. NO.	WEIGHT RATIO	STATEMENT
1	C1/C6=9	CLOC is considered an extremely important factor as compared to BCC
2	C1/C5=7	CLOC is considered very strongly important as compared to PDC
3	C1/C4=6	CLOC is considered 6 times more important than NLOC
4	C1/C3=4	CLOC is considered 4 times more important than TOC
5	C1/C2=2	CLOC is considered 2times more important than GOC
6	C2/C6=7	GOC is considered very strongly important as compared to BCC
7	C2/C5=6	GOC is considered 6 times more important than PDC
8	C2/C4=4	GOC is considered 4 times more important than NLOC
9	C2/C3=2	GOC is considered 2 times more important than TOC
10	C3/C6=5	TOC is considered essentially (strongly) important to BCC
11	C3/C5=2	TOC is considered 2 times more important than PDC
12	C3/C4=5	TOC is considered essentially (strongly) important to NLOC
13	C4/C6=3	NLOC is considered moderately important to BCC
14	C4/C5=2	NLOC is considered 2 times more important than PDC
15	C5/C6=2	PDC is considered 2 times more important than BCC

All six criteria are prioritized using 15 rules given in Table 3-3 and used to determine the entry of matrix A, given as:

$$A=\begin{bmatrix} 1 & 2 & 4 & 6 & 7 & 9 \\ 1/2 & 1 & 2 & 4 & 6 & 7 \\ 1/4 & 1/2 & 1 & 5 & 2 & 5 \\ 1/6 & 1/4 & 1/5 & 1 & 2 & 3 \\ 1/7 & 1/6 & 1/2 & 1/2 & 1 & 2 \\ 1/9 & 1/7 & 1/5 & 1/3 & 1/2 & 1 \end{bmatrix} \tag{3.19}$$

Consistency check (consistency in judgment) [91], of matrix A has been performed in the following two steps.

I. Determine the Consistency Index (CI)

$$CI=\frac{\lambda_{\max}-n}{n-1} \tag{3.20}$$

II. Calculate Consistency Ratio (CR)

$$CR=\frac{CI}{RI} \tag{3.21}$$

where, $\lambda_{\max}$ is the maximum eigenvalue of matrix A and n is the number of criteria considered. For six criteria, the average random consistency index (RI), which is empirically valued and is equal to 1.24. If the value of CR is less than 10% then the selected judgment is within the consistency limit [92]. In this work, the value of CR is calculated 0.0438 or 4.38%, which is much less than 10%.

Let LV_i is the left eigenvector of a matrix A corresponding to maximum eigenvalue $\lambda_{\max}$, then the weight vector can be represented as:

$$W_i=\frac{v_i}{\sum_{j=1}^{6} v_j} \tag{3.22}$$

where v1, v2, v3, v4, v5and v6 are the elements of LVi. Weight vector W for matrix A is determined as [0.4253, 0.2578, 0.1615, 0.0701, 0.0536, 0.0316].

Let k alternatives (optimal PMU locations) are available for PMU installation and *i* is the total number of criteria considered for the multiphase installation of PMU. Then V_{ki} defines the normalized value of each criteria associated with each alternative. For example V_{26} is the normalized value of criteria 6 (i. e. BCC) associated with 2nd alternative, which is determined by (3.15).

The PMU installation index (PMII) for kth alternative is calculated based on the weight matrix (W) and a criteria value V_{ki} for each location, given as:

$$PMII_k = \sum_{i=1}^{6} W_i V_{ki},\ where\, k = 1, 2, 3.....M \tag{3.23}$$

where $PMII_k$ provides the index value for ranking the alternatives. The six criteria normalized weights for the optimal PMU locations and PMII for 7-bus system are shown in Table 3-4.

Table 3-4: Normalized Weights and PMU Rankings for 7-bus sample system

Sl. No.	OPP Bus	CLOC	GOC	TOC	NLOC	PDC	BCC	PMII	Ranking
1	1	0.33	0.47	0.20	0.41	0.86	0.40	0.3838	4
2	2	0.81	0.79	0.80	0.77	0.70	0.80	0.7943	2
3	4	1.00	1.00	1.00	1.00	0.73	1.00	0.9857	1
4	5	0.52	0.68	0.20	0.64	1.00	0.60	0.5487	3

The PMU installation for the 7-bus sample system is assumed to be carried out in total two phases with 2 PMUs in each phase. In the given sample system, load bus 3 and 7 are the most critical buses for voltage stability monitoring as discussed in section 3. With the placement of PMUs at buses 4 and 2 according to the ranking in Table 3-4 in phase1 make the 7-bus sample system completely observable. The inclusion of 2 more PMUs at buses 5 and 1 in phase 2, makes every bus in the system observed by two PMUs, then a line outage and a PMU failure will not affect the complete observability of the network.

3.5 Simulation Results and Discussion

The effectiveness of the proposed methodology has been studied on IEEE 30-bus system [94] and NRPG 246-bus Indian systems[95]. The details of the test system are given in Appendix A. In present work, all simulation studies are carried out on Intel Core i7-2600 central processing unit, with 3.40GHz processing speed and 16GB RAM and implemented with

MATLAB version R2013a[96]. The optimal PMU numbers and locations for complete observability with conventional measurement and for N-1 contingency are obtained as discussed in chapter 2 section 2.4.

3.5.1 Multi-phase PMU installation

3.5.1.1 IEEE 30 Bus System

The optimal number and location of PMUs are obtained as given in table 2-4 in chapter 2 section 2.6.2. IEEE-30 bus system required 15 PMUs for complete observability with conventional measurement and for N-1 contingency at the buses {1, 2, 4, 5, 10, 13, 15, 17, 18, 20, 23, 25, 27, 28}. Now our objective is to rank these buses for phased PMU installation. The PMU phased installations assume to be carried out in three phases with five PMUs in each phase.

In this chapter, the phased installation is done based on voltage stability. Therefore, the next step is to identify the most critical buses in the IEEE 30 bus system. The ranking of the load buses is carried out according to the procedure as explained in section 3.2 and is shown in Table 3-5. Load bus 30 is ranked 1 with maximum loadability (Qmax) 31.9 MVAR. In this chapter, top five ranked load buses are considered as critical load buses {30, 26, 10, 29, 15}.

Table 3-5: Load bus ranking for IEEE-30 bus system

Load bus	Qmax	FVSI	Critical bus Ranking	Load Bus	Qmax	FVSI	Critical bus Ranking
30	31.9	0.98337	**1**	19	95.4	0.8704	**13**
26	39.3	0.95733	**2**	16	95.8	0.9978	**14**
10	43	0.99583	**3**	17	97.8	0.9898	**15**
29	43.9	0.99279	**4**	28	102	0.9902	**16**
15	52.5	0.98560	**5**	9	110	0.9970	**17**
25	54	0.98342	**6**	5	113	0.9957	**18**
11	70	0.71651	**7**	6	122	0.9954	**19**
14	73.6	0.98778	**8**	3	122.2	0.9930	**20**
24	74.7	0.99378	**9**	4	127.6	0.9937	**21**
18	81.9	0.99808	**10**	21	140.2	0.5548	**22**
20	89.7	0.99550	**11**	7	148.9	0.9930	**23**
12	92.5	0.99472	**12**	8	226	0.4835	**24**

IEEE 30 bus system has been partitioned using eigenvector based partitioning approach [90]. The two partitioned blocks of the system with bus numbers in block I {29 30 27 26 11 25 28 8 5 7 1 20 19 22 9} and block II {24 3 17 21 13 2 18 10 16 23 6 4 14 15 12} are shown in Figure 3-4.

Normalized weights for all the six criteria as discussed in section 3.3 are given in Table 3-6. PMU Installation Index (PMII) for all PMU buses is also given in this table. Now based on PMII values all the PMU buses are ranked for phase wise installation of PMUs. Ranking of the PMU buses are shown in Table 3-6.

A close inspection of Table 3-7 reveals that in phase -1 itself, all critical load buses are having PMUs, to aid voltage stability monitoring and control. In total, 23 buses are observed in phase 1. Moreover, in phase 2, the system becomes completely observable by installing next five PMUs. By phase 3, installing all 15 PMUs will make each of the buses observed by at least two PMUs. Thus, the system will remain observable even if a PMU fails or line outages occur.

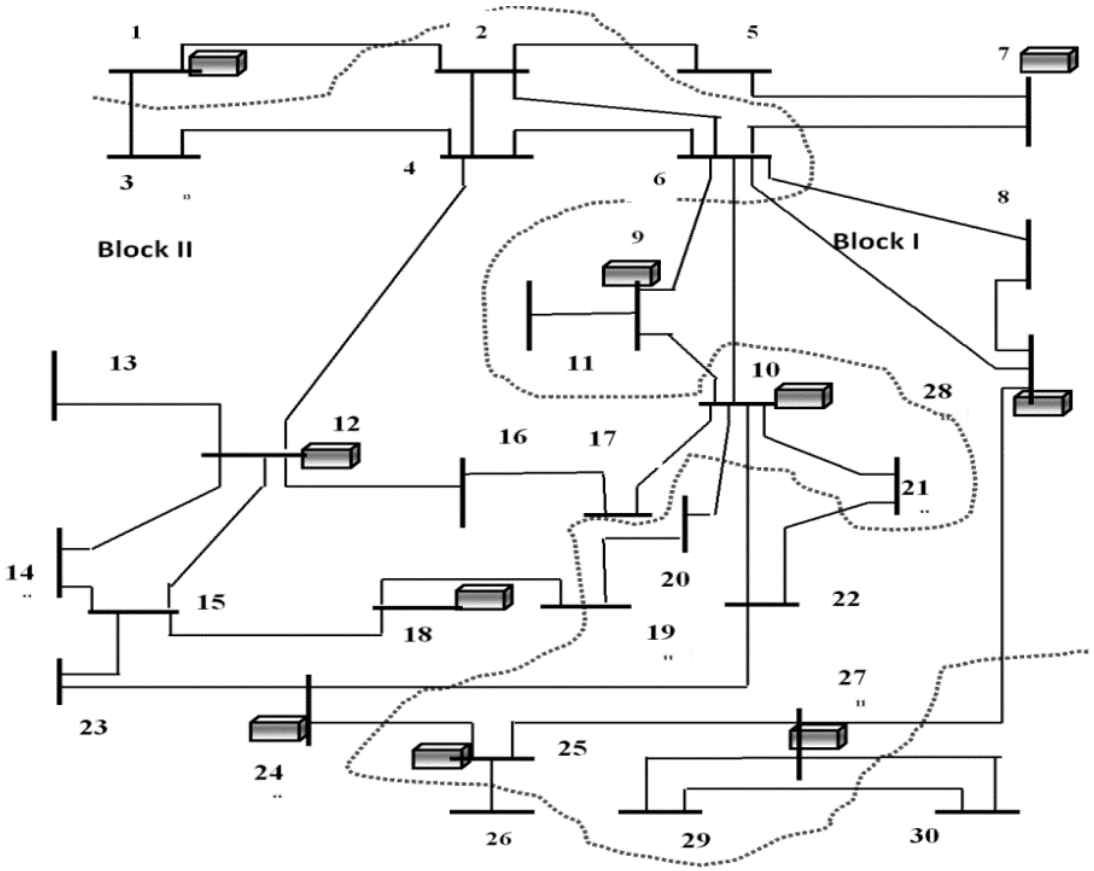

Figure 3-4: Partitioned IEEE-30 bus system with Optimal PMU Placement

Table 3-6: Normalized Weights and PMU Rankings for IEEE 30-Bus System

Sl. No.	OPP Bus	CLOC	GOC	TOC	NLOC	PDC	BCC	PMII	Ranking
1	1	0	0.609	0.429	0.342	0.666	0.429	0.299	**13**
2	2	0.115	1	0.286	0.579	0.596	0.714	0.448	**7**
3	4	0.115	0.913	0.714	0.632	0.504	0.714	0.494	**5**

Sl. No.	OPP Bus	CLOC	GOC	TOC	NLOC	PDC	BCC	PMII	Ranking
4	5	0	0.609	0	0.342	0.763	0.429	0.235	**14**
5	10	1	0.478	1	0.974	0.487	1	0.836	**1**
6	12	0.115	0.957	0.857	1	0.547	0.857	0.561	**3**
7	13	0	0.391	0.143	0.237	0.843	0.286	0.195	**15**
8	15	0.423	0.435	0.143	0.816	0.577	0.714	0.426	**9**
9	17	0.269	0.261	0.429	0.553	0.612	0.429	0.336	**11**
10	18	0.462	0.13	0	0.447	0.79	0.429	0.317	**12**
11	20	0.5	0.13	0.429	0.368	0.754	0.429	0.395	**10**
12	23	0.654	0.13	0.286	0.553	0.567	0.571	0.445	**8**
13	25	0.692	0.13	0.571	0.474	1	0.571	0.525	**4**
14	27	0.808	0.304	0.714	0.605	0.95	0.714	0.653	**2**
15	28	0.385	0.696	0.143	0.5	0.568	0.571	0.45	**6**

Table 3-7: Phased PMU placement for IEEE-30 bus system

Phase	Bus number for PMU placements
1	10, 27, 12, 25, 4
2	28, 2, 23 15, 20
3	17, 18, 1, 5, 13

3.5.1.2 Northern Regional Power Grid

The Northern Regional Power Grid (NRPG) is spreads across nine states of India viz. Jammu & Kashmir (J&K), Punjab (PB), Himachal Pradesh (HP), Uttarakhand (UK), Rajasthan (RJ), Chandigarh, Delhi (DL), Haryana (HR) and Uttar Pradesh (UP). The partitioned regions and corresponding buses in each region is shown in Table 3-8. The optimal number and location of PMUs are obtained as given in table 2-7 in chapter 2 section 2.6.4. The PMU buses are {2, 3, 4, 5, 6, 7, 9, 10, 11, 12, 15, 19, 21, 23, 24, 27, 28, 29, 30, 31, 32, 34, 35, 38, 40, 41, 44, 45, 47, 48, 49, 50, 51, 52, 53, 54, 56, 57, 61, 62, 65, 68, 69, 71, 74, 77, 78, 80, 82, 83, 84, 87, 88, 89, 93, 95, 97, 100, 101, 106, 109, 111, 112, 113, 118, 119, 120, 123, 124, 125, 126, 128, 129, 130, 132, 133, 134, 135, 139, 140, 141, 144, 145, 147, 148, 149, 151, 152, 153, 156, 157, 158, 159, 160, 163, 164, 165, 168, 172, 173, 174, 176, 177, 178, 181, 182, 185, 187, 188, 189, 190, 191, 193, 194, 195, 197, 199, 201, 202, 203, 205, 206, 208, 213, 216, 218, 219, 223, 224, 229, 230, 235, 238, 242, 243, 246 }. The PMU phased installations are assume to be carried out in five phases with 28 PMUs in 1st phase and 27 PMUs in next 4 phases. Table 3-9 shows the top 20 critical load bus identified by the method discussed in section 3.2.

Table 3-8: NRPG-246 bus system Partitioned Regions and Total Buses

No.	Name	Bus numbers	Tot
1	**J&K**	4,25,44,46,50,51,54,57,62,71,43,45,49,52,55,56	16
2	**HP**	3,5,6,7,8,9,10,11,12,42,58,60,63,77 244,245,246	17
3	**UK**	2,30,31,185,208,209,219	07
4	**UP**	1,24,26,27,28,29,32,33,36,38,39,40,41,47,48,59,139,182,184,186-207,210-218,220-228,231,233,234,235,237,239,240,241	67
5	**PB**	14,15,64-67,72-76,78-104,236,242,243	41
6	**HR**	13,16,17,34,35,53,61,68,69,70,105-131,229,232	39
7	**DL**	18,132-138,140-155,183,	25
8	**RJ**	19-23,37,156-181,230,238	34
		Total	**246**

Table 3-9: Load bus ranking for NRPG-246 bus system

Load bus	Qmax	FVSI	Critical Bus Ranking	Load Bus	Qmax	FVSI	Critical Bus Ranking
168	0.6	0.99377	**1**	194	5.5	0.9691	**11**
171	1.3	0.95833	**2**	187	5.6	0.9334	**12**
169	1.5	0.99853	**3**	193	5.8	09510	**13**
188	1.8	0.99129	**4**	189	6.3	0.8472	**14**
190	2.1	0.99010	**5**	186	7.1	0.7447	**15**
170	2.3	0.98562	**6**	184	8.5	0.7448	**16**
191	3.2	0.98550	**7**	157	17	0.9954	**17**
195	3.4	0.91160	**8**	196	18	0.9390	**18**
172	3.5	0.85164	**9**	185	18	0.9837	**19**
156	3.5	0.9838	**10**	182	35	0.9854	**20**

Normalized weights for all the six criteria as discussed in section 3.3 are given in Table 3-10. PMU Installation Index (PMII) for all PMU buses is also given in this table. Now based on PMII values all the PMU buses are ranked for phase wise installation of PMUs. Ranking of the PMU buses are shown in Table 3-10.

Table 3-10: Normalized Weights and PMU Rankings for NRPG-246 bus system

Sl. No.	OPP Bus	CLOC	GOC	TOC	NLOC	PDC	BCC	PMII	Ranking
1	2	0.225	0.075472	0.222222	0.132075	1	0.222222	0.220961	**64**
2	3	0	0.245283	0.333333	0.264151	0.243571	0.333333	0.159186	**86**
3	4	0	0.169811	0	0.169811	0.177005	0.222222	0.072207	**128**
4	5	0	0.169811	0.111111	0.132075	0.414543	0.222222	0.100242	**119**
5	6	0	0.226415	0.333333	0.226415	0.365666	0.333333	0.158224	**88**
6	7	0	0.301887	0.555556	0.45283	0.307711	0.555556	0.233357	**60**
7	9	0	0.245283	0.111111	0.245283	0.315942	0.333333	0.125863	**101**
8	10	0	0.415094	0.444444	0.339623	0.667304	0.444444	0.25244	**50**
9	11	0	0.396226	0.555556	0.433962	0.208824	0.555556	0.251054	**51**

Sl. No.	OPP Bus	CLOC	GOC	TOC	NLOC	PDC	BCC	PMII	Ranking
10	12	0	0.075472	0.222222	0.169811	0.157844	0.222222	0.082738	**126**
11	15	0	0.396226	0	0.433962	0.294543	0.555556	0.165947	**82**
12	19	0.3	0.245283	0	0.188679	0.360042	0.333333	0.233918	**58**
13	21	0.6	0.735849	0	0.54717	0.374794	0.777778	0.527979	**11**
14	23	0.275	0.245283	0	0.226415	0.376908	0.333333	0.226836	**63**
15	24	0.5	0.396226	0.111111	0.415094	0.342471	0.555556	0.397803	**29**
16	27	0.25	0.54717	0	0.528302	0.192905	0.666667	0.315874	**38**
17	28	0	0.226415	0	0.245283	0.195881	0.333333	0.096618	**121**
18	29	0	0.226415	0	0.358491	0.2968	0.444444	0.113481	**107**
19	30	0.225	0.075472	0.111111	0.132075	0.400585	0.222222	0.170871	**80**
20	31	0.175	0.075472	0.111111	0.169811	0.36753	0.222222	0.150477	**91**
21	32	0.15	0.811321	0	0.509434	0.328224	0.666667	0.347381	**32**
22	34	0.275	0.54717	0.777778	0.622642	0.25225	0.777778	0.465404	**21**
23	35	0	0.150943	0.111111	0.264151	0.28823	0.333333	0.101377	**117**
24	38	0.075	0.169811	0.111111	0.169811	0.323846	0.222222	0.129924	**95**
25	40	0.175	0.716981	0	0.490566	0.332179	0.666667	0.332579	**34**
26	41	0.075	0.169811	0	0.132075	0.155483	0.222222	0.100307	**118**
27	44	0	0.226415	0.555556	0.584906	0.157963	0.555556	0.21513	**65**
28	45	0	0.075472	0.111111	0.396226	0.19266	0.333333	0.086055	**125**
29	47	0	0.075472	0	0.301887	0.258466	0.222222	0.061516	**132**
30	48	0	0.377358	0	0.54717	0.225358	0.444444	0.1618	**85**
31	49	0	0.075472	0	0.45283	0.179539	0.333333	0.07138	**129**
32	50	0	0.264151	0	0.45283	0.183462	0.333333	0.120237	**104**
33	51	0	0.075472	0	0.301887	0.206547	0.222222	0.058731	**134**
34	52	0	0.075472	0	0.301887	0.177596	0.222222	0.057178	**135**
35	53	0	0.169811	0.111111	0.301887	0.372333	0.222222	0.109887	**110**
36	54	0	0.698113	0	0.849057	0.168865	0.666667	0.269664	**47**
37	56	0	0.943396	0.888889	0.962264	0.46344	0.888889	0.507193	**14**
38	57	0	0.433962	0.222222	0.471698	0.177574	0.444444	0.20442	**67**
39	61	0	0.245283	0.333333	0.45283	0.338371	0.333333	0.177504	**74**
40	62	0	0.396226	0.111111	0.415094	0.159087	0.444444	0.171788	**79**
41	65	0	1	1	0.90566	0.310477	1	0.531065	**8**
42	68	0	0.207547	0.333333	0.396226	0.642996	0.333333	0.180143	**72**
43	69	0	0.584906	0.555556	0.622642	0.333666	0.555556	0.319629	**37**
44	71	0	0.584906	0.555556	0.509434	0.340753	0.555556	0.312069	**40**
45	74	0	0.226415	0.666667	0.735849	0.341905	0.666667	0.257034	**49**
46	77	0.175	0.075472	0.222222	0.245283	0.38101	0.222222	0.174434	**77**
47	78	0	0.150943	0.111111	0.396226	0.191239	0.333333	0.105437	**115**
48	80	0	0.716981	0.777778	0.811321	0.269413	0.777778	0.406372	**28**
49	82	0	0.075472	0.111111	0.54717	0.167197	0.444444	0.098786	**120**
50	83	0	0.264151	0	0.90566	0.17669	0.666667	0.162166	**84**
51	84	0	0.509434	0.111111	0.698113	0.345817	0.555556	0.234351	**57**
52	87	0	0.207547	0.111111	0.396226	0.352129	0.333333	0.128661	**97**
53	88	0	0.584906	0.666667	0.660377	0.346176	0.666667	0.344398	**33**

Sl. No.	OPP Bus	CLOC	GOC	TOC	NLOC	PDC	BCC	PMII	Ranking
54	89	0	0.320755	0	0.415094	0.245779	0.444444	0.139038	**94**
55	93	0	0.245283	0	0.264151	0.296666	0.333333	0.108211	**111**
56	95	0	0	0	0.45283	0.168506	0.333333	0.05133	**136**
57	97	0	0.528302	0.333333	0.735849	0.346169	0.666667	0.281274	**42**
58	100	0	0.377358	0.444444	0.415094	0.33592	0.444444	0.23023	**62**
59	101	0	0.339623	0	0.54717	0.344453	0.444444	0.158458	**87**
60	106	0	0.264151	0.111111	0.603774	0.572061	0.444444	0.173118	**78**
61	109	0.075	0.716981	0.777778	0.811321	0.311584	0.777778	0.440534	**24**
62	111	0.075	0.075472	0.111111	0.396226	0.347513	0.333333	0.12626	**100**
63	112	0	0.132075	0	0.301887	0.450379	0.222222	0.086403	**124**
64	113	0	0.698113	0	0.773585	0.367039	0.666667	0.275	**44**
65	118	0.175	0.54717	0.666667	0.849057	0.368038	0.666667	0.423508	**26**
66	119	0	0.150943	0.111111	0.339623	0.291352	0.333333	0.106837	**113**
67	120	0	0.132075	0	0.301887	0.494496	0.222222	0.088769	**123**
68	123	0	0	0	0.301887	0.617957	0.222222	0.061338	**133**
69	124	0	0.075472	0	0.245283	0.4482	0.222222	0.067722	**131**
70	125	0	0.566038	0.111111	0.622642	0.384434	0.555556	0.245724	**54**
71	126	0	0.207547	0	0.54717	0.426225	0.444444	0.128791	**96**
72	128	0	0.264151	0	0.45283	0.334118	0.333333	0.128317	**98**
73	129	0.075	0.54717	0.111111	0.849057	0.365136	0.666667	0.291114	**41**
74	130	0	0.339623	0.555556	0.698113	0.456006	0.555556	0.268243	**48**
75	132	0.075	0.283019	0.555556	0.698113	0.259388	0.555556	0.275004	**43**
76	133	0.475	0.509434	0.555556	0.490566	0.242629	0.555556	0.488059	**18**
77	134	0.075	0.433962	0	0.471698	0.246815	0.444444	0.204152	**68**
78	135	0.075	0.169811	0.222222	0.169811	0.266289	0.222222	0.144778	**93**
79	139	0.175	0.283019	0.666667	0.849057	0.253159	0.666667	0.349241	**31**
80	140	0	0.698113	0.222222	0.90566	0.261965	0.666667	0.314509	**39**
81	141	0	0.415094	0.111111	1	0.249703	0.777778	0.233068	**61**
82	144	0	0.207547	0	0.45283	0.279039	0.333333	0.110769	**108**
83	145	0.075	0.132075	0.333333	0.45283	0.266497	0.333333	0.176361	**76**
84	147	0	0.150943	0.111111	0.490566	0.258749	0.444444	0.119186	**105**
85	148	0	0.264151	0	0.45283	0.252308	0.333333	0.12393	**103**
86	149	0	0.132075	0.111111	0.301887	0.305488	0.222222	0.096573	**122**
87	151	0	0.264151	0	0.45283	0.265082	0.333333	0.124615	**102**
88	152	0.075	0.132075	0.333333	0.45283	0.268254	0.333333	0.176455	**75**
89	153	0	0.132075	0	0.301887	0.270118	0.222222	0.076735	**127**
90	156	0.225	0.075472	0.111111	0.169811	0.704307	0.222222	0.189807	**71**
91	157	0.725	0.773585	0.111111	0.603774	0.343758	0.777778	0.611121	**5**
92	158	0.475	0.45283	0.555556	0.433962	0.653559	0.555556	0.491536	**17**
93	159	0	0.075472	0.222222	0.245283	0.459948	0.222222	0.104234	**116**
94	160	0.5	0.792453	0.222222	0.962264	0.425153	0.888889	0.571245	**7**
95	163	0.075	0.264151	0	0.45283	0.283161	0.333333	0.157485	**89**
96	164	0.075	0.075472	0	0.396226	0.338558	0.333333	0.107839	**112**
97	165	0.65	0.811321	0	0.698113	0.364423	0.777778	0.578734	**6**

Sl. No.	OPP Bus	CLOC	GOC	TOC	NLOC	PDC	BCC	PMII	Ranking
98	168	0.7	0.584906	0	0.433962	0.369125	0.666667	0.51984	**12**
99	172	0.225	0.075472	0	0.169811	0.544158	0.222222	0.163277	**83**
100	173	0.15	0.207547	0	0.396226	0.218598	0.333333	0.167358	**81**
101	174	0.175	0.207547	0	0.396226	0.236068	0.333333	0.178929	**73**
102	176	0.3	0.207547	0	0.320755	0.362481	0.333333	0.233583	**59**
103	177	0.325	0.207547	0	0.264151	0.379354	0.333333	0.241151	**56**
104	178	0.225	0.075472	0	0.169811	0.242605	0.222222	0.147103	**92**
105	181	0.475	0.45283	0.111111	0.490566	0.359394	0.555556	0.407964	**27**
106	182	0.55	0.358491	0.555556	0.433962	0.25093	0.555556	0.477518	**20**
107	185	0.525	0.45283	0.555556	0.415094	0.329047	0.555556	0.494074	**16**
108	187	0.85	0.679245	0.666667	0.415094	0.906468	0.666667	0.743106	**2**
109	188	0.525	0.207547	0	0.188679	0.549653	0.333333	0.330059	**35**
110	189	0.325	0.075472	0.111111	0.132075	0.993891	0.222222	0.245226	**55**
111	190	0.725	0.584906	0	0.509434	0.254782	0.666667	0.529634	**9**
112	191	0.675	0.679245	0.666667	0.490566	0.367209	0.666667	0.645043	**4**
113	193	0.45	0.283019	0.222222	0.339623	0.311863	0.444444	0.354843	**30**
114	194	1	0.981132	1	0.773585	0.253963	1	0.939243	**1**
115	195	0.575	0.471698	0.333333	0.433962	0.311822	0.555556	0.484723	**19**
116	197	0.6	0.471698	0.555556	0.396226	0.308908	0.555556	0.528436	**10**
117	199	0.15	0.773585	0.666667	0.698113	0.403973	0.666667	0.462592	**22**
118	201	0	0.45283	0	0.509434	0.503985	0.555556	0.197067	**69**
119	202	0	0.377358	0	0.415094	0.286553	0.444444	0.155819	**90**
120	203	0.15	0.54717	0	0.490566	0.298011	0.555556	0.27282	**46**
121	205	0.075	0.471698	0	0.415094	0.232452	0.444444	0.209141	**66**
122	206	0	0.245283	0	0.264151	0.333319	0.333333	0.110177	**109**
123	208	0.225	0.075472	0.222222	0.169811	0.411492	0.222222	0.192043	**70**
124	213	0.65	0.811321	0.777778	0.698113	0.266611	0.777778	0.699074	**3**
125	216	0.075	0.566038	0	0.584906	0.192415	0.555556	0.246737	**53**
126	218	0	0.320755	0	0.320755	0.217497	0.333333	0.127394	**99**
127	219	0.5	0.509434	0.555556	0.490566	0.364176	0.555556	0.505212	**15**
128	223	0.4	0.377358	0	0.339623	0.323067	0.444444	0.322619	**36**
129	224	0	0.075472	0	0.245283	0.455997	0.222222	0.068141	**130**
130	229	0.075	0.924528	0.888889	0.886792	0.258575	0.888889	0.517948	**13**
131	230	0.25	0.320755	0.111111	0.490566	0.347956	0.444444	0.274086	**45**
132	235	0.175	0.735849	0.666667	0.716981	0.253085	0.666667	0.456727	**23**
133	238	0.075	0.641509	0.666667	0.90566	0.69506	0.666667	0.426807	**25**
134	242	0	0.075472	0.111111	0.245283	0.819494	0.222222	0.105577	**114**
135	243	0	0.377358	0.444444	0.415094	0.710462	0.444444	0.250319	**52**
136	246	0	0.132075	0.222222	0.301887	0.323321	0.222222	0.11547	**106**

Phased PMU placement for NRPG-246 bus system is given in Table 3-11. A close inspection of phase-1 of Table 3-11 reveals that in phase -1 itself, all critical load buses are having PMUs, to aid voltage stability monitoring and control.

Table 3-11: Phased PMU placement for NRPG-246 bus system

Phase I		**Phase II**		**Phase III**		**Phase IV**		**Phase V**	
OPP Bus	Rank	OPP Bus	Rank	OPP Bus	Rank	OPP Bus	Rank	OPP Bus	Rank
194	1	24	29	177	56	172	83	53	110
187	2	193	30	84	57	83	84	93	111
213	3	139	31	19	58	48	85	164	112
191	4	32	32	176	59	3	86	119	113
157	5	88	33	7	60	101	87	242	114
165	6	40	34	141	61	6	88	78	115
160	7	188	35	100	62	163	89	159	116
65	8	223	36	23	63	202	90	35	117
190	9	69	37	2	64	31	91	41	118
197	10	27	38	44	65	178	92	5	119
21	11	140	39	205	66	135	93	82	120
168	12	71	40	57	67	89	94	28	121
229	13	129	41	134	68	38	95	149	122
56	14	97	42	201	69	126	96	120	123
219	15	132	43	208	70	87	97	112	124
185	16	113	44	156	71	128	98	45	125
158	17	230	45	68	72	218	99	12	126
133	18	203	46	174	73	111	100	153	127
195	19	54	47	61	74	9	101	4	128
182	20	130	48	152	75	151	102	49	129
34	21	74	49	145	76	148	103	224	130
199	22	10	50	77	77	50	104	124	131
235	23	11	51	106	78	147	105	47	132
109	24	243	52	62	79	246	106	123	133
238	25	216	53	30	80	29	107	51	134
118	26	125	54	173	81	144	108	52	135
181	27	189	55	15	82	206	109	95	136
80	28	--	--	--	--	--	--	--	--

3.6 Conclusion

In this chapter, multi-phase PMU placement methodology has been proposed based on RAHP approach to monitor voltage instability in a large network without any additional financial burden on the utility. In the proposed approach, first the optimal PMU number and placement locations are determined, which make the system completely observable, even under N-1 contingency. Then critical load buses are identified using FVSI. Critical Load bus Observability Criteria (CLOC), Noncritical Load bus Observability Criteria (NLOC), Generator Observability Criteria (GOC), PMUs Distribution Criteria (PDC), Tie Line Observability Criteria (TOC), and Bus Connectivity Criteria (BCC) are used to rank optimal PMU locations using RAHP. From placement results, it is observed that all critical load buses

are observed in first-phase itself. Therefore, monitoring and control scheme can be implemented after first-phase placement, which will benefit in wide-area voltage stability analysis.

In a large network, the PMUs will improve the accuracy of the SE. In the next chapter, it is discussed that how the SE accuracy improves by including the PMUs after each phase in a large power system.

Chapter 4: State Estimation in PMU Integrated Network

4.1 Introduction

One of the applications of the synchrophasor data collected by PMUs is State Estimation (SE) of the power system. However, these synchronized measurements from PMUs will not be able to replace the conventional measurements in SCADA system completely in near future. Therefore, developing a hybrid state estimator that includes both the conventional and the phasor measurements, is the current need to get the better results.

Synchrophasor measurements hoist the ideals of power system monitoring, control, and protection to a new level [1], [2]. The PMU measurements i.e. voltage and current phasors make the SE equations linear and accurate than the iterative nonlinear SE techniques [3]. The linear SE can only be applied when there are sufficient number of PMUs installed in power system grid, which make the system fully observable [4]. Therefore, research has been carried out to develop a SE technique which can utilize both the PMU measurements and the conventional SCADA measurements. Zhou et al [5] has proposed an alternative method to use phasor measurements in post processing step of the traditional weighted least square (WLS) method by keeping the existing SE model unchanged. Bi et al [6] proposed a hybrid SE method including both the PMU measurements and the traditional measurements. Ranjana et al [7] proposed two different techniques to add PMU measurements available to the existing SCADA measurements to increase the correctness of the SE. References [8] - [9] offer insight of this topic. One of the major issues in most of the state estimators is detection and identification of bad data. The most frequently used technique for bad data detection is calculating normalized measurement residuals, where predefined measurement weights are used for calculation as discussed in [10]–[13]. Jun and Abur [14] presented a rectangular coordinate formulation which enables bad data processing for both the phasor and the conventional measurements. In [15], authors have proposed projected Kalman filter approach for dynamic state estimator considering zero injection constraint. Guo et al [16] proposed a novel method for SE with accuracy evaluation of estimated value using a scalar index of correntropy. Thukaram et al. [17] proposed a linear programing approach for SE using upper bound optimization technique.

In the previous chapter, phased PMUs placement has been discussed. In this chapter, the SE of the power system with the inclusion of synchrophasor measurements obtained from PMUs has been discussed. The inclusion of synchrophasors is carried out in the same phased manner as

discussed in the previous chapter to enhance the accuracy of conventional WLS-based SE. The bad data detection and elimination in both the conventional measurement and the phasor measurements, have been carried out using the normalized residual test method. The effectiveness of the approach has been tested on IEEE-30 bus test system and the Indian Northern Region Power Grid (NRPG) 246-bus real system.

4.2 Weighted Least Square (WLS) State Estimation[97]

State Estimation (SE) is a procedure for estimating the voltage magnitude as well as voltage angles of every bus in a power system which are known as the states of the system. WLS method is the conventional method to estimate these states. In WLS method, a set of measurements consisting of non-synchronized data of real power flow and reactive power flow, real power injection and reactive power injection and slack bus voltage magnitude are considered for estimating states of the system. These measurements are nonlinear functions of the state vector x (a set of positive sequence voltage phasors at all the buses of the network) given by:

$$\begin{bmatrix} z_1 \\ z_2 \\ \vdots \\ z_m \end{bmatrix} = \begin{bmatrix} h_1(x_1, x_2, \ldots, x_n) \\ h_2(x_1, x_2, \ldots, x_n) \\ \vdots \\ h_m(x_1, x_2, \ldots, x_n) \end{bmatrix} + \begin{bmatrix} e_1 \\ e_2 \\ \vdots \\ e_m \end{bmatrix} \tag{4.1}$$

Equation (4.1) can be written as:

$$[z_I] = [h_I(x)] + [e_I] \tag{4.2}$$

where, $Z_I = [z_1, z_2, \ldots, z_m]^T$ is a set of measurement vectors, $x = [x_1, x_2, \ldots, x_n]^T$ is the state vector. $h_I = [h_1(x), h_2(x), \ldots, h_m(x)]^T$ and $h_i(x)$ is the nonlinear function relating measurement i to the state vector x. $e_I = [e_1, e_2, \ldots, e_m]^T$ is the vector of measurement errors. x is the vector of voltage magnitude (V) and voltage angle (δ) in polar form. In rectangular form x can be represented as vector of E_r *and* E_i where E_r is the real part of voltage magnitude and E_i is the imaginary part of bus voltage.

The following assumptions are made regarding the statistical properties of measurement errors:

- $E(e_i) = 0, \quad i = 1, \ldots, m.$
- Measurement errors are independent, i.e. $E[e_i e_j] = 0.$

Hence, $Cov(e) = E[e \cdot e^T] = R_I = diag\{\sigma_1^2 \sigma_2^2 \ldots, \sigma_m^2\}$. The standard deviation σ_i of each measurement i is calculated to reflect the expected accuracy of the corresponding measurements considered.

WLS estimation seeks to minimize the weighted sum of squares of the measurement errors and the solution is achieved by minimizing the following function:

$$J(x) = \sum_{i=1}^{m} \frac{(z_i - h_i(x))^2}{R_{ii}} = [z_I - h_I(x)]^T R_I^{-1} [z_I - h_I(x)] \tag{4.3}$$

At the minimum, the first-order optimality conditions have to be satisfied. These can be expressed in compact form as follows:

$$g(x) = \frac{\partial J(x)}{\partial x} = -H_I^T(x) R_I^{-1} [z_I - h_I(x)] = 0 \tag{4.4}$$

where, $H_I(x) = \left[\frac{\partial h_I(x)}{\partial x}\right]$

The non-linear function $g(x)$ can be expanded using Taylor series:

$$g(x) = g(x^k) + G(x^k)(x^{k+1} - x^k) + \ldots = 0 \tag{4.5}$$

where, x^{k+1} *and* x^k are the states of the system at $(k+1)^{th}$ *and* k^{th} instant. Neglecting the higher order terms, x^{k+1} can be represented as:

$$x^{k+1} = x^k - \left[G\left(x^k\right)\right]^{-1} \cdot g\left(x^k\right) \tag{4.6}$$

where, $G\left(x^k\right)$ is called the gain matrix and given as.

$$G\left(x^k\right) = \frac{\partial g\left(x^k\right)}{\partial x} = H_I{}^T\left(x^k\right)\cdot R_I{}^{-1}\cdot H_I\left(x^k\right) \tag{4.7}$$

$$g\left(x^k\right) = -H_I{}^T\left(x^k\right)\cdot R_I{}^{-1}\cdot\left(z_I - h_I\left(x^k\right)\right). \tag{4.8}$$

The gain matrix is sparse, positive definite and symmetric matrix. The matrix G(x) is typically not inverted but instead it is decomposed into its triangular factors, and the following sparse linear set of equations are solved using forward/back substitutions at each iteration k:

$$G\left(x^k\right)\Delta x^{k+1} = H_I{}^T\left(x^k\right)\cdot R_I{}^{-1}\cdot\left[z_I - h_I\left(x^k\right)\right] = H_I{}^T\left(x^k\right)\cdot R_I{}^{-1}\cdot\Delta z_I{}^k \tag{4.9}$$

where, $\Delta x^{k+1} = x^{k+1} - x^k$ and $\Delta z_I{}^k = \left[z_I - h_I\left(x^k\right)\right]$.

Equation (4.9) is rearranged as:

$$x^{k+1} = x^k + G^{-1}\left(x^k\right)\cdot H_I{}^T\left(x^k\right)\cdot R_I{}^{-1}\cdot\left[z_I - h_I\left(x^k\right)\right] \tag{4.10}$$

These iterations will continue until the change in state variables is within an acceptable range.

$$\max\left|\Delta x^{k+1}\right| \le \varepsilon .$$

4.3 Linear State Estimation using PMU measurements [4]

In linear SE, a set of measurements, which includes positive sequence voltage phasors and positive sequence current phasors received from the PMUs, is considered for estimating the states. The linear model of SE is formed as:

$$\left[z_{II}\right] = \begin{bmatrix} \begin{pmatrix} E_r \\ E_i \end{pmatrix}_{PMU} \\ \begin{pmatrix} I_r \\ I_i \end{pmatrix}_{PMU} \end{bmatrix} = \begin{bmatrix} H_{31} & H_{32} \\ H_{41} & H_{42} \\ H_{51} & H_{52} \\ H_{61} & H_{62} \end{bmatrix} \begin{bmatrix} E_r \\ E_i \end{bmatrix} + \mathrm{e}_{II} \tag{4.11}$$

where, z_{II} is the measurement vectors that include voltage phasors $\begin{pmatrix} E_r \\ E_i \end{pmatrix}_{PMU}$ and current phasors $\begin{pmatrix} I_r \\ I_i \end{pmatrix}_{PMU}$ obtained from the PMUs. The suffix *r* and *i* represent real and imaginary parts respectively. E_r and E_i are the real and imaginary part of bus voltages in the system.

Equation (4.11) can also be written as:

$$\left[z_{II}\right] = [H_{II}]\mathrm{x} + \mathrm{e}_{II} \tag{4.12}$$

where, e_{II} represents an error vector of measurements. All the measurement errors are independent, ensuring normal distribution with zero mean and covariance. Unlike conventional method where iterations are needed, the solution of linear model using phasor measurements is computed directly as:

$$\mathrm{x} = \left(H_{II}{}^{T} R_{II}{}^{-1} H_{II}\right)^{-1} H_{II}{}^{T} R_{II}{}^{-1} z_{II} \tag{4.13}$$

R_{II}^{-1} is the weight matrix of dimensions ($p \times p$). p is the number of phasors measurements obtained from PMUs. R_{II} is a diagonal matrix whose elements are the square of the standard deviation of ith measurement i.e. σ_i ,

Formulation of the H_{II} can be explained by considering N-bus power system. If *PM* is the number of PMUs required for making the system completely observable. Then, the matrices $[H_{31}]_{PM\times N}$ and$[H_{42}]_{PM\times N}$, with its ith row corresponding to ith PMU. These matrices have all elements as zero except for the jth column, where j corresponds to the bus position of the ith PMU in the state vector. $[H_{32}]_{PM\times N}$ and $[H_{41}]_{PM\times N}$ are zero matrices.

The elements of matrices H_{51}, H_{52}, H_{61}, and H_{62} can be explained with the help of the transmission line-π model as shown in Figure 4-1.

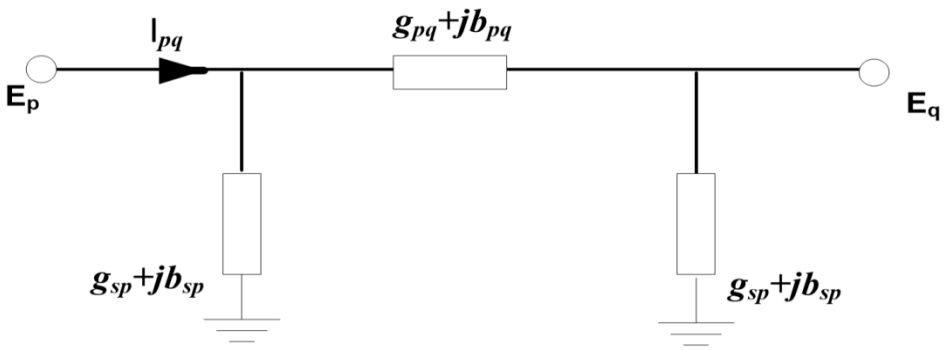

Figure 4-1: π -model of a transmission branch

In this figure, g_{pq} and b_{pq} are the line conductance and susceptance respectively. g_{sp} and b_{sp} are the shunt conductance and susceptance respectively. The current in branch p-q can be written as:

$$I_{pq_r} + jI_{pq_i} = \left[\left(g_{pq} + jb_{pq}\right) + \left(g_{sp} + jb_{sp}\right)\right]^*(E_{p_r} + jE_{p_i}) - \left(g_{pq} + jb_{pq}\right)^*(E_{q_r} + jE_{q_i}) \quad (4.14)$$

Separating the real and imaginary part of eq. (4.14), we get:

$$I_{pq_r} = (g_{pq} + g_{sp})E_{p_r} - (b_{pq} + b_{sp})E_{p_i} - g_{pq}E_{q_r} + b_{pq}E_{q_i} \quad (4.15)$$

$$I_{pq_i} = (b_{pq} + b_{sp})E_{p_r} + (g_{pq} + g_{sp})E_{p_i} - b_{pq}E_{q_r} - g_{pq}E_{q_i} \quad (4.16)$$

Equation (4.15) and (4.16) can also be represented as:

$$\begin{bmatrix} I_{pq_r} \\ I_{pq_i} \end{bmatrix} = \left[\begin{array}{cc:cc} \left(g_{pq} + g_{sp}\right) & -\left(b_{pq} + b_{sp}\right) & -g_{pq} & b_{pq} \\ \hdashline \left(b_{pq} + b_{sp}\right) & \left(g_{pq} + g_{sp}\right) & -b_{pq} & -g_{pq} \end{array}\right] \begin{bmatrix} E_{p_r} \\ E_{p_i} \\ E_{q_r} \\ E_{q_i} \end{bmatrix} \quad (4.17)$$

$$\begin{bmatrix} I_{pq_r} \\ I_{pq_i} \end{bmatrix} = \left[\begin{array}{c:c:c:c} \left(g_{pq} + g_{sp}\right) & -g_{pq} & -\left(b_{pq} + b_{sp}\right) & b_{pq} \\ \hdashline \left(b_{pq} + b_{sp}\right) & -b_{pq} & \left(g_{pq} + g_{sp}\right) & -g_{pq} \end{array}\right] \begin{bmatrix} E_{p_r} \\ E_{q_r} \\ E_{p_i} \\ E_{q_i} \end{bmatrix} \quad (4.18)$$

$$\begin{bmatrix} I_{pq_r} \\ I_{pq_i} \end{bmatrix} = \begin{bmatrix} H_{51} & H_{52} \\ H_{61} & H_{62} \end{bmatrix} \begin{bmatrix} E_{p_r} \\ E_{q_r} \\ E_{p_i} \\ E_{q_i} \end{bmatrix} \tag{4.19}$$

Therefore, $[H_{51}]_{L\times N}$ and $[H_{62}]_{L\times N}$ are the matrices whose elements are purely conductance while $[H_{52}]_{L\times N}$ and $[H_{61}]_{L\times N}$ has purely susceptance elements. Where L is the total number of current phasor measurements obtained from the PMUs and N is the number of buses in the system.

4.4 Hybrid State Estimation model

In hybrid state estimation method, consider both the set of measurements, i.e. vector [z_I], containing conventional measurements, and vector [z_{II}], a set of positive sequence voltage and current phasors obtained from the PMU measurements. In order to keep the conventional SE model unaltered, a two stage state estimation has been considered in this method. In stage-1, the conventional WLS estimator is run using the conventional measurements. In stage-2, voltage and current phasors obtained from PMUs are used to enhance the output obtained from stage-1. The appended measurement vector [***z***] is obtained combining both the stages.

$$[z] = \begin{bmatrix} z_I \\ z_{II} \end{bmatrix} = \begin{bmatrix} \begin{pmatrix} E_r \\ E_i \end{pmatrix}_{WLS} \\ \begin{pmatrix} E_r \\ E_i \end{pmatrix}_{PMU} \\ \begin{pmatrix} I_r \\ I_i \end{pmatrix}_{PMU} \end{bmatrix} \tag{4.20}$$

$$[z] = \begin{bmatrix} \begin{pmatrix} E_r \\ E_i \end{pmatrix}_{WLS} \\ \begin{pmatrix} E_r \\ E_i \end{pmatrix}_{PMU} \\ \begin{pmatrix} I_r \\ I_i \end{pmatrix}_{PMU} \end{bmatrix} = \begin{bmatrix} H_{11} & H_{12} \\ H_{21} & H_{22} \\ H_{31} & H_{32} \\ H_{41} & H_{42} \\ H_{51} & H_{52} \\ H_{61} & H_{62} \end{bmatrix} \begin{bmatrix} E_r \\ E_i \end{bmatrix} + \mathrm{e}_A \tag{4.21}$$

Equivalently (4.21) can also be written as

$$[z] = H_A x + e_A \tag{4.22}$$

where, H_A is the Jacobian matrix corresponding to both the conventional and the phasor measurements; H_{11} and H_{22} are identity matrix of size (N*N). H_{12} and H_{21} are zero matrix of size (N*N). N is the number of buses in the system. H_{31}, H_{32}, H_{41}, H_{42}, H_{51}, H_{52}, H_{61} and H_{62} are the same as explained in pervious section. x represents the state vector, and these states can be calculated using (4.22):

$$x = \left(H_A^T R_A^{-1} H_A\right)^{-1} H_A^T R_A^{-1} z \tag{4.23}$$

where, R_A is the covariance matrix of measurement error e_A.

4.5 Bad Data Processing in State Estimation [97]

State estimator designed must be capable of identifying, and removing the bad data from the measurement set. The largest normalized residual test is used to detect the presence of bad data in measurement set after SE is performed. Once the states are estimated using any SE algorithm as explained in sections 4.2 to 4.4, a largest normalized residual test is performed to identify the measurements that contain gross errors. If a measurement has error, it is discarded from the measurements set. Now the whole process is repeated until all measurements are within an acceptable error threshold.

Consider $\hat{x}$ is the estimated states of the system using hybrid SE model. Then equation (4.23) can be written as:

$$\hat{x} = \left(H_A^T R_A^{-1} H_A\right)^{-1} H_A^T R_A^{-1} z \tag{4.24}$$

Then the estimated measurement vector is given by:

$$\hat{Z} = H_A \hat{x} \tag{4.25}$$

where, $\hat{Z}$ is the estimated measurement vector using estimated state vector $\hat{x}$.

By substituting (4.24) in (4.25), we get:

$$\hat{z} = H_A \hat{x} = Kz \tag{4.26}$$

where,

$$K = H_A \left(H_A^T R_A^{-1} H_A \right)^{-1} H_A^T R_A^{-1} \tag{4.27}$$

Note that K has the property [97]:

$$(I - K) H_A = 0 \tag{4.28}$$

where I is the identity matrix.

Then the measurement residuals can be calculated as:

$$\begin{aligned} r &= z - \hat{z} = (I - K)(H_A x + e_A) \\ r &= (I - K) e_A = S * e_A \end{aligned} \tag{4.29}$$

Where $S = I - K$ is called residual sensitivity matrix.

Using the Property given below [97]:

$$S \cdot R_A \cdot S^T = S \cdot R_A \tag{4.30}$$

The covariance matrix of the measurement residual can be derived from (4.29).

$$\begin{aligned} \Omega &= E[rr^T] = S \cdot E[e_A e_A{}^T] \cdot S^T \\ \Omega &= S \cdot R_A \cdot S^T = S R_A \end{aligned} \tag{4.31}$$

The normalized value of the residual for i[th] measurement can be obtained by dividing the absolute value of residual of i[th] measurement by the square root of the corresponding diagonal entry in the residual covariance matrix:

$$r_i^N = \frac{|r_i|}{\sqrt{\Omega_{ii}}} \tag{4.32}$$

where,

$$\begin{aligned} \Omega &= S R_A = (\mathrm{I-K}) \mathrm{R}_A \\ \Omega &= \mathrm{R}_A - \mathrm{H}_A \left(\mathrm{H}_A{}^{\mathrm{T}} \mathrm{R}_A{}^{-1} \mathrm{H}_A \right)^{-1} \mathrm{H}_A{}^{\mathrm{T}} \end{aligned} \tag{4.33}$$

Based on the above formulation the bad data detection algorithm is given as:.

1. Solve SE using one of the SE algorithms explained in sections 4.2 to 4.4. From the estimated states values, obtain the elements of measurement residual vector as:

$$r_i = z_i - h_i(\hat{x}),\ i = 1, 2, ..., m \tag{4.34}$$

2. Calculate the normalized residuals using (4.32).
3. Find k such that, $r_k^N = \max\{r_i^N\}$. If r_k^N is larger than the threshold value (the threshold value considered is 3[97]), then z has a bad data else no bad data.
4. Eliminate the k^{th} measurement from z and repeat from step 1 until the normalized residual reaches below the threshold value.

4.6 Simulation Result

The effectiveness of the methodology discussed in pervious section have been studied on IEEE 30-bus system and the Northern Regional Power Grid (NRPG) 246-bus Indian system [95]. The details of both the systems are given in Appendix A. The phased PMU placement obtained in previous chapter is used in this chapter for SE.

In this work, voltage magnitude and phase angle of each bus, Real and reactive power injection and flows are obtained using the Newton Raphson load flow technique and considered as the actual/true values of measurements. A fixed value of error is added in actual/true values and considered as measured values. The standard deviations of error for different measurements used in this work are listed in Table 4-1[37].

Table 4-1Standard Deviation of Measurement error

Measurement Type	Real and Reactive Power Injection (p.u.)	Real and Reactive Power Flow (p.u.)	Voltage Magnitude (p.u.)	Angle (rad)
SCADA based conventional measurements	**0.01**	**0.008**	**0.03**	**--**
PMU based synchronized measurements	**--**	**--**	**0.001**	**0.001**

4.6.1 IEEE – 30 bus system

In order to demonstrate the effect of phasor measurements along with the conventional measurements on the performance of the state estimator, the voltage magnitude and phase angle are estimated for 4 different cases as given in Table 4-2. In each case, the PMU measurements are increased in the phased manner as obtained from the previous chapter.

Table 4-2: Different cases considered in SE for IEEE 30 bus system

Case	Measurements and SE algorithm used
1 (without any PMUs)	Traditional WLS method with 89 conventional measurements, i.e. 18 real power injections and 18 reactive power injections at different buses, 26 real power flows and 26 reactive power flows between different lines, and slack bus voltage magnitude.
2 (with PMUs after phase I)	Hybrid SE with conventional measurements considered in case 1 + PMU measurements obtained from phase 1. PMU buses are 10, 27, 12, 25 and 14.
3 (with PMUs after phase II)	Hybrid SE with conventional measurements considered in case 1 + PMU measurements obtained from phase 1 + PMU measurements obtained from phase 2. PMU buses are 10, 27, 12, 25, 14, 28, 2, 23, 15 and 20.
4 (with PMUs after phase III)	PMU placement for complete observability is considered. PMU buses are 10, 27, 12, 25, 14, 28, 2, 23, 15, 20, 17, 18, 1, 5 and 13. Linear SE algorithm is used.

To simulate the above four cases, first the load flow solution has been obtained for each bus voltage magnitude and phase angle. These values are considered as the true/actual values. Now the standard deviation of error for different measurements given in Table 4-1 has been added in the true values for the SCADA based measurements and PMU based measurements. Using this data, SE algorithms described in sections 4.2 to 4.4 have been implemented to estimate the states (Voltage magnitude and phase angle) of the system. Table 4-3 lists the real and estimated values of voltage magnitude and phase angle for all the four cases considered.

Table 4-3: True and estimated states for different cases considered

Bus Number	True		Case 1		Case 2		Case 3		Case 4	
	Magnitude (p.u)	Angle (degree)	Magnitude (p.u)	Angle (degree)	Magnitude (p.u)	Angle (degree)	Magnitude (p.u)	Angle (degree)	Magnitude (p.u)	Angle (Degree)
1	1.06	0	1.0462	0	1.0462	0	1.0615	0	1.062	0
2	1.043	-5.3543	1.0369	-5.6179	1.0424	-5.3259	1.0462	-5.376	1.0458	-5.3612
3	1.0196	-7.5308	1.0119	-7.8113	1.0119	-7.8113	1.0119	-7.8113	1.0218	-7.5205
4	1.0104	-9.284	1.0037	-9.6131	1.0098	-9.2609	1.0087	-9.2325	1.0097	-9.2385
5	1.01	-14.1738	1.0008	-14.5437	1.0008	-14.5437	1.0077	-14.143	1.0073	-14.1323
6	1.0096	-11.0581	1.0043	-11.4475	1.009	-11.0361	1.0079	-11.005	1.009	-11.0155
7	1.002	-12.8649	0.9947	-13.2677	1.0014	-12.8461	0.9947	-13.267	1.0013	-12.8236
8	1.01	-11.8193	1.0089	-12.292	1.0094	-11.7994	1.0089	-12.292	1.0094	-11.7777
9	1.0392	-14.0644	1.0306	-14.4977	1.0387	-14.0508	1.0377	-14.038	1.0386	-14.0135
10	1.0215	-15.6706	1.0129	-16.1061	1.021	-15.6809	1.0198	-15.651	1.0207	-15.6203
11	1.082	-14.0644	1.0708	-14.3906	1.0708	-14.3906	1.0708	-14.390	1.0814	-14.0152
12	1.0496	-15.1245	1.0395	-15.5448	1.0529	-15.3983	1.053	-15.401	1.0492	-15.1507
13	1.071	-15.1245	1.0595	-15.537	1.0595	-15.537	1.0595	-15.537	1.0707	-15.1494
14	1.032	-16.0018	1.0221	-16.4548	1.0327	-15.9906	1.0328	-15.993	1.0316	-15.9421
15	1.0251	-16.0084	1.0158	-16.4351	1.0256	-15.9973	1.0257	-16.004	1.0238	-15.8787
16	1.0304	-15.6251	1.0224	-16.0365	1.0224	-16.0365	1.0224	-16.036	1.03	-15.6553
17	1.0188	-15.8687	1.0099	-16.308	1.0099	-16.308	1.0171	-15.851	1.018	-15.8223
18	1.0114	-16.6067	1.0028	-17.0112	1.012	-16.5958	1.012	-16.602	1.0103	-16.5161
19	1.0066	-16.7658	0.9982	-17.1643	0.9982	-17.1643	0.9982	-17.164	1.0056	-16.6866
20	1.0095	-16.5502	1.0011	-16.9378	1.0011	-16.9378	1.0078	-16.538	1.0086	-16.4717
21	1.0082	-16.2178	0.9997	-16.6414	0.9997	-16.6414	1.0065	-16.201	1.0074	-16.1693
22	1.012	-15.9811	1.0028	-16.4362	1.0028	-16.4362	1.0102	-15.965	1.0111	-15.9351
23	1.0085	-16.2294	1	-16.6503	1.0089	-16.2204	1.009	-16.224	1.0073	-16.0986
24	0.9991	-16.3007	0.9891	-16.7613	0.9891	-16.7613	0.9891	-16.761	1	-16.2708
25	1.0032	-16.072	0.9853	-16.5601	1.0043	-16.0609	1.0039	-16.039	1.0042	-16.035
26	0.9852	-16.5038	0.9656	-17.0481	0.9656	-17.0481	0.9656	-17.048	0.9859	-16.475
27	1.0145	-15.6559	0.9937	-16.1303	1.0156	-15.6417	1.0153	-15.618	1.0156	-15.6159
28	1.0078	-11.7163	1.0017	-12.1015	1.009	-11.7035	1.0086	-11.664	1.009	-11.6843
29	0.9944	-16.9077	0.9783	-17.434	0.9956	-16.8967	0.9953	-16.869	0.9954	-16.8753
30	0.9828	-17.8067	0.9649	-18.3772	0.9839	-17.8035	0.9836	-17.769	0.9836	-17.7896

Figure 4-2 and Figure 4-3 shows the error in the estimated bus voltage magnitude and angle with respect to the true value for all the four cases. Table 4-4 shows the mean square error of the estimated states obtained by the SE methods for all the four cases. The results shown in Table 4-4 demonstrate that the addition of PMUs in different cases improves the accuracy of state estimation.

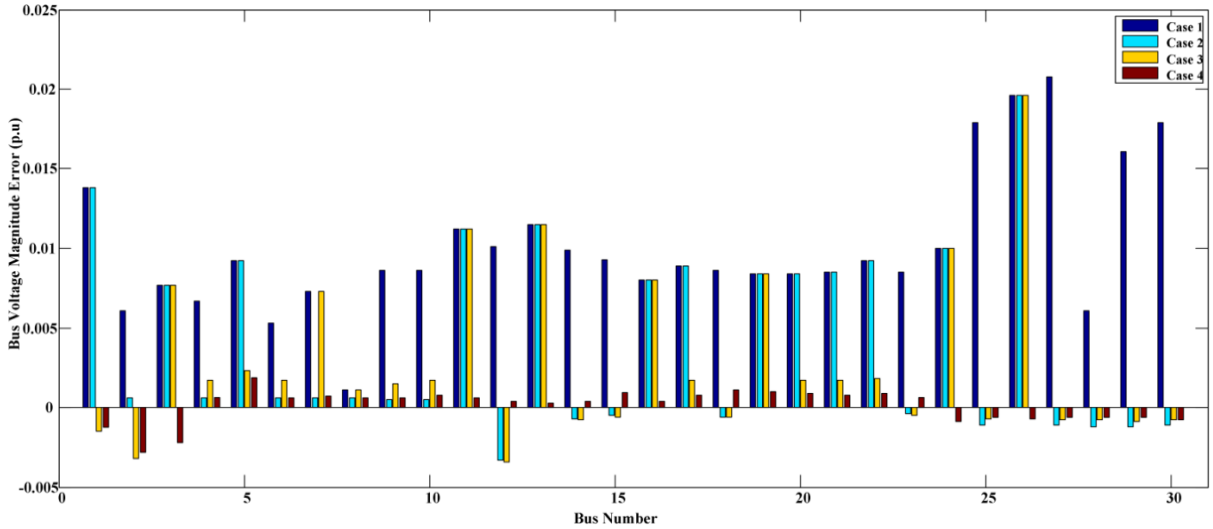

Figure 4-2: Bus voltage magnitude error for IEEE 30-bus system

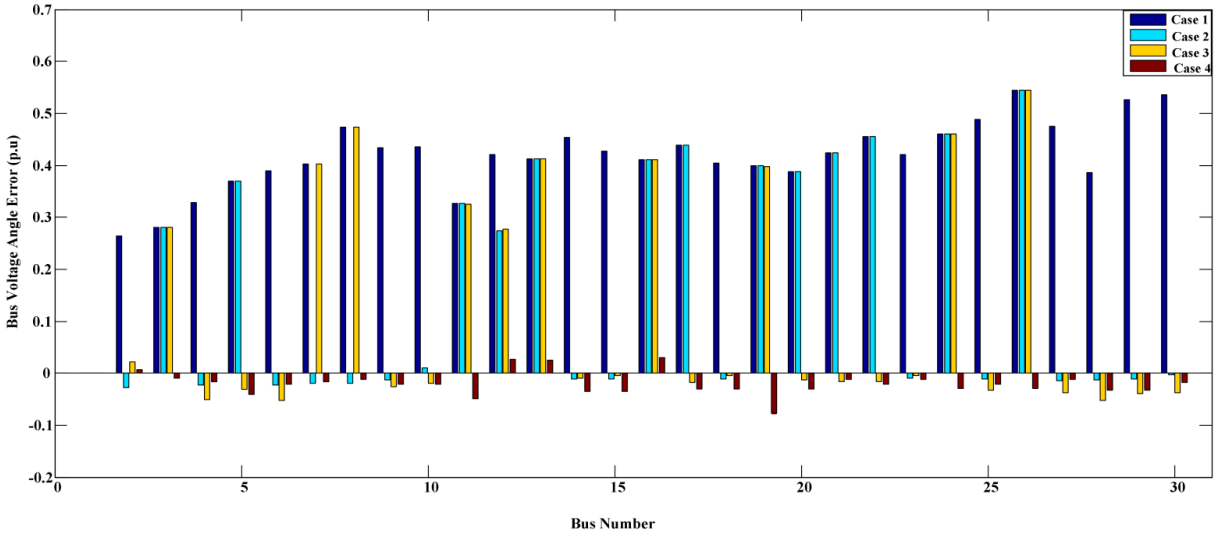

Figure 4-3: Bus voltage angle error for IEEE 30-bus system

Table 4-4: Comparison of state estimation error in IEEE 30-bus system

Performance Index (p.u.)	Case 1	Case 2	Case 3	Case 4
Mean Square Voltage Error	0.00101	4.707e-04	3.059e-04	1.518e-06
Mean Square Angle Error	1.3061	0.3899	0.3902	0.00249

The bad data analysis as discussed in section 4.5 is carried out for case 3. The threshold value of normalized residual test is assumed to be 3, i.e. $\max\left|r_i^N\right| < 3$ similar as considered in reference [38]. To validate the performance of the normalized residual test, a gross error of 10σ is added to the measurements of real power flow between bus 4 and 6 (P4-6) and of voltage magnitude bus 2 (V2). The top five normalized residuals for the given case are shown in Figure

4-4. In stage 1, the largest normalized residuals is for the voltage magnitude at bus 2 (V2) i.e. 9.267 which is greater than the threshold value, so eliminate V2 from measurement set and perform SE and calculate normalized residuals. In stage 2, P4-6 has the maximum residual, i.e. 4.096 that is greater than the threshold value so eliminates P4-6 from measurement set and repeat the same steps. In stage 3, largest normalized residual is less than the threshold value, hence all bad data has been identified and removed from the measurement set.

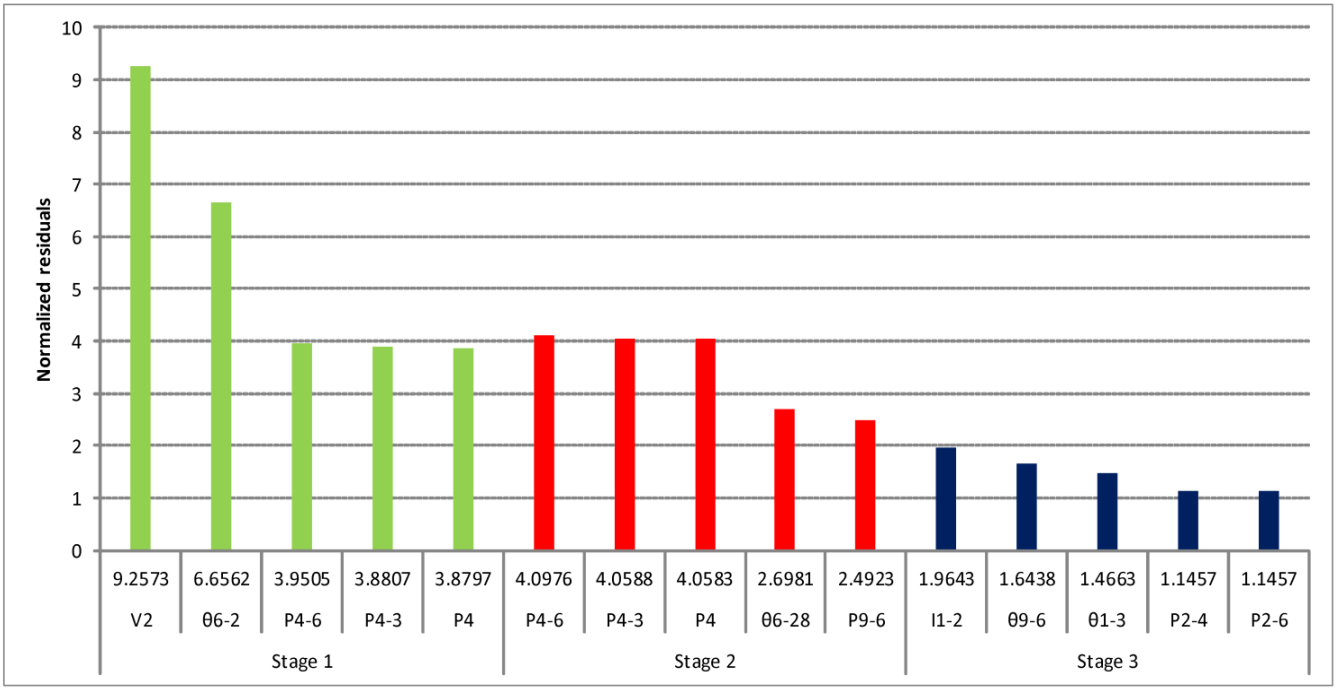

Figure 4-4: Bad data analysis using Normalized Residual Method for IEEE 30-bus system

4.6.2 Northern Regional Power Grid (NRPG) 246-bus Indian system

In NRPG 246-bus system total 136 PMUs are required for complete observability of system. These PMUs can be installed in phased manner. In the present work total 5 phases are considered for PMU installation as discussed in the previous chapter. Based on the phased PMU installation, six cases are considered for the SE. In first case, SE is done using WLS algorithm discussed in section 4.2 considering no PMU in the system. In 2^{nd}, 3^{rd}, 4^{th}, and 5^{th} cases SE analysis is done using hybrid algorithm described in section 4.4. In the last case, NRPG 246-bus system is completely observable therefore liner SE algorithm, discussed in section 4.3, is used for SE analysis. All the six cases are described in the Table 4-5.

.

Table 4-5: Different cases considered in SE for NRPG 246- bus system

Case	Measurements and SE algorithm used
1	Traditional WLS method with the conventional measurements consists of 246 voltage magnitude measurements, 376 pairs of power flow and 42 pairs of power injection measurements.
2	Hybrid SE with conventional measurements considered in case 1 + PMU measurements obtained from phase 1.
3	Hybrid SE with conventional measurements considered in case 1 + PMU measurements obtained from phase 1 + PMU measurements obtained from phase 2.
4	Hybrid SE with conventional measurements considered in case 1 + PMU measurements obtained from phase 1 + PMU measurements obtained from phase 2 + PMU measurements obtained from phase 3.
5	Hybrid SE with conventional measurements considered in case 1 + PMU measurements obtained from phase 1 + PMU measurements obtained from phase 2 + PMU measurements obtained from phase 3 + PMU measurements obtained from phase 4.
6	PMU measurements obtained from 136 PMUs placed for complete system observability are considered for SE. Linear SE algorithm is used.

To simulate the above six cases, load flow solution are considered as the true/actual values. Table 4-6 lists the real and estimated values of voltage magnitude and phase angle for all the six cases considered.

Table 4-6: True and estimated states of volatge magnitude and angle for NRPG-246 bus system

Bus Number	True		Case 1		Case 2		Case 3		Case 4		Case 5		Case 6	
	Magnitude (p.u)	Angle (degree)	Magnitude (p.u)	Angle (degree)	Magnitude (p.u)	Angle (degree)	Magnitude (p.u)	Angle (degree)	Magnitude (p.u)	Angle (Degree)	Magnitude (p.u)	Angle (Degree)	Magnitude (p.u)	Angle (Degree)
1	1.005	0	1.005	0	1.005	0	1.005	0	1.005	0	1.005	0	1.005	0
2	1.081	4.05	0.941	3.314	0.702	4.195	0.726	3.439	1.009	4.372	1.125	4.017	1.081	4.106
3	1.074	-8.482	0.858	-8.546	0.843	-8.095	0.998	-8.351	0.912	-8.41	1.115	-8.44	1.077	-8.43
4	1.085	-5.732	0.648	-6.185	1.008	-6.336	0.832	-6.319	0.81	-5.29	1.091	-5.739	1.08	-5.778
5	1.032	-4.944	0.664	-4.185	0.975	-6.06	1.098	-5.415	1.024	-5.57	1.052	-4.96	1.026	-5
6	1.048	-6.103	1.107	-6.64	0.909	-6.179	0.75	-7.183	1.088	-5.915	1.078	-6.3	1.061	-6.125
7	1.04	-7.812	0.973	-7.554	0.643	-8.707	0.69	-7.428	1.029	-7.419	1.058	-7.942	1.052	-7.888
8	1.069	-3.783	0.942	-2.694	0.661	-3.432	0.792	-3.476	1.162	-4.276	1.091	-3.629	1.081	-3.779
9	1.037	-7.318	0.618	-7.051	0.859	-7.548	0.771	-7.113	0.908	-6.655	1.017	-7.169	1.048	-7.415
10	1.101	-4.031	0.949	-3.42	0.856	-3.842	1.029	-3.01	1.076	-3.391	1.121	-3.968	1.112	-3.991
11	1.048	-9.068	1.004	-8.392	0.752	-10.2	0.812	-9.42	0.814	-9.163	1.041	-9.153	1.032	-9.109

Bus Number	True		Case 1		Case 2		Case 3		Case 4		Case 5		Case 6	
	Magnitude (p.u)	Angle (degree)	Magnitude (p.u)	Angle (degree)	Magnitude (p.u)	Angle (degree)	Magnitude (p.u)	Angle (degree)	Magnitude (p.u)	Angle (Degree)	Magnitude (p.u)	Angle (Degree)	Magnitude (p.u)	Angle (Degree)
12	1.045	-9.371	0.786	-9.84	1.132	-9.929	0.884	-9.569	1	-10.07	1.078	-9.591	1.055	-9.395
13	1.028	-7.19	0.841	-7.358	0.812	-8.143	0.857	-6.936	0.793	-7.393	1.063	-7.167	1.028	-7.153
14	1.022	-8.442	0.583	-8.282	1.097	-7.529	0.982	-8.315	1.06	-8.644	1.064	-8.464	1.007	-8.405
15	1.034	-8.679	0.573	-7.933	0.901	-8.205	0.796	-8.644	0.837	-8.945	1.038	-8.56	1.032	-8.719
16	1.057	-9.577	0.666	-10.75	0.9	-10.37	1.118	-9.207	0.835	-10.25	1.06	-9.71	1.064	-9.641
17	1.035	-7.173	0.71	-8.356	1.123	-6.534	1.185	-6.602	0.99	-6.801	1.012	-7.308	1.019	-7.097
18	1.028	-7.061	0.682	-6.513	1.092	-5.949	0.868	-6.243	0.916	-7.688	1.002	-7.222	1.012	-7.041
19	1.062	-2.958	0.623	-3.404	0.654	-2.893	0.912	-2.181	1.155	-2.331	1.05	-3.184	1.055	-3.021
20	1.089	-2.948	1.15	-3.886	0.895	-4.184	0.936	-4.007	1.116	-3.466	1.093	-2.807	1.1	-3.04
21	1.081	-3.933	0.979	-5.398	0.979	-3.415	0.849	-3.966	0.967	-3.282	1.061	-4.102	1.087	-4.032
22	1.079	3.121	1.177	1.763	0.979	2.84	0.719	2.51	0.996	3.199	1.091	3.09	1.091	3.131
23	1.089	2.667	0.692	2.913	1.105	2.933	0.719	3.045	0.844	2.475	1.105	2.713	1.086	2.675
24	1.032	-0.928	0.828	-0.016	1.05	0.201	0.685	0.133	0.89	-0.523	1.067	-0.786	1.017	-0.902
25	1.07	-7.598	0.95	-8.588	0.977	-7.699	0.888	-7.909	0.995	-8.092	1.061	-7.761	1.066	-7.594
26	1.042	2.962	1.006	4.021	0.958	2.012	0.683	3.234	0.912	3.346	1.048	2.754	1.042	2.906
27	1.074	7.818	0.854	8.741	0.743	8.345	1.16	7.432	1.169	8.256	1.13	7.66	1.07	7.764
28	1.07	24.16	0.996	24.501	0.902	25.24	1.032	23.33	1.183	23.94	1.07	23.98	1.076	24.07
29	1.076	15.40	1.135	14.259	0.921	15.96	1.206	16.25	0.898	14.69	1.051	15.42	1.069	15.454
30	1.09	-3.446	1.139	-3.794	1.117	-3.964	0.943	-3.695	1.087	-3.738	1.103	-3.364	1.093	-3.427
31	1.034	-4.681	1.093	-5.04	0.647	-4.337	0.779	-4.917	1.137	-4.303	1.039	-4.676	1.028	-4.726
32	1.085	23.72	0.939	22.347	0.813	23.20	1.135	23.62	0.836	23.05	1.08	23.77	1.087	23.783
33	1.08	23.79	1.105	23.468	0.72	24.96	0.995	23.84	1.187	23.92	1.13	23.94	1.088	23.822
34	1.018	-7.1	0.852	-5.73	0.757	-7.767	1.114	-8.204	1.12	-6.452	1.059	-7.06	1.029	-7.163
35	1.044	-6.15	0.604	-7.178	0.603	-5.966	1.027	-5.482	0.939	-5.791	1.025	-6.088	1.035	-6.101
36	1.099	6.37	0.987	5.944	0.661	7.483	0.82	6.186	1.049	5.71	1.088	6.447	1.088	6.398
37	1.099	-3.485	1.127	-3.524	1.062	-3.34	0.954	-3.82	1.218	-4.088	1.075	-3.467	1.101	-3.482
38	1.044	7.456	0.803	8.051	0.801	6.794	0.771	8.468	1.154	7.283	1.075	7.396	1.053	7.479
39	1.078	11.24	0.653	11.873	0.778	10.05	0.877	10.87	1.11	11.10	1.061	11.35	1.089	11.323
40	1.088	23.55	0.978	23.51	0.914	22.19	0.746	22.73	1.165	24.25	1.074	23.63	1.074	23.547
41	1.097	22.75	1.172	23.47	0.73	21.39	1.214	22.93	0.969	23.26	1.082	22.71	1.103	22.79
42	1.055	-8.547	1.07	-7.292	1.05	-9.677	1.108	-8.455	0.99	-8.169	1.074	-8.553	1.045	-8.564
43	1.097	-10.95	1.151	-10.06	1.129	-12.00	1.018	-10.07	1.182	-11.49	1.107	-11.09	1.095	-10.87
44	1.092	-10.65	0.748	-10.03	1.191	-11.53	0.835	-10.89	1.044	-10.53	1.07	-10.61	1.082	-10.68
45	1.101	-10.86	0.927	-10.06	1.117	-11.10	0.76	-11.75	0.861	-10.64	1.106	-11.03	1.105	-10.85
46	1.1	-10.02	0.799	-10.46	0.906	-9.918	1.236	-9.417	0.998	-9.722	1.155	-10.24	1.098	-10.06
47	1.097	17.37	0.777	16.302	0.916	18.24	1.171	18.23	0.927	17.62	1.129	17.22	1.086	17.405
48	1.105	17.87	0.862	16.846	0.993	17.37	1.022	18.53	0.833	17.93	1.149	17.90	1.096	17.913
49	1.135	-8.494	0.857	-9.5	1.064	-9.54	0.864	-8.923	1.024	-8.082	1.13	-8.629	1.122	-8.485
50	1.135	-8.456	0.708	-9.181	1.233	-7.97	0.996	-9.032	1.059	-8.608	1.187	-8.31	1.131	-8.471
51	1.138	-8.446	0.841	-9.624	0.79	-9.43	0.873	-8.792	1.05	-8.733	1.157	-8.538	1.128	-8.379
52	1.135	-8.507	0.71	-9.451	0.884	-7.491	1.192	-8.485	1.017	-8.836	1.133	-8.393	1.12	-8.442
53	1.17	-6.182	0.989	-5.393	1.023	-5.966	0.95	-5.812	0.987	-6.012	1.179	-6.042	1.161	-6.135

Bus Number	True		Case 1		Case 2		Case 3		Case 4		Case 5		Case 6	
	Magnitude (p.u)	Angle (degree)	Magnitude (p.u)	Angle (degree)	Magnitude (p.u)	Angle (degree)	Magnitude (p.u)	Angle (degree)	Magnitude (p.u)	Angle (Degree)	Magnitude (p.u)	Angle (Degree)	Magnitude (p.u)	Angle (Degree)
54	1.136	-8.421	1.151	-10.00	1.101	-7.918	0.945	-8.79	1.019	-9.156	1.176	-8.283	1.147	-8.351
55	1.136	-8.498	1.195	-7.379	0.794	-7.696	1.282	-8.689	0.97	-8.164	1.185	-8.349	1.143	-8.426
56	1.106	-9.667	0.777	-10.22	0.752	-10.11	0.848	-10.08	1.057	-10.08	1.146	-9.898	1.096	-9.613
57	1.083	-9.96	0.998	-9.205	0.714	-9.582	0.687	-9.162	0.948	-9.845	1.107	-10.01	1.093	-9.999
58	1.321	-10.47	1.018	-9.802	1.164	-11.76	1.401	-10.91	1.379	-11.03	1.298	-10.62	1.305	-10.48
59	1.113	19.21	0.822	19.592	0.68	19.11	1.065	18.75	0.884	19.35	1.11	19.12	1.103	19.202
60	1.037	-9.538	0.818	-8.732	0.674	-10.25	1.081	-10.56	1.063	-9.9	1.078	-9.681	1.02	-9.627
61	1.17	-6.182	0.841	-6.302	1.227	-5.015	0.927	-6.975	1.154	-6	1.16	-6.153	1.174	-6.213
62	1.129	-7.566	0.926	-9.019	1.098	-7.94	1.181	-6.889	1.135	-8.182	1.15	-7.754	1.12	-7.613
63	1.321	-10.47	1.128	-10.25	0.971	-10.76	0.928	-11.53	1.054	-10.89	1.317	-10.51	1.31	-10.46
64	1.062	-12.11	0.864	-12.46	0.939	-13.01	1.203	-11.47	1.113	-12.05	1.09	-11.99	1.063	-12.06
65	1.052	-7.465	0.59	-7.885	0.895	-7.968	1.18	-6.877	1.141	-7.366	1.061	-7.638	1.051	-7.553
66	1.086	-12.62	0.952	-13.36	0.662	-13.71	0.793	-11.56	0.931	-12.48	1.057	-12.74	1.082	-12.68
67	1.059	-11.86	1.089	-11.66	0.628	-13.0	0.736	-11.46	1.149	-11.82	1.058	-11.85	1.049	-11.92
68	1.053	-9.577	1.008	-10.75	0.732	-8.773	0.891	-9.118	1.101	-9.448	1.033	-9.712	1.047	-9.499
69	1.2	-9.572	0.889	-10.93	0.984	-8.872	0.935	-9.817	1.081	-8.981	1.225	-9.583	1.203	-9.654
70	1.227	-10.16	0.823	-11.01	0.823	-11.01	1.091	-9.975	1.066	-10.12	1.246	-10.02	1.216	-10.19
71	1.144	-9.399	0.662	-8.855	0.971	-8.356	0.972	-8.74	0.909	-9.608	1.137	-9.479	1.134	-9.489
72	1.145	-11.64	1.116	-12.63	1.153	-11.45	1.19	-11.44	1.028	-11.38	1.116	-11.60	1.15	-11.65
73	1.122	-11.169	0.765	-10.197	1.042	-10.749	0.995	-10.438	0.898	-11.079	1.137	-11.177	1.12	-11.137
74	1.082	-12.246	0.832	-12.359	1.019	-12.955	1.204	-13.047	0.935	-11.697	1.11	-12.326	1.091	-12.172
75	1.064	-12.212	0.922	-12.644	0.857	-11.283	1.183	-11.47	0.872	-12.227	1.068	-12.181	1.073	-12.202
76	1.06	-12.64	0.854	-13.352	1.123	-13.501	1.025	-13.096	0.97	-12.379	1.05	-12.541	1.053	-12.62
77	1.032	-6.341	0.834	-6.091	1.094	-7.176	0.835	-6.956	1.16	-5.665	1.055	-6.587	1.042	-6.413
78	1.097	-12.089	0.806	-12.875	1.105	-12.274	0.756	-11.043	1.145	-12.716	1.135	-11.973	1.104	-12.186
79	1.048	-10.955	0.702	-12.217	0.627	-10.414	0.828	-10.197	0.998	-10.571	1.071	-10.932	1.036	-10.875
80	1.064	-11.143	0.983	-9.91	0.718	-10.127	0.837	-10.132	0.965	-11.468	1.114	-10.999	1.059	-11.121
81	1.059	-10.384	1.106	-9.398	0.769	-10.811	0.827	-11.131	1.032	-9.915	1.079	-10.602	1.052	-10.483
82	1.055	-13.393	0.659	-14.582	0.621	-12.257	0.765	-12.419	0.92	-14.154	1.052	-13.386	1.039	-13.381
83	1.053	-14.71	0.919	-14.575	0.604	-13.671	0.839	-15.135	0.943	-14.764	1.065	-14.955	1.042	-14.692
84	1.128	-12.131	0.763	-11.965	0.685	-11.268	0.992	-12.082	0.944	-12.768	1.123	-12.194	1.119	-12.061
85	1.053	-15.266	1.046	-16.743	1.071	-15.238	1.021	-16.001	1.112	-15.656	1.083	-15.337	1.042	-15.288

Bus Number	True		Case 1		Case 2		Case 3		Case 4		Case 5		Case 6	
	Magnitude (p.u)	Angle (degree)	Magnitude (p.u)	Angle (degree)	Magnitude (p.u)	Angle (degree)	Magnitude (p.u)	Angle (degree)	Magnitude (p.u)	Angle (Degree)	Magnitude (p.u)	Angle (Degree)	Magnitude (p.u)	Angle (Degree)
86	1.071	-11.014	1.106	-11.865	0.644	-11.562	0.707	-10.744	0.995	-11.06	1.067	-10.931	1.076	-10.952
87	1.031	-10.324	0.587	-11.867	0.839	-11.35	1.045	-9.301	1.004	-10.535	1.008	-10.253	1.031	-10.306
88	1.064	-12.417	0.638	-11.718	1.123	-12.513	0.933	-11.831	0.793	-12.241	1.06	-12.456	1.069	-12.505
89	1.07	-10.677	0.571	-9.566	0.999	-9.604	0.813	-11.204	0.817	-10.767	1.115	-10.607	1.077	-10.72
90	1.04	-9.552	0.621	-9.305	0.647	-9.168	1.05	-9.712	0.804	-10.047	1.039	-9.776	1.044	-9.508
91	1.066	-11.84	1.144	-11.941	0.707	-12.308	0.751	-12.725	1.014	-11.55	1.09	-11.794	1.058	-11.891
92	1.052	-14.357	0.825	-14.668	1.151	-15.202	0.906	-14.947	0.874	-14.096	1.065	-14.588	1.052	-14.329
93	1.047	-10.388	0.548	-11.918	0.794	-9.94	0.696	-9.542	0.804	-10.211	1.068	-10.563	1.043	-10.369
94	1.072	-13.705	0.865	-13.783	0.73	-13.799	1.029	-14.82	1.048	-14.319	1.046	-13.688	1.079	-13.708
95	1.051	-14.704	0.627	-14.507	1.017	-15.632	0.687	-15.293	1.134	-14.144	1.097	-14.553	1.046	-14.652
96	1.035	-10.501	1.093	-12.086	1.1	-10.849	0.675	-9.453	0.95	-10.111	1.043	-10.481	1.025	-10.466
97	1.067	-10.293	0.574	-9.676	1.022	-10.488	0.893	-10.748	1.057	-10.048	1.083	-10.291	1.078	-10.259
98	1.057	-11.085	0.603	-11.681	1.1	-10.745	1.151	-11.102	0.838	-10.912	1.099	-10.963	1.04	-11.076
99	1.041	-9.888	0.803	-11.381	0.875	-9.758	0.99	-8.886	1.095	-10.278	1.052	-10.125	1.036	-9.889
100	1.033	-9.068	0.874	-9.681	0.903	-9.932	1.031	-8.246	1.077	-9.697	1.062	-8.986	1.017	-9.155
101	1.05	-10.452	0.947	-9.95	0.94	-10.145	1.054	-9.546	0.963	-9.83	1.039	-10.36	1.038	-10.521
102	1.059	-13.556	0.727	-13.75	0.672	-13.559	1.085	-13.85	1.155	-12.974	1.11	-13.604	1.071	-13.521
103	1.053	-14.993	1.145	-13.597	0.922	-14.749	1.203	-14.441	1.085	-14.315	1.056	-15.041	1.053	-15.085
104	1.07	-13.486	0.945	-14.737	1.014	-14.053	0.729	-12.727	0.94	-13.076	1.071	-13.347	1.073	-13.533
105	1.059	-13.41	0.605	-13.223	1.132	-13.686	0.959	-13.528	1.143	-12.75	1.108	-13.401	1.067	-13.484
106	1.07	-14.313	0.843	-13.817	1.05	-14.808	0.902	-15.336	0.951	-14.316	1.054	-14.393	1.058	-14.323
107	1.07	-14.158	0.885	-15.609	1.038	-14.234	1.046	-14.472	0.835	-13.823	1.052	-14.405	1.072	-14.078
108	1.046	-11.051	0.848	-11.033	1.13	-10.887	0.649	-11.53	0.975	-11.731	1.037	-11.069	1.047	-11.143
109	1.063	-9.65	0.978	-9.113	0.777	-9.691	0.672	-9.1	1.065	-10.02	1.039	-9.775	1.049	-9.687

Bus Number	True		Case 1		Case 2		Case 3		Case 4		Case 5		Case 6	
	Magnitude (p.u)	Angle (degree)	Magnitude (p.u)	Angle (degree)	Magnitude (p.u)	Angle (degree)	Magnitude (p.u)	Angle (degree)	Magnitude (p.u)	Angle (Degree)	Magnitude (p.u)	Angle (Degree)	Magnitude (p.u)	Angle (Degree)
										3				
110	1.068	-9.347	0.597	-8.2	1.163	-8.32	0.687	-8.734	0.885	-9.379	1.068	-9.193	1.069	-9.269
111	1.08	-10.068	0.591	-10.415	0.844	-9.937	0.864	-9.073	0.819	-9.485	1.051	-9.971	1.079	-10.164
112	1.119	-13.726	0.911	-12.785	0.994	-15.046	0.869	-14.145	0.984	-13.821	1.112	-13.935	1.105	-13.692
113	1.114	-12.292	0.619	-11.111	1.077	-13.122	1.081	-12.358	1.045	-12.591	1.165	-12.151	1.107	-12.382
114	1.091	-12.683	0.918	-13.025	0.833	-13.379	0.954	-12.701	1.042	-12.895	1.147	-12.535	1.085	-12.626
115	1.165	-11.048	1.01	-10.509	1.089	-11.838	1.165	-11.915	1.219	-10.977	1.15	-11.123	1.155	-10.958
116	1.054	-8.317	1.026	-8.003	1.097	-9.084	0.809	-9.419	1.003	-7.783	1.082	-8.296	1.043	-8.394
117	1.042	-6.982	1.026	-7.756	0.847	-7.974	0.764	-7.619	0.972	-7.507	1.075	-6.912	1.045	-7.054
118	1.169	-11.954	0.77	-13.129	1.179	-12.756	1.275	-11.431	0.946	-11.628	1.216	-12.164	1.182	-11.928
119	1.044	-7.076	0.708	-6.72	0.658	-8.42	1.072	-7.524	0.88	-7.14	1.084	-7.196	1.03	-7.005
120	1.147	-13.343	0.93	-14.829	0.881	-12.433	1.185	-13.979	1.023	-13.85	1.171	-13.336	1.157	-13.373
121	1.14	-11.276	0.742	-12.737	0.774	-11.106	0.947	-11.521	1.233	-11.341	1.125	-11.28	1.127	-11.262
122	1.134	-12.188	0.927	-11.406	0.815	-12.268	0.885	-12.967	1.218	-11.942	1.125	-12.112	1.119	-12.274
123	1.056	-16.034	0.825	-16.939	0.712	-15.505	0.747	-17.049	0.95	-16.627	1.028	-15.972	1.043	-16.111
124	1.077	-12.449	1.049	-12.896	0.829	-11.345	1.217	-12.81	1.018	-11.835	1.072	-12.652	1.07	-12.477
125	1.078	-12.09	0.825	-13.447	0.787	-13.423	1.116	-11.053	0.984	-12.486	1.104	-12.308	1.074	-12.17
126	1.155	-12.525	1.169	-12.932	0.876	-13.214	1.047	-11.861	1.269	-13.176	1.165	-12.685	1.154	-12.475
127	1.139	-12.397	1.207	-13.104	1.062	-11.582	1.08	-11.378	1.031	-12.393	1.131	-12.336	1.142	-12.356
128	1.072	-9.594	0.762	-10.425	0.879	-8.778	1.034	-10.627	0.944	-9.598	1.048	-9.673	1.082	-9.504
129	1.17	-11.941	0.905	-11.696	0.79	-12.574	1.285	-11.956	1.102	-11.472	1.215	-11.864	1.173	-11.868
130	1.083	-13.027	1.051	-12.381	1.153	-12.818	0.814	-13.743	1.147	-13.77	1.12	-12.919	1.071	-13.05
131	1.084	-8.547	0.94	-7.257	0.909	-7.546	1.013	-8.499	0.905	-9.161	1.112	-8.669	1.095	-8.514
132	1.064	-9.526	0.786	-9.543	0.926	-9.395	0.843	-9.563	0.868	-9.559	1.091	-9.74	1.073	-9.584
133	1.037	-7.332	0.804	-7.867	0.639	-6.504	0.884	-7.214	1.047	-7.243	1.019	-7.48	1.041	-7.364
134	1.028	-7.169	1.051	-6.606	0.781	-8.046	1.149	-8.104	0.95	-6.659	1.026	-7.346	1.016	-7.113
135	1.017	-7.212	1.016	-7.366	0.577	-8.431	0.998	-8.108	1.05	-7.901	1.072	-7.145	1.014	-7.176
136	1.038	-8.173	1.137	-7.51	0.816	-6.985	0.657	-8.524	1.089	-7.481	1.049	-8.171	1.041	-8.108

Bus Number	True		Case 1		Case 2		Case 3		Case 4		Case 5		Case 6	
	Magnitude (p.u)	Angle (degree)	Magnitude (p.u)	Angle (degree)	Magnitude (p.u)	Angle (degree)	Magnitude (p.u)	Angle (degree)	Magnitude (p.u)	Angle (Degree)	Magnitude (p.u)	Angle (Degree)	Magnitude (p.u)	Angle (Degree)
137	1.049	-8.988	0.898	-8.48	0.687	-9.478	0.687	-8.568	0.847	-8.567	1.061	-8.999	1.039	-9.005
138	1.042	-8.301	0.849	-8.853	0.884	-8.866	0.984	-7.881	1.144	-8.087	1.064	-8.525	1.029	-8.239
139	1.061	-8.109	1.065	-9.383	0.861	-7.569	0.871	-7.584	1.111	-7.484	1.039	-7.992	1.057	-8.182
140	1.072	-9.173	0.772	-10.357	1.073	-10.166	0.913	-9.685	0.802	-8.69	1.043	-9.231	1.068	-9.089
141	1.045	-8.304	1.135	-7.534	0.796	-7.868	0.739	-8.975	0.94	-8.698	1.054	-8.399	1.037	-8.375
142	1.058	-8.423	1.086	-8.22	0.628	-7.293	0.681	-9.202	0.949	-8.446	1.065	-8.378	1.061	-8.377
143	1.069	-9.507	0.597	-10.77	0.875	-8.549	1.177	-10.249	0.809	-9.314	1.105	-9.428	1.054	-9.56
144	1.069	-9.514	0.583	-8.884	0.905	-10.389	0.73	-9.008	1.158	-9.17	1.057	-9.522	1.078	-9.435
145	1.058	-8.406	1.14	-9.906	0.722	-9.055	0.899	-9.135	0.828	-8.382	1.094	-8.394	1.048	-8.45
146	1.033	-7.67	0.837	-8.127	1.082	-8.507	1.076	-8.013	0.797	-7.248	1.04	-7.576	1.036	-7.615
147	1.022	-7.278	0.604	-6.374	0.637	-7.7	1.05	-6.721	1.064	-7.064	1.025	-7.484	1.031	-7.377
148	1.04	-8.124	0.995	-9.202	1.138	-9.07	0.802	-7.905	1.102	-7.82	1.058	-8.144	1.037	-8.132
149	1.059	-10.083	0.658	-10.65	0.877	-8.974	0.88	-10.027	0.924	-10.628	1.05	-10.198	1.052	-10.095
150	1.019	-7.201	0.63	-7.441	0.745	-7.056	0.846	-7.253	1.075	-7.546	1.026	-7.128	1.013	-7.163
151	1.042	-8.374	0.765	-7.728	0.831	-7.823	0.66	-8.515	1.124	-8.174	1.032	-8.407	1.033	-8.356
152	1.058	-8.387	1.157	-7.108	0.895	-8.438	0.888	-8.087	1.039	-8.558	1.052	-8.248	1.067	-8.395
153	1.021	-7.356	0.893	-6.656	0.945	-8.446	1.116	-6.935	0.986	-7.088	0.995	-7.4	1.011	-7.364
154	1.132	-6.047	0.689	-5.73	0.901	-5.577	1.19	-6.557	1.225	-5.743	1.123	-5.997	1.122	-6.046
155	1.118	-6.376	0.81	-6.877	0.715	-6.734	1.212	-7.408	0.967	-6.066	1.125	-6.497	1.105	-6.316
156	1.06	-18.705	0.933	-20.263	0.785	-17.573	1.13	-18.967	0.966	-19.02	1.065	-18.851	1.057	-18.656
157	1.166	-4.519	0.886	-3.741	0.745	-3.723	0.946	-4.779	0.891	-4.599	1.171	-4.52	1.161	-4.552
158	1.09	-15.557	1.044	-16.428	1.136	-16.525	0.888	-16.146	1.133	-14.972	1.064	-15.626	1.095	-15.582
159	1.113	-2.026	0.87	-3.285	0.932	-1.333	1.058	-1.788	0.866	-1.41	1.131	-2.166	1.111	-1.97
160	1.189	-9.825	0.7	-9.842	1.229	-10.782	1.25	-9.769	1.046	-9.513	1.186	-9.916	1.173	-9.9
161	1.179	-9.254	0.769	-8.33	0.979	-8.933	1.115	-9.325	1.004	-9.214	1.215	-9.332	1.188	-9.264
162	1.168	-11.02	1.098	-12.053	0.889	-11.565	0.878	-12.039	1.143	-10.747	1.158	-10.889	1.171	-11.115
163	1.167	-13.455	0.858	-13.484	1.186	-12.391	1.097	-13.393	1.103	-13.773	1.209	-13.448	1.18	-13.419
164	1.182	-11.505	1.067	-10.453	0.854	-12.214	0.917	-11.865	1.268	-12.229	1.231	-11.358	1.171	-11.595
165	1.133	-9.356	0.64	-10.583	1.013	-9.454	1.12	-9.314	0.9	-9.817	1.162	-9.362	1.124	-9.381
166	1.174	-11.773	1.224	-12.279	0.78	-13.026	0.972	-11.945	1.122	-12.027	1.203	-11.883	1.164	-11.831
167	1.171	-11.663	1.121	-10.555	1.102	-11.217	0.835	-10.676	1.027	-12.094	1.212	-11.739	1.172	-11.585
168	1.13	-13.13	0.743	-14.464	1.196	-12.91	1.165	-13.87	0.961	-13.55	1.165	-13.37	1.119	-13.161

Bus Number	True		Case 1		Case 2		Case 3		Case 4		Case 5		Case 6	
	Magnitude (p.u)	Angle (degree)	Magnitude (p.u)	Angle (degree)	Magnitude (p.u)	Angle (degree)	Magnitude (p.u)	Angle (degree)	Magnitude (p.u)	Angle (Degree)	Magnitude (p.u)	Angle (Degree)	Magnitude (p.u)	Angle (Degree)
		8				8		1		9		9		
169	1.106	-10.798	1.156	-9.503	1.086	-9.894	0.992	-11.236	1.119	-10.977	1.078	-10.819	1.099	-10.879
170	1.115	-10.133	0.896	-8.852	1.169	-11.441	1.202	-9.506	1.001	-10.592	1.118	-10.292	1.1	-10.14
171	1.119	-15.359	0.739	-16.924	0.696	-15.283	1.196	-14.311	1.097	-15.247	1.134	-15.432	1.113	-15.37
172	1.154	-12.533	0.811	-13.191	1.245	-11.552	1.269	-13.177	0.958	-12.74	1.189	-12.381	1.148	-12.594
173	1.141	-15.511	1.156	-15.241	1.178	-16.174	1.248	-15.713	1.241	-15.182	1.114	-15.561	1.154	-15.545
174	1.117	-17.25	0.954	-17.363	1.21	-17.368	0.922	-17.649	0.84	-16.985	1.112	-17.257	1.104	-17.248
175	1.238	-8.951	1.128	-9.842	1.22	-8.604	1.162	-9.306	1.05	-8.28	1.235	-8.881	1.246	-8.967
176	1.173	-7.877	0.986	-6.623	1.267	-8.636	0.972	-8.456	1.3	-7.698	1.214	-7.811	1.178	-7.928
177	1.216	-8.332	0.963	-9.11	0.962	-9.305	0.894	-9.257	0.981	-7.845	1.231	-8.352	1.223	-8.34
178	1.175	-11.559	1.188	-12.263	0.991	-11.019	0.905	-11.984	0.951	-11.476	1.162	-11.776	1.172	-11.492
179	1.213	-8.281	0.77	-8.258	1.178	-8.471	0.826	-7.474	1.057	-7.811	1.26	-8.252	1.211	-8.242
180	1.143	-1.73	0.859	-2.077	1.137	-1.661	0.863	-2.263	0.91	-2.273	1.131	-1.686	1.135	-1.816
181	1.175	-10.324	1.177	-9.941	1.225	-9.534	0.81	-10.255	1.114	-10.733	1.156	-10.313	1.164	-10.346
182	1.045	-7.192	0.805	-6.304	0.942	-7.554	0.788	-7.561	1.022	-6.641	1.092	-7.237	1.05	-7.205
183	1.038	-7.285	0.579	-7.083	1.134	-8.523	1.048	-7.672	1.134	-7.816	1.088	-7.459	1.024	-7.373
184	1.105	-5.698	0.735	-7.057	0.873	-4.778	0.859	-6.151	0.826	-5.338	1.155	-5.634	1.108	-5.656
185	1.12	-4.992	0.808	-4.27	0.956	-6.132	0.888	-4.045	0.893	-4.452	1.137	-4.841	1.127	-5.075
186	1.17	0.483	0.99	0.8	1.1	0.252	0.894	1.057	1.3	0.189	1.151	0.519	1.176	0.467
187	1.175	1.051	1.119	1.477	0.866	1.14	0.914	1.751	1.026	0.319	1.202	1.088	1.184	1
188	1.135	0.846	0.894	1.995	0.774	1.65	1.11	-0.172	0.997	0.324	1.154	0.667	1.131	0.806
189	1.173	0.654	1.124	0.516	1.129	1.21	1.043	0.57	1.135	0.419	1.218	0.758	1.167	0.717
190	1.14	6.44	1.048	5.341	0.957	6.477	0.865	5.998	1.075	6.648	1.14	6.266	1.145	6.345
191	1.149	-2.552	0.702	-3.866	1.003	-2.737	0.984	-2.981	1.12	-2.268	1.159	-2.745	1.144	-2.543
192	1.044	-6.308	0.613	-7.079	0.956	-6.03	0.669	-5.412	0.988	-6.259	1.038	-6.375	1.046	-6.232
193	1.063	-7.692	0.686	-7.441	0.701	-8.502	1.118	-7.121	1.182	-7.518	1.107	-7.54	1.054	-7.623
194	1.065	-6.484	0.61	-5.978	0.625	-7.577	0.716	-6.047	1.021	-7.101	1.045	-6.532	1.068	-6.579
195	1.06	-8.02	1.053	-8.695	0.816	-8.729	0.797	-9.005	1.147	-7.329	1.077	-8.152	1.059	-8.038
196	1.054	-6.563	0.843	-7.804	1.054	-6.419	1.047	-6	1.166	-6.907	1.101	-6.689	1.06	-6.564
197	1.072	-7.626	0.796	-8.999	1.105	-7.997	0.877	-7.108	0.974	-7.433	1.094	-7.832	1.073	-7.658
198	1.026	-2.685	0.578	-1.528	0.807	-3.152	0.921	-3.133	0.905	-2.442	1.008	-2.812	1.02	-2.636
199	1.117	-1.313	0.819	-1.361	1.036	-0.445	1.196	-1.699	0.944	-1.585	1.091	-1.537	1.127	-1.355
200	1.101	-1.207	0.968	-0.192	1.054	-1.297	0.949	-1.717	1.126	-1.889	1.156	-1.051	1.11	-1.163
201	1.077	0.089	0.733	0.73	0.874	0.482	0.694	-0.722	0.909	-0.55	1.052	-0.086	1.086	0.059
202	1.078	12.54	0.687	11.288	1.079	12.236	0.985	11.976	0.916	11.744	1.055	12.686	1.088	12.448

Bus Number	True		Case 1		Case 2		Case 3		Case 4		Case 5		Case 6	
	Magnitude (p.u)	Angle (degree)	Magnitude (p.u)	Angle (degree)	Magnitude (p.u)	Angle (degree)	Magnitude (p.u)	Angle (degree)	Magnitude (p.u)	Angle (Degree)	Magnitude (p.u)	Angle (Degree)	Magnitude (p.u)	Angle (Degree)
203	1.08	9.979	0.819	10.79	0.806	8.725	0.905	11.015	1.003	10.569	1.084	9.927	1.073	9.931
204	1.124	15.936	1.173	16.972	1.193	16.026	1.213	15.696	0.888	16.441	1.138	15.828	1.121	15.842
205	1.107	12.546	0.653	12.315	1.188	13.66	1.147	11.545	0.917	11.773	1.125	12.397	1.096	12.491
206	1.08	14.311	1.148	14.767	1.023	13.095	1.141	15.184	1.007	14.876	1.102	14.356	1.081	14.302
207	1.086	13.94	0.87	14.194	1.143	12.735	1.216	13.767	0.904	13.611	1.129	13.853	1.082	13.945
208	1.142	-3.127	1.17	-4.102	0.746	-2.859	1.142	-4.151	0.998	-3.821	1.124	-3.331	1.147	-3.158
209	1.151	-3.8	1.023	-4.918	0.785	-3.276	1.174	-3.171	0.88	-3.313	1.165	-3.904	1.146	-3.769
210	1.202	3.189	0.814	2.548	1.084	2.343	1.155	3.081	1.284	2.562	1.184	3.026	1.188	3.194
211	1.179	8.17	1.133	8.32	1.186	8.04	1.255	8.964	0.953	8.841	1.173	8.129	1.175	8.134
212	1.174	-1.865	0.743	-2.393	1.037	-2.127	0.775	-2.477	1.071	-1.679	1.183	-1.87	1.158	-1.931
213	1.145	-2.593	0.817	-1.835	1.016	-3.173	1.012	-2.224	1.225	-2.25	1.147	-2.793	1.157	-2.563
214	1.153	-0.147	1.026	-0.598	0.852	0.812	1.09	0.509	0.885	-0.923	1.186	-0.277	1.152	-0.181
215	1.179	8.193	1.13	7.567	1.056	7.124	1.192	7.057	0.965	7.623	1.185	8.014	1.177	8.187
216	1.135	16.614	1.083	16.21	0.711	15.362	1.084	16.083	1.239	16.122	1.117	16.769	1.126	16.674
217	1.137	13.87	0.777	14.231	0.736	14.819	1.068	13.084	1.153	13.219	1.114	13.991	1.13	13.902
218	1.137	16.907	1.207	17.213	0.714	15.907	0.778	16.442	1.099	16.436	1.112	16.844	1.121	16.977
219	1.039	-4.974	0.728	-4.088	0.949	-6.138	0.917	-5.452	0.912	-5.529	1.09	-5.165	1.044	-5.049
220	1.057	-8.039	0.785	-9.025	0.997	-6.868	0.872	-8.159	0.81	-7.821	1.032	-7.987	1.053	-8.078
221	1.188	7.516	0.84	7.438	0.8	7.354	1.335	8.169	1.147	7.102	1.201	7.358	1.199	7.449
222	1.135	7.135	0.648	7.471	1.119	6.644	0.961	7.101	0.973	6.839	1.185	7.034	1.14	7.045
223	1.088	10.046	0.958	9.121	1.116	10.245	0.81	9.861	0.82	10.312	1.131	9.909	1.085	10.016
224	1.076	8.964	1.02	9.654	0.89	8.476	0.864	8.173	1.027	9.158	1.106	8.758	1.074	8.957
225	1.085	11.882	0.659	10.748	0.687	11.099	0.944	12.504	0.955	11.219	1.127	11.727	1.089	11.867
226	1.05	-0.005	0.667	-1.054	0.929	-0.302	0.746	-0.118	0.811	0.646	1.044	0.069	1.059	-0.102
227	1.121	6.905	0.944	5.767	1.102	6.462	0.741	6.16	0.893	6.561	1.102	7.048	1.123	6.876
228	1.06	-6.754	1.106	-6.465	1.117	-6.278	1.038	-6.477	1.132	-6.368	1.044	-6.657	1.048	-6.826
229	1.048	-6.978	0.809	-6.727	0.634	-7.961	0.759	-7.135	1.095	-7.514	1.046	-7.112	1.042	-6.981
230	1.197	-9.418	1.184	-10.602	0.965	-9.328	1.19	-9.959	1.072	-9.045	1.185	-9.311	1.203	-9.332
231	1.124	7.698	0.905	7.706	1.016	7.256	1.266	8.32	0.936	8.249	1.171	7.768	1.123	7.742
232	1.18	-11.716	1.067	-12.028	0.914	-12.683	1.278	-12.091	1.209	-11.946	1.191	-11.742	1.163	-11.731
233	1.144	-2.416	1.056	-3.102	0.809	-1.918	1.114	-1.336	1.123	-1.872	1.195	-2.447	1.136	-2.345
234	1.231	1.136	0.895	-0.345	1.148	1.294	1.213	1.057	1.221	0.638	1.218	1.26	1.243	1.136
235	1.139	-1.604	0.93	-1.843	0.858	-1.845	1.279	-1.812	1.082	-2.258	1.166	-1.652	1.136	-1.547
236	1.094	-8.785	0.72	-9.295	1.082	-8.739	1.155	-7.721	1.154	-8.554	1.079	-8.657	1.088	-8.757
237	1.171	4.284	1.148	3.972	0.743	5.249	1.076	3.347	0.995	4.562	1.165	4.376	1.172	4.353
238	1.219	-7.93	0.912	-9.311	0.927	-8.665	0.947	-8.733	1.309	-7.24	1.246	-8.076	1.224	-7.921
239	1.181	8.217	1.25	7.026	1.19	9.332	0.957	7.545	0.946	8.173	1.219	8.24	1.178	8.17
240	1.128	-4.789	0.747	-3.898	0.984	-4.706	0.885	-5.49	1.224	-5.571	1.155	-4.754	1.118	-4.844
241	1.199	15.224	0.892	16.088	0.951	16.327	1.096	15.459	1.009	14.817	1.216	15.048	1.209	15.138

Bus Number	True		Case 1		Case 2		Case 3		Case 4		Case 5		Case 6	
	Magnitude (p.u)	Angle (degree)	Magnitude (p.u)	Angle (degree)	Magnitude (p.u)	Angle (degree)	Magnitude (p.u)	Angle (degree)	Magnitude (p.u)	Angle (Degree)	Magnitude (p.u)	Angle (Degree)	Magnitude (p.u)	Angle (Degree)
242	1.013	-15.631	0.545	-14.961	0.601	-16.968	0.657	-14.895	0.795	-15.397	1.024	-15.874	1.013	-15.685
243	1.054	-9.725	1.099	-10.581	0.863	-9.883	0.66	-9.441	0.999	-9.926	1.076	-9.963	1.052	-9.698
244	1.061	-9.865	0.616	-9.063	0.817	-11.03	0.698	-10.243	0.943	-10.338	1.053	-9.942	1.049	-9.942
245	1.048	-13.177	0.842	-14.726	0.774	-12.974	0.944	-14.203	1.033	-12.644	1.102	-13.113	1.044	-13.187
246	1.1	-12.229	0.831	-12.958	0.692	-13.329	0.752	-11.36	0.918	-12.398	1.124	-12.189	1.094	-12.19

Figure 4-5 and Figure 4-6 show the error in the estimated bus voltage magnitude and angle with respect to their true value for all the six cases. Table 4-7 shows the mean square error in the estimated states, obtained by the SE methods, for all the six cases. The result demonstrates that the accuracy of state estimation improves with the addition of PMUs in each cases.

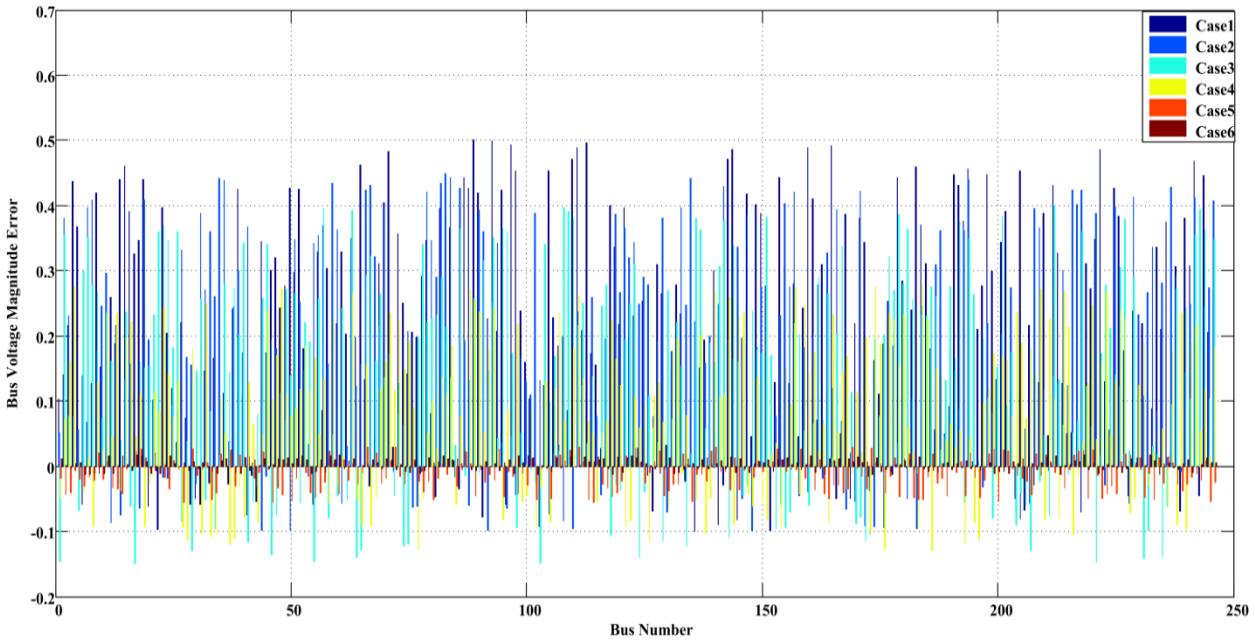

Figure 4-5: Bus voltage magnitude error for NRPG-246 bus system

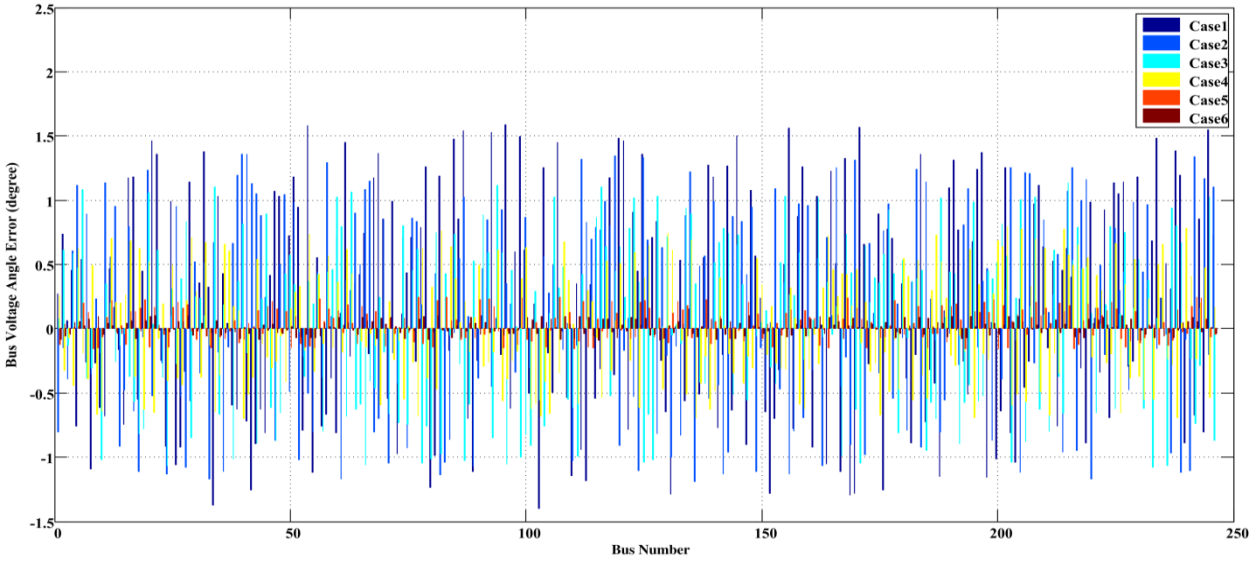

Figure 4-6: Bus voltage angle error for NRPG-246 bus system

Table 4-7: Comparison of state estimation error in NRPG – 246 bus system

Performance Index (p.u.)	Case 1	Case 2	Case 3	Case 4	Case 5	Case 6
Mean Square Voltage Error	0.07964	0.05973	0.04067	0.02162	2.563e-03	1.72e-05
Mean Square Angle Error	0.72355	0.54338	0.36321	0.18304	0.015017	0.002845

The bad data analysis as discussed in section 4.5 is carried out for case 5 of the NRPG - 246 bus system. Following the reference [38], the threshold value of normalized residual test is assumed to be 3, i.e. $\max|r_i^N| < 3$. To validate the performance of the normalized residual test, a gross error of 10σ is added to the measurements of real power flow between bus 75 and 76 (P75-76) and PMU voltage magnitude at bus 62 (V62). The five largest normalized residuals for this case are shown in Figure 4-7. In stage 1, the largest residual obtained is for voltage magnitude at bus 62 (V62) i.e. 34.1207 which is greater than the considered threshold value therefore V62 is eliminated from the measurement set and perform SE and calculate next normalized residual. In stage 2, P75-76 has the maximum residual, i.e 8.57, which is greater than threshold value. Eliminate the measurement P75-76 from the measurement set and repeat the same steps. Stage 3 shows that the largest normalized residual is less than the threshold value, hence all the bad data have been removed from the measurement set.

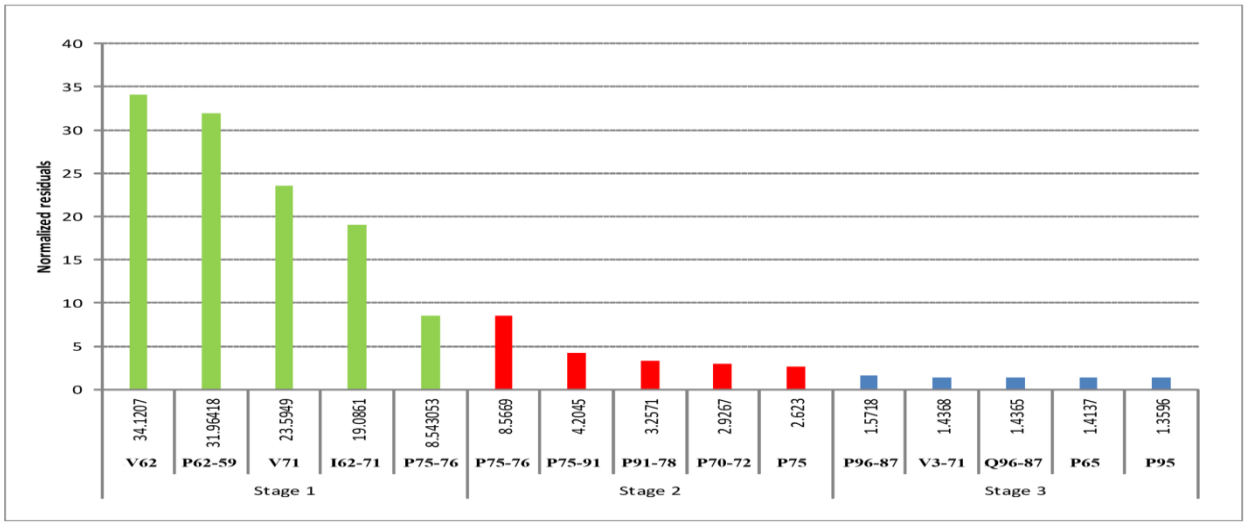

Figure 4-7:Bad data analysis using the Normalized Residual Method for NRPG-246 bus system

4.7 Conclusion

In this chapter, reduction in the state estimation error because of inclusion of phasor measurements received from PMUs have been discussed. In SE algorithm, both the phasor measurements received from the PMUs and the conventional measurements are used. The method is applied to the IEEE-30 and NRPG – 246 bus systems to validate the approach. It is clear from the results that the error between the actual and estimated values of power system states for the conventional and hybrid state estimators reduces considerably with the addition of PMUs. The normalized residual method for bad data detection performs effectively for conventional as well as PMU's data.

Once the states i.e. the voltage magnitude and voltage phase angle for all the buses in the system are estimated with maximum accuracy, the next step is to use these data for different power system application. In the next chapter, an online voltage stability monitoring technique has been proposed which utilizes bus voltage magnitudes and phase angles of the system in Support Vector Machine (SVM).

Chapter 5: Genetic algorithm based support vector machine for on-line Voltage Stability Monitoring

5.1 Introduction

In recent years, voltage collapse is a major cause for many power system blackouts [50] around the globe. The traditional method for voltage stability analysis relied on static analysis using the conventional power flow method such as Gauss-Seidel or Newton-Raphson method. In reference [52]–[56], numerous voltage stability indexes based upon conventional power flow have been proposed. The main drawback of these techniques is the singularity of the Jacobian matrix at the maximum loading point. To overcome this problem, Continuation Power Flow (CPF) method is used to compute voltage stability margin [57]. In reference [58], P-Q-V curve technique is proposed for voltage stability margin assessment which demonstrates the maximum limits of power demands and its corresponding voltage magnitude. The aforementioned techniques require comparatively large computations and are not efficient for on-line applications.

In recent years, the machine learning techniques such as artificial neural network (ANN), fuzzy logic, pattern recognition, support vector machine etc. have been used for power system analysis. Zhou et.al. [71], proposed a new online monitoring technique for voltage stability margin using synchrophasor measurement. Reference [72], introduces a method of using ANN model based approach for on-line voltage security assessment. The proposed approach uses radial basis function (RBF) networks to estimate the voltage stability level of the system under contingency state. Hashemi et al. uses wavelet transform for feature extraction of voltage profile along with RBF network to estimate voltage stability margin [73]. In [98] and [99], authors has proposed a novel algorithm for on-line monitoring of voltage instability using ANN. Usually, ANNs are considered more powerful, flexible method known for performing nonlinear regression. However, ANNs suffer from the amount of training time and the scores of the learning parameters. Support vector machine (SVM) is a new and powerful machine learning technique. It is based on the Vapnik-Chervonenkis (VC) dimension theory of statistical learning theory (SLT) and structural risk minimization principle [100]. Using this principle, SVM built optimized network structure with the right balance between the empirical error and VC- confidence interval. This balance gives a better generalization performance than

other neural network models. For the past several years, SVM has been successfully applied in solving a large range of practical problems in different areas [101]–[109].

Even though with these superior features, SVM is still limited to industrial application and academic research. It is because the user has to define various parameters known as hyper-parameters appropriately. Inappropriate selection of these parameters leads to overfitting or underfitting of SVM model. Therefore, the selection of these parameters is an important step in SVM modelling. At present, no general guidelines are available to select these parameters. The grid search (GS) method [110] is commonly used as parameter selection method for SVM. However, this method is prone to trap in local optimal points because GS is limited to the parameter value set initially [111]. It outperforms both in terms of accuracy and time efficiency. Particularly, in case when the optimized parameters are many or with large ranges, the time consumption is huge using grid algorithm method [112], [113].

In this chapter, Genetic Algorithm based Support Vector Machine (GA-SVM) approach is proposed for online monitoring of long-term voltage instability. Genetic Algorithm is used to optimize the SVM parameter such as RBF kernel (γ), regularization parameter (C) and insensitive loss function (ε) to improve the performance of SVM. GA-SVM is applied to emulate the continuation power flow for estimation of voltage stability margin index (VSMI) for steady state voltage stability analysis. The input features of GA-SVM are formed by voltage magnitude and voltage phase angle, which are assumed to be obtained from PMU. Although the PMUs have high precision level, still there are possibilities that the signal processing may introduce some errors in phasor calculation. Thus, the impact of these uncertainties in synchrophasor measurements is also analyzed to detect the deviation of VSMI at the operating point. The effectiveness of the proposed approach is tested on New England 39-bus test system and Indian Northern Region Power Grid (NRPG) 246-bus real system. Two different models, Grid Search based Support Vector Machine (GS-SVM) model and Multilayer Perceptron-back propagation neural network (MLP-BPNN) are considered in this study with same data set to compare the result of the proposed GA-SVM approach for voltage stability monitoring. The performance indices values along with Regression Receiver Operating Characteristic (RROC) curves and Area Over the RROC Curve (AOC) demonstrate that the GA-SVM outperforms the GS-SVM and MLP-BPNN models.

5.2 Problem Formulation

5.2.1 Voltage Stability Assessment (VSA)

The main objective of voltage stability analysis is to determine whether the current operating point of power system is stable, meeting various operational criteria. The voltage vs real power curve (P-V curve) [52] as shown in Figure 5-1 can be used directly to obtain voltage stability margin. Considering if at the current operating point the total active power delivered to the load is $P_{current}$ and the maximum active power transfer is $P_{\max}$, then the Voltage Stability Margin (VSM) for the load bus i, can be calculated as

$$VSM_i = P_{\max,i} - P_{current,i}, where\, i = 1, 2....l \tag{5.1}$$

Where, l is the total number of load buses in the power system. The Voltage stability margin index (VSMI) for the network is given by:

$$VSMI = \min(\frac{VSM_i}{P_{\max,i}}) \tag{5.2}$$

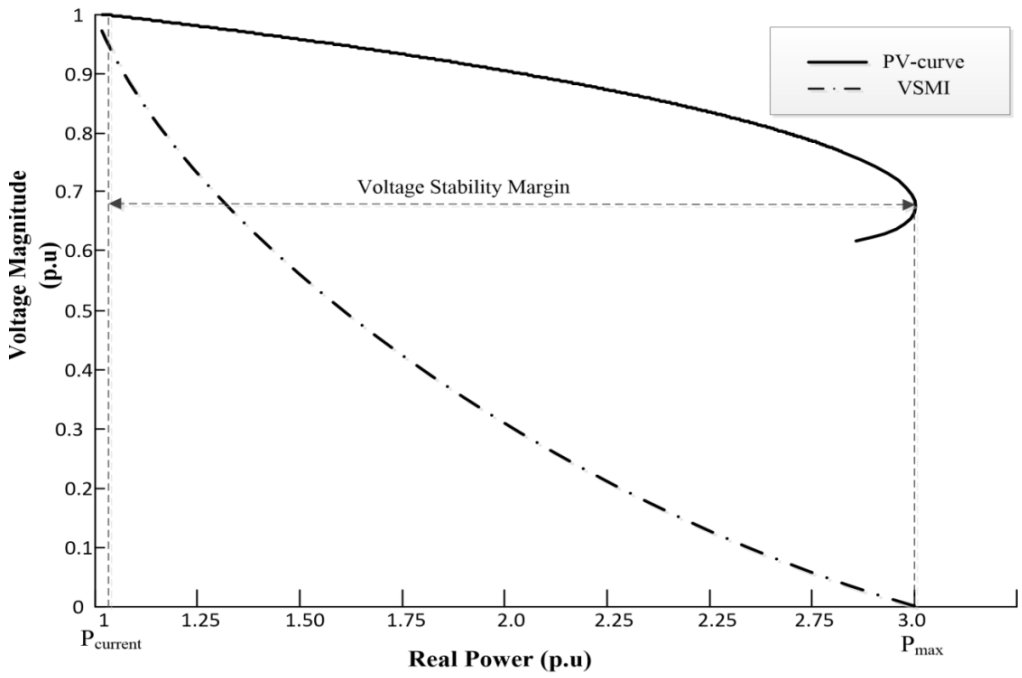

Figure 5-1: P-V Curve

VSMI is an indicator that determines the proximity to the voltage collapse point. The VSMI varies in a range between 1 (no load) and 0 (maximum loadability). Figure 5-1 shows that as the operating point moves to voltage collapse point the VSMI defined by (5.2) approaches to

zero. Therefore, VSMI is a suitable indicator for voltage stability monitoring. To determine the collapse point, PV curve is drawn using the continuous Power Flow (CPF) technique [55], [114]. CPF is used because the conventional power flow (Gauss-Seidel or Newton- Raphson) method fails to converge as the operating point reaches the nose point (voltage collapse point) of PV curve.

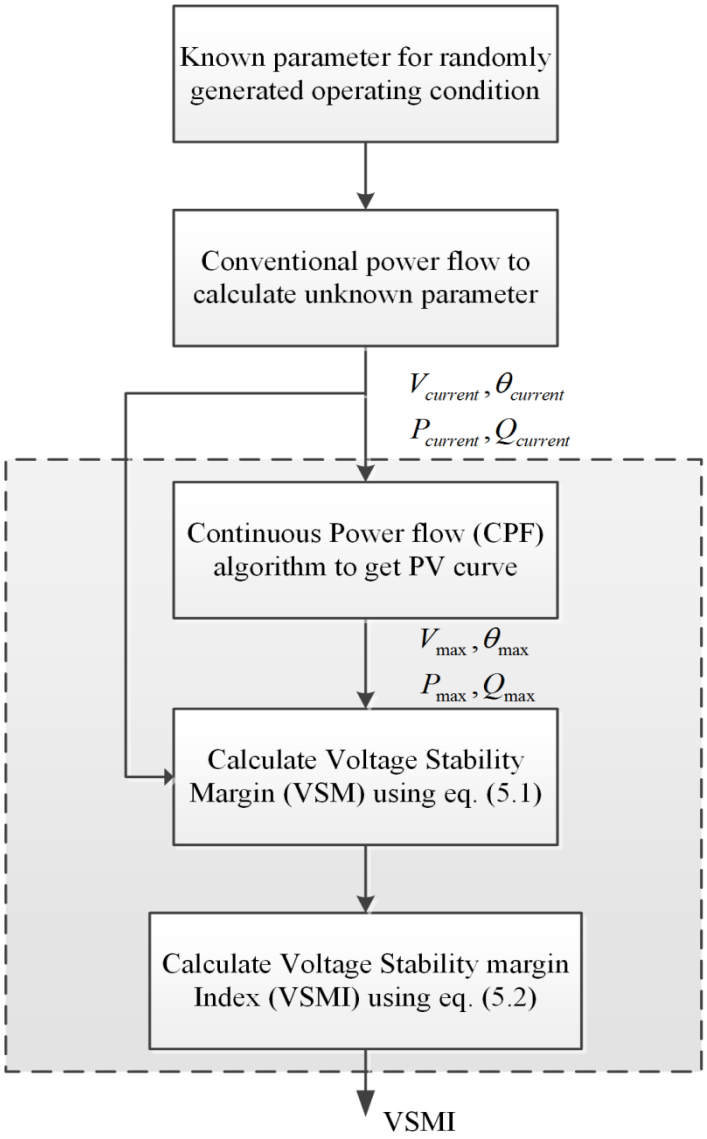

Figure 5-2: Procedure to calculate VSMI

The CPF program calculates the voltage stability limit starting from a specified initial operating point. The flow of the procedure involved in the determination of VSMI is shown in Figure 5-2. Every power network has different types of nodes. For PV-node, real power and voltage magnitude are known and for PQ-nodes, real and reactive power are specified. So these known parameters are fed to conventional power flow to calculate the values of voltage magnitude (

$V_{current}$), voltage phase angle ($\theta_{current}$), real power ($P_{current}$) and reactive power ($Q_{current}$) at the current operating condition. With these calculated values, the CPF is used to trace the PV-curve and to determine $V_{\max}, \theta_{\max}$, $P_{\max}$ and $Q_{\max}$ as the parameters corresponding to voltage collapse point. Then these parameters are used to calculate VSM and VSMI using (5.1) and (5.2), respectively.

To predict the VSMI, the computations shown inside dotted area in Figure 5-2 are replaced by GA-SVM model. The major advantage of using GA-SVM is that it avoids the traditional iterative procedure to find VSMI and can be used for real time application. The input vector to GA-SVM is voltage magnitude and voltage phase angle, which are assumed to be obtained from PMUs. PMU data suffers from the measurement uncertainties, which are discussed in the next section.

5.3 PMU Uncertainty Modeling

PMU measurements i.e. voltage magnitude and phase angle are used for the prediction of VSMI. Although, the precision level of PMU is very high, still there is a possibility of some error in the measurements. According to IEEE standard C37-118-1 [115], these uncertainties in synchrophasor measurements are considered in terms of Total Vector error (TVE). For measurement specification, TVE is an important criteria for synchrophasor and it should be less than 1% under steady state condition. TVE defines as the difference between the ideal or theoretical value and its measured representation. It is important to note that either a magnitude error of 1% alone or a phase error of 0.57^0 (0.01 rad) alone causes the TVE to be equal to 1%. The TVE can be represented as

$$TVE = \sqrt{\frac{[y_r^* - y_r]^2 + [y_i^* - y_i]^2}{y_r^2 + y_i^2}} \tag{5.3}$$

Where, y_r^* and y_i^* are the real and imaginary part of the measured values, while y_r and y_i are the real and imaginary part of the ideal values. In the present work, the TVE is modeled by inducing voltage magnitude error ΔV_i and phase angle error $\Delta\theta_i$ into real values such that TVE is always less than 1%. Therefore the value of ΔV_i and $\Delta\theta_i$ are selected randomly such that that TVE $\leq$ 1%. The new inputs with measurement uncertainty are represented as:

$$V_n^i = V_t^i(1+\Delta V_i)$$
$$\theta_n^i = \theta_t^i(1+\Delta\theta_i) \quad (5.4)$$

Where, V_n^i and θ_n^i are the new values of voltage magnitude and phase angle for i^{th} load bus, respectively and V_t^i and θ_t^i are the true values of voltage magnitude and phase angle for i^{th} load bus, respectively.

5.4 Support Vector Machine (SVM)

Support Vector Machine (SVM) is a novel machine-learning tool that has been originated from Statistical Learning Theory (SLT) developed by Vapnik [116] in 1995. SVM works on the principle of structural risk minimization seeking to minimize an upper bound of the generalization error, rather than minimize the training error. Originally, SVM has been developed to solve pattern recognition problems [117]. However, with the introduction of Vapnik's ε -insensitive loss function, SVM has been extended to solve nonlinear regression estimation problems. Therefore, SVM is capable of performing both classification and function estimation in the regression problems. SVM for regression is briefly described in this section [116], [117].

5.4.1 SVM Regression Theory

Considering a set of training data made up of input/output pairs $(x_1, y_1),.....,(x_m, y_m)$, where x_i is input attribute vector consist of voltage magnitude and voltage phase angle for ith operating point, and each $x_i \in R^n$ the input space of the sample. y_i are associated target values i.e. VSMI and m corresponds to the size of the training data. The idea of the regression problem is to determine a linear function that can approximate the relationship between the data set and can be used to estimate target VSMI with respect to an input vector of new operating point. Using mathematical notation, the regression function takes the form:

$$f(x) = \omega\phi(x) + b, \quad (5.5)$$

Where, $\omega \in R^n, b \in R$. $\phi(x)$ denotes the high dimensional feature space, which is nonlinearly mapped from the input space x. The objective is to find the value of the weight vector (ω) the values bias (b) such that values of x can be determined by minimizing the regularized risk function.

$$R_{reg}(f) = C\frac{1}{m}\sum_{i=0}^{m}\xi(f(\mathbf{x}_i) - y_i) + \frac{1}{2}\|\omega\|^2 \tag{5.6}$$

Where, ω, denotes the Euclidean norm, C denotes a cost function measuring the empirical risk and ξ (.) is a loss function. The ε –insensitive loss function is the most widely used loss functions. The function is in the form:

$$\xi(f(\mathbf{x}_i), y_i) = \begin{cases} |f(\mathbf{x}) - y| - \varepsilon & |f(\mathbf{x}) - y| \geq \varepsilon, \\ 0 & otherwise, \end{cases} \tag{5.7}$$

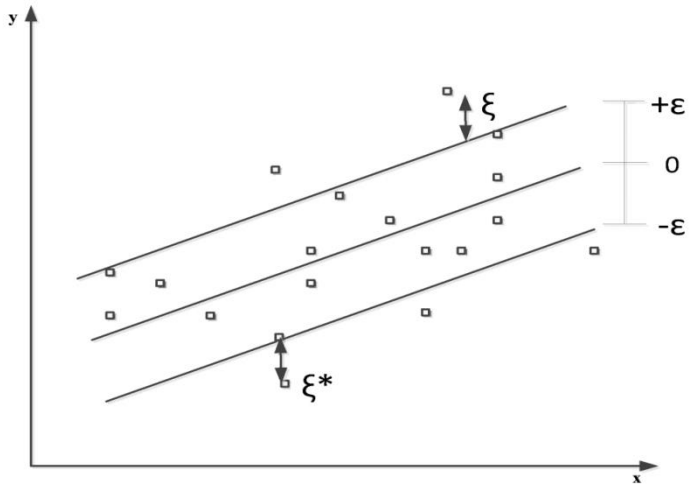

Figure 5-3: Support Vector Machine for Regression

In Eq. (5.6), the first term $C\frac{1}{m}\sum_{i=0}^{m}\xi(f(\mathbf{x}_i) - y_i)$, represents the empirical error, which is estimated by the ε-insensitive loss function in Eq. (5.7). The second item $\|\omega\|^2/2$, is the regularization term. The regularized constant C calculates the penalty when an error occurs, by determining the trade-off between the empirical risk and the regularization term, which represents the ability of prediction for regression. The ε-insensitive loss function is employed to reduce noise. Thus, ε can be viewed as a tube size equivalent to the training data accuracy in training data as shown in Figure 5-3. In the empirical analysis, C and ε are the parameters selected by users.

To estimate ω and b, Eq. (5.5) is converted to the primal function given by (5.8), by introducing ξ_i and ξ_i^*. According to Figure 5-3, the excess positive and negative deviations are represented by ξ_i and ξ_i^*, respectively. These variables are assumed non-zero values outside

the ε – tube. The SVM fits f(x) to the data such that it minimizes ξ_i , ξ_i^* and $\omega,$. Thus, SVR is formulated as minimization of the following functions:

$$\begin{aligned} &Minimize\, R_{reg}(\omega, \xi^{(*)}) = \frac{1}{2}\|\omega\|^2 + C\sum_{i=1}^{n}(\xi_i + \xi_i^*) \\ &subjected\, to \begin{Bmatrix} f(\mathbf{x}_i) - \omega\phi(x_i) - b_i\varepsilon + \xi_i \\ \omega\phi(x_i) + b_i - f(\mathbf{x}_i)\varepsilon + \xi_i^* \end{Bmatrix} \xi^{(*)} \geq 0, \end{aligned} \tag{5.8}$$

Where, ξ_i and ξ_i^* denote slack variables that measure the error of the up and down sides, respectively. The above formulae indicate that increasing ε decreases the corresponding ξ_i and ξ_i^* in the same.

Dual formulation of (5.8) leads to maximization optimization problem [117] as shown by (5.9).

$$\begin{aligned} &W(\alpha_i, \alpha_i^*) = \max(-\frac{1}{2}\sum_{i,j=1}^{m}(\alpha_i - \alpha_i^*)(\alpha_j - \alpha_j^*)K(\mathbf{x}_i \cdot \mathbf{x}_j) - \varepsilon\sum_{i=1}^{m}(\alpha_i + \alpha_i^*) + \sum_{i=1}^{m} y_i(\alpha_i - \alpha_i^*)) \\ &such\, that \\ &\quad \sum_{i=1}^{\ell}\alpha_i - \alpha_i^* = 0, \quad \alpha_i, \alpha_i^* \in [0, C] \end{aligned} \tag{5.9}$$

The Lagrange multipliers, $\alpha_i\, and\, \alpha_i^*$, represent solutions to the above quadratic problem that act as forces pushing predictions towards target value yi. Only the non-zero values of the Lagrange multipliers in equation (5.9) are useful in forecasting the regression line and are known as support vectors. For all points inside the ε – tube, the Lagrange multipliers equal to zero do not contribute to the regression function. Only if the requirement $|f(\mathbf{x}) - y| \geq \varepsilon$, as shown in Figure 5-3 is fulfilled, the Lagrange multipliers may be non-zero values and used as support vectors.

In eqn. (5.9) the term $k(x_i, x_j)$, known as the kernel function, where the value of kernel function is vectors product of two vector x_i and x_j in the feature space $\phi_i(x)$ and $\phi_j(x)$, i.e. $k(x_i, x_j) = \phi_i(x) \times \phi_j(x)$ where $i, j = 1, 2....., m.$ Kernel functions give dot product directly in higher dimensional without calculating ϕ. In machine learning theories, the popular kernel functions are:

1) Linear kernel: $k(\mathbf{x}_i, \mathbf{x}) = x_i^T x_j$

2) Polynomial kernel: $k(\mathbf{x}_i, \mathbf{x}) = (1 + x_i \bullet x_j)^d$

3) Gaussian (RBF) kernel: $k(\mathbf{x}_i, \mathbf{x}) = \exp(-\frac{\|x_i - x_j\|^2}{2\sigma^2})$

where, x_i and x_j are input vector spaces, d is the degree of the polynomial kernel, and σ^2 is the bandwidth of the RBF kernel. These parameters must be selected accurately, since they control the structure of high-dimensional feature space and manage the complexity of the final solution.

5.4.2 Selection of SVM parameter

Selection of optimal SVM parameters is an important step in SVM design. The parameters in SVM for regression are:

(1) Kernel function: The kernel function is used to build a nonlinear decision hyper-surface on the SVR input space. There are different types of kernel function as discussed in section 5.4.1. Out of these kernel functions, Gaussian (RBF) function will yield superior estimate performance [118]. Therefore, in this work the Gaussian function is used as the kernel function.

(2) Regularization parameter C: C controls the tradeoff between minimizing the model's complexity and minimizing the training error.

(3) Bandwidth of the RBF kernel function σ^2: σ^2 represents the variance of the Gaussian kernel function.

(4) ε : ε is a radius of a tube of ε-insensitive loss function within which the regression function must lie.

In [111], the author has proposed a technique to select these parameters known as grid search (GS) SVM. The grid-search is straightforward but seems time consuming. Therefore, in the proposed work a real value GA is used to determine the free parameters of SVM, known as GA-SVM, which simultaneously optimizes all SVM parameters from the training data.

5.5 GA-SVM model

In non-linear SVM, the setting of train parameters C, σ^2 and ε plays a significant role in its generalized performance. In the proposed work, genetic algorithm (GA) is used to find the

optimal values of SVM parameters. Then these optimized parameters are used to construct the SVM model in order for proceeded prediction. Figure 5-4 illustrates the proposed GA-SVM approach. The genetic algorithm randomly generates an initial population of chromosomes to search for the optimal value of SVM parameters. The SVM parameters i.e. C, σ^2 and ε, are directly coded in the chromosomes with real value data. The detailed stepwise description of the proposed GA-SVM model is as follows:

Step I Representation: The three parameters to be optimized in GA-SVM C, σ^2 and ε are coded to generate the chromosomes. The chromosomes X is represented as $X = \{x_1, x_2, x_3\}$, where x_1, x_2 and x_3 denotes the SVM parameters C, σ^2 and ε respectively.

Step II Fitness definition: To prevent overfitting and underfitting of GA-SVM model, cross validation technique is used for selection of optimal SVM parameters. In K-fold cross validation, the training set is randomly divided into K subsets of equal size. The SVM regression model is constructed with a given set of parameter using (K-1) subset as the training set. The performance of the SVM parameters is checked on the K^{th} subset. The above procedure is repeated such that each subset can be used once as testing set. In the proposed work, five-fold cross validation technique is considered. Therefore, the fitness function defined as the Mean Absolute Percentage Error (MAPEcross_val) of the five-fold validation method on the training set and is given by:

$$\min f = MAPE_{cross\_val}$$
$$MAPE_{cross\_val} = \frac{\sum_{i=1}^{m}\left|\frac{A_i - P_i}{A_i}\right|}{m} * 100\% \tag{5.10}$$

Where, m is the number of samples in the training set; is the actual value and is the predicted value. The solution with a smaller value of MAPEcross_val has a better chance of surviving in the successive generation.

Step III Population initialization: In the proposed study, the initial population composed of twenty randomly created chromosomes. The population size is selected as a trade-off between the convergence time and population diversity.

Step IV Fitness evaluation: The fitness value for each randomly generated chromosomes in step III is calculated using (5.10).

Step V Creating new population: Selection, crossover and mutation are carried out to replace the current population by the newer population. The chromosomes with better fitness values are selected into the recombination pool using the roulette wheel. Genes between two parents chromosomes are exchanged to obtain new offspring to attempt to get better solutions, the probability of creating new chromosomes in each pair is set to 0.8. Mutation is performed to alter the binary code with a probability of 0.05.

Step VI Stopping criteria: The process is repeated until from step IV to step V until the generation count reaches its limit.

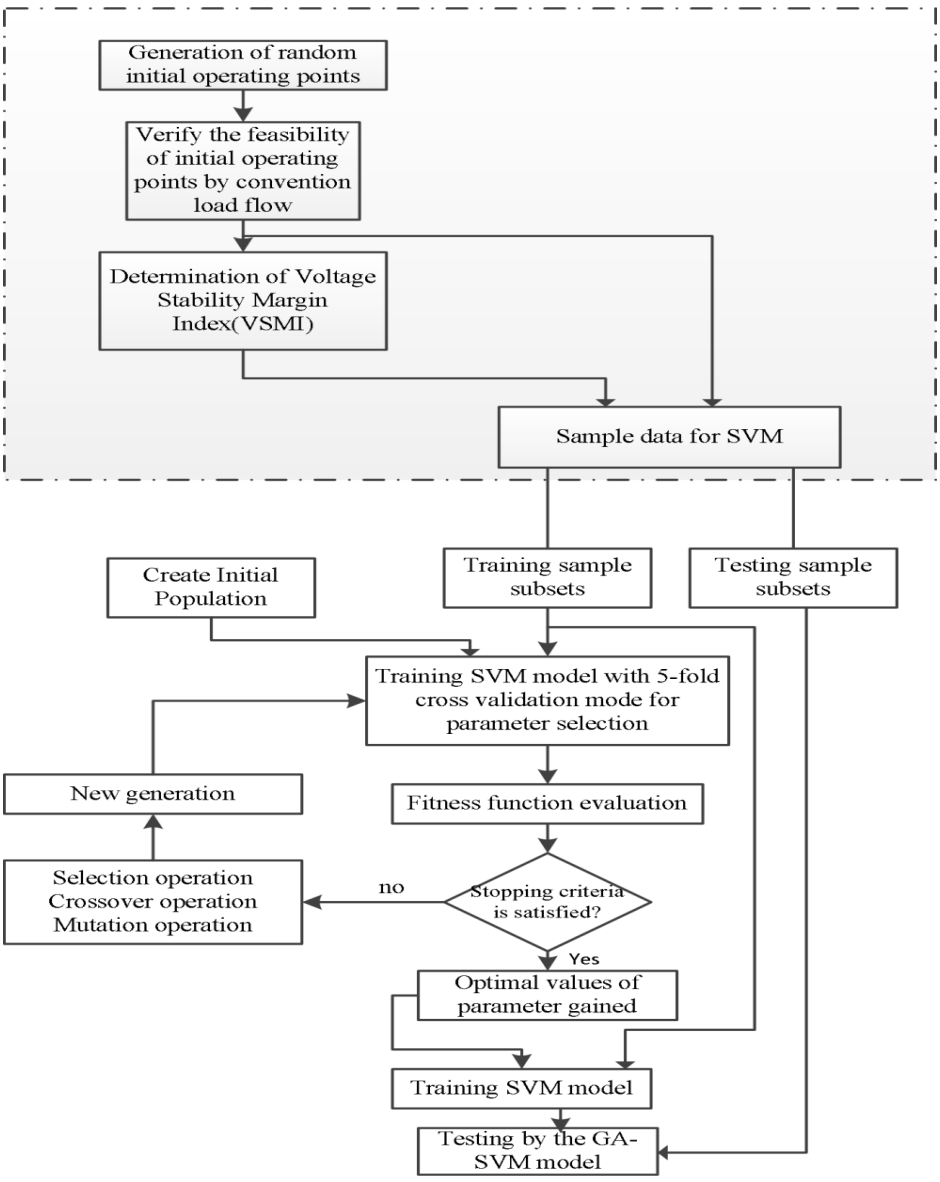

Figure 5-4: Flowchart for GA-SVM model

Table 5-1 gives the list of GA parameter settings used in the proposed GA-SVM model. The choice of these parameters is based on numerous trials, as those values provide the smallest $MAPE_{cross\_val}$ on the training set.

Table 5-1: Genetic Algorithm parameter setting

Parameters	Settings
C	0.1-1000
σ^2	0.1-100
ε	0.001-0.1
Generations	100
Population size	1000
Selection type	Standard roulette wheel
Crossover type	Simulated binary
Mutation type	Polynomial method
Crossover probability	0.8
Mutation probability	0.05

To check the performance of the overall GA-SVM model different performance indices are considered in the proposed approach. Next section gives the list of performance indices considered in this work.

5.5.1 GA-SVM performance measures

To evaluate the performance of the GA-SVM model following indices have been evaluated:

Table 5-2: Performance indices and their expressions

Indices	Expressions
Mean Absolute percentage Error (MAPE)[a]	$MAPE = \frac{1}{m}\sum_{i=1}^{m}\left\|\frac{A_i - P_i}{A_i}\right\| * 100$
Normalized Mean Square Error (NMSE)	$NMSE = \frac{1}{\delta^2 m}\sum_{i=1}^{m}(A_i - P_i)^2$ $\delta^2 = \frac{1}{m-1}\sum_{i=1}^{m}\left(A_i - \overline{A}\right)^2$
Willmott's Index of Agreement (WIA) [119]	$WIA = 1 - \frac{\sum_{i=1}^{m}(A_i - P_i)^2}{\sum_{i=1}^{m}\left(\left\|A_i - \overline{A}\right\| + \left\|P_i - \overline{A}\right\|\right)^2}$ $\overline{A} = \frac{1}{m}\sum_{i=1}^{m}A_i$

[a] A_i and P_i are the actual and predicted values

Table 5-2 shows the Performance indices and their expressions to find the deviation between the actual output and the predicted output. The smaller the value of MAPE and MPE, the closer the predicted value to actual value. The WIA measures the regression degree and varies from 0 (complete disagreement) to 1 (perfect agreement). The closer WIA is to 1, the more accurate are the predicted result.

5.6 Results

To establish the effectiveness of the proposed GA-SVM based approach for online voltage stability monitoring, it has been tested on New England 39-bus test system [120] and the Northern Regional Power Grid (NRPG) 246-bus Indian system [95]. The details of these systems are given in Appendix A.

The results of the proposed approach are compared with other machine learning models i.e. grid search (GS) SVM and multilayer perceptron-back propagation neural networks (MLP-BPNN) using same dataset. The details of these machine learning models are given in Appendix B. Selection of input features for voltage stability margin can be expressed as a function of the four variables i.e. voltage magnitude, voltage phase angle, real power and reactive power that defines the system operating point. In this work, voltage magnitude and voltage phase angle are taken as the input to the GA-SVM model. It is assumed that the values of voltage magnitude and phase angle are the output of PMUs. These PMUs are installed in the system for complete observability. This means that the data is available for all the load buses. For generating sample data for the GA-SVM, active and reactive powers at the load buses are varied randomly within ±30% of the base case values. In the present work, 3000 random operating points are generated for training and another 100 operating points are used to verify the performance of proposed GA-SVM approach.

In GA-SVM model, genetic algorithm is used to get the optimal values of SVM parameter i.e. RBF kernel function σ^2, regularization parameter (C) and insensitive loss function (ε). Table 5-3 shows the optimal values of SVM parameter for New England 39-bus system and NRPG 246-bus system. Figure 5-5(a) and Figure 5-5(b) demonstrates the best fitness values versus the number of generation for New England 39-bus system and NRPG 246-bus system respectively.

Table 5-3: SVM parameter optimized by genetic algorithm

Test System	SVM Parameter			Fitness function
	C	σ^2	ε	
New England 39-bus system	29.6946	3.9951	0.0243	0.0099
NRPG 246-bus system	45.0560	0.2463	0.001	0.0054

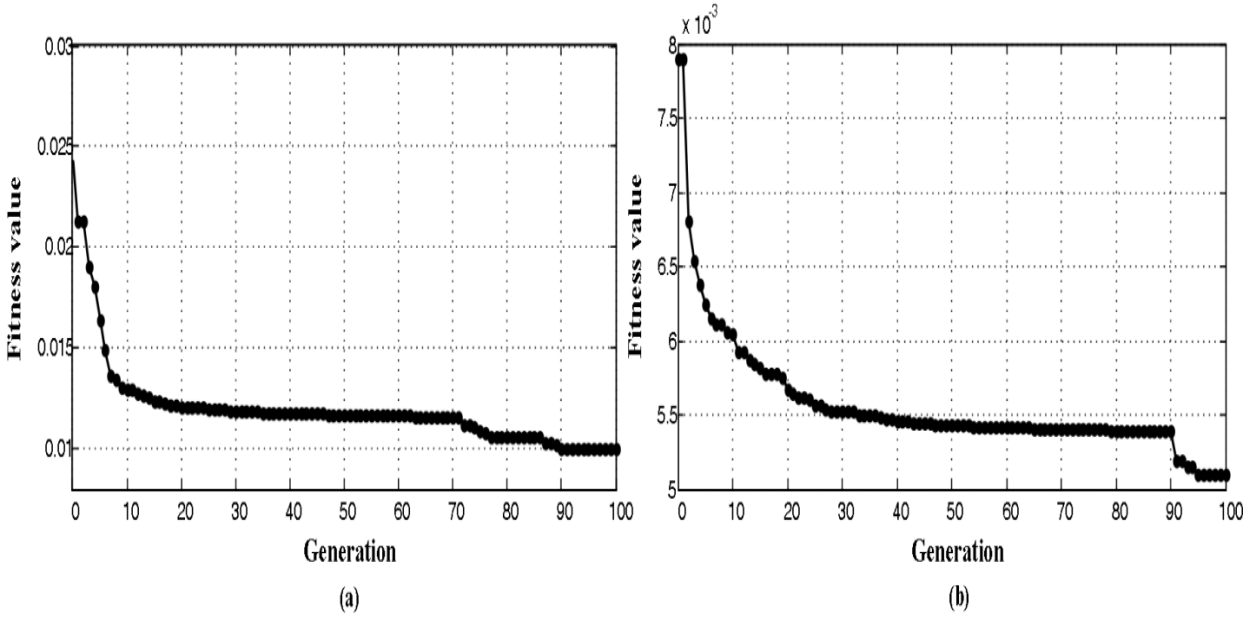

Figure 5-5: Convergence curve of GA optimization (a) New England 39-bus system; and (b) NRPG 246-bus system.

These optimal parameters are used to construct the GA-SVM models for both the test case considered in this study.

5.6.1 New England 39-bus system

The procedure as explained in section 3.2 of chapter 3 is used to identify the most critical buses in the New England 39-bus system. The most critical bus for New England 39-bus system is identified as bus number 12. To validate the VSMI proposed in this chapter, the PV curve of Load bus 12 and the corresponding VSMI for the system is shown in Figure 5-6.

This figure shows that the proposed voltage stability index obtained from CPF program is able to indicate the stability limit of the system. This means that the data is available from CPF is accurate and used for training the GA-SVM model. For generating sample data for the GA-SVM, active and reactive powers at the load buses are varied randomly within ±30% of the base case values.

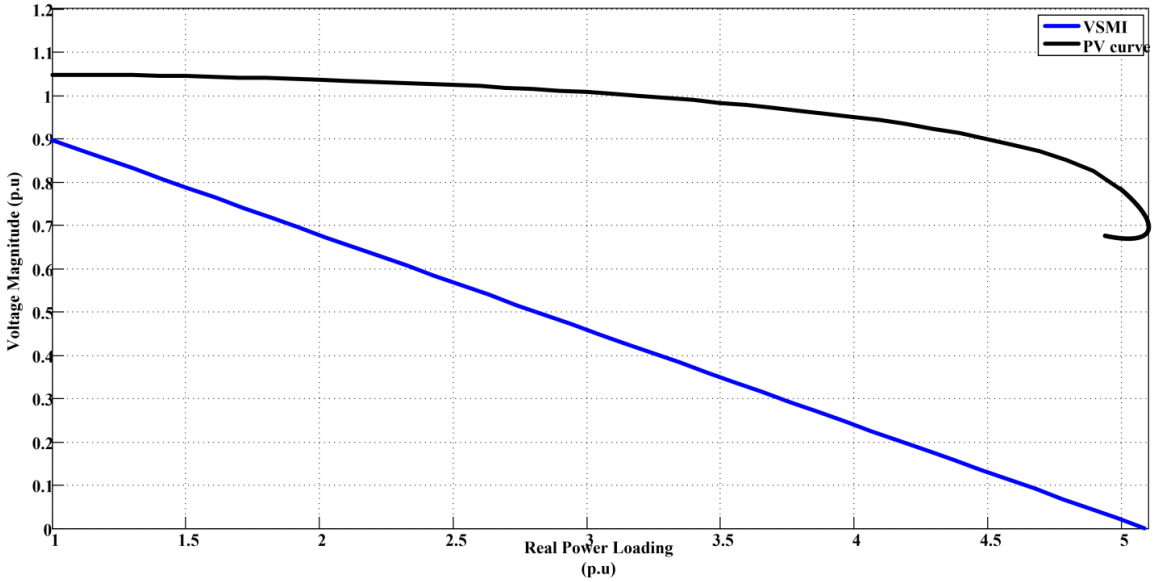

Figure 5-6: PV curve and VSMI of bus 12 in New England 39-bus system

Table 5-4 lists the performance indices of both training data used as input and the100 unseen test cases for New England 39-bus system.

Table 5-4: GA-SVM performance index on training and testing data for New England 39-bus system

Performance Indices	**New England 39-bus system**	
	Training Data	**Testing Data**
Mean Absolute percentage Error (MAPE)	0.0081	0.0025
Normalized Mean Square Error (NMSE)	0.3690	4.1997
Willmott's Index of Agreement (WIA)	0.9979	0.9994

The GA - SVM model is tested for the input having measurement error caused due to PMU uncertainty as explained in section 5.3. Table 5-5 lists the performance indices of 100 unseen test cases with and without measurement. The results show that the GA-SVM is still able to accurately predict the VSMI when measurement error is included. To estimate accuracy of the proposed GA-SVM model, it has been compared with two different models i.e. GS-SVM and MLP-BPNN model.

The performance indices obtained using these models for 100 unseen test cases are given in Table 5-6. The table shows that the GA - SVM model is superior to other models. The smaller values of performance indices MAPE and NMSE indicate a small deviation between the predicted and the actual values. Further, Regression Receiver Operating Characteristic (RROC) curves and Area Over the RROC Curve (AOC) [121] have been considered as the basis for evaluating the performance of the models. RROC curve is a two-dimensional graphs

representing over-estimation against under-estimation, plotted on the X- and Y-axis, respectively. The AOC is proportional to the error variance of the regression model. Therefore, least value of AOC indicates better model for the given operating condition.

Table 5-5: GA-SVM performance index for VSMI estimation with PMU measurement error for New England 39-bus system

Performance Indices	**New England 39-bus system**	
	Without measurement error	**With measurement error**
Mean Absolute percentage Error (MAPE)	0.0025	0.105
Normalized Mean Square Error (NMSE)	4.1997	5.543
Willmott's Index of Agreement (WIA)	0.9994	0.9981

AOC value is least for GA-SVM model indicating best model for VSMI prediction. The higher value of WIA rating indicates that VSMI predicted by GA_SVM have more precision as compared to the GS-SVM, MLP-BPNN models.

Table 5-6: Performance index for VSMI estimation from each model without measurement error for New England 39-bus system

Performance Indices	**New England 39-bus system**		
	GA-SVM	GS-SVM	MLP-BPNN
Mean Absolute percentage Error (MAPE)	0.0025	0.0059	0.0692
Normalized Mean Square Error (NMSE)	4.1997	5.3707	7.7003
Willmott's Index of Agreement (WIA)	0.9994	0.9985	0.9982
Area Over the RROC Curve(AOC)	23.9024	89.3907	100.2418

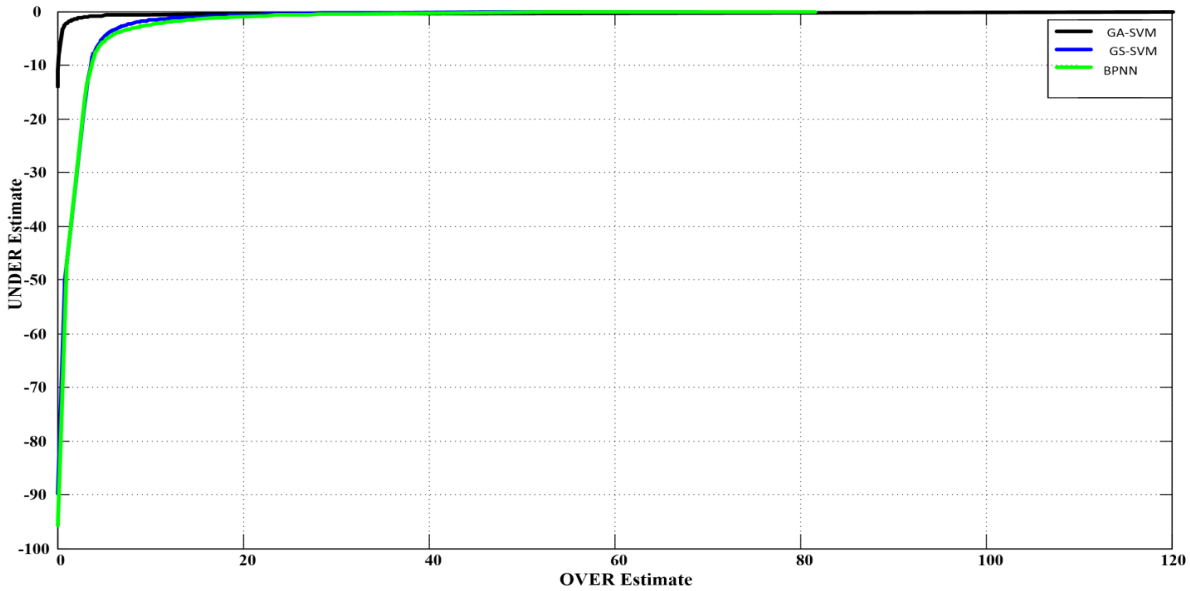

Figure 5-7: RROC curve of New England 39-bus system

Figure 5-7 shows the RROC curve of all the models considered in this work. The curve shows that GA-SVM model is more accurate when compared with other two models.

GA-SVM model has also been compared with the other models, with consideration of the uncertainty in the input data as explained in section 5.3. The result given in Table 5-7 shows that, the GA-SVM model is considerably better as compared to the other models even with measurement uncertainty.

Table 5-7: Performance index for VSMI estimation from each model with measurement error for New England 39-bus system

Performance Indices	**New England 39-bus system**		
	GA-SVM	GS-SVM	MLP-BP1
Mean Absolute percentage Error (MAPE)	0.105	0.2478	0.9064
Normalized Mean Square Error (NMSE)	5.543	7.088	8.1627
Willmott's Index of Agreement (WIA)	0.9981	0.9972	0.9969
Area Over the RROC Curve(AOC)	29.694	111.048	105.92

5.6.2 NRPG 246-bus system

Bus no 168 is identified as the most critical bus in the NRPG 246-bus system. The bus number 168 is ranked 1 as shown in table 3-9 in chapter 3. The PV curve of bus number 168 and the corresponding VSMI for the system is shown in Figure 5-8. 3000 random operating points are generated for training and another 100 operating points are used to verify the performance of proposed GA-SVM approach.

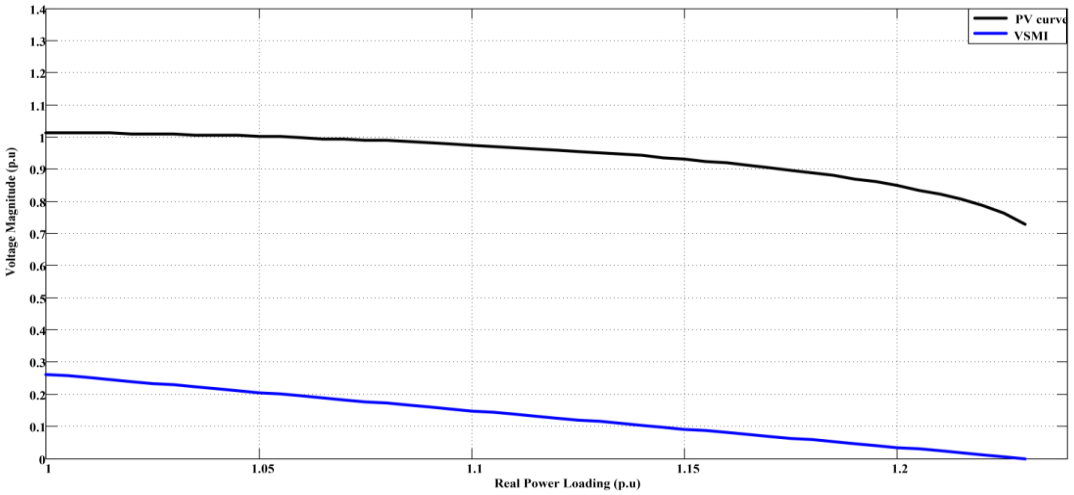

Figure 5-8: PV curve and VSMI of bus 168 in NRPG 246-bus system

The optimal parameters given in Table 5-3 are used to construct the GA-SVM models. Table 5-8 lists the performance indices of both training data used as input and the100 unseen test cases.

Table 5-8: GA-SVM performance index on training and testing data for NRPG 246-bus System

Performance Indices	**NRPG 246-bus system**	
	Training Data	**Testing Data**
Mean Absolute percentage Error (MAPE)	3.76e-4	0.0176
Normalized Mean Square Error (NMSE)	1.0962	5.3567
Willmott's Index of Agreement (WIA)	0.9990	0.9954

The GA - SVM model is tested for the input having measurement error caused due to PMU uncertainty as explained in section 5.3. Table 5-9 lists the performance indices of 100 unseen test cases with and without measurement error. The results show that the GA-SVM is able to accurately predict the VSMI when measurement error is included.

Table 5-9: GA-SVM performance index for VSMI estimation with PMU measurement error for NRPG 246-bus System

Performance Indices	**NRPG 246-bus system**	
	Without measurement error	**With measurement error**
Mean Absolute percentage Error (MAPE)	0.0176	0.0563
Normalized Mean Square Error (NMSE)	5.3567	7.4667
Willmott's Index of Agreement (WIA)	0.9954	0.9914

Table 5-10 compares the performance of GA-SVM, GS-SVM, and MLP-BPNN models for 100 unseen test cases. The table shows that the GA - SVM model is superior to other models. The smaller values of performance indices MAPE and NMSE indicate a small deviation between the predicted and the actual values. AOC value is least for GA-SVM indicating best model for VSMI prediction. The higher value of WIA rating indicates that VSMI predicted by GA_SVM have more precision as compared to the GS-SVM, and MLP-BPNN models.

Table 5-10: Performance index for VSMI estimation from each model without measurement error for NRPG 246-bus System

Performance Indices	**NRPG 246-bus system**		
	GA-SVM	GS-SVM	MLP-BPNN
Mean Absolute percentage Error (MAPE)	0.0176	0.0536	0.035
Normalized Mean Square Error (NMSE)	5.3567	7.75776	7.7908
Willmott's Index of Agreement (WIA)	0.9954	0.9843	0.9893
Area Over the RROC Curve(AOC)	7.1716	11.2459	64.4750

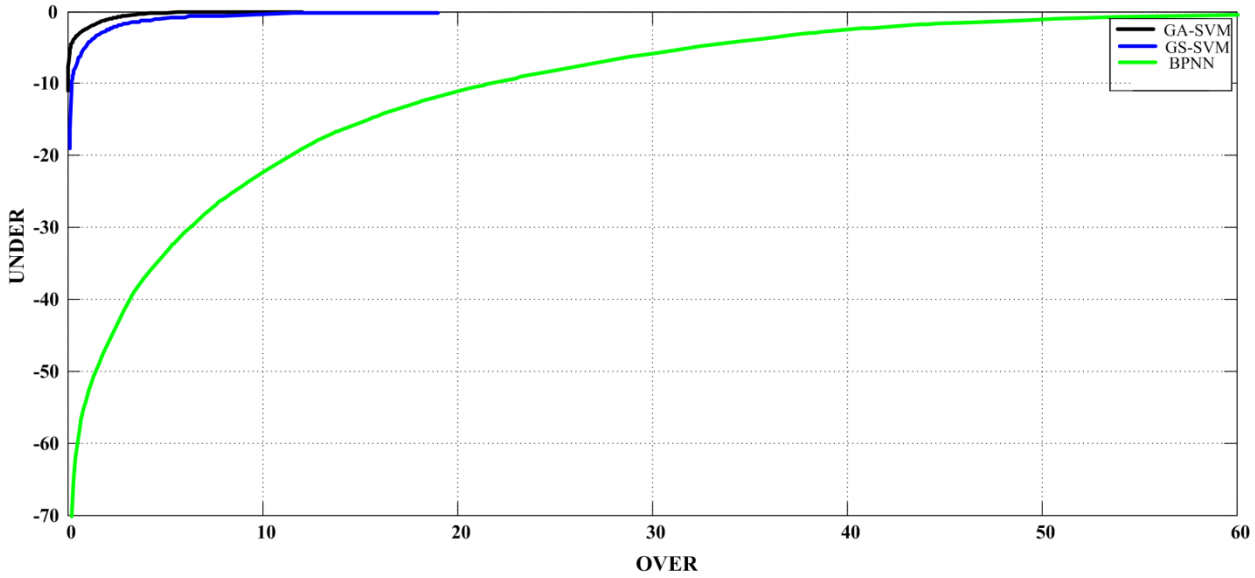

Figure 5-9: RROC curve of NRPG 246-bus system

Figure 5-9 shows the RROC curve for all the models considered in this work. TABLE 5-11 compares the results of all the three models when uncertainty is considered in the data set.

Table 5-11: Performance index for VSMI estimation from each model with measurement error for NRPG 246-bus System

Performance Indices	**NRPG 246-bus system**		
	GA-SVM	GS-SVM	MLP-BPNN
Mean Absolute percentage Error (MAPE)	0.0563	0.1928	0.112
Normalized Mean Square Error (NMSE)	7.4667	9.8135	9.9240
Willmott's Index of Agreement (WIA)	0.9914	0.9803	0.9853
Area Over the RROC Curve(AOC)	9.1982	13.601	78.3341

5.6.3 Computation Time

Computation time is also an important aspect when applying machine-learning techniques to a practical system. Table 5-12 lists the training and testing time of GA-SVM, GS-SVM and MLP-BPNN models for New England 39-bus system and NRPG 246-bus system. The computer with Intel® Core ™ i7-2600 CPU @ 3.40 GHz has been used in this study. The simulation for all three models is conducted on the same PC using 3000 sample training set, 100 unseen test cases. The result shows that selecting SVM parameter using genetic algorithm reduces computational time as compared to GS-SVM and MLP-BPNN models.

Table 5-12: Comparison of training and testing time

Test system	GA-SVM		GS-SVM		MLP-BPNN	
	Training time (sec)	Testing time (sec)	Training time (sec)	Testing time (sec)	Training time (sec)	Testing time (sec)
New England 39-bus system	3.2651	0.0112	4.148	0.0236	3.4658	0.0221
NRPG 246-bus system	8.9193	0.0524	10.3166	0.1137	19.8343	0.0530

5.7 Conclusion

In this chapter, a voltage stability-monitoring scheme suitable for online application has been proposed. This technique is based on Genetic Algorithm based Support Vector Machine (GA-SVM). The inputs to GA-SVM are the bus voltage magnitude and phase angles obtained from PMU. The GA-SVM has been used to estimate the voltage stability margin index (VSMI) with exact data and uncertain data received from PMU. The effectiveness of the proposed approach has been demonstrated by applying it to the New England 39-bus system and the Indian Northern Region Power Grid (NRPG) 246-bus real system. The results show that the GA-SVM model for online voltage stability monitoring is more suitable than GS-SVM and MLP-BPNN models. The computational time required for estimating the VSMI by the proposed technique reveals that it can be a useful approach for online voltage stability monitoring.

This real time voltage stability assessment makes it possible that the voltage controllers can quickly response to the voltage instability problem. The next chapter deals with the investigations of the dynamic operation of Static Synchronous Compensator (STATCOM) for combined reactive power compensation and voltage stabilization in an interconnected power system.

Chapter 6: Voltage Stability Control using STATCOM with Fractional Order PI Controller

6.1 Introduction

In the last decade, the advancement in the power-semiconductor devices have led to the development of the static compensator. STATCOM operation is based on gate turnoff (GTO) thyristors, and used for reactive power control and for improving power system stability [74]. The main objective of placement of a STATCOM is to regulate the voltage at the point of common coupling by dynamically absorbing or delivering reactive power from or to the transmission network respectively. In literature, most of the proposed schemes involve traditional linear control techniques in which the nonlinear model of STATCOM is linearized at a specific equilibrium point [75]–[82]. However, most of the techniques discussed in the literature uses integer order PI controller that experiences certain drawbacks especially due to the uncertainty in system parameters. The PI controller gives only a control point not the range of control. Therefore, there is still a lot of scope for improvement in the area of design of controller. In recent years, the fractional calculus has emerged as an effective control domain to increase system performance and boost system robustness. Researchers across the globe apply fractional order PID (FOPID) controller in the different fields of engineering. The authors proposed the FOPID controller in [122] for load frequency control and in [123]–[125] for automatic voltage regulation. In [126], authors used fractional order controller for the design of aerospace system to control the trajectory of the flight. In [127], author has developed a Fractional Order Proportional Integral (FOPI) controller to make the system more robust to plant uncertainties. In [128], FOPI controller is designed for the hydraulic variable pitch wind turbine system to deal with the characteristics such as slow time-varying, nonlinearization, wind load frequently changing and serious random disturbances. In[129], the author has proposed FOPI controller for congestion control of networks with traditional wired backbone and wireless terminal user supporting Internet TCP flows.

The adaptability and performance of FOPI controller in different fields encouraged to investigate its effectiveness to control the output STATCOM control. It is observed that these controllers have more degree of freedom than a conventional integer order controller and provide a complete range of control. In this chapter, an application of FOPI controller is presented for the dynamic operation of the STATCOM. The FOPI controller has been designed

using the fractional calculus. The optimal parameters for the FOPI controller are determined by the use of GA. A STATCOM connected to 230KV grid has been considered to evaluate the control performance of FOPI controller. The input signals to these controllers are voltage phasors and current phasors. In this work, it is assumed that these signals are the output of installed PMUs. The simulation results of FOPI controller has been compared with integer order PI controllers. The results show that FOPI controllers works effectively compared to integer order PI controllers. The complete FOPI control scheme of STATCOM has been tested on Real Time Digital Simulator (RTDS).

6.2 STATCOM Mathematical model and Control Strategy

6.2.1 STATCOM Mathematical model

The STATCOM is a FACTS device, which is placed in the power system for the reactive power compensation and the power quality improvement. This objective is achieved by generating a controllable three-phase AC voltage output at the Point of Common Coupling (PCC) to regulate reactive current flows by generating and absorbing controllable reactive power. The basic circuit diagram of STATCOM is shown in Figure 6-1, which consists of a Voltage source inverter and a capacitor (C). STATCOM is connected in shunt to the network through a coupling transformer. L is the leakage inductance of the coupling transformer.

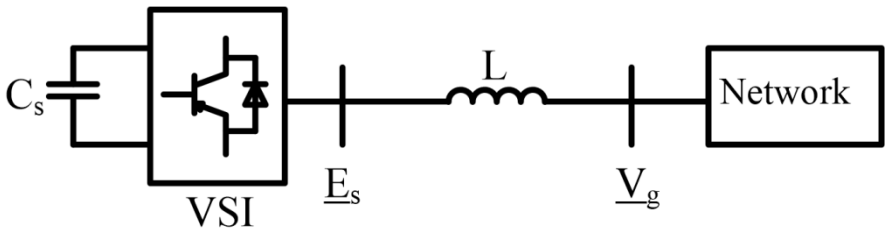

Figure 6-1: STATCOM circuit and connection to the grid

The three-phase equivalent circuit of STATCOM is shown in Figure 6-2. In this circuit, all values of parameters and variables are considered in p.u. system as given in Appendix D. The figure shows that the VSI is modeled as a voltage source with voltage $e'_{sa}, e'_{sb}, e'_{sc}$ that is connected to the grid through the inductance L'/ω_B and the resistance R'. The inductance and the resistance is used to represent the losses in the coupling circuit. The STATCOM current is represented by i' . The DC circuit is modeled as a current source (I'_{dc}) connected to the capacitor C'_s and the resistance R'_s. The resistance in DC circuit is used to represent the switching losses and the DC circuit losses. The complete mathematical model of STATCOM

[75] is explained in Appendix D. In this appendix the control strategies adopted to control the reactive power is also explained.

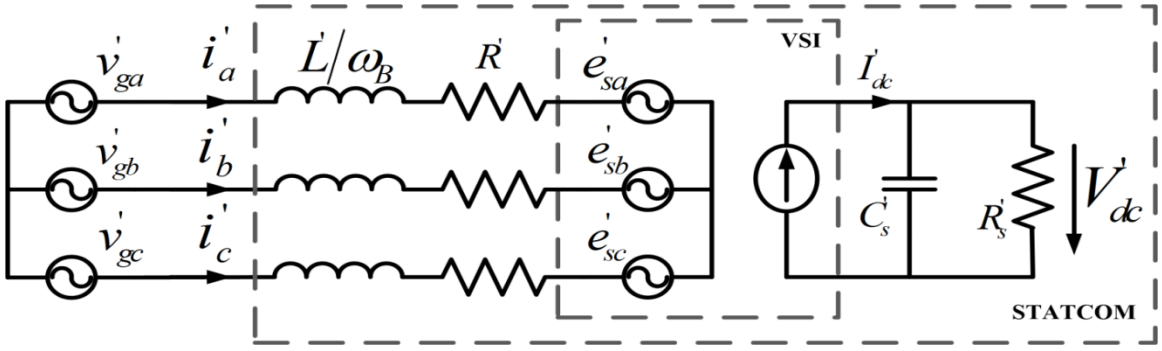

Figure 6-2: STATCOM equivalent circuit

6.3 Reactive Power Compensation by STATCOM

The power delivered by the VSI to the grid for the balanced three-phase circuit shown in Figure 6-2 can be calculated as the sum of the powers corresponding to each symmetric systems into which it is decomposed.

$$\vec{S} = P + jQ = \vec{v}'_{ga}.\vec{i}'^{*}_{a} + \vec{v}'_{gb}.\vec{i}'^{*}_{b} + \vec{v}'_{gc}.\vec{i}'^{*}_{c} \tag{6.1}$$

where, the asterisk ‘ * ’ is to denote the complex conjugate of the phasor in polar notation.

Equation (6.1) expressed in symmetric components is given by:

$$\vec{S} = 3\vec{v}'_{ga0}.\vec{i}'^{*}_{a0} + 3\vec{v}'_{ga1}.\vec{i}'^{*}_{a1} + 3\vec{v}'_{ga2}.\vec{i}'^{*}_{a2} \tag{6.2}$$

Since the STATCOM is always connected to the grid with no neutral wire and as unbalancing is not considered, therefore the zero sequence and the negative sequence component will be zero. So that:

$$\vec{S} = 3\vec{v}'_{ga1}.\vec{i}'^{*}_{a1} \tag{6.3}$$

Now, using space phasor referred to the moving frame

$$\vec{v}'_{g} = v'_{d} + jv'_{q} \tag{6.4}$$

$$\vec{i}' = i'_{d} + ji'_{q} \tag{6.5}$$

The apparent power can be expressed as

$$\vec{S} = \frac{3}{2}.\vec{v}_g^{'}.\vec{i}^{'*} = \frac{3}{2}\left[(v_{gd}^{'} + jv_{gq}^{'}).(i_d^{'} + ji_q^{'})^*\right] \tag{6.6}$$

Separating real and imaginary components,

$$\vec{S} = \frac{3}{2}(v_{gd}^{'}i_d^{'} + v_{gq}^{'}i_q^{'}) + j\frac{3}{2}(v_{gq}^{'}i_d^{'} - v_{gd}^{'}i_q^{'}) \tag{6.7}$$

It is convenient to take the direct axis of the reference frame aligned with the direct component of the grid voltage as shown in Figure 6-3. Thus $\vec{v}_g^{'} = v_{gd}^{'}$ and $v_{gq}^{'} = 0$, so the equation (6.7) is reduced to:

$$P = \frac{3}{2}v_{gd}^{'}i_{gd}^{'},\ Q = -\frac{3}{2}v_{gd}^{'}i_{gq}^{'} \tag{6.8}$$

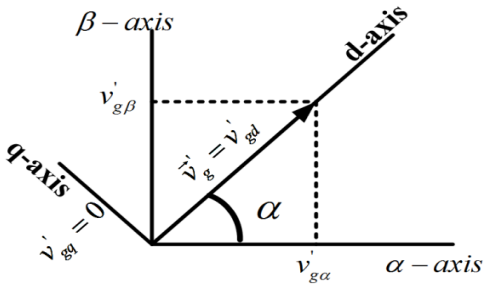

Figure 6-3: Voltage phasor aligned with d-axis of the moving frame

Figure 6-4 shows the block diagram of the STATCOM control. The main objective of the STATCOM controller is to control the active and reactive power delivered to the grid independently. The control blocks are based on the mathematical model discussed in Appendix D.

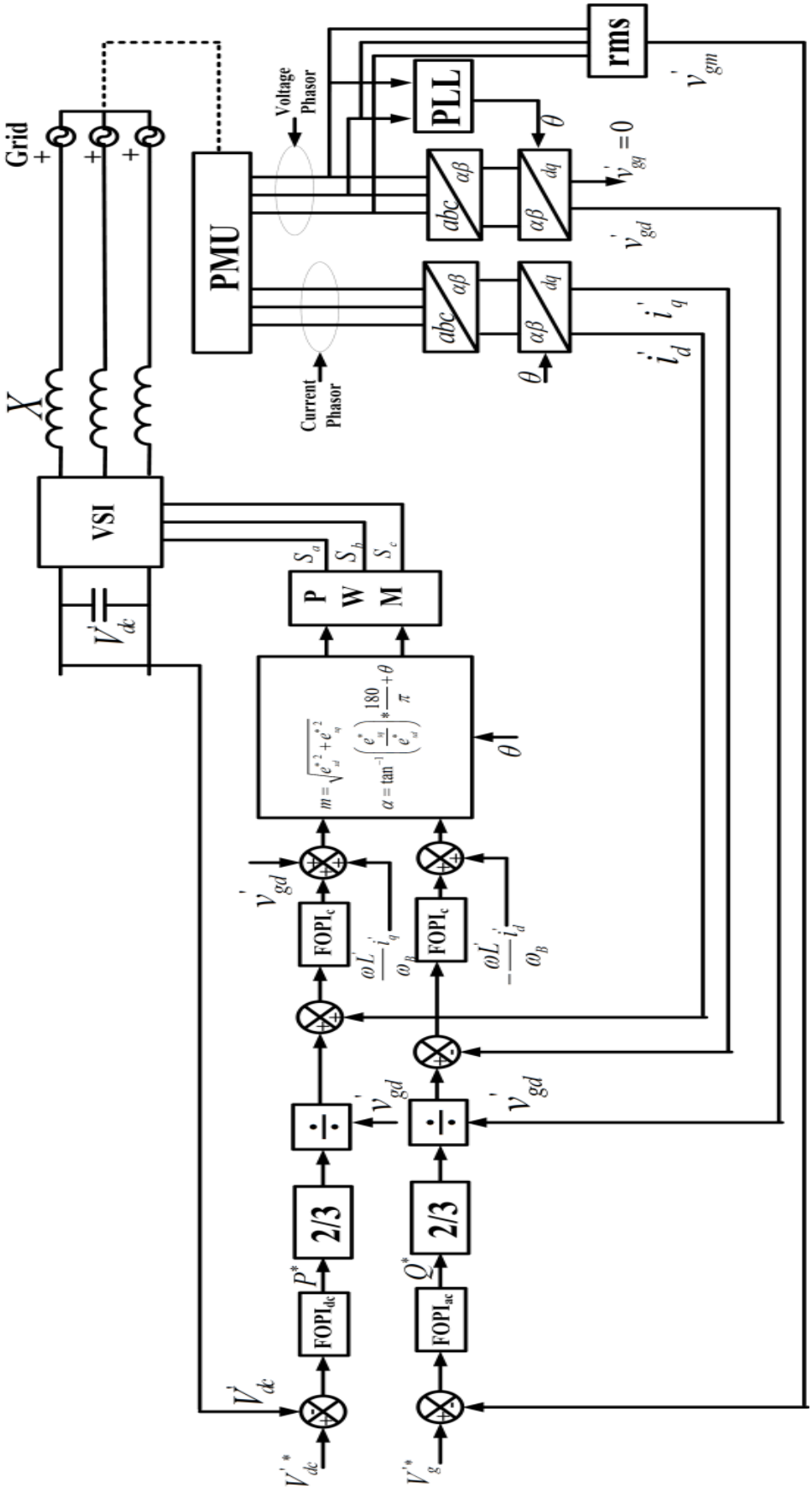

Figure 6-4: Schematic diagram of the STATCOM control

In the Figure 6-4, voltage and current phasors are the output of the PMU observing the STATCOM bus. $V_{dc}^{'*}$ is the DC voltage reference, $v_g^{'*}$ is the AC voltage reference. The active power delivered by the STATCOM to the grid is usually null, since the STATCOM is not required to generate or absorb real power. Nevertheless, since the voltage in the DC bus must be kept constant, it is necessary to compensate the electric losses in the DC side. So keeping this in reference, a DC voltage regulator ($FOPI_{dc}$) is taken in the outer loop of the D-axis. The current regulator ($FOPI_c$) in the inner loop of the same axis is to maintain the measured current (i_d') close to reference. Finally, the offset is added i.e. $v_{gd}^{'}$ *and* $\omega L^{'}/\omega_B$ in order to make the control in d-axis independent from the q-axis. In the q-axis loop the voltage difference between the measured grid voltage ($v_{gm}^{'}$) and the reference voltage ($v_g^{'*}$) is fed to the AC voltage regulator ($FOPI_{ac}$) in the outer loop of the q-axis to generate the reference reactive power (Q^*). The current regulator (FOPIc) controller in the inner loop of q-axis is used for making the $i_q^{'}$ component of STATCOM current to follow the reference current ($i_q^{'}$) calculated from the reactive power that is to be delivered to the grid. Phase Lock Loop (PLL) is a used for the synchronization of the control system with the grid with great accuracy. The block diagram of PLL is shown in Figure 6-5. The PLL algorithm measures the phase voltages of grid and then performs both the Clarke and the Park transformations to obtain $v_{gd}^{'}$ and $v_{gq}^{'}$. The PI regulator reacts by changing its output, which represents the angular speed of the grid voltage. Next, this value is integrated into the following integrator, giving a sawtooth between 0 and 2π. Progressively, the PI regulator speeds up or slows down the d-q reference frame until the V_q component becomes null. At this moment, the angular speed (ω) is the actual speed of the space vectors and the angle θ is generated so that the reference frame is aligned with the V_d component of the grid voltage. The ω_{offset} is added to the PI output to improve the transient behavior of the ω estimation at the very beginning, decreasing the settling time of this variable.

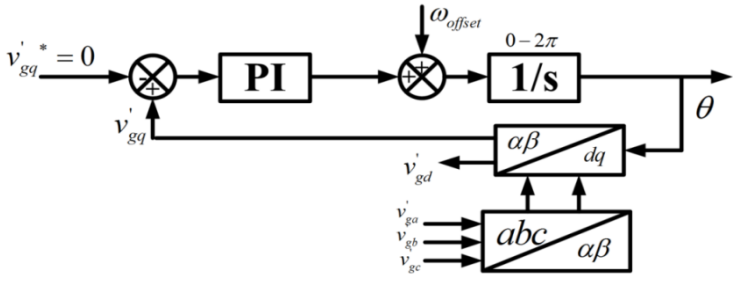

Figure 6-5: Block diagram of PLL

6.4 Fractional order Proportional Integral (FOPI) controller Design for STATCOM

The fractional order PID controller was first proposed by Podlubny in 1999 [130]. This controller is the generalization of PID controller with integrator and differentiator of real order λ and μ respectively. The theory of this controller is based on fractional calculus. Some of the details of fractional calculus is given in Appendix C. The transfer function of FOPID controller [130] has the form:

$$C(s)=\frac{U(s)}{E(s)}=K_p+T_i s^{-\lambda}+T_d s^{\mu} \tag{6.9}$$

where, K_p is the proportional constant, T_i is the integration constant and T_d is the differentiator constant. The internal structure of FOPID controller is shown in Figure 6-6.

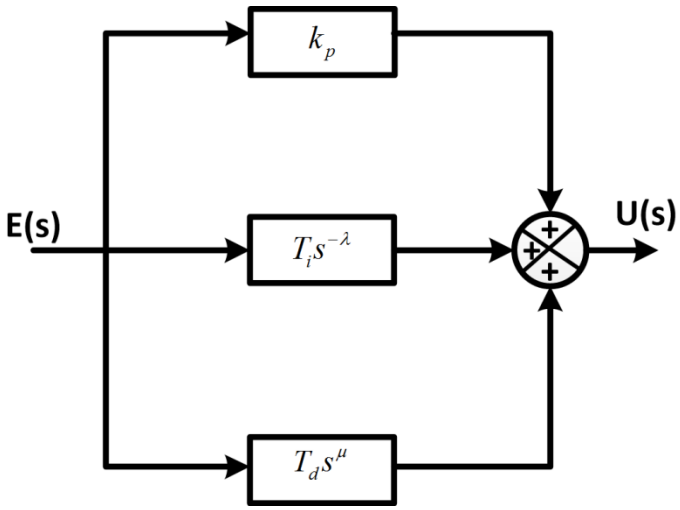

Figure 6-6: Internal structure of FOPID controller

In time domain, the transfer function (6.9) corresponds to the fractional differential equation(6.10).

$$u(t)=k_p e(t)+T_{i\,0}D_t^{-\lambda}e(t)+T_d D_t^{\mu}e(t) \tag{6.10}$$

If $\lambda=1$ and $\mu=1$, FOPID gives the integer PID structure. If $\lambda=0$ and $T_i=0$, FOPID structure is equivalent to fractional PD (PD^{μ}) controller. If $\mu=0$ and $T_d=0$ then the controller is FOPI (PI^{λ}) controller. In this work, FOPI (PI^{λ}) controller is used for STATCOM because the

derivative term amplifies the higher frequency measurement or process noise that can cause large deviations in output.

To design FOPI controller, the objective is to determine the optimal values of Kp, Ti and λ. Three FOPI controllers namely, AC voltage regulator, DC voltage regulator and current regulator are required in STATCOM. Therefore, in the proposed work nine parameters are required to be optimally determined. To determine these values the optimal problem is formulated in the following manner.

$$J = \min(ITAE) = \min\left(\int_0^{\infty} t\left(\Delta V\right) dt\right);\ where, \Delta V = v_g^* - v_{gm}$$

Subjected to

$$\begin{aligned} & K_{P_{\min}} < K_{P_j} < K_{P_{\max}}; \\ & T_{i_{\min}} < T_{i_j} < T_{i_{\max}}; \\ & \lambda_{\min} < \lambda_j < \lambda_{\max};\ where\ j = 1,2,3 \end{aligned} \tag{6.11}$$

where, v_g^* is the desired reference voltage and v_{gm} is the measured grid voltage and the objective is to minimize the Integral Time Absolute Error (IATE) between the reference voltage and the measured grid voltage subjected to the constraints as shown in (6.11).

The Genetic Algorithm (GA) is used in this work to determine these parameters. The following steps are used to determine the FOPI parameters:

Step I Representation: The three parameters of the controller Kp, Ti and λ are to be optimized in each FOPI controller are coded to generate the chromosomes. The chromosomes X is represented as $X = \{x_1, x_2, ..., x_9\}$, where, x_1 to x_9 denotes the nine parameters to be determined i.e $\left\{K_{p_{ac}}, T_{i_{ac}}, \lambda_{ac}, K_{p_c}, T_{i_c}, \lambda_c, K_{p_{dc}}, T_{i_{dc}}, \lambda_{dc}\right\}$ where $K_{p_{ac}}, T_{i_{ac}}, \lambda_{ac}$ are the FOPI controller parameters of AC regulator, $K_{p_c}, T_{i_c}, \lambda_c$ are the FOPI controller parameters of current regulator and $K_{p_{dc}}, T_{i_{dc}}, \lambda_{dc}$ are the FOPI controller parameters for DC regulator.

Step II Fitness definition: The fitness function is considered defined in (6.11).

Step III Population initialization: The initial population is composed of randomly created chromosomes X.

Step IV Fitness evaluation: The fitness value for each randomly generated chromosomes in step III is calculated using eqn.(6.11).

Step V Creating new population: Selection, crossover, and mutation are carried out to replace the current population by the newer population. The chromosomes with better fitness values are selected into the recombination pool using the roulette wheel. Genes between two parent chromosomes are exchanged to obtain new offspring to attempt to get better solutions, the probability of creating new chromosomes in each pair is set to 0.8. Mutation is performed to alter the binary code with a probability of 0.05.

Step VI Stopping criteria: The process is repeated from step IV to step V until the generation count reaches its limit.

The flowchart of the GA is given in Figure 2-5.

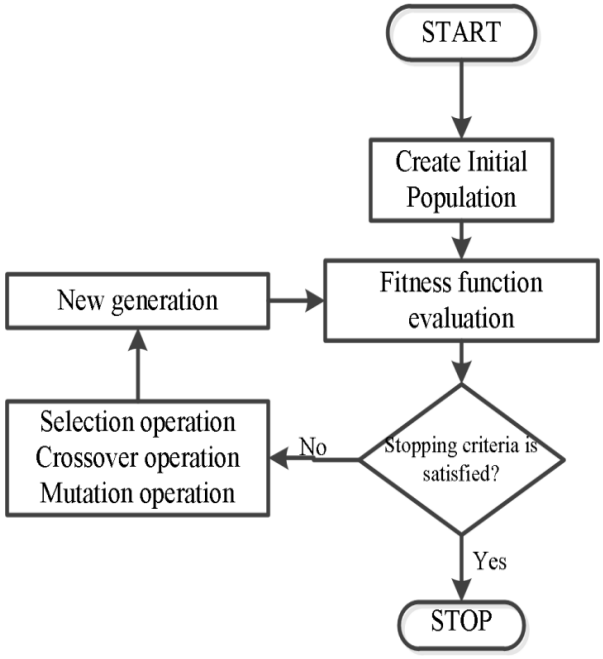

Figure 6-7: GA flowchart for tuning FOPI controller

6.5 The Test System

The single line diagram of the system on which the proposed scheme has been verified is shown in Figure 6-8 [82]. The system has 15kV, 100 MVAR STATCOM is connected to bus 2 i.e. 230kV bus. The values of system parameters are given in

Table 6-1. In this section, the performance of both the integer order PI controller and the FOPI controller has been analyzed.

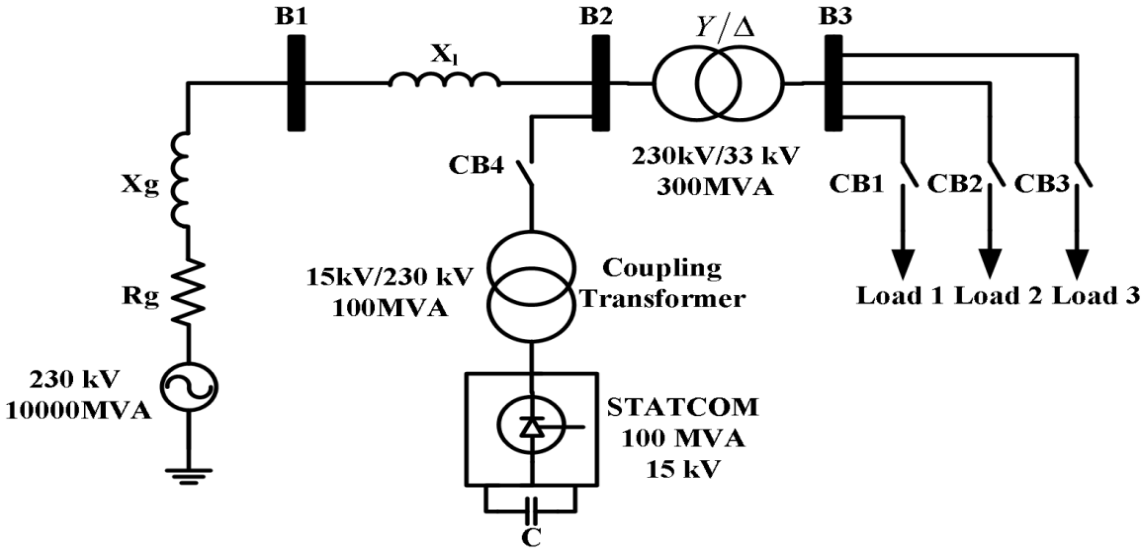

Figure 6-8: Test system with STATCOM connected at Bus 2

Table 6-1: System parameters[82]

Three Phase AC Source		Active Power	0.7 [pu]
Rated Voltage	230*1.03 [kV]	Reactive Power	0.5 [pu]
Frequency	60 [Hz]	**Load 3**	
S.C Level	10000 [MVA]	Active Power	0.6 [pu]
Base Voltage	230 [kV]	Reactive Power	0.4 [pu]
X/R	8	**STATCOM**	
Transmission Line		Primary Voltage	138 [kV]
Resistance	0.05 [pu]	Secondary Voltage	15 [kV]
Reactance	0.2 [pu]	Nominal Power	100 [MVAR]
Power Transformer		Frequency	60 [Hz]
Nominal Power	300 [MVA]	Eq. Capacitance	750 [μF]
Frequency	60 [Hz]	**Coupling Transformer**	
Prim. Voltage	230 [kV]	Nominal Power	100 [MVA]
Sec. Voltage	33 [kV]	Frequency	60 [Hz]
Magnetization Resist.	500	Prim. Voltage	138 [kV]
Magnetization React.	500	Sec. Voltage	230 [kV]
Three Phase Loads		**GTO Switches**	
Load 1		Snubber Resistance	1e5 [ohm]
Active Power	1 [pu]	Snubber Cap.	inf
Reactive Power	0.8 [pu]	Internal Resistance	1e-4 [ohm]
Load 2		No. of Bridge arm	3

List of GA parameter settings and the FOPI controller parameters limits used for tuning FOPI controller is given in Table 6-2. The optimal parameters of IOPI and FOPI controller are shown in Table 6-3.

Table 6-2: Genetic Algorithm parameter setting

Parameters	**Settings**
Generations	100
Population size	1000
Selection type	Standard roulette wheel
Crossover type	Simulated binary
Mutation type	Polynomial method
Crossover probability	0.8
Mutation probability	0.05
Propotional constant(K_p)	$0 < K_{P_j} < 5000;\ \ j = 1,2,3$
Integration Constant (T_i)	$0 < T_{i_j} < 5000;\ \ j = 1,2,3$
Fractional order (λ)	$0 < \lambda_j < 2;\ \ j = 1,2,3$

Table 6-3: STATCOM controller parameters

Controller parameters	FOPI controller			Integer order PI	
	K_p	**K_i**	**λ**	**K_p**	**K_i**
AC voltage regulator	0.55	2500	1.2382	12	3000
Current regulator	0.8	200	1.7674	5	40
DC voltage regulator	0.001	0.15	1.2063	0.001	0.02

6.6 Simulation Results

In this section the results obtained from the simulation studies carried out with MATLAB version 2013a have been discussed. At the beginning of the simulation, the circuit breaker CB4 is open, i.e. STATCOM is inactive. It is considered that the capacitor connected to the DC side of STATCOM is pre-charged to 1p.u. voltage. Simulations studies have been carried out with different switching instants, as given below:

- Time t=0 to t=0.1sec only circuit breaker CB1 is closed, all other circuit breakers are open. During this period the inductive load (load 1) with P=1 p.u and Q = 0.8 p.u. connected to bus 3. The bus B2 voltage at the beginning is 0.975 p.u. for the uncompensated network.
- Time t =0.1sec to t=0.5sec, circuit breaker CB1 and CB4 are closed and other breakers are open.
- Time t=0.5sec to t=1sec, circuit breaker CB1, CB2 and CB4 are closed and CB3 is open.
- Time t=1sec to t=1.5sec, all the circuit breakers are closed.
- Time t=1.5sec to t=2sec, circuit breaker CB3 and CB4 are closed and other breakers are open.

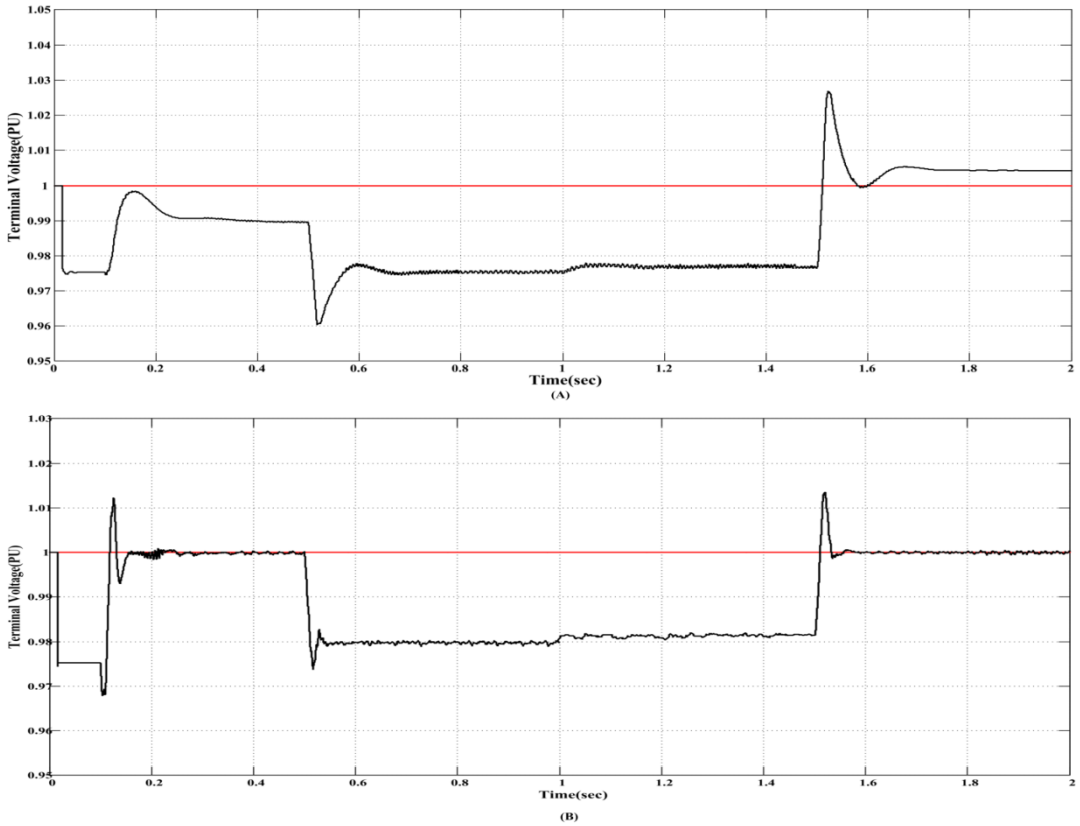

Figure 6-9: Terminal voltage of STATCOM: (A) Integer order PI controller (B) FOPI controller

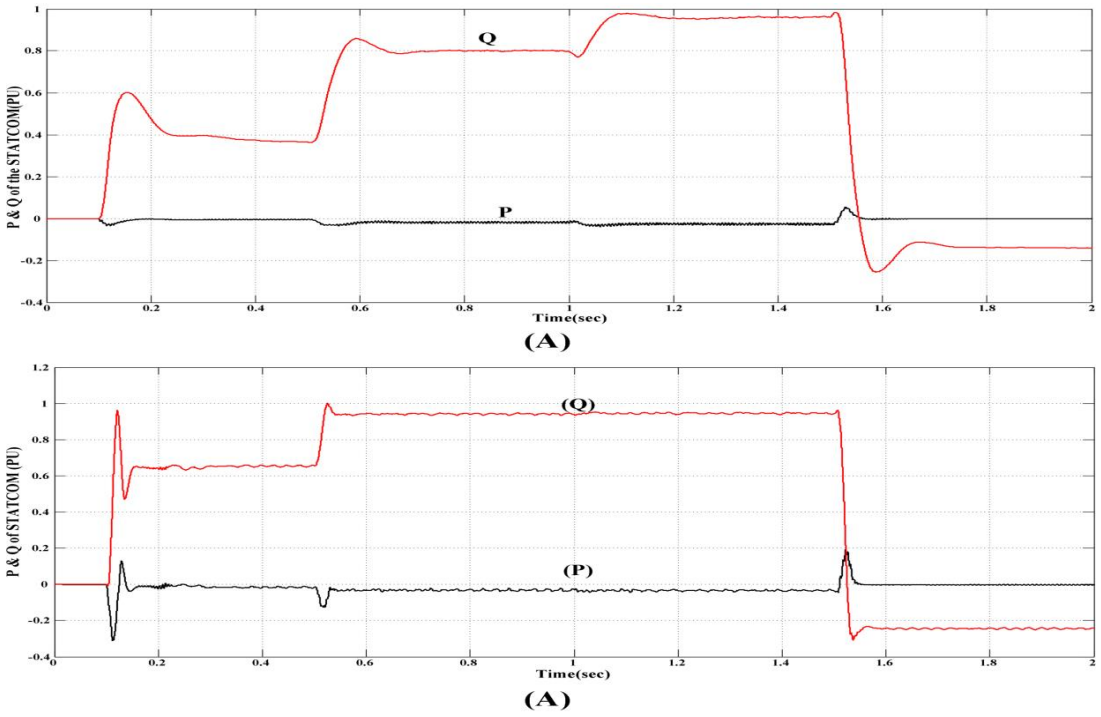

Figure 6-10: Active and Reactive power of STATCOM: (A) Integer order PI controller (B) FOPI controller

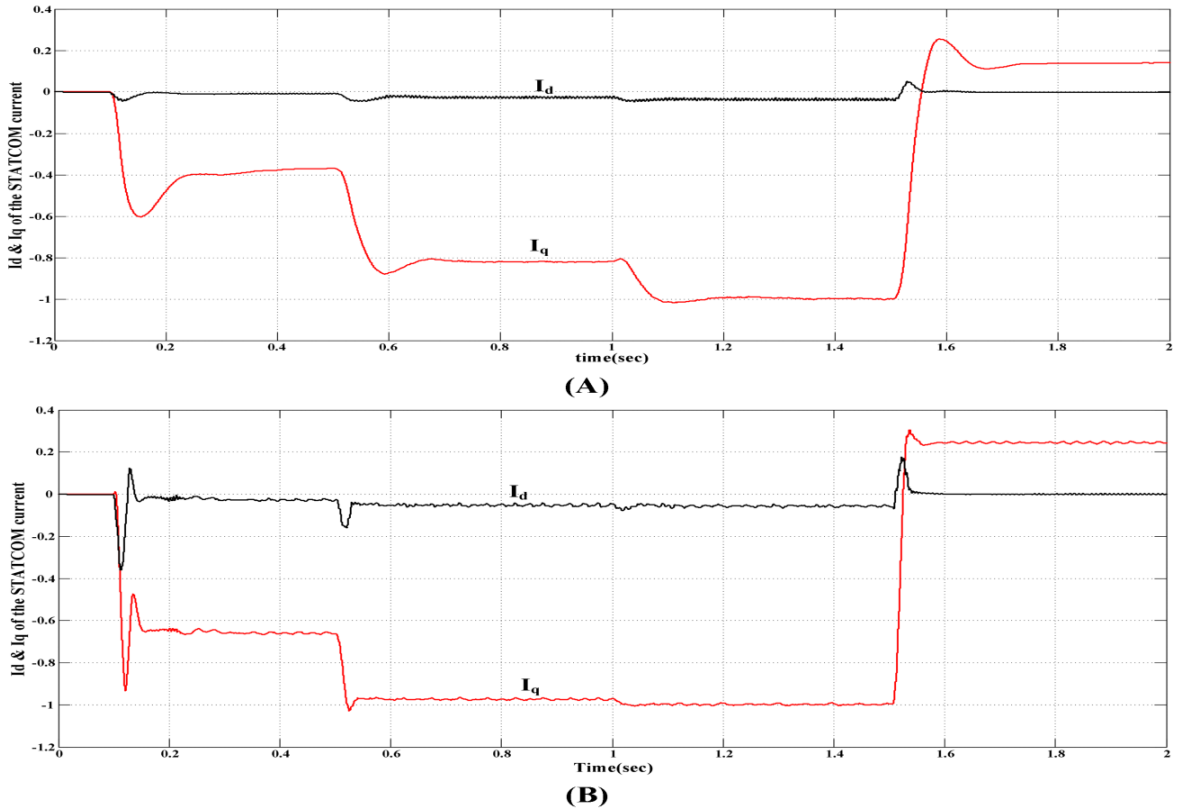

Figure 6-11: Id and Iq of STATCOM current: (A) Integer order PI controller (B) FOPI controller

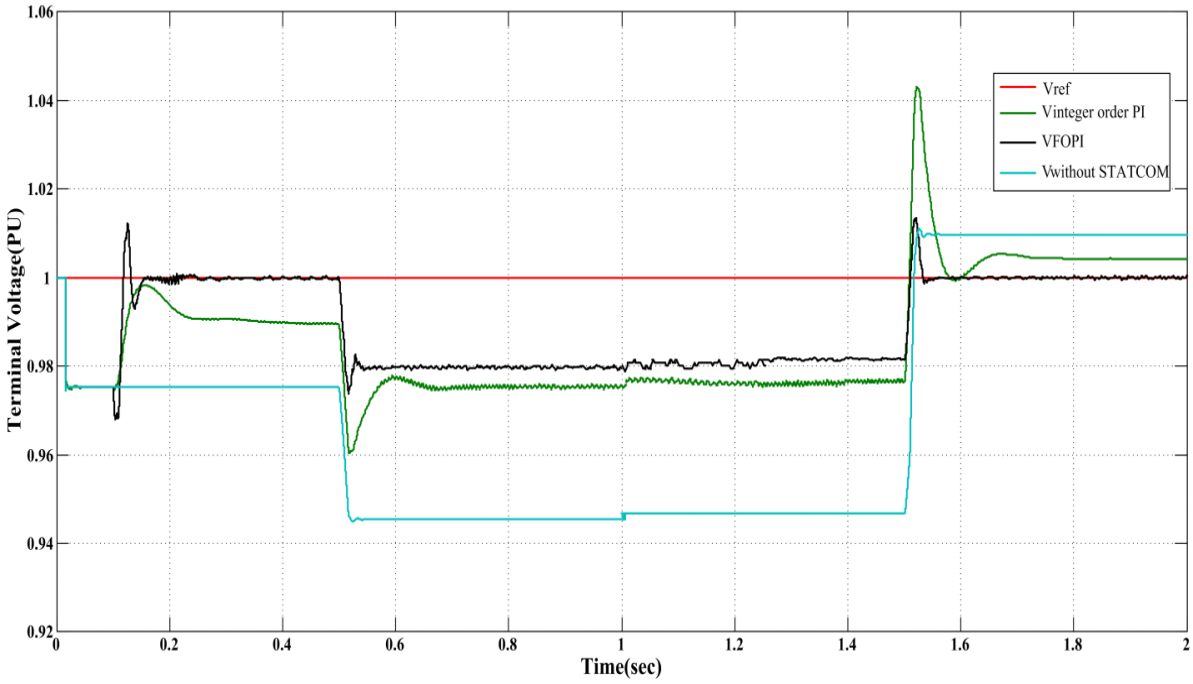

Figure 6-12: Terminal voltage of STATCOM (comparison)

The effect of the switching is explained in the following:

Step I. At t = 0.1 sec.: The circuit breaker CB4 is closed to connect the STATCOM to the 230 kv grid. Initially the voltage at bus B2 is below the desired voltage. Therefore, the STATCOM operate in capacitive mode and inject reactive power to the grid to maintain the voltage at bus B2 as shown in Figure 6-9. The reactive power injected by the STATCOM with IOPI controller is 0.4 p.u. as shown in Figure 6-10(A) (t=0.1 to t=0.5) and regulate bus B2 voltage to 0.99 p.u. as shown in Figure 6-9(A) (t=0.1 to t=0.5). The STATCOM with FOPI controller inject 0.65 p.u. reactive power as shown in Figure 6-10(B) (t=0.1 to t=0.5) and enhance the voltage at B2 to 1 p.u. as shown in Figure 6-9(B) (t=0.1 to t=0.5). Figure 6-11 shows the id and iqs current components. It is clear from the results that id=0 (except transients) i.e. the total STATCOM current is the reactive current.

Step II. At t = 0.5 sec.: The second inductive load (Load 2) with P = 0.7 p.u. and Q = 0.5 p.u. is added at the bus B3; therefore more reactive power compensation is required. The reactive power injected by the STATCOM with integer order PI controller is increased to 0.8 p.u. as shown in Figure 6-10(A) (t=0.5 to t=1.0) and voltage regulated at bus B2 is now about 0.975 p.u. as shown in Figure 6-9(A) (t=0.5 to t=1.0). The STATCOM with FOPI controller inject 0.95 p.u. reactive power as shown in Figure 6-10(B) (t=0.5 to t=1.0) and the voltage at B2 is 0.98 p.u. as shown in Figure 6-9(B) (t=0.5 to t=1.0).

Step III. At t = 1 sec.: The capacitive load (Load 3) with P = 0.6 p.u. and Q = 0.4 p.u. is added to the bus B3. The voltage regulated at bus B2 is now about 0.978 p.u. as shown in Figure 6-9(A) (t=1.0 to t=1.5). The STATCOM with FOPI controller inject 0.95 p.u. reactive power as shown in Figure 6-10(B) (t=1.0 to t=1.5) and the voltage at B2 is 0.982 p.u. as shown in Figure 6-9(B) (t=1.0 to t=1.5).

Step IV. At t = 1.5 sec.: Both the inductive loads (Load 1 and Load 2) are removed from bus B3 and only the capacitive load (Load 3) remain connected to bus B3. This is a sever load rejection condition. The STATCOM voltage leads the bus voltage. As a result, the STATCOM will operate in inductive mode and absorb reactive power from the grid to maintain the voltage at bus B2. The reactive power absorbed by the STATCOM with IOPI controller is 0.18 p.u. as shown in Figure 6-10(A) (t=1.5 to t=2.0) and voltage regulated at bus B2 is 1.005 p.u. as shown in Figure 6-9(A) (t=1.5 to t=2.0). The STATCOM with FOPI controller absorb 0.25 p.u. reactive power as shown in Figure 6-10(B) (t=1.5 to t=2.0) and the voltage at B2 is 1.0 p.u. as shown in Figure 6-9(B) (t=1.5 to t=2.0). Figure 6-11(t=1.5 to t=2.0) shows the d-q STATCOM current components is inductive current.

The bus B2 voltage regulation of the IOPI and FOPI controllers are compared in Figure 6-12. Between t= 0.1sec to t=0.5sec IOPI controller shows a steady state error while FOPI controller regulates the voltage at 1p.u. Between t=0.5 sec to t=1.5 sec reactive load is very high therefore the voltage of bus 2 is lower than 1p.u. with both the controllers. In this case also the performance of FOPI controller is better than the FOPI controller. Between time t=1.5 to t=2.0 sec the net load is very low. For this case, the FOPI controller maintain the bus voltage at 1p.u. while the bus voltage with IOPI controller is higher than 1 p.u.(1.05p.u.).

6.6.1 Validation of STATCOM controller using RTDS

The simulation of the proposed FOPI controller based STATCOM has been carried out Real Time digital Simulator (RTDS). The RTDS is a fully digital power system simulator that is precise, fast, and reliable simulation tool used for real-time simulation, prototype, and

hardware-in-loop testing [131]. The model of the test system considered for the demonstration of the proposed scheme has been developed in RSCAD/RTDS as shown in Figure 6-13.

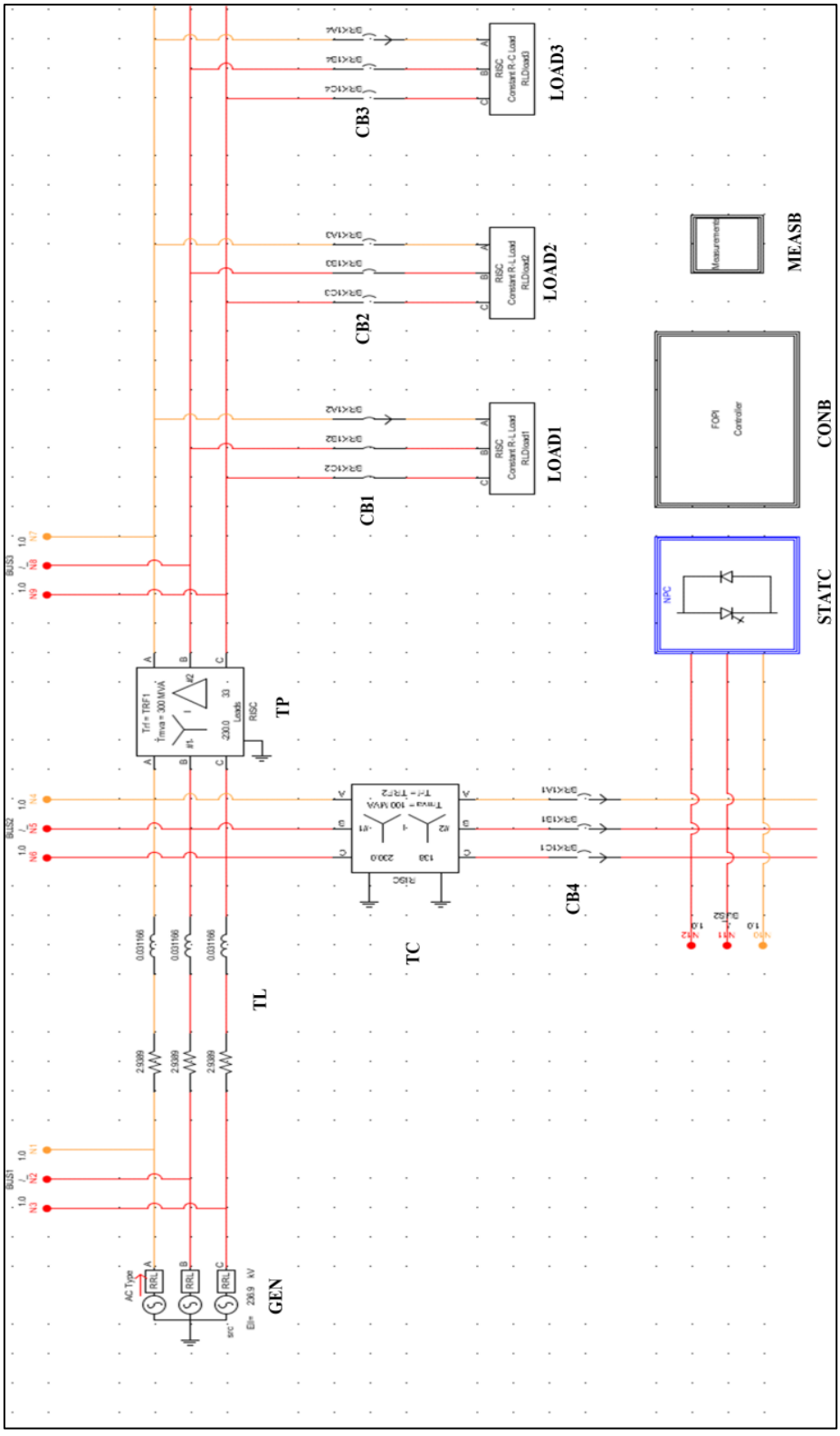

Figure 6-13: Test system modeled in RTDS

Table 6-4: System model label

Components	Label	Components	Label
Three-phase AC source	GEN	Circuit breaker	CB1, CB2, CB3, CB4
Transmission line	TL	STATCOM	STATC
Power Transformer	TP	Controller Block	CONB
Coupling Transformer	TC	Measurement block	MEASB
Loads	LOAD1, LOAD2, LOAD3		

The component of the test system as mentioned in Figure 6-8 and Table 6-1 are labeled in the RSCAD/RTDS model shown in Figure 6-13 as per the Table 6-4. The block STATC in Figure 6-14 represents the model of STATCOM. In the present work 48-pulse STATCOM have been developed in RSCAD/RTDS. The switching GTOs of the VSI is controlled by a controller. The FOPI controller as discussed in section 6.4, has been modelled in RSCAD/RTDS having the schematic as shown in Figure 6-15. The performance of the controller has been validated considering the same test cases given in section 6.5.

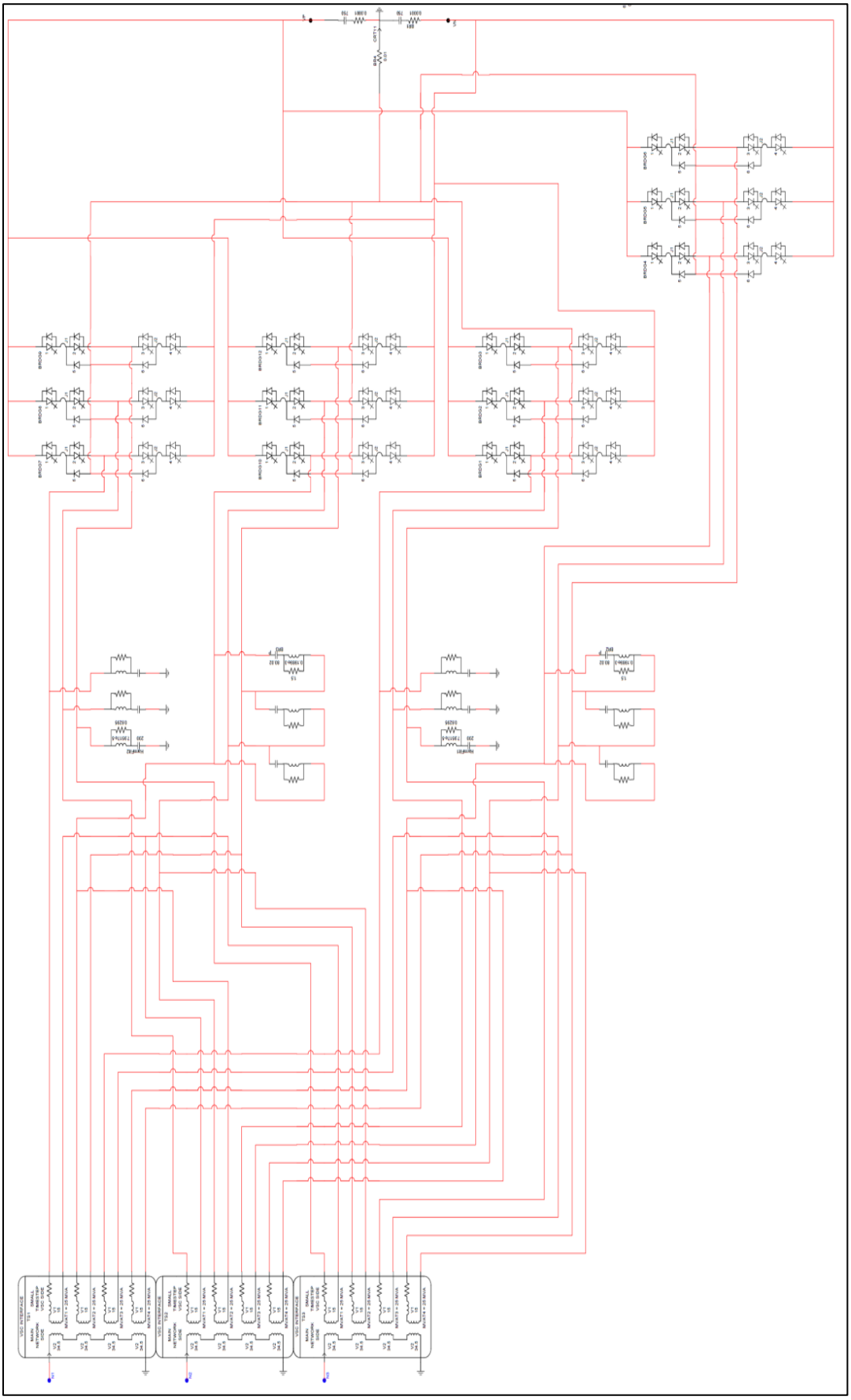

Figure 6-14: STATCOM modeling in RSCAD/RTDS

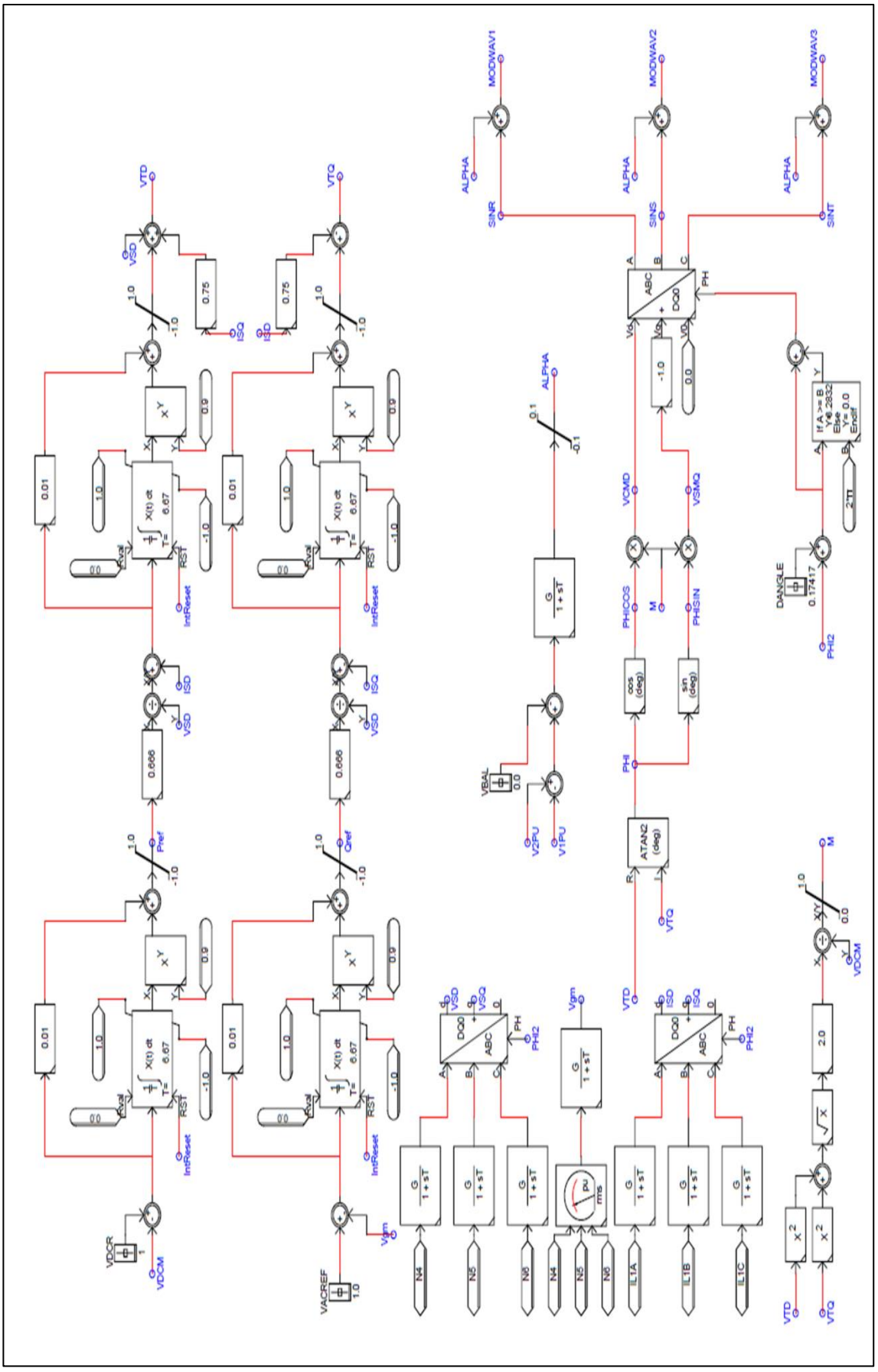

Figure 6-15: STACOM controller in RSCAD/RTDS

To generate the various cases using the time switching of the circuit breakers, a sequencer is used in RSCAD/RTDS. At time t = 0.6 sec the sequencer has switched ON. The switching instances of RTDS simulator equivalent time to MATLAB simulation is given in Table 6-5

Table 6-5: Switching instances in RTDS and MATLAB simulation

RSCAD/RTDS simulation instance	MATLAB simulation instance	Action
time t = 0.6 – 0.7 sec	time t = 0.0 – 0.1 sec	Simulation started with only CB1 closed all other circuit breakers are open
time t = 0.7 – 1.1 sec	time t = 0.1 – 0.5 sec	CB1 and CB4 are closed and all other circuit breakers are open
time t = 1.1 – 1.6 sec	time t = 0.5 – 1.0 sec	CB1, CB2 and CB4 are closed and CB3 is open
time t = 1.6 – 2.1 sec	time t = 1.0 – 1.5 sec	All the circuit breakers are closed
time t = 2.1 – 3 sec	time t = 1.5 – 2.0 sec	CB3 and CB4 are closed and all other circuit breakers are open

Figure 6-16 to Figure 6-18 shows the RTDS result for the test system considered in this work. Figure 6-16 shows the grid voltage variation by the switching sequences given in Table 6-5. The dotted line in the figure shows the switch instant when the sequencer is switched ON i.e time t=0 in MATLAB simulation. The variation in the voltage matches with the MATLAB simulation after t=0.6 sec in RTDS results. Similarly, the same variation can be seen at each switching instances in STATCOM currents (Id and Iq) shown in Figure 6-17 and the real and reactive power of STATCOM as shown in Figure 6-18.

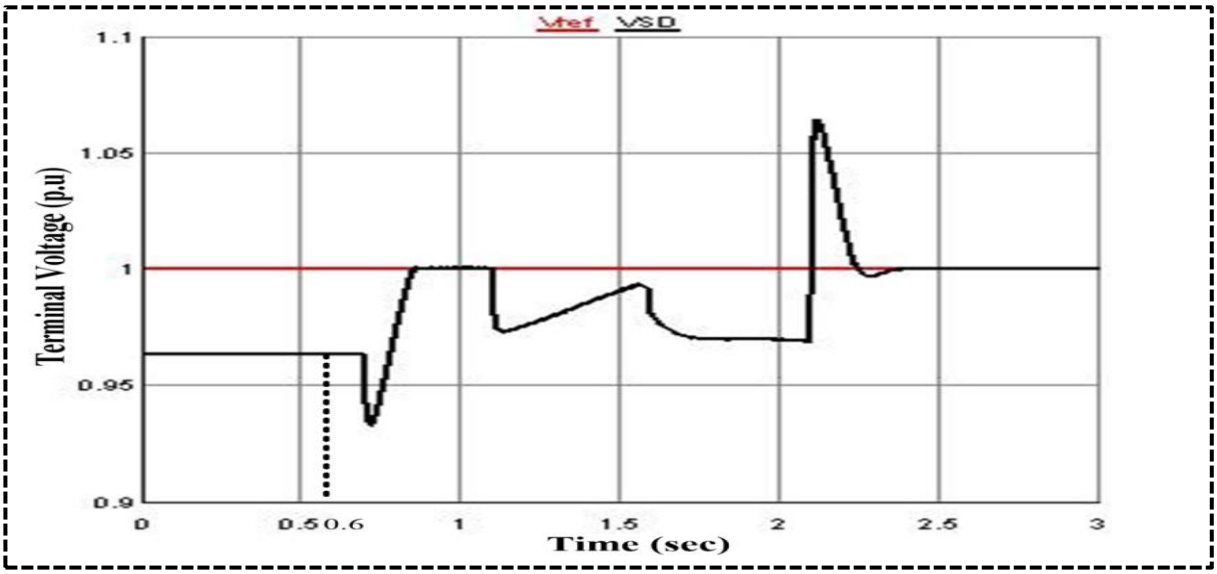

Figure 6-16: Terminal voltage of STATCOM with FOPI controller (RTDS result)

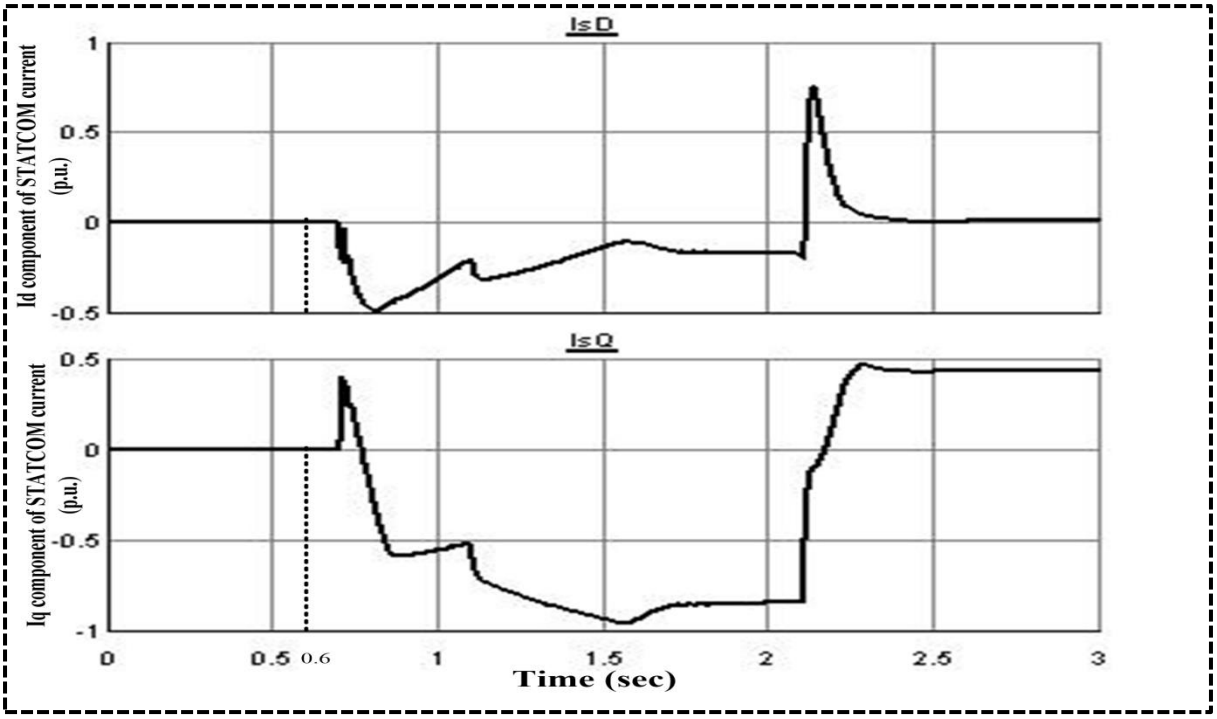

Figure 6-17: Id and Iq of STATCOM current with FOPI controller (RTDS result)

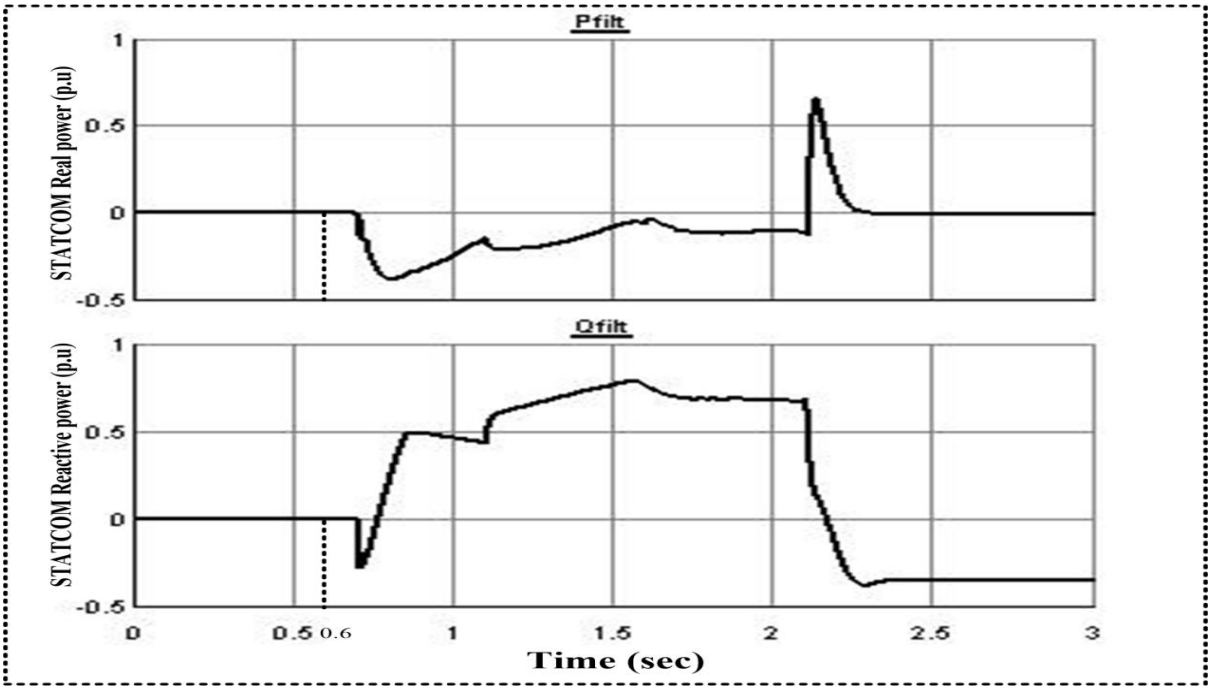

Figure 6-18: Active and Reactive power of STATCOM with FOPI controller (RTDS result)

The real time simulation results shown in Figure 6-16, Figure 6-17 and Figure 6-18 are compared with the MATLAB results shown in Figure 6-9(B), Figure 6-11(B) and Figure 6-10(B) respectively. In between different switching instances, variation in the bus B2 voltage is approximately similar to shown in Figure 6-16 and Figure 6-9(B). The STATCOM current (Id and Iq) shown in Figure 6-17 and Figure 6-11(B) are also similar in between the switching

instance. Similarly real and reactive power are also similar in both the environment. It can be concluded from this comparison that the proposed FOPI controller for STATCOM works satisfactorily in real time environment.

In a power system network if reactive power compensation is sufficient, the voltage stability margins can be increased sufficiently. In the following, it is shown that how the voltage stability margins can be improved by using the reactive power compensation in IEEE 30-bus system. In this system, the candidate bus, at which STATCOM is installed, is the most critical bus identified by the approach discussed in section 3.2 of chapter 3. From table 3.5 of chapter 3, the most critical bus is bus 30. A STATCOM is installed at bus 30. The maximum loadability of the system is computed using continuation power flow [114]. The dynamic PV curve simulation results with and without STATCOM are shown in Figure 6-19. The figure shows that the maximum loading factor (λ_{max}) is increased from 2.994 to 3.850, which means voltage stability limit of IEEE 30-bus system is increased by 29% with the placement of STATCOM at bus 30.

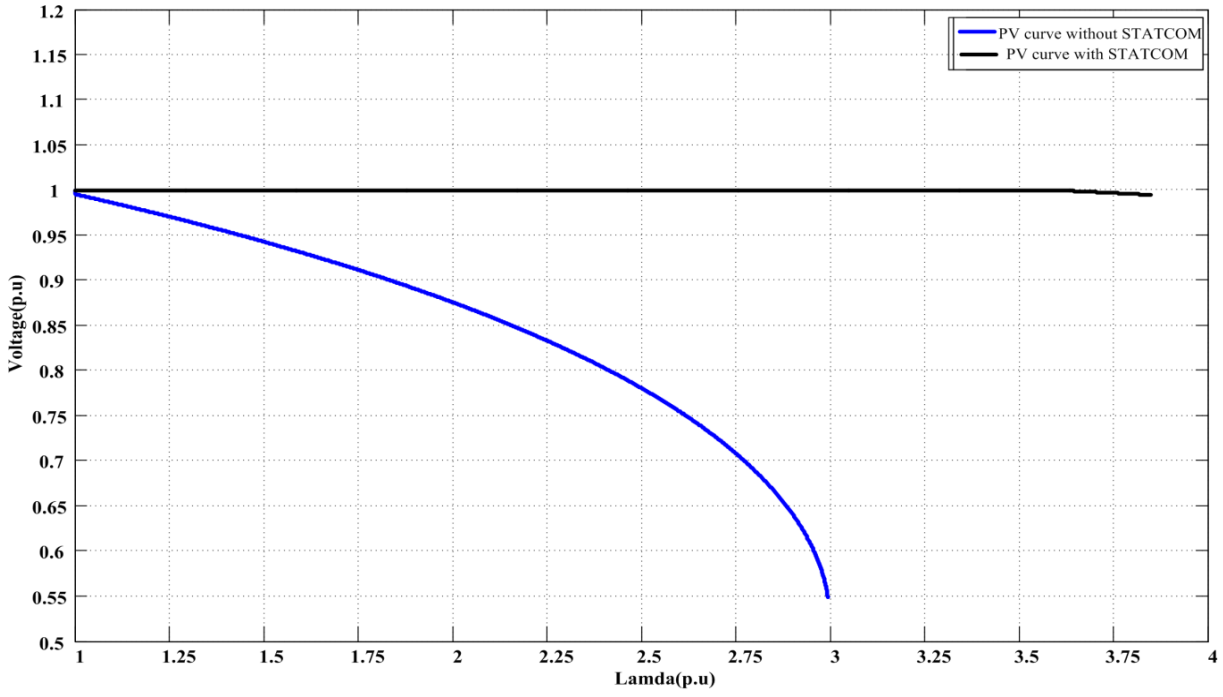

Figure 6-19: PV curve of bus 30 in IEEE 30-bus system

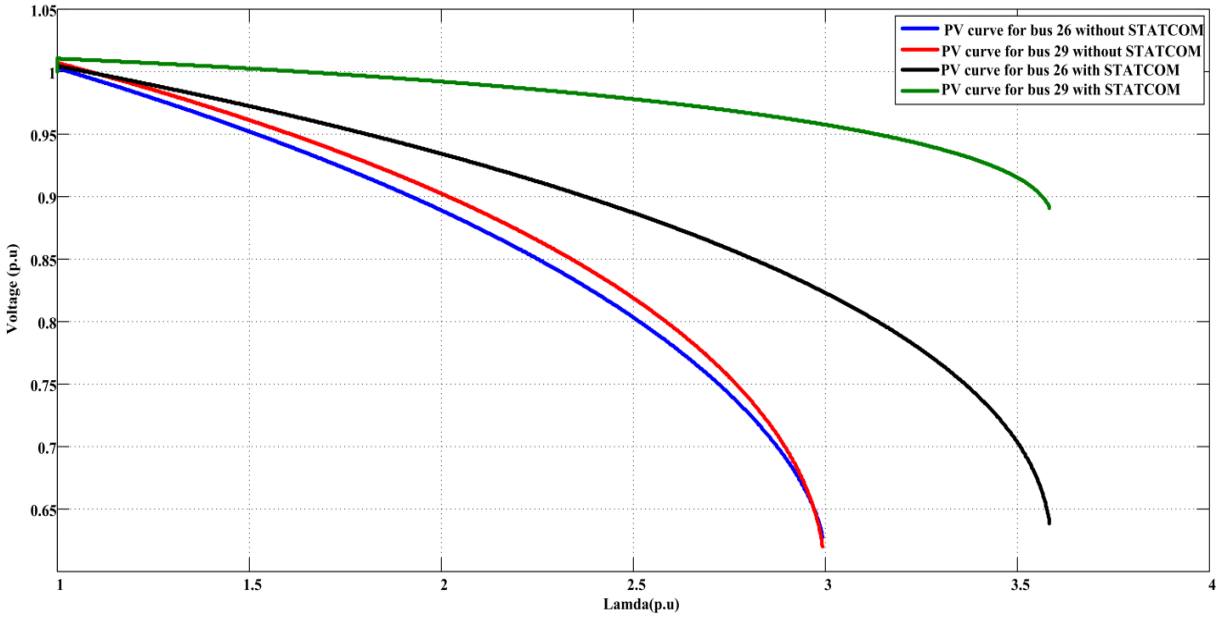

Figure 6-20: PV curve of bus 26 and 29 in IEEE 30-bus system

Figure 6-20 shows the PV curve for bus 26 and bus 29 (next critical buses from table 3.5 of chapter 3) of IEEE 30-bus system with and without STATCOM. The figure shows that the placement of STATCOM at bus 30 also improves the voltage profile of other week buses.

6.7 Conclusion

In this chapter, a FOPI controller to control the reactive power of STATCOM has been proposed. The FOPI controller has been designed using the fractional calculus. The optimal parameters of this controller have been determined using GA. The results of FOPI controllers are compared with the IOPI controller. A 48-pulse STATCOM model has been used to check the performance of both the controllers. First, the simulation studies have been carried out in MATLAB/SIMULINK for both the controllers, then the result of FOPI controller has been validated in RTDS. Results shows that the FOPI controller is more effective compared to IOPI controller.

Chapter 7: Conclusion and Future Scope

7.1 General

The power systems are continuously developing which increases their complexity in real time monitoring, analysis and control. Therefore, this requires accurate and reliable power system measurements delivered at a faster rate than the measurements currently provided by the SCADA systems. In a large interconnected and geographically distributed power grid, along with highly accurate measurements, time synchronization of these measurements also become one of the important requirements to have the coherent view of network. Wide Area Measurement System (WAMS) with Phasor Measurement Units (PMUs) provides synchronized phasor measurements with fast reporting rate and accurate measurements, hence is the most suitable solution for today's ever-changing power system. Therefore, this thesis has carried out studies on the emerging concept of synchrophasor technology based WAMS and various issues related to the optimal placement of PMUs and effective utilization of the PMU measurements in three applications viz. power system state estimation, voltage stability monitoring and voltage stability control. Since the proper deployment of PMUs plays a significant role in voltage stability monitoring. Therefore, developed methodologies will be beneficial for monitoring and control of voltage stability in real-time. Thus, presented work will be helpful in preventing power system from severe voltage collapse.

In the present chapter, various outcomes of the conducted research work are summarized first and later some suggestions for future work in this area are given.

7.2 Summary of the Main Findings

In Chapter 2, a new approach has been proposed for the Optimal Placement of PMUs (OPP) with optimal number of current phasor measurements. The overall approach comprises of two steps. The first step finds the optimal locations of PMUs using Genetic Algorithm (GA). Second step utilizes the results of the first step to obtain the optimal set of branch current phasor measurement. The proposed approach has been carried out for different cases of observability. In first case, the OPP formulation is done for the complete observability. In second case, the optimal PMU placement problem formulation is done for the incomplete observability of types Depth-of-One unobservability and Depth-of-Two unobservability. In another case, the OPP problems have been formulated that ensures complete power system

observability even under a branch outage or a PMU failure. The formulated problem is of Binary Integer Linear Programming (BILP) problem. The GA based approach has been used to solve this BILP problem. Developed algorithm has been tested on IEEE-14, IEEE-30, IEEE-57 bus systems and the Northern Regional Power Grid (NRPG) 246-bus system. From results obtained in this chapter following conclusions are drawn.

- The proposed approach is able to reduce the number of current phasor measurements to a considerable amount; hence, the overall cost has been reduced.
- In general, PMUs are required to be placed at about $1/3^{rd}$ of the total numbers of buses in the power system, in order to completely observe the system with only phasor measurements.

In a large power system, large number of PMUs are needed to be deployed for full observability and will entail high capital cost in their installation. These requirements pose physical and financial constraints on the PMU installation process. Therefore, most of the utilities would like to install the PMUs in their power system in multi-phases. For this purpose, a new multiphase PMU placement procedure based on voltage stability has been proposed in chapter 3. To achieve this objective Revised Analytical Hierarchy Process (RAHP) is used for decision-making for phasing of PMU locations. Critical buses are identified using fast voltage stability index (FVSI) which are more prone to voltage collapse. To get the maximum priority to critical buses in the multiphase installation of PMUs, Critical Load bus Observability Criteria (CLOC) has been introduced in the decision making process along with five other observability criteria (OB) i.e. Noncritical Load bus Observability Criteria (NLOC), Generator Observability Criteria (GOC), PMUs Distribution Criteria (PDC), Tie Line Observability Criteria (TOC), and Bus Connectivity Criteria (BCC). The results obtained from IEEE 30-bus system and NRPG 246-bus system provide following conclusion.

- The proposed approach can be utilized by the utilities in deciding the multi-phase PMU installations, while ensuring maximum advantage in terms of critical load buses and generator buses observability.
- With the proposed approach, monitoring and control scheme can be implemented just after first-phase of PMUs placement, which will benefit in wide-area voltage stability analysis.
- By the proposed method, the system becomes complete observable by the end of the last phase ensuring complete observability with N-1 contingency.

One of the applications of the synchrophasor data collected from PMUs is State Estimation (SE) of the power system. However, these synchronized measurements received from PMU will not be able to replace the conventional measurements in SCADA system completely in near future. Therefore, developing a hybrid state estimator that includes both the conventional and the phasor measurements is the current need to get better results. In Chapter 4, hybrid state estimator has been developed, utilizing the available phasor measurements along with the conventional SCADA measurements to improve the estimation accuracy. The inclusion of synchrophasors is carried out in the same phased manner as discussed in chapter 3. The bad data detection in both the conventional measurement and the phasor measurements has been carried out using the normalized residual test method. The effectiveness of the approach has been tested using the IEEE-30 bus test system and NRPG 246-bus real system. Following are the important findings of this work.

- The developed hybrid SE algorithm with the addition of PMUs provides more accurate results than the conventional Weighted Least Square (WLS) SE method.
- The normalized residual method for bad data detection works effectively for conventional as well as PMU's data.
- The proposed hybrid method does not change the structure of the conventional WLS-SE method and requires almost the same computational time.
- The accuracy of the hybrid SE model increases with number of PMUs included in the system.

In Chapter 5, an approach for online monitoring of long-term voltage instability condition in the power system has been developed with the use of GA-SVM. GA is used to optimize the SVM parameter such as RBF kernel, regularization parameter and insensitive loss function to improve the performance of SVM. GA-SVM is applied to emulate the continuation power flow for estimation of voltage stability margin index (VSMI) for steady state voltage stability analysis. The input features of GA-SVM are formed by voltage magnitude and voltage phase angle, which are assumed to be obtained from PMU. The effectiveness of the proposed approach is tested on New England 39-bus test system and NRPG 246-bus real system. Two different models, Grid Search based Support Vector Machine (GS-SVM) model and Multilayer Perceptron-Back Propagation Neural Network (MLP-BPNN) are considered to compare the performance of the proposed GA-SVM approach for voltage stability monitoring. Followings are the important findings of the work.

- The performance indices values along with Regression Receiver Operating Characteristic (RROC) curves and Area Over the RROC Curve (AOC) demonstrate that the GA-SVM model for online voltage stability monitoring is more suitable than GS-SVM and MLP-BPNN models.
- The GA-SVM model is able to accurately predict the VSMI even in the presence of uncertainties in synchrophasor measurements.
- The computational time required for estimating the VSMI by the proposed technique reveals that it can be a useful approach for online voltage stability monitoring.

In chapter 6, Fractional Order Proportional Integral (FOPI) controller is presented for the dynamic operation of the STATCOM. The FOPI controller has been designed using the fractional calculus. The optimal parameters of the FOPI controller are determined by using GA. The results of FOPI controllers are compared with the IOPI controller. A STATCOM of rating 15KV, 100 Mvar has been connected to 230KV grid to evaluate the performance of controllers. The complete control scheme of STATCOM has been tested on Real Time Digital Simulator (RTDS). The simulation results of FOPI controller has been compared with integer order PI controller. The main findings of this chapter are as follows.

- The simulation studies revealed that the FOPI controller used for reactive power compensation of STATCOM is more effective compared to IOPI controller.
- RTDS results show that the proposed FOPI controller for STATCOM works satisfactorily in real time environment.
- The voltage stability margins can be improved by placing the STATCOM at the weakest bus.

7.3 Scope of Future Research

As a result of the investigations carried out in this thesis, following topics are identified for future research in this area.

- ❖ Proposed PMU placement method can be extended by considering reliability of system observability.
- ❖ The main objective of the proposed multi phased PMU placement scheme is voltage stability monitoring. The proposed approach can be further extended for transient and dynamic stability analysis.

- In the present work, STATCOM has been used to improve the voltage stability control. This work can be extended by using other FACTS devices.
- The Present thesis is primarily focused on application of synchrophasor measurements to the voltage stability monitoring and control. The proposed scheme in this work can be applied to other possible applications in the power system.
- In this work, STATCOM is placed only on single bus. In a large network more number of STATCOMs at different weak buses can be placed.

BIBLIOGRAPHY

[1] A. G. Phadke, "Synchronized phasor measurements in power systems," *IEEE Comput. Appl. Power*, vol. 6, no. 2, pp. 10–15, Apr. 1993.

[2] M. Chenine and L. Nordström, "Investigation of communication delays and data incompleteness in multi-PMU Wide Area Monitoring and Control Systems," in *International Conference on Electric Power and Energy Conversion Systems, 2009. EPECS '09.*, 2009, pp. 1–6.

[3] "IEEE Std C37.118.2-2011 (Revision of IEEE Std C37.118-2005)," *IEEE Std C37.118.2-2011 (Revision of IEEE Std C37.118-2005)*. pp. 1–53, 2011.

[4] A. G. Phadke, J. S. Thorp, and K. J. Karimi, "State Estimation with Phasor Measurements," *IEEE Trans. Power Syst.*, vol. 1, no. 1, pp. 233–238, 1986.

[5] C. Madtharad, S. Premrudeepreechacharn, N. R. Watson, and R. Saeng-Udom, "An Optimal Measurement Placement Method for Power System Harmonic State Estimation," *IEEE Trans. Power Deliv.*, vol. 20, no. 2, pp. 1514–1521, Apr. 2005.

[6] X. Dongjie, H. Renmu, W. Pen, and X. Tao, "Comparison of several PMU placement algorithms for state estimation," in *Eighth IEE International Conference on Developments in Power System Protection*, 2004, vol. 2004, pp. 32–35.

[7] B. Mohammadi-Ivatloo and S. H. Hosseini, "Optimal PMU placement for power system observability considering secondary voltage control," in *2008 Canadian Conference on Electrical and Computer Engineering*, 2008, pp. 000365–000368.

[8] K. Mazlumi, H. Askarian Abyaneh, S. H. H. Sadeghi, and S. S. Geramian, "Determination of optimal PMU placement for fault-location observability," in *2008 Third International Conference on Electric Utility Deregulation and Restructuring and Power Technologies*, 2008, pp. 1938–1942.

[9] A. G. Phadke, J. S. Thorp, and K. J. Karimi, "State Estimation with Phasor Measurements," *IEEE Power Eng. Rev.*, vol. PER-6, no. 2, pp. 48–48, Feb. 1986.

[10] T. L. Baldwin, L. Mili, M. B. Boisen, and R. Adapa, "Power system observability with minimal phasor measurement placement," *IEEE Trans. Power Syst.*, vol. 8, no. 2, pp. 707–715, May 1993.

[11] L. Mili, T. Baldwin, and R. Adapa, "Phasor measurement placement for voltage stability analysis of power systems," in *29th IEEE Conference on Decision and Control*, 1990, pp. 3033–3038 vol.6.

[12] B. Milosevic and M. Begovic, "Nondominated sorting genetic algorithm for optimal phasor measurement placement," *IEEE Trans. Power Syst.*, vol. 18, no. 1, pp. 69–75, Feb. 2003.

[13] S. Chakrabarti and E. Kyriakides, "Optimal Placement of Phasor Measurement Units for Power System Observability," *IEEE Trans. Power Syst.*, vol. 23, no. 3, pp. 1433–1440, Aug. 2008.

[14] S. Chakrabarti, E. Kyriakides, and D. G. Eliades, "Placement of Synchronized Measurements for Power System Observability," *IEEE Trans. Power Deliv.*, vol. 24, no. 1, pp. 12–19, Jan. 2009.

[15] S. Chakrabarti, G. K. Venayagamoorthy, and E. Kyriakides, "PMU placement for power system observability using binary particle swarm optimization," in *Power Engineering*

Conference, 2008. AUPEC '08. Australasian Universities, 2008, pp. 1–5.

[16] K. Jamuna and K. S. Swarup, "Multi-objective biogeography based optimization for optimal PMU placement," *Appl. Soft Comput.*, vol. 12, no. 5, pp. 1503–1510, May 2012.

[17] A. Abur, "Observability analysis and measurement placement for systems with PMUs," in *IEEE PES Power Systems Conference and Exposition, 2004.*, 2004, pp. 1472–1475.

[18] B. Gou, "Optimal Placement of PMUs by Integer Linear Programming," *IEEE Trans. Power Syst.*, vol. 23, no. 3, pp. 1525–1526, Aug. 2008.

[19] B. Gou, "Generalized Integer Linear Programming Formulation for Optimal PMU Placement," *IEEE Trans. Power Syst.*, vol. 23, no. 3, pp. 1099–1104, Aug. 2008.

[20] M. Korkali and A. Abur, "Placement of PMUs with channel limits," in *2009 IEEE Power & Energy Society General Meeting*, 2009, pp. 1–4.

[21] R. Sodhi, S. C. Srivastava, and S. N. Singh, "Optimal PMU placement method for complete topological and numerical observability of power system," *Electr. Power Syst. Res.*, vol. 80, no. 9, pp. 1154–1159, Sep. 2010.

[22] R. F. Nuqui and A. G. Phadke, "Phasor Measurement Unit Placement Techniques for Complete and Incomplete Observability," *IEEE Trans. Power Deliv.*, vol. 20, no. 4, pp. 2381–2388, Oct. 2005.

[23] D. Dua, S. Dambhare, R. K. Gajbhiye, and S. A. Soman, "Optimal Multistage Scheduling of PMU Placement: An ILP Approach," *IEEE Trans. Power Deliv.*, vol. 23, no. 4, pp. 1812–1820, Oct. 2008.

[24] R. Sodhi, S. C. Srivastava, and S. N. Singh, "Multi-criteria decision-making approach for multi-stage optimal placement of phasor measurement units," *IET Gener. Transm. Distrib.*, vol. 5, no. 2, p. 181, 2011.

[25] A. Pal, G. A. Sanchez-Ayala, V. A. Centeno, and J. S. Thorp, "A PMU Placement Scheme Ensuring Real-Time Monitoring of Critical Buses of the Network," *IEEE Trans. Power Deliv.*, vol. 29, no. 2, pp. 510–517, Apr. 2014.

[26] C. Sharma and B. Tyagi, "Ranking of phasor measurement units based on control strategy for small-signal stability," *Int. Trans. Electr. Energy Syst.*, vol. 25, no. 10, pp. 2359-2375, Jul. 2014.

[27] F. C. Schweppe and J. Wildes, "Power System Static-State Estimation, Part I: Exact Model," *Trans. Power Appar. Syst.*, vol. PAS-89, no. 1, pp. 120–125, 1970.

[28] F. C. Schweppe and D. B. Rom, "Power System Static-State Estimation, Part II: Approximate Model," *IEEE Trans. Power Appar. Syst.*, vol. PAS-89, no. 1, pp. 125–130, 1970.

[29] F. C. Schweppe, "Power System Static-State Estimation, Part III : Implementation," *IEEE Trans. Power Appar. Syst.*, vol. PAS-89, no. 1, pp. 130–135, 1970.

[30] J. S. Thorp, a. G. Phadke, and K. J. Karimi, "Real Time Voltage-Phasor Measurement For Static State Estimation," *IEEE Trans. Power Appar. Syst.*, vol. PAS-104, no. 11, pp. 3098–3106, 1985.

[31] M. Zhou, V. A. Centeno, J. S. Thorp, and A. G. Phadke, "An Alternative for Including Phasor Measurements in State Estimators," *IEEE Trans. Power Syst.*, vol. 21, no. 4, pp. 1930–1937, Nov. 2006.

[32] S. a. Dowi and G. Li, "A new approach for including synchronized phasor measurements in dynamic state estimation," *2013 2nd Int. Symp. Instrum. Meas. Sens. Netw. Autom.*, no. 1, pp. 389–394, 2013.

[33] L. Zhao and a. Abur, "Multi area state estimation using synchronized phasor measurements," *Power Syst. IEEE Trans.*, vol. 20, no. 2, pp. 611–617, 2005.

[34] T. S. Bi, X. H. Qin, and Q. X. Yang, "A novel hybrid state estimator for including synchronized phasor measurements," *Electr. Power Syst. Res.*, vol. 78, no. 8, pp. 1343–1352, Aug. 2008.

[35] S. K. Mallik, S. Chakrabarti, and S. N. Singh, "A Robust Regularized Hybrid State Estimator for Power Systems," *Electr. Power Components Syst.*, vol. 42, no. 7, pp. 671–681, Apr. 2014.

[36] E. A. Zamora-Cárdenas, B. A. Alcaide-Moreno, and C. R. Fuerte-Esquivel, "State estimation of flexible AC transmission systems considering synchronized phasor measurements," *Electr. Power Syst. Res.*, vol. 106, pp. 120–133, Jan. 2014.

[37] R. Sodhi, S. C. Srivastava, and S. N. Singh, "Phasor-assisted Hybrid State Estimator," *Electr. Power Components Syst.*, vol. 38, no. 5, pp. 533–544, Mar. 2010.

[38] G. N. Korres and N. M. Manousakis, "State estimation and bad data processing for systems including PMU and SCADA measurements," *Electr. Power Syst. Res.*, vol. 81, no. 7, pp. 1514–1524, Jul. 2011.

[39] X. Qin, T. Bi, and Q. Yang, "Hybrid Non-linear State Estimation with Voltage Phasor Measurements," in *2007 IEEE Power Engineering Society General Meeting*, 2007, pp. 1–6.

[40] Ding Junce and Cai Zexiang, "Mixed Measurements State Estimation Based on Wide-Area Measurement System and Analysis," in *2005 IEEE/PES Transmission & Distribution Conference & Exposition: Asia and Pacific*, 2005, pp. 1–5.

[41] S. Chakrabarti, E. Kyriakides, G. Ledwich, and A. Ghosh, "A comparative study of the methods of inclusion of PMU current phasor measurements in a hybrid state estimator," in *IEEE PES General Meeting*, 2010, pp. 1–7.

[42] T. Cutsem, M. Ribbens-Pavella, and L. Mili, "Bad Data Identification Methods In Power System State Estimation-A Comparative Study," *IEEE Trans. Power Appar. Syst.*, vol. PAS-104, no. 11, pp. 3037–3049, Nov. 1985.

[43] K. A. Clements and P. W. Davis, "Multiple Bad Data Detectability and Identifiability: A Geometric Approach," *IEEE Trans. Power Deliv.*, vol. 1, no. 3, pp. 355–360, 1986.

[44] I. W. Slutsker, "Bad data identification in power system state estimation based on measurement compensation and linear residual calculation," *IEEE Trans. Power Syst.*, vol. 4, no. 1, pp. 53–60, 1989.

[45] J. Chen and A. Abur, "Placement of PMUs to Enable Bad Data Detection in State Estimation," *IEEE Trans. Power Syst.*, vol. 21, no. 4, pp. 1608–1615, Nov. 2006.

[46] J. Zhu and A. Abur, "Bad Data Identification When Using Phasor Measurements," in *2007 IEEE Lausanne Power Tech*, 2007, pp. 1676–1681.

[47] Y. Yang, W. Hu, and Y. Min, "Projected unscented Kalman filter for dynamic state estimation and bad data detection in power system," in *12th IET International Conference on Developments in Power System Protection (DPSP 2014)*, 2014, p. 12.30.

[48] Y. Guo, W. Wu, B. Zhang, and H. Sun, "A method for evaluating the accuracy of power system state estimation results based on correntropy," *Int. J. Electr. Power Energy Syst.*, vol. 60, pp. 45–52, Sep. 2014.

[49] T. Dhadbanjan and S. S. K. Vanjari, "Linear Programming Approach for Power System State Estimation Using Upper Bound Optimization Techniques," *Int. J. Emerg. Electr.*

Power Syst., vol. 11, no. 3, Jan. 2010.

[50] J. De La Ree, V. Centeno, J. S. Thorp, and A. G. Phadke, "Synchronized Phasor Measurement Applications in Power Systems," *IEEE Trans. Smart Grid*, vol. 1, no. 1, pp. 20–27, Jun. 2010.

[51] T. Van Cutsem, "Voltage instability: phenomena, countermeasures, and analysis methods," *Proc. IEEE*, vol. 88, no. 2, pp. 208–227, Feb. 2000.

[52] P. Kessel and H. Glavitsch, "Estimating the Voltage Stability of a Power System," *IEEE Trans. Power Deliv.*, vol. 1, no. 3, pp. 346–354, 1986.

[53] A. Tiranuchit and R. J. J. Thomas, "A posturing strategy against voltage instabilities in electric power systems," *IEEE Trans. Power Syst.*, vol. 3, no. 1, pp. 87–93, 1988.

[54] C. W. Taylor, *Power System Voltage Stability. EPRI Power System Engineering Series*. McGraw-Hill, 1993.

[55] J. Hongjie, Y. Xiaodan, and Y. Yixin, "An improved voltage stability index and its application," *Int. J. Electr. Power Energy Syst.*, vol. 27, no. 8, pp. 567–574, Oct. 2005.

[56] R. Tiwari, K. R. Niazi, and V. Gupta, "Line collapse proximity index for prediction of voltage collapse in power systems," *Int. J. Electr. Power Energy Syst.*, vol. 41, no. 1, pp. 105–111, Oct. 2012.

[57] V. Ajjarapu and C. Christy, "The continuation power flow: a tool for steady state voltage stability analysis," *IEEE Trans. Power Syst.*, vol. 7, no. 1, pp. 416–423, 1992.

[58] C.-Y. Lee, S.-H. Tsai, and Y.-K. Wu, "A new approach to the assessment of steady-state voltage stability margins using the P–Q–V curve," *Int. J. Electr. Power Energy Syst.*, vol. 32, no. 10, pp. 1091–1098, Dec. 2010.

[59] V. Terzija, G. Valverde, P. Regulski, V. Madani, J. Fitch, S. Skok, M. M. Begovic, A. Phadke, Deyu Cai, P. Regulski, V. Madani, J. Fitch, S. Skok, M. M. Begovic, and A. Phadke, "Wide-Area Monitoring, Protection, and Control of Future Electric Power Networks," *Proc. IEEE*, vol. 99, no. 1, pp. 80–93, Jan. 2011.

[60] S. Corsi, "Wide area voltage regulation and protection: When their co-ordination is simple," in *2005 IEEE Russia Power Tech*, 2005, pp. 1–8.

[61] M. Donolo, M. Venkatasubramanian, A. Guzman, and F. de Villiers, "Monitoring and mitigating the voltage collapse problem in the Natal network," in *2009 IEEE/PES Power Systems Conference and Exposition*, 2009, pp. 1–5.

[62] W. Nakawiro and I. Erlich, "Optimal Load Shedding for Voltage Stability Enhancement by Ant Colony Optimization," in *2009 15th International Conference on Intelligent System Applications to Power Systems*, 2009, pp. 1–6.

[63] S. S. Biswas and A. K. Srivastava, "A novel method for distributed real time voltage stability monitoring using synchrophasor measurements," in *2013 IREP Symposium Bulk Power System Dynamics and Control - IX Optimization, Security and Control of the Emerging Power Grid*, 2013, pp. 1–6.

[64] S. S. Biswas, C. B. Vellaithurai, and A. K. Srivastava, "Development and real time implementation of a synchrophasor based fast voltage stability monitoring algorithm with consideration of load models," in *2013 IEEE Industry Applications Society Annual Meeting*, 2013, pp. 1–9.

[65] S. S. Biswas and A. K. Srivastava, "Performance analysis of a new synchrophasor based real time voltage stability monitoring (RT-VSM) tool," in *2014 North American Power Symposium (NAPS)*, 2014, pp. 1–6.

[66] Y. Gong, N. Schulz, and A. Guzman, "Synchrophasor-Based Real-Time Voltage Stability Index," in *2006 IEEE PES Power Systems Conference and Exposition*, 2006, pp. 1029–1036.

[67] L.-J. Cai and I. Erlich, "Power System Static Voltage Stability Analysis Considering all Active and Reactive Power Controls - Singular Value Approach," in *2007 IEEE Lausanne Power Tech*, 2007, pp. 367–373.

[68] R. Chendur Kumaran, T. G. Venkatesh, and K. S. Swarup, "Voltage stability – Case study of saddle node bifurcation with stochastic load dynamics," *Int. J. Electr. Power Energy Syst.*, vol. 33, no. 8, pp. 1384–1388, Oct. 2011.

[69] N. Amjady, "Voltage security evaluation by a new framework based on the load domain margin and continuation method," in *IEEE Power Engineering Society General Meeting, 2005*, 2005, pp. 582–588.

[70] P. Bhagwat Chitare, V. S. K. M. Balijepalli, and S. A. Khaparde, "Online Assessment of Voltage Stability in Power Systems with PMUs," *Int. J. Emerg. Electr. Power Syst.*, vol. 14, no. 4, p. 373, Jan. 2013.

[71] D. Q. Zhou, U. D. Annakkage, and A. D. Rajapakse, "Online Monitoring of Voltage Stability Margin Using an Artificial Neural Network," *IEEE Trans. Power Syst.*, vol. 25, no. 3, pp. 1566–1574, Aug. 2010.

[72] D. Devaraj and J. Preetha Roselyn, "On-line voltage stability assessment using radial basis function network model with reduced input features," *Int. J. Electr. Power Energy Syst.*, vol. 33, no. 9, pp. 1550–1555, Nov. 2011.

[73] S. Hashemi and M. R. Aghamohammadi, "Wavelet based feature extraction of voltage profile for online voltage stability assessment using RBF neural network," *Int. J. Electr. Power Energy Syst.*, vol. 49, no. 0, pp. 86–94, Jul. 2013.

[74] F. Fran Li, J. Kueck, T. Rizy, and T. King, "A Preliminary Analysis of the Economics of Using Distributed Energy as a Source of Reactive Power Supply," 2006.

[75] C. Schauder and H. Mehta, "Vector analysis and control of advanced static VAR compensators," *IEE Proc. C Gener. Transm. Distrib.*, vol. 140, no. 4, p. 299, Jul. 1993.

[76] P. W. Lehn and M. R. Iravani, "Experimental evaluation of STATCOM closed loop dynamics," *IEEE Trans. Power Deliv.*, vol. 13, no. 4, pp. 1378–1384, 1998.

[77] P. Rao, M. L. Crow, and Z. Yang, "STATCOM control for power system voltage control applications," *IEEE Trans. Power Deliv.*, vol. 15, no. 4, pp. 1311–1317, 2000.

[78] L. Dong, M. L. Crow, Z. Yang, C. Shen, L. Zhang, and S. Atcitty, "A Reconfigurable FACTS System for University Laboratories," *IEEE Trans. Power Syst.*, vol. 19, no. 1, pp. 120–128, Feb. 2004.

[79] D. Soto and R. Pena, "Nonlinear Control Strategies for Cascaded Multilevel STATCOMs," *IEEE Trans. Power Deliv.*, vol. 19, no. 4, pp. 1919–1927, Oct. 2004.

[80] M. Saeedifard, H. Nikkhajoei, and R. Iravani, "A Space Vector Modulated STATCOM Based on a Three-Level Neutral Point Clamped Converter," *IEEE Trans. Power Deliv.*, vol. 22, no. 2, pp. 1029–1039, Apr. 2007.

[81] R. Sternberger and D. Jovcic, "Analytical Modeling of a Square-Wave-Controlled Cascaded Multilevel STATCOM," *IEEE Trans. Power Deliv.*, vol. 24, no. 4, pp. 2261–2269, Oct. 2009.

[82] M. S. El-Moursi and A. M. Sharaf, "Novel Controllers for the 48-Pulse VSC STATCOM and SSSC for Voltage Regulation and Reactive Power Compensation," *IEEE Trans.*

Power Syst., vol. 20, no. 4, pp. 1985–1997, Nov. 2005.

[83] P. Gopakumar, M. J. B. Reddy, and D. K. Mohanta, "Stability Control of Smart Power Grids with Artificial Intelligence and Wide-area Synchrophasor Measurements," *Electr. Power Components Syst.*, vol. 42, no. 10, pp. 1095–1106, Jun. 2014.

[84] K. Seethalekshmi, S. N. Singh, and S. C. Srivastava, "Adaptive Scheme for Minimal Load Shedding Utilizing Synchrophasor Measurements to Ensure Frequency and Voltage Stability," *Electr. Power Components Syst.*, vol. 38, no. 11, pp. 1211–1227, Aug. 2010.

[85] M. Hajian, A. M. Ranjbar, T. Amraee, and A. R. Shirani, "Optimal Placement of Phasor Measurement Units: Particle Swarm Optimization Approach," in *2007 International Conference on Intelligent Systems Applications to Power Systems*, 2007, pp. 1–6.

[86] "SEL Offers Economical Dedicated Phasor Measurement Units," 2010. [Online]. Available: https://www.selinc.com/news.aspx?id=6883. [Accessed: 26-Sep-2014].

[87] N. H. Abbasy and H. M. Ismail, "A Unified Approach for the Optimal PMU Location for Power System State Estimation," *IEEE Trans. Power Syst.*, vol. 24, no. 2, pp. 806–813, May 2009.

[88] I. Musirin and T. K. A. Rahman, "Estimating Maximum Loadability for Weak Bus Identification Using FVSI," *IEEE Power Eng. Rev.*, vol. 22, no. 11, pp. 50–52, 2002.

[89] Sung-Hwan Song, Ho-Chul Lee, Yong Tae Yoon, and Seung-Il Moon, "Cluster design compatible with market for effective reactive power management," in *2006 IEEE Power Engineering Society General Meeting*, 2006, pp. 1 – 7.

[90] I. O. Habiballah, "Integer-linear-programming eigenvector-based approach for multipartitioning power system state-estimation networks," *IEE Proc. - Gener. Transm. Distrib.*, vol. 141, no. 1, p. 11, 1994.

[91] V. Belton and T. Gear, "On a short-coming of Saaty's method of analytic hierarchies," *Omega*, vol. 11, no. 3, pp. 228–230, 1983.

[92] E. Triantaphyllou and S. H. Mann, "Using the Analytic Hierarchy Process for Decision Making in Engineering Applications : Some Challenges," *Int. J. Ind. Eng. Theory, Appl. Pract.*, vol. 2, no. 1, pp. 35–44, 1995.

[93] J. Zietsman, L. R. Rilett, and S.-J. Kim, "Transportation Corridor Decision-Making With Multi-Attribute Utility Theory," *Int. J. Manag. Decis. Mak.*, vol. 7, no. 2/3, 2006.

[94] "Power Systems Test Case Archive - UWEE." [Online]. Available: http://www.ee.washington.edu/research/pstca/. [Accessed: 26-Sep-2014].

[95] "Northern Regional Power Grid (NRPG) 246-bus system," 2013 Avaliable:http://www.iitk.ac.in/ee/labs/lab_files/NRPG-DATA.pdf.

[96] "Matlab User Guide." [Online]. Available: http://www.mathworks.in/help/pdf_doc/matlab/getstart.pdf. [Accessed: 26-Sep-2014].

[97] A. G. E. Ali Abur, *Power System State Estimation: Theory and Implementation - CRC Press Book*. 2004.

[98] W. Nakawiro and I. Erlich, "Online voltage stability monitoring using Artificial Neural Network," in *2008 Third International Conference on Electric Utility Deregulation and Restructuring and Power Technologies*, 2008, pp. 941–947.

[99] S. Kamalasadan, A. K. Srivastava, and D. Thukaram, "Novel algorithm for online voltage stability assessment based on feed forward neural network," in *2006 IEEE Power Engineering Society General Meeting*, 2006, p. 7 pp.

[100] S. R. Gunn, "Support Vector Machines for Classification and Regression," Image Speech and Intelligent Systems Research Group, University of Southampton, 1997.

[101] M. A. H. Farquad, V. Ravi, and S. B. Raju, "Support vector regression based hybrid rule extraction methods for forecasting," *Expert Syst. Appl.*, vol. 37, no. 8, pp. 5577–5589, Aug. 2010.

[102] W.-C. Hong, "Hybrid evolutionary algorithms in a SVR-based electric load forecasting model," *Int. J. Electr. Power Energy Syst.*, vol. 31, no. 7–8, pp. 409–417, Sep. 2009.

[103] L. M. Saini, S. K. Aggarwal, and A. Kumar, "Parameter optimisation using genetic algorithm for support vector machine-based price-forecasting model in National electricity market," *IET Gener. Transm. Distrib.*, vol. 4, no. 1, pp. 36 – 49, 2010.

[104] B. Ravikumar, D. Thukaram, and H. P. Khincha, "Application of support vector machines for fault diagnosis in power transmission system," *Generation, Transmission & Distribution, IET*, vol. 2, no. 1. pp. 119–130, 2008.

[105] Q. Wu, "A hybrid-forecasting model based on Gaussian support vector machine and chaotic particle swarm optimization," *Expert Syst. Appl.*, vol. 37, no. 3, pp. 2388–2394, Mar. 2010.

[106] A. R. Phadke, M. Fozdar, and K. R. Niazi, "A new technique for computation of closest saddle-node bifurcation point of power system using real coded genetic algorithm," *Int. J. Electr. Power Energy Syst.*, vol. 33, no. 5, pp. 1203–1210, Jun. 2011.

[107] K. Seethalekshmi, S. N. Singh, and S. C. Srivastava, "A Classification Approach Using Support Vector Machines to Prevent Distance Relay Maloperation Under Power Swing and Voltage Instability," *Power Delivery, IEEE Transactions on*, vol. 27, no. 3. pp. 1124–1133, 2012.

[108] H. S. Kim and S. Y. Sohn, "Support vector machines for default prediction of SMEs based on technology credit," *Eur. J. Oper. Res.*, vol. 201, no. 3, pp. 838–846, Mar. 2010.

[109] J. N. Hu, J. J. Hu, H. B. Lin, X. P. Li, C. L. Jiang, X. H. Qiu, and W. S. Li, "State-of-charge estimation for battery management system using optimized support vector machine for regression," *J. Power Sources*, vol. 269, no. 0, pp. 682–693, Dec. 2014.

[110] K. Duan, S. S. Keerthi, and A. N. Poo, "Evaluation of simple performance measures for tuning SVM hyperparameters," *Neurocomputing*, vol. 51, no. 0, pp. 41–59, Apr. 2003.

[111] S. S. Keerthi and C.-J. Lin, "Asymptotic behaviors of support vector machines with Gaussian kernel," *Neural Comput.*, vol. 15, no. 7, pp. 1667–1689, 2003.

[112] Y. JinLiang, Z. Yongli, and Y. Guoqin, "Power transformer fault diagnosis based on support vector machine with cross validation and genetic algorithm," *Advanced Power System Automation and Protection (APAP), 2011 International Conference on*, vol. 1. pp. 309–313, 2011.

[113] M. Li, X. Zhou, X. Wang, and B. Wu, "Genetic algorithm optimized SVM in object-based classification of quickbird imagery," in *Proceedings 2011 IEEE International Conference on Spatial Data Mining and Geographical Knowledge Services*, 2011, pp. 348–352.

[114] A. J. A. J. Flueck, K. S. K. S. Shah, N. Balu, and H. D. Chiang, "CPFLOW: a practical tool for tracing power system steady-state stationary behavior due to load and generation variations," *IEEE Trans. Power Syst.*, vol. 10, no. 2, pp. 623–634, May 1995.

[115] "IEEE Standard for Synchrophasor Measurements for Power Systems," *IEEE Std C37.118.1-2011 (Revision of IEEE Std C37.118-2005)*. pp. 1–61, 2011.

[116] C. Cortes and V. Vapnik, "Support-Vector Networks," *Mach. Learn.*, vol. 20, no. 3, pp. 273–297, 1995.

[117] A. Smola, V. Vapnik, H. Drucker, C. J. C. Burges, L. Kaufman, A. Smola, and V. Vapnik, "Support vector regression machines," *Adv. Neural Inf. Process. Syst.*, vol. 9, pp. 155–161, 1997.

[118] A. J. Smola and B. Schölkopf, "A tutorial on support vector regression," *Stat. Comput.*, vol. 14, no. 3, pp. 199–222, 2004.

[119] C. Willmott, "On the evaluation of model performance in physical geography," *Spat. Stat. Model. Springer*, vol. 40, pp. 443–460, 1984.

[120] P. W. Sauer and M. A. Pai, *Power System Dynamics and Control*. Upper Saddle River, NJ: Prentice-Hall, 1998.

[121] J. Hernández-Orallo, "ROC curves for regression," *Pattern Recognit.*, vol. 46, no. 12, pp. 3395–3411, Dec. 2013.

[122] S. Sondhi and Y. V. Hote, "Fractional order PID controller for load frequency control," *Energy Convers. Manag.*, vol. 85, pp. 343–353, Sep. 2014.

[123] I. Pan and S. Das, "Chaotic multi-objective optimization based design of fractional order PIλDμ controller in AVR system," *Int. J. Electr. Power Energy Syst.*, vol. 43, no. 1, pp. 393–407, Dec. 2012.

[124] M. Zamani, M. Karimi-Ghartemani, N. Sadati, and M. Parniani, "Design of a fractional order PID controller for an AVR using particle swarm optimization," *Control Eng. Pract.*, vol. 17, no. 12, pp. 1380–1387, Dec. 2009.

[125] Y. Tang, M. Cui, C. Hua, L. Li, and Y. Yang, "Optimum design of fractional order PIλDμ controller for AVR system using chaotic ant swarm," *Expert Syst. Appl.*, vol. 39, no. 8, pp. 6887–6896, Jun. 2012.

[126] M. A. S. Aboelela, M. F. Ahmed, and H. T. Dorrah, "Design of aerospace control systems using fractional PID controller," *J. Adv. Res.*, vol. 3, no. 3, pp. 225–232, Jul. 2012.

[127] C. A. Monje, A. J. Calderon, B. M. Vinagre, Y. Chen, and V. Feliu, "On Fractional PI? Controllers: Some Tuning Rules for Robustness to Plant Uncertainties," *Nonlinear Dyn.*, vol. 38, no. 1–4, pp. 369–381, Dec. 2004.

[128] Qian Yanping, Zhang Ning, Wang Bin, and Wang Wancheng, "Fractional order proportional integral (FOPI) controller design for the hydraulic variable pitch wind turbine system," in *Control Conference (CCC), 2012 31st Chinese*, 2012, pp. 6789–6793.

[129] Qian Yanping, Hu Wenkui, Lin Xiangze, and Wang Bing, "Fractional order proportional integral controller for active queue management of wireless network," in *Control Conference (CCC), 2011 30th Chinese*, 2011, pp. 4406–4410.

[130] I. Podlubny, *Fractional Differential Equations*. ACADEMIC PRESS, 1999.

[131] R. Technologies, "Real Time Digital Simulator Power System and Control User Manual," 2009.

[132] S. S. Keerthi and C.-J. Lin, "Asymptotic behaviors of support vector machines with Gaussian kernel.," *Neural Comput.*, vol. 15, no. 7, pp. 1667–89, Jul. 2003.

[133] K. L. Priddy and P. E. Keller, *Artificial Neural Networks: An Introduction*. SPIE Press, 2005.

[134] I. Papič and P. Žunko, "UPFC converter-level control system using internally calculated system quantities for decoupling," *Int. J. Electr. Power Energy Syst.*, vol. 25, no. 8, pp. 667–675, Oct. 2003.

APPENDIX A

In this appendix, line data and the bus data of IEEE-14 bus system, IEEE-30 bus system, IEEE-57 bus system, New England-39 bus system and Northern Region Power Grid (NRPG) 246-bus Indian system used in this thesis are given. In column 'Type' for the bus data, type 1 represents slack bus, type 2 represents generator bus and type 3 represents load bus.

A.1 IEEE-14 bus system

A.1.1 Line Data

Line No.	From bus	To bus	R	X	Bsh/2	Tab ratio
1	1	2	0.01938	0.05917	0.0264	1
2	1	5	0.05403	0.22304	0.0246	1
3	2	3	0.04699	0.19797	0.0219	1
4	2	4	0.05811	0.17632	0.017	1
5	2	5	0.05695	0.17388	0.0173	1
6	3	4	0.06701	0.17103	0.0064	1
7	4	5	0.01335	0.04211	0	1
8	4	7	0	0.20912	0	0.978
9	4	9	0	0.55618	0	0.969
10	5	6	0	0.25202	0	0.932
11	6	11	0.09498	0.1989	0	1
12	6	12	0.12291	0.25581	0	1
13	6	13	0.06615	0.13027	0	1
14	7	8	0	0.17615	0	1
15	7	9	0	0.11001	0	1
16	9	10	0.03181	0.0845	0	1
17	9	14	0.12711	0.27038	0	1
18	10	11	0.08205	0.19207	0	1
19	12	13	0.22092	0.19988	0	1
20	13	14	0.17093	0.34802	0	1

A.1.2 Bus data

Bus	Type	Vm(p.u)	P_G(MW)	Q_G(MVar)	P_L(MW)	Q_L(MVar)	Q_{min}(MVar)	Q_{max}(MVar)
1	1	1.06	0	0	0	0	0	0
2	2	1.045	40	42.4	21.7	12.7	-40	50
3	2	1.01	0	23.4	94.2	19	0	40
4	3	1	0	0	47.8	-3.9	0	0
5	3	1	0	0	7.6	1.6	0	0
6	2	1.07	0	12.2	11.2	7.5	-6	24

Bus	Type	Vm(p.u)	P_G(MW)	Q_G(MVar)	P_L(MW)	Q_L(MVar)	Q_{min}(MVar)	Q_{max}(MVar)
7	3	1	0	0	0	0	0	0
8	2	1.09	0	17.4	0	0	-6	24
9	3	1	0	0	29.5	16.6	0	0
10	3	1	0	0	9	5.8	0	0
11	3	1	0	0	3.5	1.8	0	0
12	3	1	0	0	6.1	1.6	0	0
13	3	1	0	0	13.5	5.8	0	0
14	3	1	0	0	14.9	5	0	0

A.2 IEEE-30 bus system

A.2.1 Line Data

Line No.	From bus	To bus	R	X	Bsh/2	Tab ratio
1	1	2	0.0192	0.0575	0.0264	1
2	1	3	0.0452	0.1652	0.0204	1
3	2	4	0.057	0.1737	0.0184	1
4	3	4	0.0132	0.0379	0.0042	1
5	2	5	0.0472	0.1983	0.0209	1
6	2	6	0.0581	0.1763	0.0187	1
7	4	6	0.0119	0.0414	0.0045	1
8	5	7	0.046	0.116	0.0102	1
9	6	7	0.0267	0.082	0.0085	1
10	6	8	0.012	0.042	0.0045	1
11	6	9	0	0.208	0	0.978
12	6	10	0	0.556	0	0.969
13	9	11	0	0.208	0	1
14	9	10	0	0.11	0	1
15	4	12	0	0.256	0	0.932
16	12	13	0	0.14	0	1
17	12	14	0.1231	0.2559	0	1
18	12	15	0.0662	0.1304	0	1
19	12	16	0.0945	0.1987	0	1
20	14	15	0.221	0.1997	0	1
21	16	17	0.0824	0.1923	0	1
22	15	18	0.1073	0.2185	0	1
23	18	19	0.0639	0.1292	0	1
24	19	20	0.034	0.068	0	1
25	10	20	0.0936	0.209	0	1
26	10	17	0.0324	0.0845	0	1
27	10	21	0.0348	0.0749	0	1
28	10	22	0.0727	0.1499	0	1
29	21	23	0.0116	0.0236	0	1
30	15	23	0.1	0.202	0	1

Line No.	From bus	To bus	R	X	Bsh/2	Tab ratio
31	22	24	0.115	0.179	0	1
32	23	24	0.132	0.27	0	1
33	24	25	0.1885	0.3292	0	1
34	25	26	0.2544	0.38	0	1
35	25	27	0.1093	0.2087	0	1
36	28	27	0	0.396	0	0.968
37	27	29	0.2198	0.4153	0	1
38	27	30	0.3202	0.6027	0	1
39	29	30	0.2399	0.4533	0	1
40	8	28	0.0636	0.2	0.0214	1
41	6	28	0.0169	0.0599	0.065	1

A.2.2 Bus data

Bus	Type	Vm(p.u)	P_G(MW)	Q_G(MVar)	P_L(MW)	Q_L(MVar)	Q_{min}(MVar)	Q_{max}(MVar)
1	1	1.06	0	0	0	0	0	0
2	2	1.043	40	50	21.7	12.7	-40	50
3	3	1	0	0	2.4	1.2	0	0
4	3	1.06	0	0	7.6	1.6	0	0
5	2	1.01	0	37	94.2	19	-40	40
6	3	1	0	0	0	0	0	0
7	3	1	0	0	22.8	10.9	0	0
8	2	1.01	0	37.3	30	30	-10	40
9	3	1	0	0	0	0	0	0
10	3	1	0	0	5.8	2	0	0
11	2	1.082	0	16.2	0	0	-6	24
12	3	1	0	0	11.2	7.5	0	0
13	2	1.071	0	10.6	0	0	-6	24
14	3	1	0	0	6.2	1.6	0	0
15	3	1	0	0	8.2	2.5	0	0
16	3	1	0	0	3.5	1.8	0	0
17	3	1	0	0	9	5.8	0	0
18	3	1	0	0	3.2	0.9	0	0
19	3	1	0	0	9.5	3.4	0	0
20	3	1	0	0	2.2	0.7	0	0
21	3	1	0	0	17.5	11.2	0	0
22	3	1	0	0	0	0	0	0
23	3	1	0	0	3.2	1.6	0	0
24	3	1	0	0	8.7	6.7	0	0
25	3	1	0	0	0	0	0	0
26	3	1	0	0	3.5	2.3	0	0
27	3	1	0	0	0	0	0	0
28	3	1	0	0	0	0	0	0
29	3	1	0	0	2.4	0.9	0	0
30	3	1	0	0	10.6	1.9	0	0

A.3 IEEE-57 bus system

A.3.1 Line Data

Line No.	From bus	To bus	R	X	Bsh/2	Tab ratio
1	1	2	0.0083	0.028	0.0645	1
2	2	3	0.0298	0.085	0.0409	1
3	3	4	0.0112	0.0366	0.019	1
4	4	5	0.0625	0.132	0.0129	1
5	4	6	0.043	0.148	0.0174	1
6	6	7	0.02	0.102	0.0138	1
7	6	8	0.0339	0.173	0.0235	1
8	8	9	0.0099	0.0505	0.0274	1
9	9	10	0.0369	0.1679	0.022	1
10	9	11	0.0258	0.0848	0.0109	1
11	9	12	0.0648	0.295	0.0386	1
12	9	13	0.0481	0.158	0.0203	1
13	13	14	0.0132	0.0434	0.0055	1
14	13	15	0.0269	0.0869	0.0115	1
15	1	15	0.0178	0.091	0.0494	1
16	1	16	0.0454	0.206	0.0273	1
17	1	17	0.0238	0.108	0.0143	1
18	3	15	0.0162	0.053	0.0272	1
19	4	18	0	0.555	0	0.97
20	4	18	0	0.43	0	0.978
21	5	6	0.0302	0.0641	0.0062	1
22	7	8	0.0139	0.0712	0.0097	1
23	10	12	0.0277	0.1262	0.0164	1
24	11	13	0.0223	0.0732	0.0094	1
25	12	13	0.0178	0.058	0.0302	1
26	12	16	0.018	0.0813	0.0108	1
27	12	17	0.0397	0.179	0.0238	1
28	14	15	0.0171	0.0547	0.0074	1
29	18	19	0.461	0.685	0	1
30	19	20	0.283	0.434	0	1
31	21	20	0	0.7767	0	1.043
32	21	22	0.0736	0.117	0	1
33	22	23	0.0099	0.0152	0	1
34	23	24	0.166	0.256	0.0042	1
35	24	25	0	1.182	0	1
36	24	25	0	1.23	0	1
37	24	26	0	0.0473	0	1.043
38	26	27	0.165	0.254	0	1
39	27	28	0.0618	0.0954	0	1
40	28	29	0.0418	0.0587	0	1

Line No.	From bus	To bus	R	X	Bsh/2	Tab ratio
41	7	29	0	0.0648	0	0.967
42	25	30	0.135	0.202	0	1
43	30	31	0.326	0.497	0	1
44	31	32	0.507	0.755	0	1
45	32	33	0.0392	0.036	0	1
46	34	32	0	0.953	0	0.975
47	34	35	0.052	0.078	0.0016	1
48	35	36	0.043	0.0537	0.0008	1
49	36	37	0.029	0.0366	0	1
50	37	38	0.0651	0.1009	0.001	1
51	37	39	0.0239	0.0379	0	1
52	36	40	0.03	0.0466	0	1
53	22	38	0.0192	0.0295	0	1
54	11	41	0	0.749	0	0.955
55	41	42	0.207	0.352	0	1
56	41	43	0	0.412	0	1
57	38	44	0.0289	0.0585	0.001	1
58	15	45	0	0.1042	0	0.955
59	14	46	0	0.0735	0	0.9
60	46	47	0.023	0.068	0.0016	1
61	47	48	0.0182	0.0233	0	1
62	48	49	0.0834	0.129	0.0024	1
63	49	50	0.0801	0.128	0	1
64	50	51	0.1386	0.22	0	1
65	10	51	0	0.0712	0	0.93
66	13	49	0	0.191	0	0.895
67	29	52	0.1442	0.187	0	1
68	52	53	0.0762	0.0984	0	1
69	53	54	0.1878	0.232	0	1
70	54	55	0.1732	0.2265	0	1
71	11	43	0	0.153	0	0.958
72	44	45	0.0624	0.1242	0.002	1
73	40	56	0	1.195	0	0.958
74	56	41	0.553	0.549	0	1
75	56	42	0.2125	0.354	0	1
76	39	57	0	1.355	0	0.98
77	57	56	0.174	0.26	0	1
78	38	49	0.115	0.177	0.0015	1
79	38	48	0.0312	0.0482	0	1
80	9	55	0	0.1205	0	0.94

A.3.2 Bus Data

Bus	Type	Vm(p.u)	P_G(MW)	Q_G(MVar)	P_L(MW)	Q_L(MVar)	Q_{min}(MVar)	Q_{max}(MVar)
1	1	1.04	0	0	0	0	0	0
2	2	1.01	3	88	0	-0.8	50	-17
3	2	0.985	41	21	40	-1	60	-10
4	3	1	0	0	0	0	0	0
5	3	1	13	4	0	0	0	0
6	2	0.98	75	2	0	0.8	25	-8
7	3	1	0	0	0	0	0	0
8	2	1.005	150	22	450	62.1	200	-140
9	2	0.98	121	26	0	2.2	9	-3
10	3	1	5	2	0	0	0	0
11	3	1	0	0	0	0	0	0
12	2	1.015	377	24	310	128.5	155	-150
13	3	1	18	2.3	0	0	0	0
14	3	1	10.5	5.3	0	0	0	0
15	3	1	22	5	0	0	0	0
16	3	1	43	3	0	0	0	0
17	3	1	42	8	0	0	0	0
18	3	1	27.2	9.8	0	0	0	0
19	3	1	3.3	0.6	0	0	0	0
20	3	1	2.3	1	0	0	0	0
21	3	1	0	0	0	0	0	0
22	3	1	0	0	0	0	0	0
23	3	1	6.3	2.1	0	0	0	0
24	3	1	0	0	0	0	0	0
25	3	1	6.3	3.2	0	0	0	0
26	3	1	0	0	0	0	0	0
27	3	1	9.3	0.5	0	0	0	0
28	3	1	4.6	2.3	0	0	0	0
29	3	1	17	2.6	0	0	0	0
30	3	1	3.6	1.8	0	0	0	0
31	3	1	5.8	2.9	0	0	0	0
32	3	1	1.6	0.8	0	0	0	0
33	3	1	3.8	1.9	0	0	0	0
34	3	1	0	0	0	0	0	0
35	3	1	6	3	0	0	0	0
36	3	1	0	0	0	0	0	0
37	3	1	0	0	0	0	0	0
38	3	1	14	7	0	0	0	0
39	3	1	0	0	0	0	0	0
40	3	1	0	0	0	0	0	0
41	3	1	6.3	3	0	0	0	0
42	3	1	7.1	4.4	0	0	0	0

Bus	Type	Vm(p.u)	P_G(MW)	Q_G(MVar)	P_L(MW)	Q_L(MVar)	Q_{min}(MVar)	Q_{max}(MVar)
43	3	1	2	1	0	0	0	0
44	3	1	12	1.8	0	0	0	0
45	3	1	0	0	0	0	0	0
46	3	1	0	0	0	0	0	0
47	3	1	29.7	11.6	0	0	0	0
48	3	1	0	0	0	0	0	0
49	3	1	18	8.5	0	0	0	0
50	3	1	21	10.5	0	0	0	0
51	3	1	18	5.3	0	0	0	0
52	3	1	4.9	2.2	0	0	0	0
53	3	1	20	10	0	0	0	0
54	3	1	4.1	1.4	0	0	0	0
55	3	1	6.8	3.4	0	0	0	0
56	3	1	7.6	2.2	0	0	0	0
57	3	1	6.7	2	0	0	0	0

A.4 New England-39 bus system

A.4.1 Line Data

Line No.	From bus	To bus	R	X	Bsh/2	Tab ratio
1	1	2	0.0035	0.0411	0.3493	1
2	1	39	0.001	0.025	0.375	1
3	2	3	0.0013	0.0151	0.1286	1
4	2	25	0.007	0.0086	0.073	1
5	2	30	0	0.0181	0	1.025
6	3	4	0.0013	0.0213	0.2214	1
7	3	18	0.0011	0.0133	0.1107	1
8	4	5	0.0008	0.0128	0.0671	1
9	4	14	0.0008	0.0129	0.0691	1
10	5	8	0.0008	0.0112	0.0738	1
11	6	5	0.0002	0.0026	0.0217	1
12	6	7	0.0006	0.0092	0.0565	1
13	6	11	0.0007	0.0082	0.06945	1
14	7	8	0.0004	0.0046	0.039	1
15	8	9	0.0023	0.0363	0.1902	1
16	9	39	0.001	0.025	0.6	1
17	10	11	0.0004	0.0043	0.0365	1
18	10	13	0.0004	0.0043	0.0365	1
19	10	32	0	0.02	0	1.07
20	12	11	0.0016	0.0435	0	1.006
21	12	13	0.0016	0.0435	0	1.006
22	13	14	0.0009	0.0101	0.0862	1
23	14	15	0.0018	0.0217	0.183	1

Line No.	From bus	To bus	R	X	Bsh/2	Tab ratio
24	15	16	0.0009	0.0094	0.0855	1
25	16	17	0.0007	0.0089	0.0671	1
26	16	19	0.0016	0.0195	0.152	1
27	16	21	0.0008	0.0135	0.1274	1
28	16	24	0.0003	0.0059	0.034	1
29	17	18	0.0007	0.0082	0.066	1
30	17	27	0.0013	0.0173	0.1608	1
31	19	33	0.0007	0.0142	0	1.07
32	19	20	0.0007	0.0138	0	1.06
33	20	34	0.0009	0.018	0	1.009
34	21	22	0.0008	0.014	0.1283	1
35	22	23	0.0006	0.0096	0.0923	1
36	22	35	0	0.0143	0	1.025
37	23	24	0.0022	0.035	0.1805	1
38	23	36	0.0005	0.0272	0	1
39	25	26	0.0032	0.0323	0.2565	1
40	25	37	0.0006	0.0232	0	1.025
41	26	27	0.0014	0.0147	0.1198	1
42	26	28	0.0043	0.0474	0.3901	1
43	26	29	0.0057	0.0625	0.5145	1
44	28	29	0.0014	0.0151	0.1245	1
45	29	38	0.0008	0.0156	0	1.025
46	31	6	0	0.025	0	1

A.4.2 Bus Data

Bus	Type	Vm(p.u)	P_G(MW)	Q_G(MVar)	P_L(MW)	Q_L(MVar)	Q_{min}(MVar)	Q_{max}(MVar)
1	3	1	0	0	0	0	0	0
2	3	1	0	0	0	0	0	0
3	3	1	0	0	32.2	0.24	0	0
4	3	1	0	0	50	18.4	0	0
5	3	1	0	0	0	0	0	0
6	3	1	0	0	0	0	0	0
7	3	1	0	0	23.38	8.4	0	0
8	3	1	0	0	52.2	17.6	0	0
9	3	1	0	0	0	0	0	0
10	3	1	0	0	0	0	0	0
11	3	1	0	0	0	0	0	0
12	3	1	0	0	0.75	8.8	0	0
13	3	1	0	0	0	0	0	0
14	3	1	0	0	0	0	0	0
15	3	1	0	0	32	15.3	0	0
16	3	1	0	0	32.9	3.23	0	0
17	3	1	0	0	0	0	0	0
18	3	1	0	0	15.8	3	0	0

Bus	Type	Vm(p.u)	P_G(MW)	Q_G(MVar)	P_L(MW)	Q_L(MVar)	Q_{min}(MVar)	Q_{max}(MVar)
19	3	1	0	0	0	0	0	0
20	3	1	0	0	62.8	10.3	0	0
21	3	1	0	0	27.4	11.5	0	0
22	3	1	0	0	0	0	0	0
23	3	1	0	0	24.75	8.46	0	0
24	3	1	0	0	30.86	-9.2	0	0
25	3	1	0	0	22.4	4.72	0	0
26	3	1	0	0	13.9	1.7	0	0
27	3	1	0	0	28.1	7.55	0	0
28	3	1	0	0	20.6	2.76	0	0
29	3	1	0	0	28.35	2.69	0	0
30	2	1.0475	25	6.389	0	0	-45	510
31	1	0.982	52.3	13.475	0.92	0.46	-60	550
32	2	0.9831	65	13.8	0	0	-70	800
33	2	0.9972	63.2	3.773	0	0	0	350
34	2	1.0123	50.8	13.979	0	0	-20	275
35	2	1.0493	65	30.135	0	0	0	365
36	2	1.0635	56	14.427	0	47.2	-20	109
37	2	1.0278	54	5.218	0	0	-20	109
38	2	1.0265	83	5.764	0	0	-40	205
39	2	1.03	100	38.285	110.4	25.05	0	550

A.5 Northern Regional Power Grid (NRPG) – 246 bus system

A.5.1 Line Data

Line No.	From bus	To bus	R	X	Bsh	Tab ratio
1	59	48	0	0.0125	0	1
2	61	53	0	0.0125	0	1
3	62	54	0	0.0125	0	1
4	71	56	0	0.0125	0	1
5	6	5	0	0.0125	0	1
6	10	8	0	0.0125	0	1
7	69	115	0	0.0125	0	1
8	70	232	0	0.0125	0	1
9	72	84	0	0.0125	0	1
10	72	84	0	0.00625	0	1
11	72	84	0	0.00417	0	1
12	73	74	0	0.0125	0	1
13	236	97	0	0.0125	0	1
14	131	109	0	0.0125	0	1
15	240	139	0	0.0125	0	1
16	154	140	0	0.0125	0	1
17	155	141	0	0.0125	0	1

Line No.	From bus	To bus	R	X	Bsh	Tab ratio
18	180	157	0	0.0125	0	1
19	179	160	0	0.0125	0	1
20	23	22	0	0.0125	0	1
21	209	185	0	0.0125	0	1
22	210	187	0	0.0125	0	1
23	211	190	0	0.0125	0	1
24	212	191	0	0.0125	0	1
25	213	194	0	0.0125	0	1
26	214	199	0	0.0125	0	1
27	215	27	0	0.0125	0	1
28	33	28	0	0.0125	0	1
29	216	204	0	0.0125	0	1
30	217	205	0	0.0125	0	1
31	221	222	0	0.0125	0	1
32	233	229	0	0.0125	0	1
33	238	230	0	0.0125	0	1
34	239	231	0	0.0125	0	1
35	237	36	0	0.0125	0	1
36	235	38	0	0.0125	0	1
37	43	44	0.0035	0.01855	0.1278	1
38	43	45	0.0035	0.01855	0.1278	1
39	44	56	0.00464	0.02475	0.1704	1
40	44	57	0.0071	0.0379	0.0653	1
41	44	80	0.0071	0.0379	0.0653	1
42	45	56	0.00619	0.03299	0.2272	1
43	46	56	0.00155	0.00825	0.0568	1
44	46	57	0.0077	0.0412	0.071	1
45	46	80	0.0192	0.1023	0.1761	1
46	47	48	0.00155	0.00825	0.0142	1
47	59	48	0	0.052	0	1
48	48	204	0.0161	0.0858	0.1477	1
49	49	50	0.00154	0.00825	0.0568	1
50	49	54	0.00132	0.00701	0.04828	1
51	50	55	0.00232	0.01238	0.0852	1
52	51	54	0.00348	0.01856	0.1278	1
53	52	54	0.00077	0.00413	0.0284	1
54	54	55	0.00038	0.00206	0.0142	1
55	55	56	0.01455	0.07755	0.534	1
56	56	25	0.00232	0.01238	0.3408	1
57	56	80	0.0081	0.0433	0.2982	1
58	25	57	0.00479	0.02557	0.17608	1
59	2	187	0.0075	0.04315	0.301	1
60	63	58	0	0.0198	0	1
61	59	32	0.00149	0.0166	1.776	1

Line No.	From bus	To bus	R	X	Bsh	Tab ratio
62	59	216	0.0019	0.0207	0.555	1
63	3	71	0.00186	0.02075	0.555	1
64	3	73	0.00155	0.0173	1.8538	1
65	4	62	0.00086	0.00965	1.0323	1
66	61	154	0.00101	0.01439	2.2514	1
67	62	71	0.00174	0.0194	2.0757	1
68	63	70	0.00151	0.02137	3.3434	1
69	6	65	0.00123	0.0066	0.1023	1
70	7	65	0.00195	0.0103	0.071	1
71	7	67	0.00665	0.03545	0.2442	1
72	7	79	0.00395	0.02105	0.1448	1
73	7	105	0.01733	0.09239	0.15904	1
74	8	65	0.00435	0.0231	0.159	1
75	64	67	0.00485	0.026	0.179	1
76	64	11	0.00507	0.02693	0.4176	1
77	64	88	0.0011	0.00575	0.0398	1
78	64	102	0.00773	0.04124	0.071	1
79	9	11	0.0149	0.0792	0.1363	1
80	9	60	0.00928	0.04949	0.0852	1
81	65	67	0.00605	0.03215	0.2216	1
82	65	68	0.0248	0.132	0.2272	1
83	65	90	0.00605	0.03215	0.2216	1
84	65	100	0.00555	0.0297	0.2044	1
85	65	110	0.00867	0.0462	0.31808	1
86	66	67	0.00605	0.03215	0.2216	1
87	66	98	0.0054	0.0289	0.0497	1
88	66	118	0.0088	0.047	0.3238	1
89	66	130	0.00541	0.02887	0.1988	1
90	67	91	0.00155	0.00825	0.0568	1
91	68	108	0.0074	0.0396	0.0386	1
92	10	69	0.0065	0.0726	1.9425	1
93	10	131	0.0048	0.0533	1.4263	1
94	69	70	0.0007	0.0073	0.1943	1
95	69	154	0.0023	0.0259	0.6937	1
96	70	72	0.00195	0.0218	2.331	1
97	70	154	0.003	0.0332	0.888	1
98	70	238	0.0052	0.0581	1.554	1
99	71	72	0.00105	0.02375	3.8058	1
100	72	73	0.00065	0.00725	0.777	1
101	74	86	0.00885	0.02353	0.1618	1
102	74	88	0.00109	0.00577	0.03976	1
103	74	104	0.00348	0.01856	0.1278	1
104	74	246	0.01006	0.05362	0.3692	1
105	75	76	0.0023	0.01235	0.0852	1

Line No.	From bus	To bus	R	X	Bsh	Tab ratio
106	75	91	0.00195	0.0103	0.071	1
107	78	84	0.00265	0.014	0.0966	1
108	78	91	0.0025	0.0132	0.0908	1
109	79	88	0.00365	0.0194	0.1334	1
110	11	86	0.0065	0.0346	0.0596	1
111	11	60	0.00696	0.03712	0.0639	1
112	80	82	0.00147	0.00784	0.48564	1
113	80	12	0.00139	0.00743	0.20448	1
114	80	86	0.0045	0.0239	0.1648	1
115	81	97	0.00232	0.01238	0.0852	1
116	81	101	0.00232	0.01238	0.0852	1
117	82	83	0.0031	0.0165	0.1136	1
118	82	92	0.0027	0.01444	0.0994	1
119	83	95	0.00194	0.01031	0.071	1
120	83	102	0.00634	0.03382	0.05822	1
121	83	103	0.00155	0.00825	0.0568	1
122	83	104	0.00348	0.01856	0.1278	1
123	84	89	0.0035	0.01855	0.1278	1
124	84	94	0.0068	0.0363	0.0625	1
125	85	94	0.0031	0.0165	0.1136	1
126	85	103	0.00155	0.00825	0.0568	1
127	87	96	0.00232	0.01238	0.0852	1
128	87	100	0.0027	0.01444	0.0994	1
129	88	13	0.0081	0.0433	0.2982	1
130	88	94	0.00315	0.0169	0.1164	1
131	89	93	0.0027	0.01445	0.0994	1
132	89	15	0.00426	0.02269	0.1562	1
133	13	90	0.00243	0.013	0.358	1
134	13	91	0.0071	0.03795	0.2612	1
135	13	100	0.00356	0.01897	0.13064	1
136	90	96	0.0025	0.0132	0.0908	1
137	90	97	0.00365	0.0194	0.1334	1
138	91	97	0.0097	0.052	0.0895	1
139	92	95	0.00194	0.01031	0.071	1
140	93	14	0.00385	0.0206	0.142	1
141	96	101	0.00696	0.03712	0.2556	1
142	97	98	0.0085	0.0454	0.0781	1
143	98	15	0.00465	0.02475	0.1704	1
144	14	15	0.00116	0.00619	0.0426	1
145	15	99	0.00332	0.01774	0.12212	1
146	99	101	0.00325	0.01733	0.11928	1
147	105	107	0.00503	0.02681	0.1846	1
148	105	245	0.00534	0.02846	0.19596	1
149	106	107	0.00116	0.00619	0.0426	1

Line No.	From bus	To bus	R	X	Bsh	Tab ratio
150	106	123	0.00402	0.02144	0.14768	1
151	106	130	0.0031	0.0165	0.1136	1
152	108	109	0.0108	0.0577	0.0994	1
153	109	16	0.00042	0.00228	0.0624	1
154	109	110	0.00967	0.05155	0.355	1
155	109	121	0.017	0.0907	0.1562	1
156	109	132	0.00299	0.01595	0.24708	1
157	16	113	0.0059	0.03135	0.2158	1
158	16	125	0.0031	0.0165	0.1136	1
159	111	121	0.0091	0.0487	0.0838	1
160	111	128	0.00155	0.00825	0.0568	1
161	112	122	0.00557	0.0297	0.05112	1
162	113	114	0.00285	0.01525	0.105	1
163	113	126	0.01006	0.05362	0.0923	1
164	113	127	0.00348	0.01856	0.1278	1
165	113	129	0.0093	0.0495	0.0852	1
166	114	125	0.0031	0.0165	0.1136	1
167	114	130	0.0023	0.01235	0.0852	1
168	115	118	0.0045	0.0239	0.1648	1
169	115	121	0.00135	0.00722	0.1988	1
170	116	128	0.0031	0.0165	0.1136	1
171	116	229	0.00185	0.0099	0.0682	1
172	17	121	0.0181	0.09651	0.16614	1
173	17	229	0.00026	0.00137	0.0213	1
174	17	34	0.00185	0.0099	0.0682	1
175	117	119	0.00115	0.0062	0.0426	1
176	117	35	0.00194	0.01031	0.071	1
177	118	129	0.0008	0.0041	0.0071	1
178	118	162	0.0178	0.0949	0.1633	1
179	118	232	0.0011	0.00575	0.0398	1
180	119	229	0.00154	0.00825	0.0568	1
181	120	126	0.00619	0.033	0.0568	1
182	121	122	0.00325	0.01733	0.11928	1
183	121	162	0.00649	0.03465	0.23856	1
184	121	229	0.01779	0.09486	0.1633	1
185	124	125	0.00372	0.0198	0.13632	1
186	125	130	0.0031	0.0165	0.1136	1
187	126	129	0.00464	0.02475	0.1704	1
188	127	129	0.00503	0.02681	0.1846	1
189	129	232	0.00075	0.0041	0.0284	1
190	132	139	0.00215	0.01155	0.0796	1
191	132	140	0.00095	0.00495	0.034	1
192	132	149	0.0017	0.00905	0.0624	1
193	133	18	0.0003	0.00165	0.0114	1

Line No.	From bus	To bus	R	X	Bsh	Tab ratio
194	133	139	0.0011	0.00575	0.0398	1
195	133	182	0.0012	0.0066	0.0114	1
196	133	183	0.0002	0.0008	0.0014	1
197	18	134	0.0001	0.0004	0.0028	1
198	134	146	0.00045	0.00245	0.017	1
199	134	147	0.001	0.00535	0.037	1
200	135	34	0.00045	0.00245	0.017	1
201	136	138	0.0004	0.00205	0.0142	1
202	136	141	0.0011	0.00575	0.0398	1
203	136	229	0.0023	0.01235	0.0852	1
204	136	34	0.0013	0.007	0.0482	1
205	137	140	0.0017	0.00905	0.0624	1
206	137	141	0.0007	0.0037	0.0256	1
207	138	141	0.00031	0.00165	0.01136	1
208	138	151	0.00055	0.0029	0.0198	1
209	139	145	0.00055	0.0029	0.0198	1
210	139	152	0.0007	0.0037	0.0256	1
211	140	143	0.00095	0.00495	0.034	1
212	140	144	0.00085	0.00455	0.0312	1
213	141	148	0.00031	0.00165	0.01136	1
214	141	151	0.0014	0.0074	0.0512	1
215	142	145	0.00055	0.0029	0.0198	1
216	142	152	0.00025	0.00125	0.0086	1
217	143	144	0.00045	0.00245	0.017	1
218	146	148	0.00055	0.0029	0.0198	1
219	147	150	0.00075	0.0041	0.0284	1
220	147	153	0.0004	0.00205	0.0142	1
221	150	34	0.00025	0.00125	0.0086	1
222	154	155	0.00015	0.0026	0.439	1
223	154	240	0.00015	0.00195	0.3326	1
224	181	158	0.0131	0.0701	0.1207	1
225	181	172	0.01083	0.05774	0.0994	1
226	181	230	0.0024	0.0125	0.086	1
227	181	37	0.01701	0.09074	0.6248	1
228	156	158	0.00465	0.02475	0.1704	1
229	19	21	0.00385	0.0206	0.142	1
230	19	169	0.0223	0.1188	0.2045	1
231	20	21	0.00773	0.04124	0.071	1
232	20	168	0.03496	0.18643	0.32092	1
233	20	170	0.01291	0.06888	0.47428	1
234	20	37	0.01702	0.09074	0.1562	1
235	157	162	0.0192	0.1023	0.1761	1
236	157	175	0.0232	0.1237	0.213	1
237	157	176	0.00413	0.022	0.3408	1

Line No.	From bus	To bus	R	X	Bsh	Tab ratio
238	157	177	0.0221	0.118	0.2031	1
239	157	22	0.01315	0.07011	0.4828	1
240	158	160	0.0183	0.0973	0.1676	1
241	158	34	0.0227	0.1213	0.2087	1
242	159	199	0.0037	0.0198	0.1364	1
243	160	161	0.0048	0.02555	0.176	1
244	160	162	0.0102	0.05445	0.3748	1
245	160	164	0.00485	0.026	0.179	1
246	160	21	0.01087	0.05803	0.8988	1
247	160	230	0.0024	0.0125	0.086	1
248	161	162	0.0131	0.0701	0.1207	1
249	161	176	0.00284	0.01512	0.2343	1
250	163	164	0.013	0.0693	0.1193	1
251	163	167	0.0147	0.07837	0.1349	1
252	165	21	0.01045	0.0557	0.3834	1
253	165	167	0.01315	0.07012	0.1207	1
254	165	170	0.0087	0.0462	0.0795	1
255	165	171	0.0316	0.1683	0.2897	1
256	165	174	0.0328	0.1749	0.301	1
257	165	37	0.0139	0.07425	0.5112	1
258	166	21	0.0156	0.0833	0.5736	1
259	166	167	0.00464	0.02475	0.1704	1
260	166	173	0.01392	0.07424	0.1278	1
261	166	175	0.01934	0.10311	0.71	1
262	21	37	0.00385	0.0206	0.142	1
263	168	169	0.017	0.0907	0.1562	1
264	168	170	0.0173	0.0924	0.159	1
265	168	171	0.0153	0.0817	0.1406	1
266	168	178	0.0119	0.0635	0.4374	1
267	169	170	0.0062	0.033	0.0568	1
268	173	174	0.01083	0.05774	0.0994	1
269	175	177	0.0247	0.1319	0.2272	1
270	179	238	0.0003	0.0031	0.333	1
271	23	180	0.00153	0.01712	1.8315	1
272	24	191	0.0139	0.0742	0.1278	1
273	24	192	0.0122	0.0652	0.1122	1
274	24	198	0.0035	0.01855	0.1278	1
275	24	1	0.0054	0.0289	0.0497	1
276	182	183	0.0011	0.0058	0.0099	1
277	182	194	0.00185	0.0099	0.0682	1
278	182	228	0.0039	0.0206	0.0355	1
279	183	194	0.00433	0.0231	0.03976	1
280	183	34	0.0031	0.0165	0.0284	1
281	184	191	0.0105	0.0561	0.0966	1

Line No.	From bus	To bus	R	X	Bsh	Tab ratio
282	184	197	0.00773	0.04124	0.071	1
283	185	197	0.00696	0.03712	0.2556	1
284	185	30	0.0081	0.0433	0.2982	1
285	185	219	0.0127	0.0676	0.1164	1
286	186	187	0.0064	0.03425	0.2358	1
287	186	188	0.0145	0.0775	0.1335	1
288	187	189	0.0064	0.03425	0.05895	1
289	187	191	0.00695	0.0371	0.2556	1
290	188	190	0.0149	0.0792	0.1363	1
291	190	222	0.0031	0.0165	0.1136	1
292	190	223	0.0093	0.0495	0.0852	1
293	190	227	0.0046	0.0247	0.0426	1
294	191	208	0.00232	0.01238	0.0852	1
295	192	193	0.0071	0.0379	0.0653	1
296	193	194	0.0071	0.0379	0.0653	1
297	193	197	0.00187	0.0099	0.1533	1
298	194	195	0.0124	0.066	0.1136	1
299	194	198	0.0054	0.02885	0.1988	1
300	194	220	0.0063	0.0338	0.0582	1
301	194	228	0.00077	0.00413	0.0284	1
302	195	196	0.00535	0.02845	0.196	1
303	195	197	0.00295	0.01565	0.108	1
304	195	220	0.0062	0.033	0.0568	1
305	196	219	0.00625	0.0334	0.23	1
306	198	1	0.0035	0.01855	0.1278	1
307	1	199	0.0152	0.0808	0.1392	1
308	1	226	0.0058	0.03095	0.213	1
309	199	200	0.0046	0.0247	0.0426	1
310	199	36	0.0144	0.0767	0.5282	1
311	200	201	0.0087	0.0462	0.0795	1
312	201	26	0.0165	0.08785	0.605	1
313	201	226	0.00465	0.02475	0.1704	1
314	201	231	0.01315	0.07011	0.4828	1
315	26	27	0.03094	0.16498	0.284	1
316	27	203	0.00695	0.0371	0.2556	1
317	27	222	0.0023	0.01235	0.0852	1
318	27	231	0.00232	0.01238	0.0852	1
319	28	202	0.01113	0.0594	0.9201	1
320	202	203	0.01005	0.0536	0.3692	1
321	202	225	0.0059	0.0313	0.054	1
322	203	224	0.0108	0.0577	0.0994	1
323	203	39	0.0023	0.01235	0.0852	1
324	204	207	0.00554	0.06174	0.1511	1
325	205	29	0.0058	0.03095	0.213	1

Line No.	From bus	To bus	R	X	Bsh	Tab ratio
326	205	225	0.0101	0.0536	0.0923	1
327	29	206	0.0079	0.0421	0.0724	1
328	29	207	0.0116	0.0619	0.1065	1
329	206	207	0.0116	0.0619	0.1065	1
330	31	219	0.0004	0.00265	0.0164	1
331	209	212	0.003	0.0332	0.888	1
332	209	213	0.00339	0.03777	1.0101	1
333	210	221	0.00224	0.0249	2.664	1
334	211	212	0.00616	0.06868	1.83705	1
335	211	217	0.0027	0.0301	0.8047	1
336	211	221	0.00102	0.01141	0.30525	1
337	211	40	0.0075	0.084	2.2478	1
338	212	213	0.0025	0.0274	0.7326	1
339	213	214	0.00354	0.03943	1.0545	1
340	213	215	0.0074	0.082	2.1923	1
341	213	235	0.0009	0.0104	0.2775	1
342	214	221	0.00466	0.05188	1.3875	1
343	215	33	0.0072	0.0803	2.1479	1
344	215	221	0.00074	0.0083	0.222	1
345	215	239	0.00005	0.00052	0.0555	1
346	32	33	0.0007	0.0079	0.2109	1
347	32	218	0.00493	0.05499	1.47075	1
348	32	221	0.00286	0.06547	2.62463	1
349	32	40	0.0005	0.0056	0.1498	1
350	33	217	0.0043	0.0477	1.2765	1
351	216	217	0.0023	0.0259	0.6937	1
352	216	218	0.00065	0.00726	0.19425	1
353	219	77	0.0027	0.01444	0.0994	1
354	223	227	0.0108	0.0577	0.0994	1
355	223	39	0.0013	0.007	0.0482	1
356	229	35	0.00132	0.00701	0.04828	1
357	231	39	0.0058	0.03094	0.852	1
358	233	234	0.0034	0.0373	0.999	1
359	233	235	0.0005	0.0055	0.5882	1
360	233	238	0.00404	0.04503	1.20435	1
361	233	239	0.00735	0.0533	2.19225	1
362	234	237	0.00175	0.0193	2.0646	1
363	234	238	0.0048	0.0537	1.4374	1
364	234	239	0.0047	0.0519	1.3875	1
365	40	239	0.00819	0.0913	2.442	1
366	40	41	0.0004	0.00435	0.4662	1
367	40	241	0.00217	0.02412	2.5807	1
368	235	236	0.00577	0.06433	1.7205	1
369	235	240	0.00025	0.00365	0.6118	1

Line No.	From bus	To bus	R	X	Bsh	Tab ratio
370	239	241	0.00217	0.02412	2.5807	1
371	42	243	0.00418	0.02227	0.03834	1
372	42	244	0.00773	0.04124	0.071	1
373	42	245	0.02027	0.10806	0.18602	1
374	243	242	0	0.3968	0	1
375	243	245	0.01702	0.09074	0.1562	1
376	244	245	0.02119	0.11301	0.19454	1

A.5.2 Bus Data

Bus	Type	Vm(p.u)	P_G(p.u)	Q_G(p.u)	P_L(p.u)	Q_L(p.u)	Q_{min}(p.u)	Q_{max}(p.u)
1	1	1.0052	3.852	-0.4175	2.141	0.0754	-2.0717	2.427
2	2	1.0319	1.107	0.0132	0	0	-0.414	0.213
3	2	1.0242	3.6	-0.2894	0	0	-1.8564	0.952
4	2	1.0353	3.6	-0.1099	0	0	-1.72	1.545
5	2	1.032	2	0.3725	0.248	0.082	-0.74	0.38
6	2	1.0287	2	-0.1271	0	0	-0.74	0.38
7	2	1.0209	5	0.8543	0	0	-2.2683	1.16
8	2	1.0499	3.6	0.4218	0	0	-1.6995	0.871
9	2	1.0377	1.2	0.3395	0	0	-0.6804	0.349
10	2	1.0519	3	-1.1329	0	0	-1.133	0.58
11	2	1.0183	3	0.271	0.124	0.041	-1.2354	0.633
12	2	0.9952	4	-0.594	0	0	-1.63	1.465
13	2	1.0189	10	1.401	0.944	0.298	-4.8366	5.657
14	2	1.0027	3.6	0.2649	1.771	0.582	-1.6892	1.977
15	2	1.0043	3.8	0.1776	0	0	-1.6096	1.884
16	2	1.0274	7.2	2.6917	3.057	1.005	-3.3009	3.861
17	2	1.0159	1.2	0.505	4.662	1.532	-0.6898	0.809
18	2	1.018	8.75	4.2745	2.216	0.728	-3.512	4.66
19	2	1.0429	2	0.5666	0	0	-1.6892	1.975
20	2	1.0495	3.8	0.5954	0	0	-1.6935	1.971
21	2	1.0311	7.5	-1.1163	3.862	0.965	-3.2623	3.814
22	2	1.0499	4.5	1.2244	1.659	0.549	-1.9213	2.246
23	2	1.039	4.5	-1.9233	0	0	-1.9235	2.257
24	2	1.0127	3	0.5921	0	0	-1.8041	2.112
25	2	1.0203	4.5	-0.6983	0	0	-1.9756	1.013
26	2	1.0329	1.6	0.5433	1.64	0.539	-0.8446	0.989
27	2	1.0249	1.4	-0.4024	3.016	1.254	-0.8446	0.989
28	2	1.05	4	1.8732	-0.432	0.209	-1.7311	2.022
29	2	1.0368	2.6	1.483	0	0	-1.2668	1.483
30	2	1.04	0.6	0.106	0	0	-0.207	0.106
31	2	1.0248	1.74	0.3171	0	0	-0.618	0.317
32	2	1.035	14	-0.213	0	0	-6.2647	7.321
33	2	1.03	8	-2.3954	0	0	-3.8415	4.494
34	2	1.0188	5.5	3.0559	0	0	-2.7658	3.234

Bus	Type	Vm(p.u)	P_G(p.u)	Q_G(p.u)	P_L(p.u)	Q_L(p.u)	Q_{min}(p.u)	Q_{max}(p.u)
35	2	1.0243	3.6	0.9468	0	0	-1.5779	1.605
36	2	1.0499	5.8	0.0376	0	0	-2.7847	3.948
37	2	1.0499	3.6	0.9789	0	0	-1.5846	1.854
38	2	1.0447	15	1.6075	0	0	-6.3594	7.441
39	2	1.0486	7.2	1.3595	0	0	-3.2214	3.769
40	2	1.038	18	-4.0049	0	0	-15.36	8.988
41	2	1.0475	9	-3.9419	12.584	-6.34	-3.949	4.689
42	2	1.0256	2.4	0.4335	0	0	0	0
43	3	1.0089	0	0	0.425	0.197	0	0
44	3	1.0094	0	0	0.556	0.165	0	0
45	3	1.0111	0	0	0.628	0.219	0	0
46	3	1.0163	0	0	0.71	0.173	0	0
47	3	0.9815	0	0	1.45	0.844	0	0
48	3	0.9909	0	0	0.958	0.576	0	0
49	3	1.0344	0	0	0.36	0.261	0	0
50	3	1.0342	0	0	-0.155	0.307	0	0
51	3	1.0376	0	0	0	0	0	0
52	3	1.0356	0	0	0.489	0.121	0	0
53	3	1.0279	0	0	0	0	0	0
54	3	1.0364	0	0	0	0	0	0
55	3	1.0363	0	0	0.435	-0.063	0	0
56	3	1.0203	0	0	0	0	0	0
57	3	1.012	0	0	1.426	0.217	0	0
58	3	1.0456	0	0	0	0	0	0
59	3	1.0037	0	0	0	0.57	0	0
60	3	1.0181	0	0	1.102	0.265	0	0
61	3	1.0279	0	0	0	0	0	0
62	3	1.0378	0	0	0	0	0	0
63	3	1.0456	0	0	0	0	0	0
64	3	0.9945	0	0	0.496	0.163	0	0
65	3	1.0233	0	0	0.127	0.055	0	0
66	3	0.9972	0	0	1.489	0.49	0	0
67	3	0.9944	0	0	4.271	1.172	0	0
68	3	1.0068	0	0	-0.43	0.168	0	0
69	3	1.0256	0	0	0	0	0	0
70	3	1.0285	0	0	0	0	0	0
71	3	1.0298	0	0	0	0	0	0
72	3	1.013	0	0	0	0	0	0
73	3	1.0151	0	0	0	0	0	0
74	3	0.9989	0	0	0	0	0	0
75	3	0.9906	0	0	0	0	0	0
76	3	0.9854	0	0	0.724	0.315	0	0
77	3	1.0146	0	0	1.81	0.306	0	0
78	3	0.9976	0	0	0.291	0.066	0	0

Bus	Type	Vm(p.u)	P_G(p.u)	Q_G(p.u)	P_L(p.u)	Q_L(p.u)	Q_{min}(p.u)	Q_{max}(p.u)
79	3	0.9992	0	0	1.397	0.418	0	0
80	3	0.9938	0	0	0	0	0	0
81	3	1.0005	0	0	0	0	0	0
82	3	0.975	0	0	2.81	0.935	0	0
83	3	0.9658	0	0	2.986	1.173	0	0
84	3	1.0017	0	0	4.662	1.757	0	0
85	3	0.9617	0	0	2.634	0.866	0	0
86	3	1.0048	0	0	0	0	0	0
87	3	0.9973	0	0	1.401	0.46	0	0
88	3	0.9913	0	0	4.095	1.612	0	0
89	3	0.9995	0	0	0.387	0.127	0	0
90	3	1.0042	0	0	2.534	0.833	0	0
91	3	0.9942	0	0	1.773	0.583	0	0
92	3	0.9676	0	0	0.65	0.214	0	0
93	3	0.9955	0	0	1.411	0.464	0	0
94	3	0.9797	0	0	0.537	0.176	0	0
95	3	0.9652	0	0	0.65	0.214	0	0
96	3	0.9968	0	0	1.66	0.546	0	0
97	3	1.001	0	0	1.708	0.561	0	0
98	3	0.996	0	0	1.136	0.373	0	0
99	3	0.9996	0	0	0.65	0.214	0	0
100	3	1.0072	0	0	1.231	0.405	0	0
101	3	0.9989	0	0	0.65	0.214	0	0
102	3	0.9796	0	0	0	0	0	0
103	3	0.9639	0	0	0	0	0	0
104	3	0.9831	0	0	0	0	0	0
105	3	0.9901	0	0	0.701	0.23	0	0
106	3	0.9878	0	0	0.46	0.151	0	0
107	3	0.9888	0	0	0	0	0	0
108	3	1.0006	0	0	1.235	0.406	0	0
109	3	1.0252	0	0	1.401	0.461	0	0
110	3	1.0253	0	0	0.573	0.188	0	0
111	3	1.003	0	0	0.637	0.209	0	0
112	3	0.9779	0	0	1.21	0.398	0	0
113	3	1.012	0	0	1.095	0.36	0	0
114	3	1.0062	0	0	0.683	0.224	0	0
115	3	1.0151	0	0	0.599	0.197	0	0
116	3	1.0096	0	0	1.115	0.366	0	0
117	3	1.0171	0	0	1.302	0.428	0	0
118	3	1.0151	0	0	1.821	0.552	0	0
119	3	1.0166	0	0	0.528	0.173	0	0
120	3	1.0028	0	0	0.6	0.213	0	0
121	3	1.0068	0	0	2.318	0.762	0	0
122	3	0.9967	0	0	0	0	0	0

Bus	Type	Vm(p.u)	P_G(p.u)	Q_G(p.u)	P_L(p.u)	Q_L(p.u)	Q_{min}(p.u)	Q_{max}(p.u)
123	3	0.9698	0	0	1.656	0.544	0	0
124	3	1.0077	0	0	0.36	0.118	0	0
125	3	1.01	0	0	0.705	0.232	0	0
126	3	1.0127	0	0	0	0	0	0
127	3	1.013	0	0	0.475	0.156	0	0
128	3	1.0046	0	0	0.348	0.114	0	0
129	3	1.0167	0	0	0	0	0	0
130	3	1.0013	0	0	0.348	0.114	0	0
131	3	1.0352	0	0	0	0	0	0
132	3	1.0061	0	0	2.552	0.839	0	0
133	3	1.0135	0	0	2.202	0.724	0	0
134	3	1.0171	0	0	0.743	0.244	0	0
135	3	1.0177	0	0	0.883	0.29	0	0
136	3	1.0099	0	0	3.239	1.065	0	0
137	3	1.0045	0	0	3.323	1.092	0	0
138	3	1.0093	0	0	0.701	0.23	0	0
139	3	1.0102	0	0	1.234	0.406	0	0
140	3	1.0072	0	0	0.477	0.157	0	0
141	3	1.0097	0	0	0.855	0.281	0	0
142	3	1.007	0	0	0.715	0.235	0	0
143	3	1.0036	0	0	1.36	0.447	0	0
144	3	1.0035	0	0	1.655	0.544	0	0
145	3	1.0071	0	0	2.005	0.659	0	0
146	3	1.0135	0	0	0.92	0.302	0	0
147	3	1.0167	0	0	0	0	0	0
148	3	1.0106	0	0	0.91	0.299	0	0
149	3	1.0003	0	0	1.276	0.419	0	0
150	3	1.0177	0	0	1.192	0.392	0	0
151	3	1.0087	0	0	0.68	0.223	0	0
152	3	1.0073	0	0	0.968	0.318	0	0
153	3	1.0159	0	0	0.743	0.244	0	0
154	3	1.0247	0	0	0	0	0	0
155	3	1.022	0	0	0	0	0	0
156	3	0.8723	0	0	2.698	0.887	0	0
157	3	1.0308	0	0	0.835	0.275	0	0
158	3	0.9128	0	0	1.747	0.624	0	0
159	3	0.9824	0	0	0.799	0.263	0	0
160	3	0.9986	0	0	2.532	0.832	0	0
161	3	1.0019	0	0	0.968	0.318	0	0
162	3	0.9999	0	0	2.094	0.688	0	0
163	3	0.9683	0	0	1.235	0.406	0	0
164	3	0.9835	0	0	0.884	0.29	0	0
165	3	1.008	0	0	0.508	0.183	0	0
166	3	0.9948	0	0	1.381	0.459	0	0

Bus	Type	Vm(p.u)	P_G(p.u)	Q_G(p.u)	P_L(p.u)	Q_L(p.u)	Q_{min}(p.u)	Q_{max}(p.u)
167	3	0.9953	0	0	0	0	0	0
168	3	0.978	0	0	2.3	0.888	0	0
169	3	0.9926	0	0	1.189	0.338	0	0
170	3	0.9992	0	0	1.336	0.469	0	0
171	3	0.9535	0	0	1.375	0.469	0	0
172	3	0.9576	0	0	0.945	0.342	0	0
173	3	0.9407	0	0	0.486	0.183	0	0
174	3	0.9133	0	0	1.698	0.676	0	0
175	3	1.0371	0	0	0	0	0	0
176	3	1.0085	0	0	1.38	0.454	0	0
177	3	1.0273	0	0	0.593	0.195	0	0
178	3	1.0062	0	0	-0.71	-0.106	0	0
179	3	1.007	0	0	0	0	0	0
180	3	1.0355	0	0	0	0	0	0
181	3	0.9876	0	0	0.714	0.235	0	0
182	3	1.0096	0	0	1.147	0.377	0	0
183	3	1.0131	0	0	0	0	0	0
184	3	0.9947	0	0	0.258	0.114	0	0
185	3	1.0245	0	0	0.8	0.287	0	0
186	3	1.0044	0	0	0.43	0.096	0	0
187	3	1.0176	0	0	2.2	0.216	0	0
188	3	0.9741	0	0	1.524	0.556	0	0
189	3	1.0137	0	0	0.281	0.092	0	0
190	3	1.0093	0	0	4.079	1.198	0	0
191	3	1.0098	0	0	1.231	0.351	0	0
192	3	0.9856	0	0	0.86	0.283	0	0
193	3	0.9865	0	0	1.528	0.616	0	0
194	3	1.0057	0	0	2.687	1.292	0	0
195	3	0.989	0	0	1.974	0.671	0	0
196	3	1.0043	0	0	-0.131	0.252	0	0
197	3	0.9895	0	0	1.807	0.613	0	0
198	3	1.0026	0	0	1.853	0.535	0	0
199	3	0.9895	0	0	3.283	1.093	0	0
200	3	0.9908	0	0	0.49	0.161	0	0
201	3	1.0026	0	0	2.111	0.694	0	0
202	3	1.0048	0	0	2.375	0.813	0	0
203	3	1.035	0	0	1.388	0.222	0	0
204	3	0.9973	0	0	0.889	0.347	0	0
205	3	1.0002	0	0	3.646	1.237	0	0
206	3	1.0212	0	0	0.388	0.127	0	0
207	3	1.0051	0	0	1.277	0.646	0	0
208	3	1.0007	0	0	1.147	0.552	0	0
209	3	1.0292	0	0	0	0	0	0
210	3	1.0178	0	0	0	0	0	0

Bus	Type	Vm(p.u)	P_G(p.u)	Q_G(p.u)	P_L(p.u)	Q_L(p.u)	Q_{min}(p.u)	Q_{max}(p.u)
211	3	1.0144	0	0	0	0	0	0
212	3	1.0217	0	0	0	0	0	0
213	3	1.0242	0	0	0	0	0	0
214	3	0.9954	0	0	0	0	0	0
215	3	1.0335	0	0	0	0	0	0
216	3	0.9998	0	0	0	0	0	0
217	3	1.0036	0	0	0	0	0	0
218	3	1.002	0	0	1.595	0.368	0	0
219	3	1.0233	0	0	-0.662	-0.208	0	0
220	3	0.9898	0	0	0.95	0.312	0	0
221	3	1.0239	0	0	0	0	0	0
222	3	1.0212	0	0	0	0	0	0
223	3	1.0387	0	0	0.78	0.256	0	0
224	3	1.0275	0	0	0.357	0.117	0	0
225	3	0.9972	0	0	0.7	0.23	0	0
226	3	1.0062	0	0	0	0	0	0
227	3	1.0123	0	0	0.75	0.247	0	0
228	3	1.0049	0	0	0.92	0.302	0	0
229	3	1.0178	0	0	0	0	0	0
230	3	1.0008	0	0	0	0	0	0
231	3	1.0337	0	0	0	0	0	0
232	3	1.019	0	0	0	0	0	0
233	3	1.0293	0	0	0	0	0	0
234	3	1.045	0	0	0	0	0	0
235	3	1.0411	0	0	-12.584	-7	0	0
236	3	1.0058	0	0	0	0	0	0
237	3	1.0536	0	0	0	0	0	0
238	3	1.0096	0	0	0	0	0	0
239	3	1.0344	0	0	0	0	0	0
240	3	1.0276	0	0	0	0	0	0
241	3	1.0559	0	0	0	0	0	0
242	3	0.9725	0	0	0.277	0.091	0	0
243	3	1.016	0	0	0	0	0	0
244	3	1.0186	0	0	0	0	0	0
245	3	0.9864	0	0	2.007	0.996	0	0
246	3	1.0037	0	0	-0.07	0.108	0	0

APPENDIX B

The proposed GA-SVM approach for on-line voltage stability monitoring presented in chapter 5 are compared with other machine learning models i.e. grid search (GS) SVM and multilayer perceptron-back propagation neural networks (MLP-BPNN) using same dataset. The details of these machine-learning models are given below.

B1 Grid Search based Support Vector Machine (GS-SVM)

In [132], the author has proposed a technique to select this parameter known as grid search (GS) SVM. In GS-SVM, five-fold cross validation technique is considered. To evaluate the optimal parameter of GS-SVM same fitness function is considered as discussed in chapter 5 section 5.5 equation (5.10). An interactive grid search has been carried out for the selection of SVM parameters with C in the range of $[2^{-1}, 2^{10}]$, σ^2 varying in the range $[2^{-5}, 2^{10}]$ and ε varying in the range $[2^{-10}, 2^{3}]$. The best fitness value for New England 39-bus system is 0.0110 with parameter values C = 16, σ^2 = 4 and ε = 0.0625, and the best fitness value for NRPG 246-bus system is 0.0169 with parameter values C = 32, σ^2 = 0.5 and ε = 0.0313.

B2 Multilayer Perceptron-Back Propagation Neural Network (MLP-BPNN)

The ANN model used in this work is multilayer perceptron-back propagation neural network (MLP-BPNN). The detailed description on MIP-BPNN is given in [133]. MIP-BPNN is constituted of a hidden layer with five neurons using log-sigmoid transfer function (logsig) whereas the output uses a pure linear output function. This model contains multiple layers of nodes, which is fully connected to each other. Except for the input nodes, each node is a neuron with an activation function. The activation function used is sigmoidal function. The output layer is compared to a target and the error is applied in a back propagation process to adjust the weights. The network is trained for a maximum of 100 epochs or until the network training mean-squared error falls below 1e-5. A learning rate of 0.01 and a momentum constant of 0.9 are used in chapter 5.

APPENDIX C

C.1 Definition of Fractional Derivatives and Integrals

Fractional calculus is a the generalization of integration and differentiation to non-integer order fundamental operator ${}_aD_t^\alpha$, where a and t are the bounds of the operation and $\alpha \in R$. The ${}_aD_t^\alpha$ operator is defined as:

$$ {}_aD_t^\alpha = \begin{cases} \dfrac{d^\alpha}{dt^\alpha}, & \alpha > 0 \\ 1 & \alpha = 0 \\ \int_\alpha^t (d\tau)^\alpha & \alpha < 0 \end{cases} \tag{C.1} $$

The three most commonly used definition for the fractional integral and derivatives are Grunwald-Letnikov (GL) definition, the Riemann-Liouville (RL) and the Caputo definition [130]. In this work, Riemann-Liouville (RL) is used and explained below.

C.2 Riemann-Liouville Fractional Integrals and Derivatives

The expression for n-fold integral considering Riemann-Liouville (RL) definition is expressed as:

$$ \underbrace{\int_a^t \int_a^{t_n} \int_a^{t_{n-1}} \cdots\cdots \int_a^{t_3} \int_a^{t_2} f(t_1)\, dt_1 dt_2 \cdots\cdots dt_{n-1} dt_n}_{n-fold} = \frac{1}{\Gamma(n)} \int_a^t \frac{f(\tau)}{(t-\tau)^{1-n}}\, d\tau \tag{C.2} $$

where $n \in N, n > 0.$

Fractional integral of order α for the function f(t) can be expressed as:

$$ {}_aI_t^\alpha f(t) \equiv {}_aD_t^{-\alpha} f(t) = \frac{1}{\Gamma(-\alpha)} \int_a^t \frac{f(\tau)}{(t-\tau)} \tag{C.3} $$

For $\lambda, a \in R, \alpha < 0.$

From relation (C.3), the formula for the Riemann-Liouville definition of fractional integral of the order α can be written in the following form,

$$ {}_{a}D_{t}^{\alpha} f(t) = \frac{1}{\Gamma(n-\alpha)} \frac{d^n}{dt^n} \int_a^t \frac{f(\tau)}{(t-\tau)^{\alpha-n+1}} d\tau; \quad where\ n-1 < \alpha < n, \tag{C.4} $$

where *a* and *t* are the limits of operation ${}_{a}D_{t}^{\alpha} f(t)$.

Now, for $0 < \alpha < 1$ and $f(t)$ is causal function i.e. $f(t) = 0,$ for t<0, the fractional integral is defined as:

$$ {}_{0}D_{t}^{\alpha} f(t) = \frac{1}{\Gamma(\alpha)} \int_0^t \frac{f(\tau)}{(t-\tau)^{1-\alpha}} d\tau; \quad 0 < \alpha < 1, \ \ t > 0 \tag{C.4} $$

The fractional order derivative can be expressed as:

$$ {}_{0}D_{t}^{\alpha} f(t) = \frac{1}{\Gamma(n-\alpha)} \frac{d^n}{dt^n} \int_a^t \frac{f(\tau)}{(t-\tau)^{\alpha-n+1}} d\tau \tag{C.5} $$

Where, $\Gamma(.)$ is Euler's Gamma function.

C.2.1 Laplace transform of fractional integrals

The Laplace form of (C.4) is expressed by convolution of the functions $g(t) = t^{p-1}$ *and* $f(t)$.

$$ {}_{0}D_{t}^{-p} f(t) = \frac{1}{\Gamma(p)} \frac{d^n}{dt^n} \int_0^t (t-\tau)^{p-1} f(\tau) d\tau = t^{p-1} * f(t) \tag{C.6} $$

The Laplace transform of the function t^{p-1} is

$$ G(s) = L\left\{t^{p-1}; s\right\} = \Gamma(p) s^{-p} \tag{C.7} $$

Therefore using the formula for the Laplace transform of the convolution, the Laplace transform of the Riemann-Liouville fractional integrals of order λ can be obtained as:

$$ L\left\{ {}_{0}D_{t}^{-\lambda} f(t) : s\right\} = L\left\{ {}_{0}D_{t}^{-\lambda} f(t) : s\right\} = s^{-\lambda} F(s) \tag{C.8} $$

C.2.2 Laplace transform of fractional derivatives

The Laplace transform of the Riemann-Liouville fractional derivative can be expressed as:

$$ {}_{0}D_{t}^{p} f(t) = g^{(n)}(t), \tag{C.9} $$

$$g(t) = {}_0D_t^{-(n-p)} f(t) \frac{1}{\Gamma(k-p)} \int_0^t (t-\tau)^{n-p-1} f(\tau) d\tau \quad \text{(C.10)}$$

$$n-1 \le p < n$$

The Laplace transform of (C.9) can be expressed as:

$$L\left\{ {}_0D_t^p f(t) : s \right\} = s^n G(s) - \sum_{k=0}^{n-1} s^k g^{(n-k-1)}(0) \quad \text{(C.11)}$$

The Laplace transform of the function *g(t)* is evaluated by (C.8)

$$G(s) = s^{-(n-p)} F(s) \quad \text{(C.12)}$$

Additionally, from the definition of the Riemann-Liouville fractional derivative we have

$$g^{(n-k-1)}(t) = \frac{d^{n-k-1}}{dt^{n-k-1}} {}_0D_t^{-(n-p)} f(t) = {}_0D_t^{p-k-1} f(t) \quad \text{(C.13)}$$

On putting (C.12) and (C.13) into (C.11), the final expression for the Riemann-Liouville fractional derivative for *p>0*, can be written as

$$L\left\{ {}_0D_t^p f(t) : s \right\} = s^n F(s) - \sum_{k=0}^{n-1} s^k [{}_0D_t^{p-k-1} f(t)]_{t=0}; \; n-1 \le p < n \quad \text{(C.14)}$$

For zero initial condition the Laplace transform of the fractional derivatives of order μ can be written as:

$$L\left\{ {}_0D_t^{\mu} f(t) \right\} = s^{\mu} F(s) \quad \text{(C.15)}$$

APPENDIX D

D.1 Mathematical modeling of STATCOM

The mathematical modeling of STATCOM is done in per-unit. i_B *and* V_B are the base values and ω_B is the angular speed of the system at the nominal frequency [75]. The parameters and the variables shown in figure 6.2 can be represented in p.u. as given below.

$$\begin{aligned}
&i_a^{'} = \frac{i_a}{i_B} \quad i_b^{'} = \frac{i_b}{i_B} \quad i_c^{'} = \frac{i_c}{i_B} \\
&e_{sa}^{'} = \frac{e_{sa}}{v_B} \quad e_{sb}^{'} = \frac{e_{sb}}{v_B} \quad e_{sc}^{'} = \frac{e_{sc}}{v_B} \\
&v_{ga}^{'} = \frac{v_{ga}}{v_B} \quad v_{gb}^{'} = \frac{v_{gb}}{v_B} \quad v_{gc}^{'} = \frac{v_{gc}}{v_B} \\
&z_B = \frac{v_B}{i_B} \quad L^{'} = \frac{\omega_B L}{z_B} \quad R^{'} = \frac{R}{z_B} \\
&V_{dc}^{'} = \frac{V_{dc}}{v_B} \quad I_{dc}^{'} = \frac{I_{dc}}{i_B} \quad C_s^{'} = \frac{1}{\omega_B C z_B} \quad R_s^{'} = \frac{R_s}{z_B}
\end{aligned} \tag{D.1}$$

The differential equation for STATCOM current can be written as:

$$\frac{d}{dt}\begin{bmatrix} i_a^{'} \\ i_b^{'} \\ i_c^{'} \end{bmatrix} = \frac{-R^{'}\omega_B}{L^{'}}\begin{bmatrix} i_a^{'} \\ i_b^{'} \\ i_c^{'} \end{bmatrix} + \frac{\omega_B}{L^{'}}\begin{bmatrix} v_{ga}^{'} - e_{sa}^{'} \\ v_{gb}^{'} - e_{sb}^{'} \\ v_{gc}^{'} - e_{sc}^{'} \end{bmatrix} \tag{D.2}$$

In (D.2) $v_{ga}^{'}, v_{gb}^{'}, v_{gc}^{'}$ is the three-phase grid voltage, $i_a^{'}, i_b^{'}, i_c^{'}$ is the three-phase STATCOM current. The voltage difference between the grid voltage and the STATCOM voltage results in the STACOM current through the coupling circuit. The DC side current $I_{dc}^{'}$ can be expressed as:

$$I_{dc}^{'} = \frac{1}{\omega_B C_s^{'}} \frac{dV_{dc}^{'}}{dt} + \frac{V_{dc}^{'}}{R_s^{'}} \tag{D.3}$$

To describe the relation between the AC and DC side, it is considered that the instantaneous power on the DC side of the VSI is always equal to the power on AC side:

$$V_{dc}^{'} I_{dc}^{'} = e_{sa}^{'} i_a^{'} + e_{sb}^{'} i_b^{'} + e_{sc}^{'} i_c^{'} \tag{D.4}$$

The connection between the VSI AC and DC side voltage can be explained with the switching signal $S_a, S_b \text{ and } S_c$ as:

$$\begin{bmatrix} e'_{sa} \\ e'_{sb} \\ e'_{sc} \end{bmatrix} = k_p \begin{bmatrix} S_a \\ S_b \\ S_c \end{bmatrix} V'_{dc} \tag{D.5}$$

where the value of k_p depends on the type of VSI. By substituting (D.5) into (D.4), the DC side current will be:

$$I'_{dc} = k_p S_a i'_a + k_p S_b i'_b + k_p S_c i'_c \tag{D.6}$$

The complete mathematical equation describing the STATCOM operation can be obtained by combining (D.2), (D.3), (D.6) and is given by:

$$\frac{d}{dt}\begin{bmatrix} i'_a \\ i'_b \\ i'_c \\ I'_{dc} \end{bmatrix} = \begin{bmatrix} \frac{-R'\omega_B}{L'} & 0 & 0 & \frac{k_p\omega_B}{L'}S_a \\ 0 & \frac{-R'\omega_B}{L'} & 0 & \frac{k_p\omega_B}{L'}S_b \\ 0 & 0 & \frac{-R'\omega_B}{L'} & \frac{k_p\omega_B}{L'}S_c \\ k_p\omega_B C'_s S_a & k_p\omega_B C'_s S_b & k_p\omega_B C'_s S_b & \frac{\omega_b C'_s}{R'_s} \end{bmatrix} \begin{bmatrix} i'_a \\ i'_b \\ i'_c \\ I'_{dc} \end{bmatrix} + \frac{\omega_B}{L'}\begin{bmatrix} v'_{ga} \\ v'_{gb} \\ v'_{gc} \\ 0 \end{bmatrix} \tag{D.7}$$

The mathematical model explained above in three-phase is converted to $\alpha - \beta$ coordinate system using Clarke transformation $T_{\alpha\beta}$ given by:

$$T_{\alpha\beta} = \frac{2}{3}\begin{bmatrix} 1 & \frac{-1}{2} & -\frac{1}{2} \\ 0 & \frac{\sqrt{3}}{2} & -\frac{\sqrt{3}}{2} \\ \frac{1}{2} & \frac{1}{2} & \frac{1}{2} \end{bmatrix} \tag{D.8}$$

$$\begin{bmatrix} x_\alpha \\ x_\beta \\ x_0 \end{bmatrix} = T_{\alpha\beta}\begin{bmatrix} x_a \\ x_b \\ x_c \end{bmatrix} \tag{D.9}$$

Where, $x_{a,}\ x_b$ *and* x_c are individual phases of any electrical parameter in three-phase.

Applying the above transformation in (D.9) to the three-phase model in (D.2) yields mathematical model in $\alpha-\beta$ frame as:

$$\frac{d}{dt}\begin{bmatrix} i_\alpha^{'} \\ i_\beta^{'} \end{bmatrix}=\begin{bmatrix} \frac{-R^{'}\omega_B}{L^{'}} & 0 \\ 0 & \frac{-R^{'}\omega_B}{L^{'}} \end{bmatrix}\begin{bmatrix} i_\alpha^{'} \\ i_\beta^{'} \end{bmatrix}+\frac{\omega_B}{L^{'}}\begin{bmatrix} v_{g\alpha}^{'}-e_{s\alpha}^{'} \\ v_{g\beta}^{'}-e_{s\beta}^{'} \end{bmatrix} \tag{D.10}$$

Where the zero sequence is omitted because STATCOM is connected to network with three wire system.

In order to include the DC side circuit into the mathematical model the equation (D.5) and (D.6) are transformed to $\alpha-\beta$ frame.

$$\begin{aligned} e_{s\alpha}^{'} &= k_p S_\alpha V_{dc}^{'} \\ e_{s\beta}^{'} &= k_p S_\beta V_{dc}^{'} \end{aligned} \tag{D.11}$$

$$I_{dc}^{'}=\frac{3}{2}\left(k_p S_\alpha i_\alpha^{'}+k_p S_\beta i_\beta^{'}\right) \tag{D.12}$$

Where the average switching function in $\alpha-\beta$ coordinate is given by:

$$\begin{bmatrix} S_\alpha \\ S_\beta \end{bmatrix}=m_s\begin{bmatrix} \cos\delta \\ \sin\delta \end{bmatrix} \tag{D.13}$$

The complete STATCOM model in $\alpha-\beta$ coordinates can be written as:

$$\frac{d}{dt}\begin{bmatrix} i_\alpha^{'} \\ i_\beta^{'} \\ V_{dc}^{'} \end{bmatrix}=\begin{bmatrix} \frac{-R^{'}\omega_B}{L^{'}} & 0 & \frac{-k_p\omega_B}{L^{'}}S_\alpha \\ 0 & \frac{-R^{'}\omega_B}{L^{'}} & \frac{-k_p\omega_B}{L^{'}}S_\beta \\ \frac{3k_p\omega_B C_s^{'}}{2}S_\alpha & \frac{3k_p\omega_B C_s^{'}}{2}S_\beta & \frac{-\omega_B C_s^{'}}{R_s^{'}} \end{bmatrix}\begin{bmatrix} i_\alpha^{'} \\ i_\beta^{'} \\ V_{dc}^{'} \end{bmatrix}+\begin{bmatrix} \frac{\omega_B}{L^{'}}v_{g\alpha}^{'} \\ \frac{\omega_B}{L^{'}}v_{g\beta}^{'} \\ 0 \end{bmatrix} \tag{D.14}$$

In the next step, the mathematical model of STATCOM given in (D.7) is transformed into d-q synchronous frame using the classical transformation matrix [75] given by:

$$T_{dq} = \frac{2}{3}\begin{bmatrix} \cos(\omega t) & \cos(\omega t - \frac{2\Pi}{3}) & \cos(\omega t + \frac{2\Pi}{3}) \\ -sin(\omega t) & -sin(\omega t - \frac{2\Pi}{3}) & -sin(\omega t + \frac{2\Pi}{3}) \end{bmatrix} \quad \text{(D.15)}$$

The zero sequence components is not considered because three-wire STATCOM cannot generate zero sequence current. Then using the above transformation (D.2) is transformed as:

$$\frac{d}{dt}\begin{bmatrix} i_d^{'} \\ i_q^{'} \end{bmatrix} = \begin{bmatrix} \frac{-R^{'}\omega_B}{L^{'}} & \omega \\ -\omega & \frac{-R^{'}\omega_B}{L^{'}} \end{bmatrix}\begin{bmatrix} i_d^{'} \\ i_q^{'} \end{bmatrix} + \frac{\omega_B}{L^{'}}\begin{bmatrix} v_{gd}^{'} - e_{sd}^{'} \\ v_{gq}^{'} - e_{sq}^{'} \end{bmatrix} \quad \text{(D.16)}$$

The power balance equation between the AC side and DC side of VSI in d-q frame is given by:

$$V_{dc}^{'} I_{dc}^{'} = \frac{3}{2}(e_{sd}^{'} i_d^{'} + e_{sq}^{'} i_q^{'}) \quad \text{(D.17)}$$

The connection between the AC and DC side voltage in d-q frame represented with the switching function is expressed as:

$$\begin{bmatrix} e_{sd}^{'} \\ e_{sq}^{'} \end{bmatrix} = k_p \begin{bmatrix} S_d \\ S_q \end{bmatrix} V_{dc}^{'} \quad \text{(D.18)}$$

Substituting (D.18) in (D.17)

$$I_{dc}^{'} = \frac{3}{2}\left(k_p S_d i_d^{'} + k_p S_q i_q^{'}\right) \quad \text{(D.19)}$$

The complete mathematical model in d-q coordinate system in given by:

$$\frac{d}{dt}\begin{bmatrix} i_d^{'} \\ i_q^{'} \\ V_{dc}^{'} \end{bmatrix} = \begin{bmatrix} \frac{-R^{'}\omega_B}{L^{'}} & \omega & \frac{-k_p\omega_B}{L^{'}} S_d \\ -\omega & \frac{-R^{'}\omega_B}{L^{'}} & \frac{-k_p\omega_B}{L^{'}} S_q \\ \frac{3k_p\omega_B C_s^{'}}{2} S_d & \frac{3k_p\omega_B C_s^{'}}{2} S_q & \frac{-\omega_B C_s^{'}}{R_s^{'}} \end{bmatrix}\begin{bmatrix} i_d^{'} \\ i_q^{'} \\ V_{dc}^{'} \end{bmatrix} + \begin{bmatrix} \frac{\omega_B}{L^{'}} v_{gd}^{'} \\ \frac{\omega_B}{L^{'}} v_{gq}^{'} \\ 0 \end{bmatrix} \quad \text{(D.20)}$$

Where, ω is the angular speed of the fundamental frequency of voltage component. Figure D-1 shows the block diagram of the STATCOM model in the rotating d-q frame.

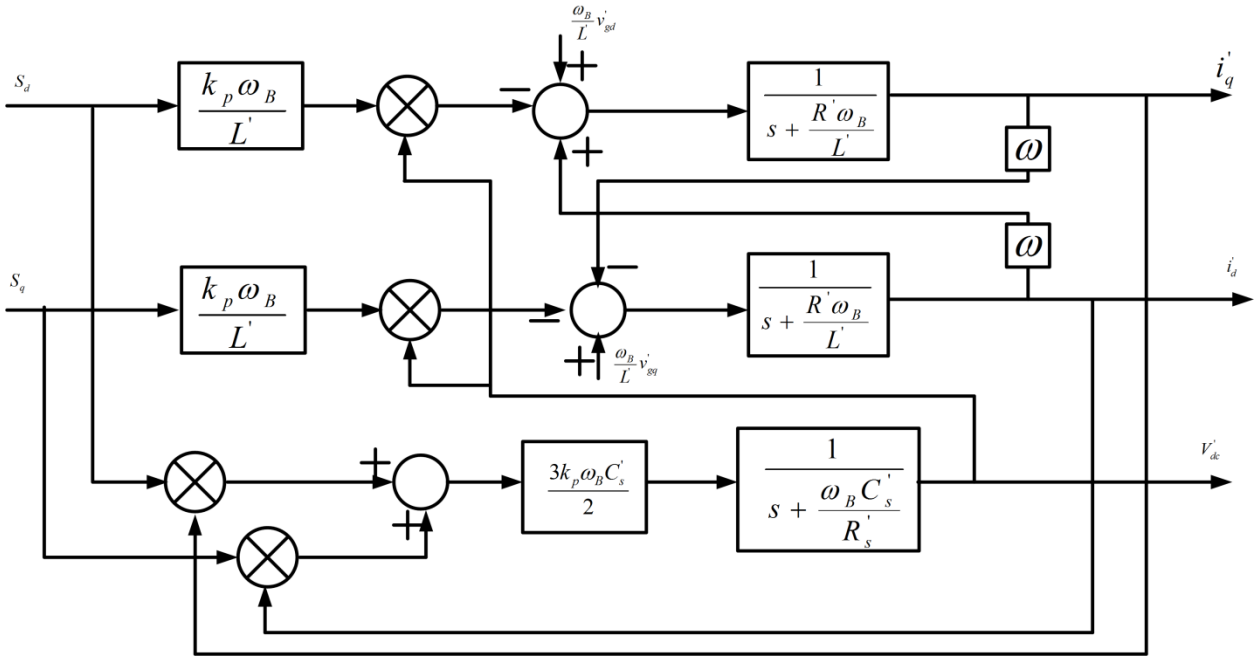

Figure D-1: Equivalent block diagram of STATCOM mathematical model in the d-q frame

D.2 STATCOM control strategy

The development of control algorithm is described using the mathematical model discussed above. Figure D-1 shows that there are two controllable parameters S_d and S_q and three variables i'_d, i'_q *and* V'_{dc} . Therefore, two variables can be controlled independently, while the third one is a dependent variable. To develop the control algorithm, variables w'_d and w'_q are introduced to represent the voltage drop on the coupling circuit and variable w'_{dc} which is proportional to the DC –side current [134].

$$\begin{bmatrix} w'_d \\ w'_q \\ w'_{dc} \end{bmatrix} = \begin{bmatrix} 0 & 0 & \frac{-k_p\omega_B}{L'}S_d \\ 0 & 0 & \frac{-k_p\omega_B}{L'}S_q \\ \frac{3k_p\omega_B C'_s}{2}S_d & \frac{3k_p\omega_B C'_s}{2}S_q & 0 \end{bmatrix} \begin{bmatrix} i'_d \\ i'_q \\ V'_{dc} \end{bmatrix} + \begin{bmatrix} \frac{\omega_B}{L'}v'_{gd} \\ \frac{\omega_B}{L'}v'_{gq} \\ 0 \end{bmatrix} \quad \text{(D.21)}$$

Combining (D.21) and (D.20), the STATCOM mathematical model is transformed as:

$$\frac{d}{dt}\begin{bmatrix} i_d^{'} \\ i_q^{'} \\ V_{dc}^{'} \end{bmatrix} = \begin{bmatrix} \frac{-R^{'}\omega_B}{L^{'}} & \omega & 0 \\ -\omega & \frac{-R^{'}\omega_B}{L^{'}} & 0 \\ 0 & 0 & \frac{-\omega_B C_s^{'}}{R_s^{'}} \end{bmatrix} \begin{bmatrix} i_d^{'} \\ i_q^{'} \\ V_{dc}^{'} \end{bmatrix} + \begin{bmatrix} w_d^{'} \\ w_q^{'} \\ w_{dc}^{'} \end{bmatrix} \quad \text{(D.22)}$$

Next, the decoupling between q and d axes is made. The block diagram of the STATCOM control algorithm is shown in Figure D-2. The variable $w_d^{'}, w_q^{'}$ *and* $w_{dc}^{'}$ form the outputs of Proportional-Integral (PI) controller. The input to PI controllers is the difference between the reference and measured values. The output of the current PI controllers would therefore be the voltage drop on the coupling circuit that is required in order that the desired reference current is generated. The output of the DC-side voltage PI controller is proportional to the DC-side current that is required to maintain the DC-side voltage at the reference value.

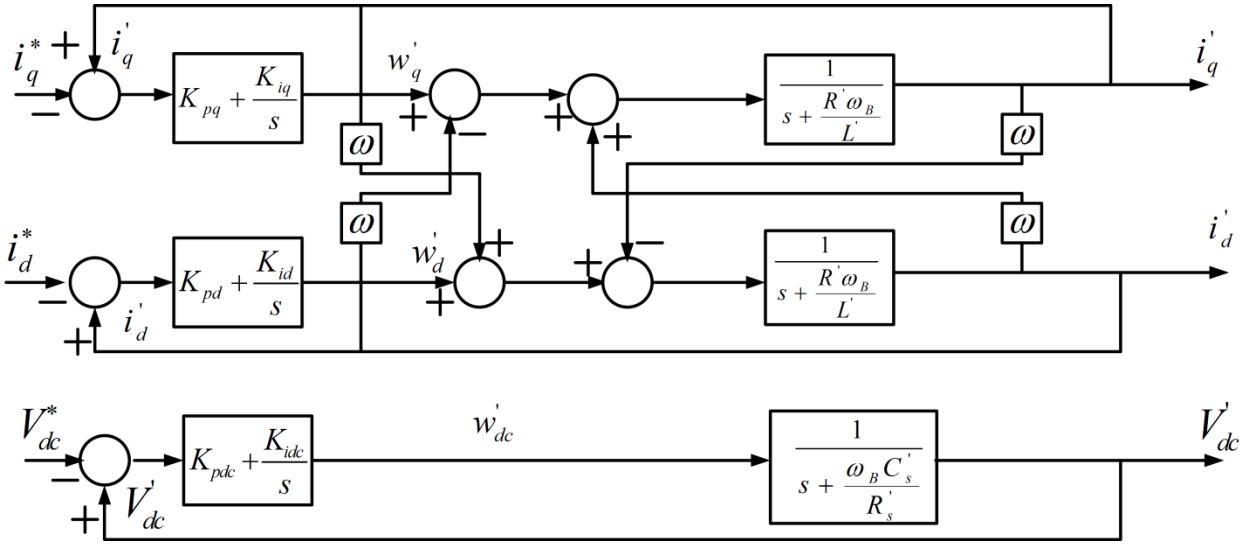

Figure D-2: Bock diagram of the STATCOM control algorithm

LIST OF PUBLICATIONS

On the basis of research work carried out, following papers have been published/under review in international journals and published in proceedings of international/ national conferences.

International Journals-

[1.] K S Sajan, Vishal Kumar and Barjeev Tyagi, "Genetic Algorithm based Support Vector Machine for On-line Voltage Stability Monitoring", International Journal of Electrical Power & Energy Systems, vol. 73, pp. 200–208, Dec. 2015

[2.] K S Sajan, A K Mishra, Vishal Kumar and Barjeev Tyagi, "Phased Optimal PMU Placement Based on Revised Analytical Hierarchy Process", in Electr. Power Components Syst. Taylor & Francis. (*Accepted*) December 2015.

[3.] K S Sajan, Vishal Kumar and Barjeev Tyagi, ""State Estimation and Bad Data Processing for Complete and Incomplete Observability in PMU Integrated Network"", in International Journal of Emerging Electric Power Systems (IJEEPS). (*Under-review*)

[4.] K S Sajan, Vishal Kumar and Barjeev Tyagi, "Reactive power control of STATCOM using Fractional Order PI controller", in IEEE Transaction on Power System. (*communicated*).

Conferences-

[1.] K. S. Sajan and Barjeev Tyagi, "Optimal placement of PMU with optimal branch current phasors for complete and incomplete observability," in 2011 IEEE Power and Energy Society General Meeting, 2011, pp. 1–5.

[2.] K S Sajan, A K Mishra, Vishal Kumar and Barjeev Tyagi, "Phased PMU Installation using Revised Analytical Hierarchy Process," in Asia Smart Grids and Electromobility (ASGE) conference, 29-30 October 2013 at Marina Bay Sands, Singapore. (poster presentation).

[3.] K S Sajan, Vishal Kumar, Barjeev Tyagi, "Genetic Algorithm based Artificial Neural Network model for Voltage Stability Monitoring" proceedings of 2014 18th NPSC, IIT Guwahati, 18-20 December, 2014.

[4.] K S Sajan, Vishal Kumar, Barjeev Tyagi, "ICA based Artificial Neural Network model for Voltage Stability Monitoring" proceedings of 2015 TENCON IEEE Region 10 Conference, 1-4 November, 2015.